



SENIOR DESIGN:
MAE 4351 Project

Ref.: MAE 4351-001-2021
Date: 11. Aug. 2023
Name: Gayathri Kola
Status: Complete

Designing a Hypersonic Spirit of St. Louis: Aerodynamics, Stability and Control Study

Signatures:

	Name:	Signature:	Dept.:	Date:
Author:	Gayathri Kola		MAE	8/11/2023
Seen:	Dr. Bernd Chudoba		MAE	

Summary:

The University of Texas at Arlington's Senior Design capstone is a multidisciplinary project that aims to expose students to industry structure to aircraft conceptual design. The class is split into competing teams that collaboratively develop a conceptual aircraft using modern sizing and convergence methodologies to grossly estimate the required vehicle size. This team, ATLANTIX is tasked with re-imagining the Spirit of St. Louis. The team was tasked to design a wing-body hypersonic Spirit of St. Louis and perform a feasibility study for single and dual flow path, 3D intakes for Mach numbers 5, 7.5 and 10. A total of vehicles were to be assessed for feasibility. Through our process, the Mach 10 dual flow path vehicle was concluded to be infeasible due to high internal combustion temperatures of the scramjet engines, thereby leading to dangerous aerothermal effects.

This report covers the Stability and Control, and Aerodynamics of the configurations. For the aerodynamics part, the neutral point location is of primary focus. The aircraft control surface sizing procedure and results are built up. The sizing results yield a higher elevon size requirement for takeoff rotation. With increased elevon size, and increased elevon chord length was generated. This required all the configured vehicles to have larger wingspans, hence needed to be resized. Initial vertical tail estimates from the configuration layout (CL) phase were very large, and with sizing assessment for control power during the asymmetric thrust condition and crosswind landings, the overall sizes were reduced for most vehicles.

With the sized areas for the control effectors, a stability assessment was performed for all configured vehicles. The results yielded in poor lateral stability during subsonic flight and without any tail dihedral. The vehicles were stable longitudinally, however, decreased in the directional stability when approaching hypersonic speeds, this was an expected result since the initial designs do not feature drooped wings or ventral tail fins that can improve yaw.

Distribution:

Institution:	Dept.:	Name:
The University of Texas at Arlington	MAE	Dr. Bernd Chudoba



SENIOR DESIGN:
MAE 4351 Project

Ref.: MAE 4351-001-2021
Date: 11. Aug. 2023
Name: Gayathri Kola
Status: Complete

Work Disclosure Statement

The work I performed to document the results presented in this report was performed by me, or it is otherwise acknowledged.

Date: 8/11/2023

Signature:

A handwritten signature in black ink, appearing to read "Gayathri".



Table of Contents

WORK DISCLOSURE STATEMENT	2
LIST OF FIGURES.....	5
LIST OF TABLES.....	8
NOMENCLATURE	9
1 INTRODUCTION	11
1.1 BACKGROUND ON PLANES	11
1.2 PROJECT OVERVIEW	14
1.3 TEAM STRUCTURE AND BREAKDOWN.....	15
2 LITERATURE REVIEW	16
2.1 HYPERSONIC REVIEW.....	16
2.2 STABILITY AND CONTROL RESOURCE LIST.....	19
3 CONCEPTUAL DESIGN BREAKDOWN	21
3.1 PARAMETRIC SIZING	21
3.2 CONFIGURATION LAYOUT	23
3.3 CONFIGURATION EVALUATION	24
4 STABILITY AND CONTROL.....	25
4.1 BACKGROUND	25
4.2 VOLUME COEFFICIENT APPROACH	26
4.3 CONTROL SURFACE SIZING.....	27
4.4 FLIGHT CONDITIONS TO ADDRESS	29
4.5 AXIS SYSTEMS	33
4.6 STATIC STABILITY	33
4.7 DYNAMIC STABILITY	34
4.8 LONGITUDINAL STABILITY.....	34
4.9 METHODOLOGY FOR STABILITY AND CONTROL DERIVATIVES	35
4.10 VALIDATION METHODS.....	40
4.11 SIZING RESULTS FOR S&C.....	45
4.12 AIRCRAFT TRIM ANALYSIS	70
4.13 STABILITY RESULTS.....	74
5 AERODYNAMICS.....	78
5.1 BACKGROUND	78
5.2 METHODOLOGY FOR AERODYNAMICS IN PS.....	81
5.3 METHODOLOGY FOR CL AND CE	95
5.4 VALIDATION METHODS.....	96
5.5 RESULTS AND DISCUSSION FOR AERODYNAMICS	99
6 CONCLUSIONS.....	100
7 HISTORICAL DEVELOPMENT.....	101
7.1 WEEK 1.....	101
7.2 WEEK 2.....	101
7.3 WEEK 3.....	101
7.4 WEEK 4.....	102
7.5 WEEK 5.....	102
7.6 WEEK 6.....	102



7.7	WEEK 7-10	102
8	ABET ACCREDITATION.....	102
8.1	OUTCOME 2.....	102
8.2	OUTCOME 3.....	103
8.3	OUTCOME 4.....	104
8.4	OUTCOME 5.....	104
8.5	OUTCOME 7.....	105
	APPENDIX	106
	APPENDIX A	106
	APPENDIX B.....	109
	APPENDIX C	116
	REFERENCES	146

List of Figures

Fig. 1 The Spirit of St. Louis was built back in 1927 [1].....	11
Fig. 2 The Gulfstream G700 was launched in 2020 [3].....	12
Fig. 3 The SR-71 Blackbird was built in 1964 [4].....	12
Fig. 4 Hermeus Quarterhorse, expected flight in 2024 [5]	13
Fig. 5 Hermeus Darkhorse, expected to launch in 2025 [7].....	13
Fig. 6 Hermeus Halcyon with drooped wings is expected to launch in 2029 [9].	14
Fig. 7 Hypersonic Spirit of St. Louis progression [10].....	15
Fig. 8 Atlantix logo created by Wesley Junell [11]	15
Fig. 9 Atlantix team structure by Noah Blakely [12].....	16
Fig. 10 Different aircraft configurations for hypersonic vehicle concepts [13].....	16
Fig. 11 The North American X-15 [15].....	17
Fig. 12 X-43A mission trajectory [16].....	17
Fig. 13 Space Shuttle Orbiter with a wing-body configuration [17].....	18
Fig. 14 Concorde and Tupolev Tu-144 [18].....	18
Fig. 15 Aircraft design phases [25].....	21
Fig. 16 Atlantix vehicle design points [11].....	22
Fig. 17 Wight and volume budgets for convergence [42].....	23
Fig. 18 Stability and Control IDA for CL.....	23
Fig. 19 Stability and Control CE IDA.	24
Fig. 20 Stable, unstable, and neutral equilibrium [32].....	25
Fig. 21 Stability and Control overview.....	25
Fig. 22 Types of tail configurations available to the designer [34].	26
Fig. 23 Canard designs on supersonic aircraft.....	27
Fig. 24 Elevons features in supersonic and hypersonic aircraft.....	28
Fig. 25 High-speed aircrafts with twin vertical tails.....	28
Fig. 26 Single vertical tail used in high-speed aircraft.	29
Fig. 27 Ground clearance required for takeoff rotation [28].....	30
Fig. 28 Forces and moments during takeoff rotation [28]	30
Fig. 29 Asymmetric thrust condition [28]	32
Fig. 30 Control surface sizing IDA for CE.....	32
Fig. 31 Axis Systems with body frame.....	33
Fig. 32 Static stability requirements overview [35].....	34
Fig. 33 Interactions between disciplines for longitudinal stability.	34
Fig. 34 Static stability assessment roadmap [35].....	36
Fig. 35 Axis system and forces acting on a tailless wing-body [25].....	38
Fig. 36 Subsonic and supersonic pitching moment derivative verification attempt.	41
Fig. 37 Flight test data for XB-70 used for verification [66].....	42
Fig. 38 XB-70 pitching moment derivative data for given Mach (Column 7) [66].....	42
Fig. 39 Elevon control derivative verification using SR-71 data.....	43
Fig. 40 Flight test results for baseline SR-71 configuration from LASRE [21]	43
Fig. 41 Dimensions used for Space Shuttle Orbiter [50].	44
Fig. 42 Hypersonic elevon control derivative, same plots with chosen points for verification.	44
Fig. 43 Method verification plots used from Space Shuttle Orbiter data [68].....	45
Fig. 44 Elevon design procedure [28].....	47
Fig. 45 Vertical tail and rudder design procedure [28].....	47
Fig. 46 W&B C.G. location results for Mach 5.0 configurations, for single and dual flow [12].....	48
Fig. 47 W&B C.G. location results for Mach 7.5 configurations, for single and dual flow [12].....	48
Fig. 48 W&B C.G. location results for Mach 10.0 configurations, for single and dual flow [12].....	49
Fig. 49 P&T results needed for S&C sizing and evaluation [71].....	49
Fig. 50 P&T trajectory results for Mach 5 single flow path [71].....	49
Fig. 51 P&T trajectory results for Mach 5 dual flow path [71].....	50
Fig. 52 P&T trajectory results for Mach 7.5 single flow path [71].....	50

Fig. 53 P&T trajectory results for Mach 7.5 dual flow path [71].	50
Fig. 54 P&T trajectory results for Mach 10.0 single flow path [71].	51
Fig. 55 P&T trajectory results for Mach 10.0 dual flow path [71].	51
Fig. 56 Flight trajectory for distance travelled [72].	51
Fig. 57 Angle of attacks as a function of trajectory [72].	52
Fig. 58 Lift-curve-slope given for Mach 5 configuration [72].	52
Fig. 59 AX-110 Design point results [11,12,69].	53
Fig. 60 Vertical tail geometry with rudder [28].	54
Fig. 61 AX-110 initial dimensions decided by Aerodynamics, Propulsion & Geometry [69].	54
Fig. 62 AX-110 initial control surface dimensions based on initial geometry [67].	55
Fig. 63 AX-110 dimensions used for elevon sizing at takeoff [69].	55
Fig. 64 Sized elevons for CE of AX-110.	55
Fig. 65 Stacked turbines of AX-110 [69].	56
Fig. 66 AX-110 Vertical tail sizing results for inlet unstart and crosswind landing.	56
Fig. 67 Control surface dimensions based on AX-105 geometry given [67].	56
Fig. 68 Mach 5, Single flow path dimensions from CL [69].	57
Fig. 69 Mach 5 AX-105 vertical tail geometry [67,69].	57
Fig. 70 Hand-drawn control surface definitions given to Geometry.	58
Fig. 71 AX-105 dimensions needed for elevon sizing at takeoff rotation [69].	58
Fig. 72 Simplified moment diagram at takeoff rotation [69].	59
Fig. 73 AX-105 elevon sizing analysis at takeoff rotation – increased elevon size.	59
Fig. 74 AX-105 elevon sizing analysis at takeoff rotation – original CL elevon size.	59
Fig. 75 New elevon size needed for AX-105 to takeoff with given landing gear configuration [69].	60
Fig. 76 The C.G. movement with example SM bounds provided by Noah Blakely [12].	60
Fig. 77 AX-105 engines out during takeoff [69].	60
Fig. 78 AX-105 ramjet's inlet unstart at cruise [69].	61
Fig. 79 AX-105 during crosswind landing conditions [69].	61
Fig. 80 Rudder and Vertical tail geometry for AX-105 [69].	62
Fig. 81 Mach 7.5 AX-175 dimensions provided by Austin Prior [69].	62
Fig. 82 Control surface dimensions provided to Geometry based on AX-175 dimensions.	63
Fig. 83 AX-175 dimensions needed for elevon sizing at takeoff rotation [69].	63
Fig. 84 AX-175 elevon sizing analysis at takeoff rotation – increased elevon size.	64
Fig. 85 AX-175 elevon sizing analysis at takeoff rotation – original CL elevon size.	64
Fig. 86 CL and CE vertical tail sizes for AX-175 at takeoff and cruise.	65
Fig. 87 CL and CE vertical tail sizes for AX-175 at crosswind landing.	65
Fig. 88 AX-205 dimensions used from CAD models [69].	65
Fig. 89 Sized AX-205 elevons for takeoff rotation.	66
Fig. 90 Re-sized elevons for AX-205 after reducing elevon chord lengths.	66
Fig. 91 AX-205 Dimensions used for engines-out [69].	66
Fig. 92 Vertical tail sizing results for AX-205 at takeoff and cruise.	66
Fig. 93 Vertical tail sizing results for AX-205 at landing.	67
Fig. 94 AX-275 dimensions used from CAD models [69].	67
Fig. 95 Sized elevons for AX-275 at takeoff rotation.	68
Fig. 96 Resize needed for AX-275 wings to accommodate shorter elevon chord lengths.	68
Fig. 97 AX-275 Dimensions used for engines-out [69].	68
Fig. 98 Rudder sizing results for AX-275 at takeoff and cruise.	69
Fig. 99 Rudder sizing results for AX-275 at crosswind landing.	69
Fig. 100 Initial trim code results.	71
Fig. 101 Initial trim code results.	71
Fig. 102 Initial trim code results.	71
Fig. 103 Initial trim code results.	72
Fig. 104 Initial trim code results.	72
Fig. 105 Initial trim code results.	72
Fig. 106 Takeoff trim results for AX-105.	73

Fig. 107 Hypersonic cruise trim results for AX-105	74
Fig. 108 Stability results as a function of Mach number for AX-105.....	75
Fig. 109 Stability results as a function of Mach number for AX-175.....	75
Fig. 110 Stability results as a function of Mach number for AX-110.....	76
Fig. 111 Stability results as a function of Mach number for AX-205.....	77
Fig. 112 Stability results as a function of Mach number for AX-275.....	77
Fig. 113 Spectrum of aerodynamic issues to address [74].....	79
Fig. 114 Common types of delta wings [75]	80
Fig. 115 Lift formation due to free vortices on various aircraft bodies [25].....	81
Fig. 116 Chart for determining constant for non-linear lift coefficient [25].....	82
Fig. 117 Empirical charts to estimate maximum lift coefficient [30]	84
Fig. 118 Correlation for supersonic lift-curve-slope of delta wing-body configuration [13].	84
Fig. 119 Lift-to-drag relations for Mach numbers 2, 5 and 12 [39].....	86
Fig. 120 Concorde aerodynamic analysis geometric parameters [79]	87
Fig. 121 DATCOM Subsonic lift curve slope [29].....	90
Fig. 122 DATCOM empirical relations for subsonic, supersonic aerodynamic center calculation [29]	91
Fig. 123 Trendlines for subsonic DATCOM aerodynamic center empirical method.....	91
Fig. 124 Trendlines for subsonic DATCOM aerodynamic center empirical method.....	92
Fig. 125 Trendlines for supersonic DATCOM aerodynamic center empirical method.....	92
Fig. 126 Trendlines for supersonic DATCOM aerodynamic center empirical method.....	93
Fig. 127 Fig. 128 DATCOM empirical relations for supersonic normal force slope [29].....	93
Fig. 129 Trend fitted graphs from DATCOM supersonic plots.....	94
Fig. 130 Trend fitted graphs from DATCOM supersonic plots.....	94
Fig. 131 Trend fitted graphs from DATCOM supersonic plots.....	95
Fig. 132 Mission profile chosen for PS phase created by Noah Blakely [12]	95
Fig. 133 Subsonic lift-curve-slope of Nicolai's method.....	96
Fig. 134 XB-70 parasite drag test using Raymer's method.....	96
Fig. 135 Zero-lift drag coefficient verification of XB-70 [Raymer].....	97
Fig. 136 Comparison of DATCOM Neutral point method with SR-71 data [26].....	98
Fig. 137 DATCOM method extended to hypersonic speeds using SR-71 data [29]	98
Fig. 138 SR-71 method verification of DATCOM's neutral point method using regression.....	99
Fig. 139 Neutral point movement for single flow path vehicles.....	99
Fig. 140 Neutral point movement for dual flow path vehicles.	100
Fig. 141 Assumptions to calculate pitching moment as a function of angle of attack from DATCOM [29]	106
Fig. 142 Specific wing-body geometry for calculating 3D lift-curve slope of the wing [29]	106
Fig. 143 Wing geometry parameter definitions [29].....	107
Fig. 144 Method to find lift ratio for estimating pitching moments [29].....	107
Fig. 145 Wing geometries presented to estimate the lift-curve slope [29].	108
Fig. 146 Pitching moment as a function of angle of attack for subsonic speed.....	108
Fig. 147 Static margin change for subsonic speed.....	108
Fig. 148 Neutral point shift for subsonic speed.....	109
Fig. 149 NASA LASRE verification data for pitching moment derivative [21].	109



List of Tables

Table 1. Selected Aircraft Characteristics	14
Table 2. Literature Review for Stability and Control.	19
Table 3. Literature Review for Aerodynamics.	20
Table 4. Important longitudinal and lateral stability derivatives [34].....	26
Table 5. Similar aircraft control surface dimensions [24,49–51].....	27
Table 6. Sign requirements for main stability derivatives [25].....	35
Table 7. Stability and Control derivatives in Jan Roskam [20,38,63]	39
Table 8. Stability and Control Verification Literature.....	40
Table 9. Stability and Control Verification Road Map.....	40
Table 10. Results from Space Shuttle hypersonic elevon control derivative [68].	45
Table 11. Results from PS for Single Flow Path design points [11,12,69].....	46
Table 12. Results from PS for Dual Flow Path design points [11,12,69]	46
Table 13. Landing gear information provided by Structures team for single flow paths [70].	49
Table 14. List of Dimensions Used.	52
Table 15. Configuration Layout (CL) Results for S&C Control Surface Estimates.....	69
Table 16. Configuration Evaluation (CE) Results for S&C Control Surface Sizes.	70
Table 17. Stability Results Summary for Assessed Configurations.	78
Table 18. Concept vehicles aerodynamic estimates for PS phase.	80
Table 19. Aircraft with similar TOGW as our conceptual vehicles.....	82
Table 20. Data using Raymer's method for subsonic maximum lift coefficient [78].....	84
Table 21. The XB-70 data used for parasite drag verification [78].	97
Table 22. Verification data for neutral point methodology [49,78,84]......	97

Nomenclature

\bar{c}_{HT}	= horizontal tail volume coefficient	M	= Mach number
c_{VT}	= vertical tail volume coefficient	x_{cp}	= x-dist from nose to center of pressure
S_{HT}	= horizontal tail area	$C_{l\beta}$	= rolling moment efficient due to sideslip
S_{VT}	= vertical tail area	C_y	= sideforce coefficient
l_{HT}	= horizontal tail moment area from C.G.	C_l	= rolling moment coefficient
l_{VT}	= vertical tail moment area from C.G.	$C_{y\beta}$	= sideforce coefficient due to sideslip
b	= wingspan	C_{l_0}	= rolling moment bias (at zero α)
S_{ref}	= wing or reference area	C_{n_0}	= yawing moment bias (at zero α)
l_{ref}	= aircraft reference length (fuselage end)	g	= acceleration due to gravity, 9.81 m/s^2
S_e	= elevon area	ϕ	= roll angle
α_{TO}	= angle of attack at takeoff	θ	= pitch angle
δ_e	= elevon deflection angle	ψ	= yaw angle
$C_{L\alpha}$	= lift-curve-slope	L_A	= rolling moment about aircraft axis
C_{m_0}	= pitching moment bias (at zero α)	M_A	= pitching moment about aircraft axis
$C_{m\alpha}$	= pitching moment as function of α	N_A	= yawing moment about aircraft axis
C_L	= lift coefficient	L_T	= rolling moment about thrust line
$C_{m\delta e}$	= pitching moment due to elevon deflection	M_T	= yawing moment about thrust line
$C_{L\delta e}$	= lift coefficient due to elevon deflection	N_T	= pitching moment about thrust line
M_{cg}	= moment about center of gravity	X_A	= reaction force (drag) on aircraft axis
$I_{yy mg}$	= moment of inertia of main landing gear	Y_A	= reaction force (sideforce) on aircraft axis
$\ddot{\theta}$	= angular acceleration	Z_A	= reaction force (lift) on aircraft axis
M_W	= moment about wing	X_T	= reaction force (drag) on thrust line
M_D	= moment about drag force	Y_T	= reaction force (sideforce) on thrust line
M_T	= moment about thrust force from engine	Z_T	= reaction force (lift) on thrust line
M_{Lwf}	= moment about wing-fuselage lift		
$M_{ac wf}$	= moment about wing-fuselage a.c.	OEI	= one engine inoperative
M_{Lh}	= moment about horizontal tail lift vector	SM	= static margin
M_a	= moment about linear acceleration vector	LEX	= leading edge extensions
$X_{ac h}$	= x-dist from nose to horizontal tail a.c.	AR	= aspect ratio
X_{mg}	= x-dist from nose to main landing gear	TO	= takeoff
X_{cg}, x_{cg}	= x-dist from nose to center of gravity	$T&P$	= trajectory and performance
$X_{ac wf}$	= x-dist from nose to wing-fuselage a.c.	$T&P$	= trajectory and performance
Z_{cg}	= z-dist from bottom to C.G. centerline	$T&P$	= trajectory and performance
Z_T	= z-dist from bottom to thrust line	$HTHL$	= horizontal takeoff horizontal landing
Z_D	= z-dist from bottom to drag centerline	$VTHL$	= vertical takeoff horizontal landing
m	= aircraft mass	UAS	= unmanned aerial system
a	= linear acceleration	PAX	= number of passengers
T	= thrust force	IC	= industry capability
D	= drag force	$RBCC$	= rocket-based combined cycle
F_r	= friction force	$TBCC$	= turbine-based combined cycle
W	= aircraft weight	$SSTC$	= single stage to cruise
L_h	= lift force on horizontal tail	$SSTO$	= single stage to orbit
L_{wf}	= lift force on wing-fuselage	$TSTO$	= two stage to orbit
D_{trim}	= trim drag	AB	= all-body configuration
η_T	= tail efficiency	WB	= wing-body configuration
q_∞, \bar{q}	= dynamic pressure	BB	= blended-body configuration
C_{LT}	= lift coefficient on tail	SAS	= stability augmentation system
S_T	= tail area	ACS	= active control system
L_v	= lift coefficient on vertical tail		



y_T	= y-dist from fuselage centerline to engine	FCS	= flight control system
\bar{c}, c	= mean aerodynamic chord	HGV	= hypersonic glide vehicle
β	= sideslip angle	DOF	= degree of freedom
T_L	= thrust line	EOM	= equations of motion
$C_{n\delta r}$	= yawing moment due to rudder deflection	PS	= parametric sizing
$C_{n\delta e}$	= yawing moment due to elevon deflection	CL	= configuration layout
$C_{l\delta r}$	= rolling moment due to rudder deflection	CE	= configuration evaluation
$C_{l\delta e}$	= rolling moment due to elevon deflection	CD	= conceptual design
$C_{m\delta r}$	= pitching moment due to rudder deflection	PD	= preliminary design
δ_r	= rudder deflection angle	DD	= detailed design
$C_{n\beta}$	= yawing moment due to sideslip	$C.G.$	= center of gravity
C_n	= yawing moment coefficient	COP	= center of pressure
α	= angle of attack	$TOGW$	= takeoff gross weight
x_w	= w	OEW	= operating empty weight
C_{L_0}	= lift coefficient bias (at zero α)	OWE	= operating weight empty
$C_{l\alpha VT}$	= lift coefficient due to α on vertical tail	TPS	= thermal protection system
V_{TO}	= take-off velocity	$S&C$	= stability and control
\bar{X}_{np}	= neutral point from nose divided by \bar{c}	$W&B$	= weights and balance
\bar{X}_{cg}	= C.G. location from nose divided by \bar{c}	$T&P$	= trajectory and performance

	SENIOR DESIGN: MAE 4351 Project	Ref.: MAE 4351-001-2021 Date: 11. Aug. 2023 Name: Gayathri Kola Status: Complete
---	---	---

1 Introduction

Hypersonic vehicle concepts are frequently emerging in today's market. This quest for a high-speed transport vehicle whether it be supersonic or hypersonic is rampant among commercial companies all over the world. While these vehicles do achieve top speeds, their range is often compromised due to their high fuel consumption.

The goal of this project is to perform a feasibility study for a hypothetical hypersonic Spirit of St. Louis with a wing-body (WB) configuration. The other competing teams will be addressing an all-body (AB) and a blended-body (BB) configuration. For this reason, it is important to understand the background of the plane and the characteristics that made it possible to fly from New York to Paris, with a range of 4,100 miles, without any additional refueling back in 1927. Then, we will look into the progression of planes from the Spirit of St. Louis to hypersonic planes that are under development today.

1.1 Background on planes

1.1.1 Spirit of St. Louis [1].

The Spirit of St. Louis, designed in 1927 by Donald A. Hall was one of a kind back in its era [2]. Piloted by Charles Lindbergh on a single-fueled flight from New York to Paris over the North Atlantic Ocean, this plane stayed in flight for an incredible 33 hours. It flew at a very low speed of 133 nautical miles (Mach 0.173) with a radial piston engine named Wright J-5C. This was a propeller-driven airplane with two blades and a rectangular wing connected to the fuselage by trusses. It had its landing gear intact with an aft tail containing elevators, a single vertical tail, and a rudder. The horizontal stabilizer was supported by smaller trusses. This tail dragger was a lightweight structure with a gross weight of approximately 2,888 lb.



Fig. 1 The Spirit of St. Louis was built back in 1927 [1].

1.1.2 Gulfstream G700 [3]

The private jet Gulfstream G700 is a subsonic aircraft cruising at Mach 0.90 with a long range of 7,500 nautical miles. Its swept wing with winglets reduces aerodynamic drag thus improving its fuel efficiency and critical Mach number making flight close to sonic speed possible. Its slender fuselage is built to hold up to 13 passengers and sleeps 8 passengers. Its maximum cruise altitude is 51,000 ft. It has a T-tail configuration that helps avoid the downwash from the wing's plane. It has two Rolls-Royce Pearl 700 engines mounted at the aft section of the fuselage above the centerline. This has several benefits: reduces cabin noise, improves longitudinal stability at high speeds, the landing gear can be shorter, and if an engine fails, it wouldn't immediately harm the passengers.

ATLANTIX 	SENIOR DESIGN: MAE 4351 Project	Ref.: MAE 4351-001-2021 Date: 11. Aug. 2023 Name: Gayathri Kola Status: Complete
--	---	---



Fig. 2 The Gulfstream G700 was launched in 2020 [3].

1.1.3 SR-71 Blackbird

This legendary aircraft set the speed record in 1964 at Mach 3.2 with its maximum speed capability classified. To this day, many projects are trying to beat this record with a Horizontal-Takeoff-Horizontal-Landing (HTHL) vehicle. Designed by the infamous Skunk Works chief engineer Clarence (Kelly) Johnson, new design thinking and re-engineering manufacturing made this reconnaissance plane possible. Its lightweight titanium alloy structure allowed it to withstand an incredible amount of heat generated while cruising at Mach 3.0. Its engines had to be combined: turbojet and ramjet in order to takeoff at a conventional runway. Its engine featured a 3D circular inlet with spikes that controlled the location of the normal shock wave. The addition of chines did a lot: they added lift, contributed to directional stability, and helped with avoiding the radar. Its high service ceiling and long-range kept it mostly undetectable.



Fig. 3 The SR-71 Blackbird was built in 1964 [4].

1.1.4 Darkhorse [5,6]

Hermeus is an aerospace startup based in Atlanta, Georgia with a target to make reusable hypersonic transport aircraft. The Hermeus Darkhorse will be the second iteration of the hypersonic Unmanned-Aerial-System (UAS), after its test iteration named Quarterhorse. The Quarterhorse, which is currently in development with an expected launch in 2024, also features a remote piloting capability [5]. Its expected maximum speed is at Mach 4+ intending to break the speed 50-year-old speed record set by the SR-71. Its propulsion system features a single Turbojet/Ramjet engine combination named Chimera. This engine contains a repurposed J85 turbojet engine to allow for takeoff at

runways before switching to ramjet at Mach 3.0. The Chimera is housed in the fuselage of the Quarterhorse, and the design features a wing-body configuration with an aft-tail section, single vertical tail, and highly swept delta wing.

The Darkhorse has a few distinguishable features compared to Quarterhorse. There is no aft tail, instead, the fuselage is extended further to mount twin vertical tails canted outward. The wing features multiple sweeps, with a high sweep on the front fuselage section (somewhat like chines) with a reduced sweep at the rear. Looks like a normal delta wing in the back with elevons on either side of the fuselage. Its propulsion system utilizes a Turbofan/Ramjet configuration instead of the turbojet, increasing its speed to Mach 5.0.

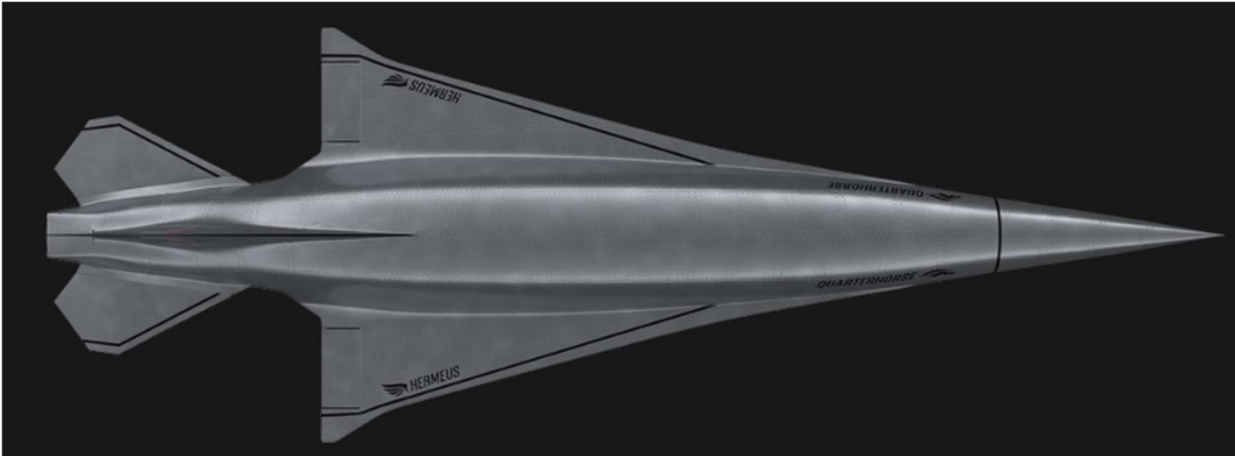


Fig. 4 Hermeus Quarterhorse, expected flight in 2024 [5].



Fig. 5 Hermeus Darkhorse, expected to launch in 2025 [7].

1.1.5 Halycon [8].

The last concept of Hermeus is the reusable hypersonic transport with a payload of 20 passengers and 2 crew as shown in Fig. 6. The unique design features a flat bottom and a slender bulged fuselage. It has a double delta wing with a high sweep in the forward fuselage section. Additionally, it also has drooped wing tips that add to directional stability and gives additional lift due to shock waves. It is to have two engines propelling to a speed of Mach 5.0, flying at an altitude of 90,000 ft. Its expected range is 4,600 miles, expected to make a flight from New York to Paris in 90 minutes. Its structure is made of titanium alloy with twin vertical tails similar to the Darkhorse. It is currently in development with an expected launch in 2029.



Fig. 6 Hermeus Halcyon with drooped wings is expected to launch in 2029 [9].

Table 1. Selected Aircraft Characteristics

Aircraft Name	Max Speed [mph]	Range [nmi]	Engine Type	Year	Crew, Passengers	Gross Weight [lb]
Spirit of St. Louis	133 (Mach 0.173)	3,600	Radial piston engine	1927	1, 0 PAX	2,888
Gulfstream	611 (Mach 0.925)	7,500	Pearl 700 Turbofan	2021	2, 13 PAX	56,365
SR-71 Blackbird	2,500 (Mach 3.00+)	2,824	J-58, TBCC	1964	1-2, 0 PAX	152,000
Darkhorse (UAS)	3,850 (Mach 5.000)	-	Turbofan-Ramjet	2025	0, 0 PAX	-
Halcyon	3,850 (Mach 5.000)	4,600	"Ramburner"	2029	2, 20 PAX	-

1.2 Project Overview

As mentioned earlier, the goal of this capstone project is to design a hypersonic aircraft that has the same range as the Spirit of St. Louis. Our team Atlantix is tasked with creating a wing-body hypersonic demonstrator that is of Industry Capability (IC). The aim is to create a solution space topology using a convergence methodology that screens all possible designs and produces a feasible baseline configuration. This solution space topology must also include the aircraft Gulfstream G700, Hermeus Darkhorse, and Halcyon. Finally, an overall market assessment of these vehicle designs must be conducted in terms of cost and technology available [10]. A mission profile must be made in agreement with the other two competing teams. The project's progress will be documented with weekly reports and presentations.

1.2.1 Mission Details [10]

The following are the mission details:

- The flight path must be similar to that of the Spirit of St. Louis.
- Has two main crew members: the pilot and the co-pilot. No additional crew members.
- Payload: 20 military personnel.
- Required solution spaces must be screened for designated trades. These are Mach numbers 5, 7.5, and 10.
- No rocket acceleration. That means the vehicle cannot be powered by either a rocket engine or Rocket-Based-Combined-Cycle (RBCC) engine.

1.2.2 Vehicle Details [10]

The following are the vehicle details:

- The engine must be of Turbine-Based-Combined-Cycle (TBCC). There are two vehicle designs: one with a single engine and the other with a twin engine. Both vehicles must have a 3D engine intake.
- Horizontal-Takeoff-Horizontal-Landing (HTHL) capability with Single-Stage-To-Cruise (SSTC).
- Fuel must be any form of Kerosene.
- Wing-body configuration for Atlantix.

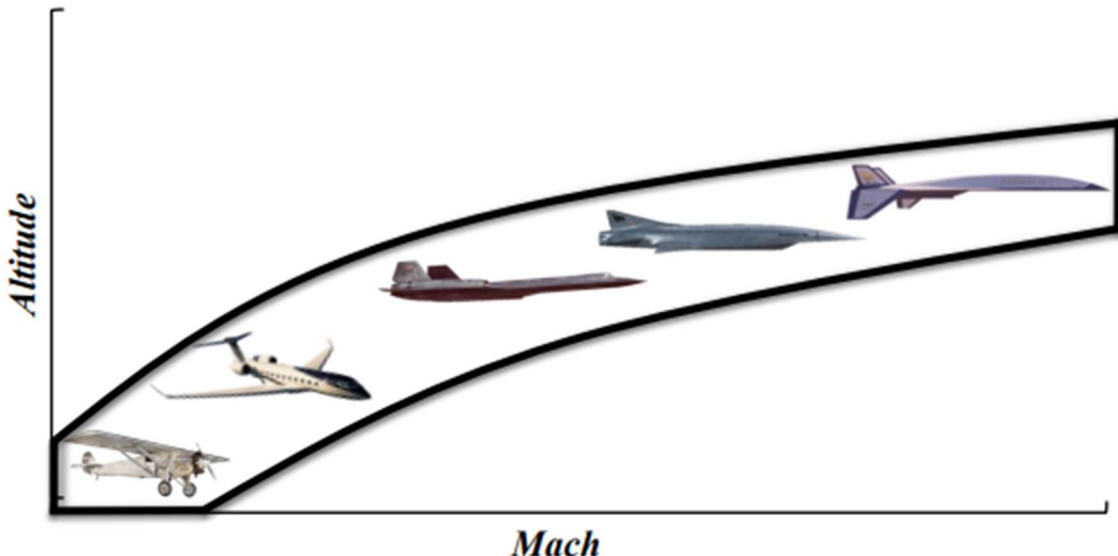


Fig. 7 Hypersonic Spirit of St. Louis progression [10].

1.3 Team Structure and Breakdown

The team name “Atlantix” was inspired by the transatlantic route the designed vehicle will take from New York to Paris over the North Atlantic Ocean. The following team logo was created by the Chief Engineer, Wesley Junell.



Fig. 8 Atlantix logo created by Wesley Junell [11].

The following in Fig. 9 below is the team structure and discipline breakdown created by team member Noah Blakely. There are 9 disciplines in total with some disciplines that have additional sub-disciplines such as Structures & Materials and Geometry & Weights. The focus of this report will be on Stability and Control, and Aerodynamics. The author is the Stability and Control team lead; hence it will be the primary discipline and Aerodynamics is the secondary discipline.

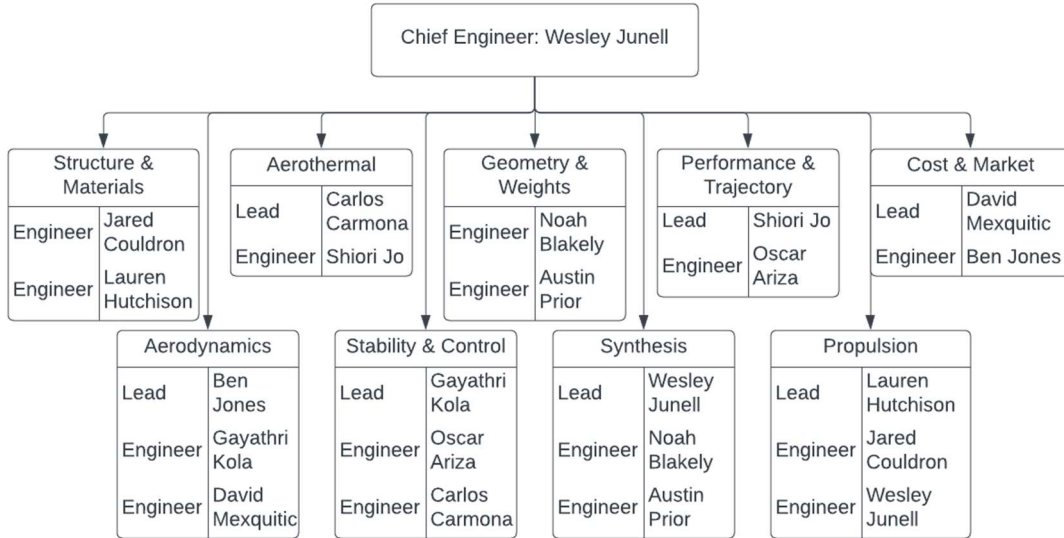


Fig. 9 Atlantix team structure by Noah Blakely [12].

2 Literature Review

Before designing any new aircraft, it is essential to first perform an extensive literature review in order to find any similar aircraft configurations that can aid with the design process and validation. In this section, we will first have a brief review of Hypersonics, followed by past hypersonic aircraft programs, particularly the U.S. Air Force X planes.

2.1 Hypersonic Review

The following in Fig. 10 gives the distinction between Wing-Body (WB), Blended-Body (BB), and All-Body (AB). As illustrated, the WB configuration is less integrated with a set of distinct wings, engines, and fuselage. We will review the characteristics of an AB configuration aircraft – X-43A Hyper X, along with a WB configuration vehicle namely the Space Shuttle Orbiter. The weight of the Orbiter alone is significantly less compared to our concept aircraft, hence, other supersonic WB aircraft within similar weight categories will also be discussed.

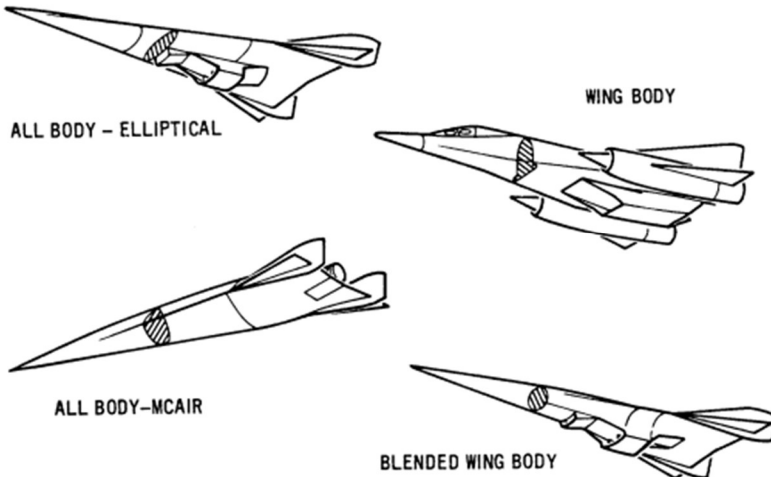


Fig. 10 Different aircraft configurations for hypersonic vehicle concepts [13]

2.1.1 X-15

The X-15 was an experimental plane built in the 90's. It was a rocket-powered aircraft that was dropped from a mothership – NB-52. This aircraft had a tiny, tapered wing attached to the top of its cylindrical fuselage. Additionally, it featured ventral and dorsal vertical tail fins, to improve its directional stability. This hypersonic research aircraft set the record on 3 October 1967 for a top speed of Mach 6.7 at an altitude of 102,100 feet, piloted by William J. Knight. There were a total of three X-15s built. The interesting aspect of the X-15 is the large wedge tails. These were meant to improve directional stability at hypersonic speeds, however, they also created enormous amounts of base drag. This research aircraft has been published [14].



Fig. 11 The North American X-15 [15].

2.1.2 X-43A Hyper-X

The X-43-A was another experimental hypersonic unmanned aerial vehicle (UAV) that was built by Microcraft. A total number of three X-43s were built of which two had a successful flight. They were propelled by the Pratt & Whitney SJ-Y61, a scramjet engine. Both successful flights flew to Mach 9.74 and Mach 9.689, using the air-breathing propulsion system. This proved scramjet engines can operate. However, their operation range is very high, from 100,000 ft onwards. Unfortunately, the project ended due to funding depletion. The X-43-A was also dropped from a mothership, B-52 at an altitude of 20,000 ft. The mission trajectory for the X-43A is given below in Fig. 12. It was boosted by a Pegasus rocket to an altitude of 100,000 ft after which the scramjet fired for about 15 seconds, then it descended by gliding back to land. For context, our aim for this project is to develop a Horizontal-Takeoff-Horizontal-Landing (HTHL) hypersonic aircraft. At the time of this writing, there is no public HTHL hypersonic aircraft known.

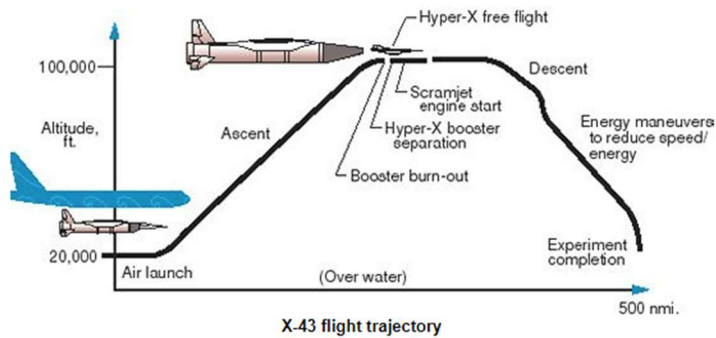


Fig. 12 X-43A mission trajectory [16]

2.1.3 Space Shuttle Orbiter

The Space Shuttle Orbiter is a Vertical-Takeoff-Horizontal-Landing (VTHL) aircraft that was boosted out of the Earth's atmosphere using two solid rocket boosters. The main reason for mentioning this aircraft in this report is due to its WB configuration. When viewed from the front, it has a distinct wing and a distinct fuselage, with very little blending at the intersection of the two. It features a low sweep angle, a large delta wing that during the descent into the atmosphere is meant to block heat during maximum dynamic pressure while re-entry. The re-entry speeds are up to Mach 25 [17]. Large aspect ratio vehicles are rare in hypersonic design because the drag is very high at hypersonic speeds.

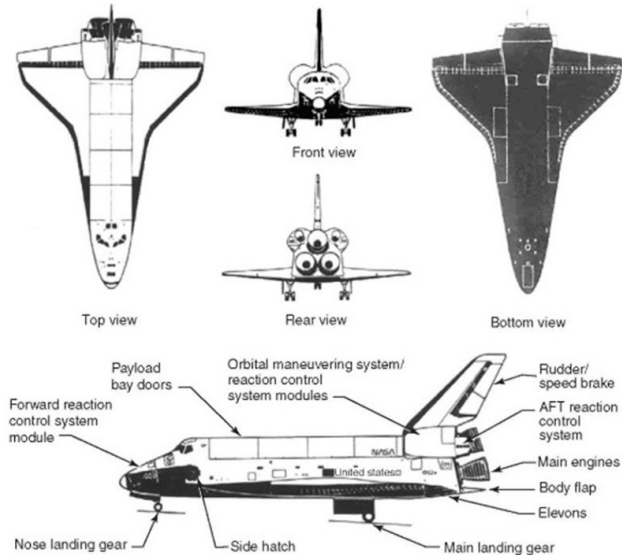


Fig. 13 Space Shuttle Orbiter with a wing-body configuration [17]

2.1.4 Wing-body Supersonic Transport

Apart from the Space Shuttle Orbiter, WB aircraft transport aircraft can be found in the supersonic regime. The most successful supersonic passenger aircraft was the Concorde. Its competitor, the Tupolev TU-144 features a similar design, except it has distinct double-delta wings and the Concorde has ogive wings. Both serve to improve subsonic flight efficiency. Their supersonic speeds were up to Mach 2.0, however, the TU-144 initially had older, inefficient engines that reduced its performance. The TU-144 also featured retractable canards to lower the angle of attack at landing. The lessons from these planes give ideas on features that could be incorporated to improve our conceptual hypersonic aircraft's feasibility.



Fig. 14 Concorde and Tupolev Tu-144 [18].

2.2 Stability and Control Resource List

As mentioned in the mission details section, it is important to first build a Data-Base (DB) to begin the literature review process. To start, that means collecting all the relevant books, articles, journals, and conference papers for a particular aircraft, configuration, or component. Here, an initial search is performed for each discipline.

Table 2. Literature Review for Stability and Control.

Serial No.	Title	Author	Year	Category
1	Stability & Control of Conventional & Unconventional Aerospace Vehicle Configurations [19]	Chudoba, B.	2019	Book
2	Airplane Design Part VII: Determination of Stability, Control, and Performance Characteristics [20]	Roskam, J.	2017	Book
3	Stability and Control Estimation Flight Test Results for the SR-71 Aircraft with Externally Mounted Experiments [21]	Moes, T. R.	2002	Book
4	Flight Stability and Control and Performance Results from the Linear Aerospike SR-71 Experiment (LASRE) [22]	Moes, T. Et al.	1998	Conference Paper
5	Longitudinal Handling Qualities of the Tu-144LL Airplane and Comparisons with Other Large, Supersonic Aircraft [23]	Cox, T. H Marshall, A.	2000	Journal Article
6	Development of the Vehicle Configuration Compendium: A Comprehensive Data-Information-Knowledge System to Aid in High-Speed Vehicle Design [24]	Simon, S.	2021	Master's Thesis
7	Fundamentals of Aircraft and Airship Design. Volume I – Aircraft Design [25]	Nicolai, L. M. Carichner, G.	2010	Book
8	Aircraft Performance and Design [26]	Anderson, J.D	1999	Book
9	Introduction to Aircraft Flight Mechanics, Performance, Static Stability, Dynamic Stability, and Classical Feedback Control [27]	Yechout, T. R. Et al.	2003	Book
10	Aircraft Design: A Systems Engineering Approach [28]	Sadruey, M.	2013	Book
11	USAF Stability and Control DATCOM [29]	Hoak, D. E.	1978	Data
12	Aircraft Design: A Conceptual Approach [30]	Finck, R. D	2018	Sheets
13	Airplane Flight Dynamics and Automatic Flight Controls [31]	Raymer, D.	2018	Book
14	Mechanics of Flight [32]	Roskam, J.	1998	Book
15	On Stability and Control of Hypersonic Vehicles [33]	Philips, W. F	2004	Book
16	A Generic Stability and Control Tool for Conceptual Design Prototype System Overview [34]	Coleman, C. C Faruqi, F. A	2009	Review Paper
17	A Generic Stability and Control Tool for Flight Vehicle Conceptual Design: AeroMech Software Development [35].	Coleman, G. Chudoba, B. Coleman, G.	2007	Conference Paper
				Master's thesis

2.2.1 USAF Stability and Control DATCOM [29].

This document is a database containing equations for stability and control derivatives at various speed regimes ranging from subsonic to hypersonic. However, upon further review, it appears that coverage for hypersonic equations is fairly limited, only two derivatives were found to have equations solely for hypersonic speeds. Further, these equations are for wing and tail-body configurations only. A software version of this database is available online which requires knowledge of the programming language: FORTRAN. The author is currently looking into the way this resource can be used.

2.2.2 On Stability and Control of Hypersonic Vehicles [33].

This paper explains the most common issues associated with the stability and control of hypersonic vehicles and emphasizes the need for an Active-Control-System (ACS) or Stability-Augmentation-System (SAS). One caveat is that this paper primarily discusses hypersonic missiles and Hypersonic Glide Vehicle (HGV). It gives basic information on the range for L/D for supersonic and hypersonic vehicles and also explains how lift and drag coefficients remain constant for speeds over Mach 6.

2.2.3 A Generic Stability & Control Tool for Conceptual Design Prototype System Overview [35].

The author of this thesis acknowledges the fact that stability and control analysis for novel designs is difficult, especially with limited data, and also time-consuming. A generic solution for stability and control analysis is presented called *AeroMech* and the software development and integration process are described. Techniques for analyzing control power for control surface sizing, static and dynamic stability derivatives, and 6-degree-of-freedom (DOF) trimmed equations-of-motion (EOM) are presented. Various tailplane configurations are presented, and critical flight

conditions are discussed. Finally, the Appendix B of this thesis contains a user guide to Digital DATCOM that is simpler to read and follow.

2.2.4 Jan Roskam's Design Books [20,31,36]

The author discovered simpler methodology that could be implemented within time in Jan Roskam's design books for S&C. The Part VI for the series gives extensive methods for calculating several types of steady state, stability, and control derivatives. This resource is being used currently to develop the S&C code for Configuration Evaluation (CE). If some of the methods are not applicable for supersonic and hypersonic flight, then DATCOM will be used to sort for the derivatives. The Part VII of the series gives flight conditions to address and methods for computation.

2.2.5 Aircraft Design: A Systems Engineering Approach [28]

This text was excellent for providing generic methodology for sizing control surface effectors chosen. It provides methods, illustrations for takeoff rotation to size pitch control effectors, engine out scenarios and crosswind landings for vertical tail and rudder sizing. Some of the examples in the next were used to build the sizing code and test if the results match the text examples.

Table 3. Literature Review for Aerodynamics.

Serial No.	Title	Author	Year	Category
1	Fundamentals of Aerodynamics [37]	Anderson, J. D	2017	Book
2	Airplane Design Part VI: Preliminary Calculation of Aerodynamic, Thrust, and Power Characteristics, Vol 1 [38]	Roskam, J.	1987	Book
3	Aircraft Conceptual Design: An Adaptable Parametric Sizing Methodology [39]	Coleman, G.	2010	Thesis
4	Transatlantic Launcher Sizing (Chapter 16): Scramjet Propulsion [40]	Czysz, P. Jean, V.	2000	Book
5	Future Spacecraft Propulsion Systems and Integration: Enabling Technologies for Space Exploration [41]	Czysz, P. Et al.	2018	Book
6	Development of the Vehicle Configuration Compendium: A Comprehensive Data-Information-Knowledge System to Aid in High-Speed Vehicle Design [24]	Simon, S.	2021	Master's Thesis
7	Fundamentals of Aircraft and Airship Design. Volume I – Aircraft Design [25]	Nicolai, L. M. Carichner, G.	2010	Book
8	Hypersonic Convergence: Background and Methodology [42]	Ledford, T. Harris, C.	2023	Guest Lecture
9	Solution-Space Screening of a Hypersonic Endurance Demonstrator [43]	Chudoba, B. Et al	2012	Journal Article
10	Computational Methods in Hypersonic Aerodynamics [44]	Murthy, T.K.S	1991	Book
11	Aerodynamic Problems of Hypersonic Vehicles (AGARD) [45]	Enkenhus, K. Et al.	1972	Lecture Series
12	Hypersonic Flow [46]	Rasmussen, M.	1994	Book
13	Hypersonic and High-Temperature Gas Dynamics [47].	Anderson, J.	2006	Book

2.2.6 Fundamentals of Aerodynamics by John D. Anderson [37].

Chapter 14 of this text covers the basics of hypersonic aerodynamics. This resource can be especially useful to develop a background in this field before attempting to find a suitable methodology. The key takeaway from this chapter was understanding that the word hypersonic does not necessarily relate to Mach 5.0. There is nothing special about this number. The drag does not dramatically increase at Mach 5 when compared to the exponential rise at Mach 1.0. Many other factors go into characterizing hypersonic flow.

2.2.7 Development of the Vehicle Configuration Compendium, Simon. S [24]

This thesis is an excellent resource for getting started with the parameters required, and understanding the roles of a discipline in PS, CL, and CE. It is easy to get lost in a literature search when trying to design a novel airplane concept such as hypersonic transport. This thesis gives classifications for wing-body (WB), all-body (AB), and blended-body (BB) configurations. There are many hypersonic aircraft from the past that help identify the body configuration such as Sanger II, X-43A, and SR-71. A compilation of comparisons between such aircraft is made as an example for the development of their Vehicle Configuration Compendium (VCC) software. For the Aerodynamics team, this is a great starting point for the parameters of interest and how they are required by other disciplines.

	SENIOR DESIGN: MAE 4351 Project	Ref.: MAE 4351-001-2021 Date: 11. Aug. 2023 Name: Gayathri Kola Status: Complete
---	--	---

2.2.8 Future Spacecraft Propulsion Systems and Integration [41]

In the PS phase, the Synthesis team has opted to use Hypersonic Convergence as their methodology. This book, along with Scramjet Propulsion by Czysz, P and Jean, V gives a lot of information on the equations needed for the convergence logic. For the Aerodynamics team, it gives a way to estimate an initial maximum lift-to-drag (L/D) based on the Mach number and the zero lift-drag coefficient. It becomes very useful for hypersonic vehicles where information is scarce very early in the design process.

2.2.9 Hypersonic Research Facilities Study Phase 2 Parametric Studies

This resource along with Gary Coleman's thesis on parametric methodology are considered for the estimation of aerodynamic coefficients. Specifically, there are methods for estimating the lift-to-drag ratio, lift estimation method, and lift-curve-slope empirical relations for delta WB combinations. Additionally, a drag estimation method is presented for high Mach number vehicle concepts.

2.2.10 Raymer and USAF Stability and Control DATCOM [29,30]

Raymer was initially used as the neutral point methodology. However, this proved to be difficult as the terms in the equations were not clearly defined by the text. Additionally, the method was more applicable to the transonic commercial wing-body aircraft than aircraft with delta and double delta planforms. Instead, the USAF DATCOM was used to approximate neutral point locations for delta wings using empirical charts. These charts were converted to equations by trend-fitting them to the highest order.

3 Conceptual Design Breakdown

The aircraft design pyramid starts with Conceptual Design (CD) at the top, followed by Preliminary Design (PD) and Detailed Design (DD). Since this project will be taking a multi-disciplinary approach to designing the hypersonic aircraft, it becomes essential to lay down the groundwork for the chosen convergence methodology.

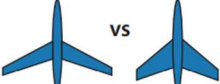
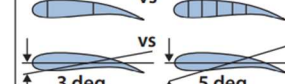
Phase 1 Conceptual Design		Phase 2 Preliminary Design	Phase 3 Detail Design
	vs		
Known	Basic Mission Requirements Range, Altitude, & Speed Basic Material Properties σ/p E/p $$/lb$	Aeroelastic Requirements Fatigue Requirements Flutter Requirements Overall Strength Requirements	Local Strength Requirements Producibility Functional Requirements
Results	Geometry Airfoil Type R t/c λ Δ	Design Objectives Drag Level Weight Goals Cost Goals	Basic Internal Arrangement Complete External Configuration <i>Camber & Twist Distribution</i> <i>Local Flow Problems Solved</i> Major Loads, Stresses, Deflections
Output	Feasible Design	Mature Design	Shop Designs
TRL	2 – 3	4 – 5	6 – 7

Fig. 15 Aircraft design phases [25].

3.1 Parametric Sizing

In order to design an aircraft, we must first know the size of what is trying to be built. If the aircraft will be a fighter jet or a passenger transport. In the Parametric Sizing (PS) process, the aircraft is grossly sized using a method to converge to a solution. A solution space is created giving a visualization for the list of feasible designs. These feasible designs will be given to all disciplines. The Synthesis team has chosen to use Hypersonic Convergence as their sizing method.

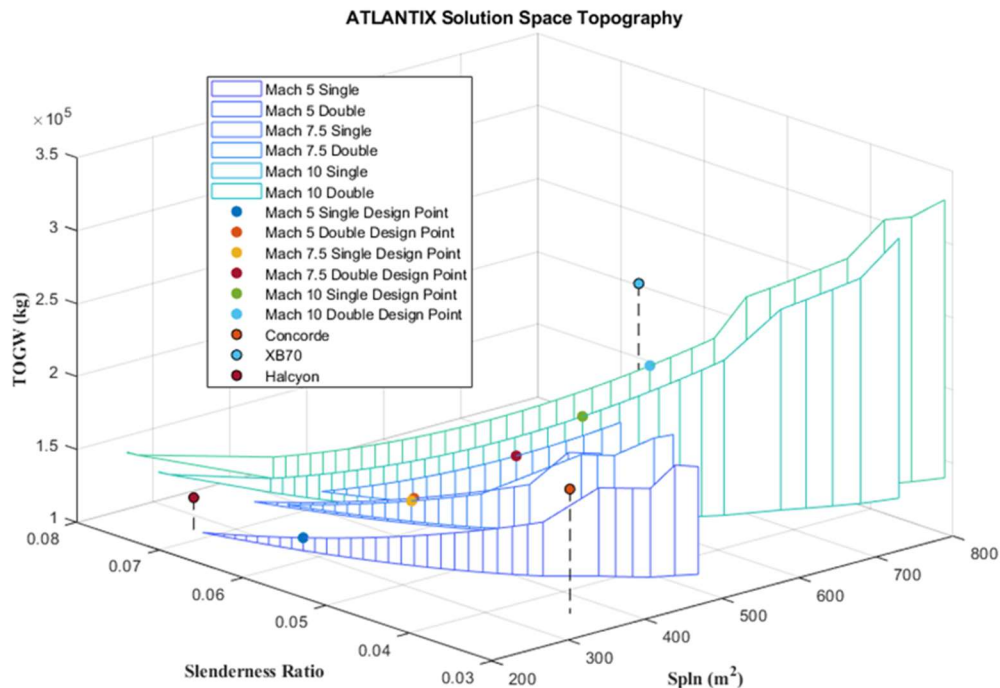


Fig. 16 Atlantix vehicle design points [11].

3.1.1 Hypersonic Convergence

Traditional convergence methods require defining many constraints to come up with a solution space. One such method is Loftin Sizing, where constraints such as stall speed, takeoff, and landing field length, and climb gradients are made. To size the aircraft, usually, first, the wing and engines are sized, and the empennage is added in the end. However, to design high-speed hypersonic aircraft, the sizing for wings, engines, and control efforts must be fully integrated to ensure optimal performance. For that reason, transitional methods become redundant as convergence becomes difficult. Hypersonic Convergence is a method that streamlines this process by fully integrating multiple design aspects into two main convergence equations. Before utilizing these equations (Fig.), the gross vehicle geometry must be known. Two new variables are introduced: slenderness ratio τ and area ratio k_w . These parameters relate to the volume, planform area, and wetted area of the vehicle. The convergence process is iterated for a range of slenderness ratios to obtain an estimate of the Takeoff-Gross-Weight (TOGW), and the ratio of volume available to volume from variables OEW (Operating-Empty-Weight) and OWE (Operating-Weight-Empty). After the iteration process, and landing constraint is given, and a solution space is generated. For this, the Synthesis team will be creating a solution space code to output baseline design parameters such as TOGW, planform area, wing area, slenderness ratio, weight (OEW), and volume (OWE) budgets [42].

With these parameters, the disciplines can start to define the approximate wing area, engine size, horizontal and vertical tail areas, aspect ratios, components weights, overall aircraft weight, C.G. location, internal aircraft structure and loads, Thermal-Protection-System (TPS) weights, and approximate cost of the aircraft.

Several of the constants given in the equations in Fig. are estimated based on the type of aircraft being built, whether it is a Single-Stage-To-Orbit (SSTO) or Two-Stage-To-Orbit (TSTO).

	SENIOR DESIGN: MAE 4351 Project	Ref.: MAE 4351-001-2021 Date: 11. Aug. 2023 Name: Gayathri Kola Status: Complete
---	--	---

Weight budget

$$W_{OEW} = \frac{I_{str} K_w S_{pln} + C_{sys} + \frac{(T/W)_{Max} W_R (W_{pay} + W_{crew}) + W_{cprv}}{E_{TW}}}{1 + \mu_a - f_{sys} + \frac{(T/W)_{Max} W_R}{E_{TW}}}$$

Structure Geometry Systems Propulsion Mission Requirements

Volume budget

$$W_{OWE} = \frac{\tau S_{pln}^{1.5} (1 - k_{vv} - k_{vs}) - v_{fix} - N_{crw}(v_{crw} - k_{crw}) - W_{pay}/\rho_{pay}}{\frac{W_R - 1}{\rho_{ppl}} + (k_{ve} (T/W)_{Max} W_R)}$$

Where:

$$W_{OWE} = W_{OEW} + W_{pay} + W_{crew}$$

Fig. 17 Weight and volume budgets for convergence [42].

Responsibilities of the Aerodynamics team in PS:

- Calculating L/D and giving it to the Performance/Propulsion team so they can calculate thrust requirements that will go into the Synthesis convergence logic. Additionally, to compute the lift and drag coefficients.

Responsibilities of the Stability/Control team in PS:

- Stability/Control is not involved in PS because this stage involves grossly sizing a vehicle, most variables (from Geometry, Weights, Thrust) are unknown to perform stability analysis.

3.2 Configuration Layout

Once a list of feasible designs is obtained from the PS phase, along with values for weight and volume to be allocated, the designs can be made in the CL phase. Here, the creativity of the multi-disciplinary design process comes into play. Each discipline will give its input on how best the geometry can be made based on mission criteria. For example, the Aerodynamics team may suggest having delta wings or modified versions of highly swept wings when laying a hypersonic aircraft. Then, the Propulsion team may suggest optimal engine placements and if the fuselage length needs to be extended based on the engine dimensions available. The Stability and Control team may input how many control effectors are needed based on historical data. A few designs are made with tweaks in geometries and placement of essential features. These designs are then evaluated in the final CE phase.

Responsibilities of the Aerodynamics team in CL:

- Coming up with a wing design: defining leading-edge sweep angles, shock angles, and fuselage length.
- Maximum lift coefficient, $c_{l_{max}}$
- Estimating the wing area, canard area, horizontal tailplane area, and fuselage area ruling.
- Center of pressure location (or neutral point) in percent chord.
- Aerodynamic center in percent chord.

Stability and Control (CL)
Objective:
<ul style="list-style-type: none"> • Determine the most control surface types • Decided on control surface configuration: TAC, FWC, FCC • Utilize Volume Coefficient approach to estimate size • Determine optimal geometry & number of control surfaces
Inputs:
<ul style="list-style-type: none"> • Wing area, wingspan, moment arms, elevon area, vertical tail area, rudder area of similar aircraft
Analysis:
<ul style="list-style-type: none"> • Volume Coefficient approach
Output:
<ul style="list-style-type: none"> • Approximate elevon area • Approximate vertical tail area • Approximate elevon and vertical tail geometry

Fig. 18 Stability and Control IDA for CL.

	SENIOR DESIGN: MAE 4351 Project	Ref.: MAE 4351-001-2021 Date: 11. Aug. 2023 Name: Gayathri Kola Status: Complete
---	--	---

The following in Fig. 18 is the Stability and Control IDA for CL. Responsibilities of the Stability/Control team in CL:

- Choosing control surfaces: number, layout, and placement.
- Common method using the Volume coefficient approach: looking through historical aircraft and making comparisons to gauge an approximate size of control effectors – output areas to Geometry & Synthesis.
- Computing maximum control surface deflection ranges.

3.3 Configuration Evaluation

The outputs from the CL phase are a list of feasible designs available. These designs will be evaluated for the entire mission profile during the CE phase. Many teams will be interacting with one another to meet different aspects of their discipline requirements. For example, the Stability and Control team must interact with the Propulsion team for thrust data and the WB team for C.G. location and placement to ensure adequate stability for the takeoff phase. Usually, the control surfaces will be sized based on the inputs provided by these teams for asymmetric thrust conditions, etc. Higher fidelity methods are typically used in CE to complete this analysis with the best accuracy. Finally, the Synthesis team will decide which discipline is important at a particular flight phase while meeting all basic discipline requirements.

Stability and Control (CE)	
Takeoff	Climb
Objective: <ul style="list-style-type: none"> • Critical conditions: OEI, Trim Drag, Takeoff Rotation • Interact with Propulsion, W&B, Geometry, Aerodynamics, Sythesis to size control surfaces • Determine maximum elevon and rudder deflections • Assess static stability Inputs: <ul style="list-style-type: none"> Propulsion: Thrust, Engine drag W&B: C.G location Aerodynamics: neutral point or aerodynamic center Geometry & Synthesis: TOGW, planform area, aircraft dimensions Analysis: <ul style="list-style-type: none"> • Longitudinal: Nicolai, Raymer • Lateral: Nicolai • Directional: Nicolai Output: <ul style="list-style-type: none"> • Maximum elevon and rudder deflection angles • Stability derivatives once stability is achieved 	Objective: <ul style="list-style-type: none"> • Critical conditions: Trim Drag • Interact with Synthesis, Geometry, Aerodynamics, W&B to ensure less trim drag • Determine elevon and rudder deflections to trim • Assess static stability Inputs: <ul style="list-style-type: none"> Aerodynamics: neutral point or aerodynamic center W&B: C.G location Geometry: aircraft dimensions Analysis: <ul style="list-style-type: none"> • Longitudinal: Nicolai, Raymer • Lateral: Nicolai • Directional: Nicolai Output: <ul style="list-style-type: none"> • Maximum elevon and rudder deflection angles • Stability derivatives once stability is achieved
Cruise	Landing
Objective: <ul style="list-style-type: none"> • Critical conditions: Trim Drag, One-Engine-Inoperative (OEI) • Interact with Propulsion, Synthesis, Geometry, Aerodynamics, W&B to check for adequate control authority • Determine maximum elevon and rudder deflections • Assess static stability Inputs: <ul style="list-style-type: none"> Propulsion: Thrust, Engine drag W&B: C.G location Aerodynamics: neutral point or aerodynamic center Geometry & Synthesis: TOGW, planform area, aircraft dimensions Analysis: <ul style="list-style-type: none"> • Longitudinal: Nicolai, Raymer • Lateral: Nicolai • Directional: Nicolai Output: <ul style="list-style-type: none"> • Maximum elevon and rudder deflection angles • Stability derivatives once stability is achieved 	Objective: <ul style="list-style-type: none"> • Critical conditions: Trim Drag, Crosswind landing • Interact with Propulsion, Synthesis, Geometry, Aerodynamics, W&B to check for adequate control authority • Determine elevon and rudder deflections to trim • Assess static stability Inputs: <ul style="list-style-type: none"> Aerodynamics: neutral point or aerodynamic center W&B: C.G location Geometry: aircraft dimensions Analysis: <ul style="list-style-type: none"> • Longitudinal: Nicolai, Raymer • Lateral: Nicolai • Directional: Nicolai Output: <ul style="list-style-type: none"> • Maximum elevon and rudder deflection angles • Stability derivatives once stability is achieved

Fig. 19 Stability and Control CE IDA.

Responsibilities of the Stability/Control team in CE:

- Assess the stability of the aircraft throughout the mission profile for all flight phases.

- Consider speed regimes to calculate longitudinal, lateral, and directional stability derivatives.
- Consider critical conditions as per MIL-SPEC requirements to size control surfaces.

The following in Fig. 19 is the CE IDA for Stability and Control discipline. Additional details will be added once method verification has been completed. The IDA template is credited to David Mexquitic [48].

Responsibilities of the Aerodynamics team in CE:

- Computing the total lift and drag forces, lift and drag coefficients, and induced drag coefficient.
- Lift-curve slopes, zero-lift drag coefficient.
- Determination of the aircraft neutral point.

4 Stability and Control

4.1 Background

Before beginning with any methodology, it is important to give some background on stability and control, and its role in aircraft design. The stability of an aircraft can be broken down into four main speed regimes, namely subsonic, transonic, supersonic, and hypersonic. It also depends on the kind of body configuration we are looking at; whether it is a wing-body, all-body, or a blended body. Most information is available for calculating the stability derivatives of the subsonic regime. Additionally, aircraft stability can be split into two main categories: static stability and dynamic stability.

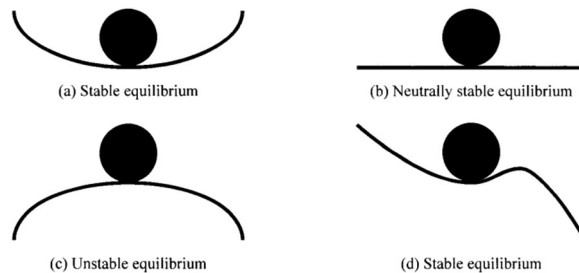


Fig. 20 Stable, unstable, and neutral equilibrium [32].

Static stability relates to when an aircraft inherently returns to its equilibrium position when disturbed by external forces due to its weight distribution. When an aircraft continues to deviate from equilibrium, meaning it is unstable in straight-line flight, it is known to have static instability. Most transport aircraft are designed to have static stability and these requirements are given in documents such as FAR 23, FAR 25, and MIL-SPEC-1797.

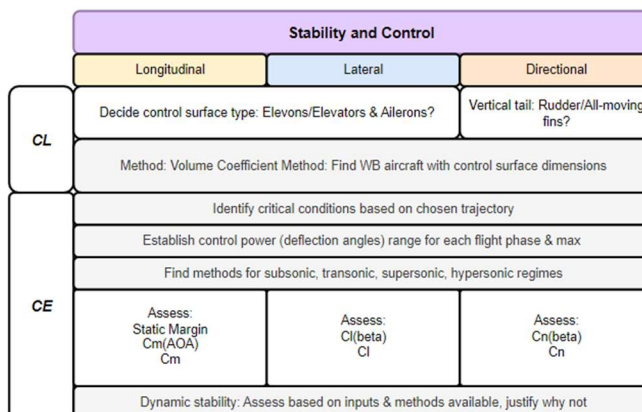


Fig. 21 Stability and Control overview.

During conceptual design phase, static stability will be of primary consideration. Dynamic stability analysis requires more detailed data and accuracy is limited this early in design phase.

After looking at the basics of Stability and Control, it is essential to look into the various kinds of tail configuration options available to the designer. The following Fig. shows the various types of tail configurations in general.

TAC	Tail-Aft Configuration	symmetric
TFC	Tail-First Configuration	symmetric
TSC	Three-Surface Configuration	symmetric
FWC	Flying-Wing Configuration	symmetric
OWC	Oblique-Wing Configuration	asymmetric
OWFC	Oblique Flying-Wing Configuration	asymmetric



Tail-Aft Configuration



Tail-First Configuration



Three-Surface Configuration



Flying-Wing Configuration



Oblique-Wing Configuration



Oblique Flying-Wing Configuration

Fig. 22 Types of tail configurations available to the designer [34].

The most common stability derivatives are given below in table:

Table 4. Important longitudinal and lateral stability derivatives [34].

Symbol	Parameter Name	Category
$C_{L\alpha}$	Variation of lift coefficient with angle of attack	Longitudinal
$C_{D\alpha}$	Variation of drag coefficient with angle of attack	Longitudinal
$C_{m\alpha}$	Variation of pitching moment coefficient with angle of attack	Longitudinal
C_{Lq}	Variation of lift coefficient with pitch rate	Longitudinal
C_{mq}	Variation of pitching moment coefficient with pitch rate	Longitudinal
$C_{Y\beta}$	Variation of sideforce coefficient with angle of sideslip	Directional
$C_{l\beta}$	Variation of rolling moment coefficient with angle of sideslip	Lateral
$C_{n\beta}$	Variation of yawing moment coefficient with angle of sideslip	Directional
C_{Yp}	Variation of sideforce coefficient with roll rate	Lateral
C_{lp}	Variation of rolling moment coefficient with roll rate	Lateral
C_{np}	Variation of yawing moment coefficient with roll rate	Lateral
C_{Yr}	Variation of sideforce coefficient with yaw rate	Directional
C_{lr}	Variation of rolling moment coefficient with yaw rate	Directional
C_{nr}	Variation of yawing moment coefficient with yaw rate	Directional

4.2 Volume Coefficient Approach

One of the most common methods used to estimate the size of control surfaces is by a method known as the volume coefficient method. In this method, similar aircraft are chosen where control surface dimensions are available. It gives a means of comparison to get a base estimate when the C.G. location of the aircraft is unknown in CL phase. The following is the way to calculate volume coefficient below [28].

$$\bar{c}_{HT} = \frac{S_{HT} l_{HT}}{S_{ref} b} \quad (1)$$

$$\bar{c}_{VT} = \frac{S_{VT} l_{VT}}{S_{ref} b} \quad (2)$$

	SENIOR DESIGN: MAE 4351 Project	Ref.: MAE 4351-001-2021 Date: 11. Aug. 2023 Name: Gayathri Kola Status: Complete
---	---	---

The following are the aircraft that are the most similar to the mission. Hypersonic vehicles with wing-body configuration are rare and difficult to find. Supersonic vehicles with WB configurations such as Concorde and XB-70 were considered for comparison purposes as well.

Table 5. Similar aircraft control surface dimensions [24,49–51].

Aircraft Name	Speed (M)	Body Type	Tail Volume (VT)	Tail Volume (HT)	Elevon Area [ft ²]	Vertical Tail Area [ft ²]	Wingspan [ft]	Fuselage Length [ft]
Concorde	2.1	WB	0.045	0.095	172.20	365.00	83.80	184.50
TU-144	2.1	WB				717.80	94.50	215.50
XB-70	3.0	WB	0.031	0.037	197.70	233.96	150.00	185.75
Space Shuttle	25	WB	0.078	0.154	210.00	413.25	78.06	122.26
SR-71	3.0	BB	0.051	0.084	91.50	150.76	55.70	107.42

*NASP X-30 was originally intended to be Mach 25 capability vehicle that was cancelled due to cost increments [24]. Note, the dimensions obtained are for space shuttle elevon area is for single side [50]. Similarly, for the SR-71, the elevon area is the combination of the inboard and outboard areas of a single side. The vertical tail area is for a single tail [52].

4.3 Control Surface Sizing

The control surface sizing is done in the CE phase once a rough geometry is obtained from CL. Once the horizontal tail volume coefficient is known, the elevons or other combinations can be decided. Most high-speed aircraft use elevons, a dual control capability control effector. It can control the lateral and longitudinal motion to vary pitch and roll.

Questions to address for control surface sizing:

- The question becomes what types of control surfaces are needed and why? How many are required?
- Type of control surface: elevons, canard, vertical tail, twin tails, etc.
- Number of elevons
- Elevon geometry
- Type of control surface: ailerons. Why not?
- Number of vertical tails
- Vertical tail dihedral angle

4.3.1 Canards

There are different types of tail configurations. One of them is Tail-Forward-Configuration (TFC). This includes canards that are used for either control or trim. Having a canard serves to modify the longitudinal stability and decrease the angle of attack during takeoff and landing for delta winged aircraft. One drawback of high sweep for an aircraft is the decrease in the maximum lift coefficient which usually occurs at high angles of attack. This means the aircraft may stall at a higher angle of attack, which is very beneficial, but it reduces the maximum lift at given speed. Having canards on the forward fuselage negates this imbalance by reducing the landing angle of attack. For pitch stability, this can reduce the stability of an aircraft. This is desirable especially in overly stable flight such as hypersonic aircraft.



(a) XB-70 Fixed Canards [53].



(b) TU-144 Retractable Canards [54]

Fig. 23 Canard designs on supersonic aircraft.

The following in the **Fig. 23** are some aircraft canard designs for reference. In the **Fig. 23** above, the XB-70 features a fixed canard that can be used for control. The Tupolev TU-144 has retractable canards that are mainly used for trim and reducing the angle of attack at landing [49]. The retractable nature of these devices makes them more useful for supersonic speeds where the drag can be reduced. Chines are another form of longitudinal stability feature. Although more applicable for adding directional stability, the addition of chines on the SR-71 also significantly prohibited the aft movement of neutral point at high supersonic speeds [26]. Adding too much of a blend between the fuselage and wings can change the aircraft design to a Blended-Body configuration.

4.3.2 Elevons

The elevons are dual control effectors used for pitch and roll control, used by many famous supersonic and hypersonic aircraft designs. The manner of their movement dictates whether the aircraft will pitch or roll. If the elevons are deflected up or down simultaneously on either side, the aircraft will change pitch. If the elevons are deflected in opposite directions, the aircraft will roll. Most design texts are resources that do not give a separate method to calculate the control power for elevons, except Nicolai. Usually, the control power for ailerons and elevators are calculated and sized based on which movement requires greater control authority. A method to calculate the trim of aircraft using elevons is given in section 4.4.3. The following are example aircraft featuring elevons in **Fig. 24**.

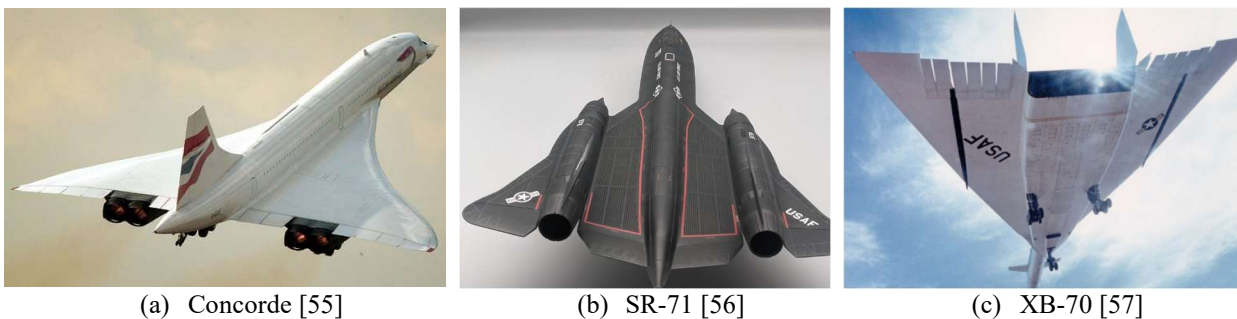


Fig. 24 Elevons features in supersonic and hypersonic aircraft.

Notice the three different designs for elevons. The SR-71 and Concorde have both inboard and outboard elevons and the XB-70 just features outboard elevons. The elevons are inboard when they are placed in between engines location and fuselage centerline. The large delta wing of Concorde has straight elevons that are extension of the wing itself. For SR-71, the elevons have a rather distinct geometry with curvature near the engines. The elevons are also rounded at the edges. The XB-70's elevons do not extend throughout the wingspan. A sub-section of elevons are a part of the drooped wing section and each are smaller in size.

4.3.3 Twin Vertical tails

For twin tails, the dihedral angle determines the kind of lateral stability the aircraft will have. If the tails are canted inwards such as for SR-71, the increase lateral stability during high-speed flight. Having outward dihedral is effective for maneuverability, most commonly found of fighter aircraft. The Hermeus Halcyon design features twin vertical tails with an outward dihedral.



Fig. 25 High-speed aircrafts with twin vertical tails.

Having a single large tail for a hypersonic aircraft may produce a lot of drag compared to twin tails of smaller size. Following are examples of twin tail high-speed aircraft. Note that the Halcyon is currently still a conceptual aircraft and many design iterations are expected to be made in the future. The hypersonic aircraft X-43A Hyper X also features straight, no-dihedral twin vertical tails. The number of tails will be a trade to be explored in the CL phase. Tail dihedral is another trade being used of CL. If twin vertical tails are used, they must be placed behind the passenger cabin for safety.

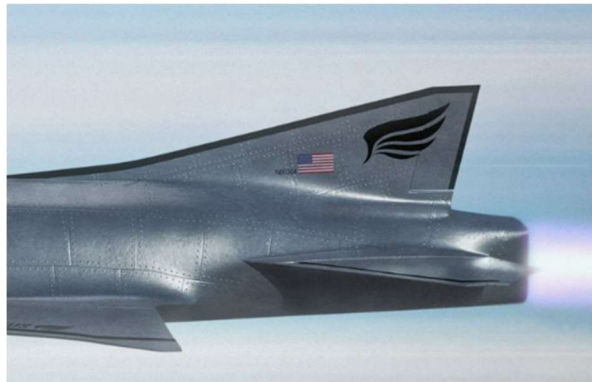
An advantage of twin vertical tails is that the aircraft directional controllability is improved compared to a long-span vertical tail. The added dihedral helps with roll control. Since the vertical tails are typically placed some distance away from the fuselage centerline, they are not obstructed by the fuselage wake region. However, twin vertical tails are slightly heavier than commonly used single vertical tails [28].

4.3.4 Single Vertical tail

The two supersonic commercial transports, Concorde and TU-144 both feature a single vertical tail with two rudders aligned vertically. Having a single tail has the benefit of less maintenance since it is a common feature. However, large vertical tails require stronger structural support compared to smaller twin vertical tails. The Hermeus Quarterhorse, unmanned plane features a single, highly swept vertical tail as well. Following are example designs of single vertical tail in **Fig. 26**.



(a) Concorde [60]



(b) Quarterhorse (Concept 2023) [5]

Fig. 26 Single vertical tail used in high-speed aircraft.

The Concorde has a large vertical stabilizer with two rudders, mainly for redundancy. They are connected to two separate systems, so if one fails, the other can be used instead. The Quarterhorse uses a single tail, however, notice the high sweep. This could decrease aerodynamic drag at hypersonic speeds. The Quarterhorse is also currently just a conceptual design and may have design alterations in the future.

4.4 Flight Conditions to address

When it comes to control surface sizing, these areas are sized to have enough control authority during critical flight conditions. For longitudinal control, these conditions are takeoff rotation, trim drag at cruise, high-g maneuver, and low speed at high angle of attacks. Since the concept is for a hypersonic passenger transport vehicle, the longitudinal control is assessed primarily for takeoff rotation and trim drag. For directional control, critical conditions such as crosswind landings, asymmetric thrust due to one-engine-inoperative (OEI) and adverse yaw must be taken into consideration for the sizing process. For lateral control, the deflections of elevons or ailerons will not be adding to lateral stability of the aircraft. They only function of roll control. The roll stability comes from the wing, vertical tail and fuselage configuration [25]. However, the elevon can be sized for lateral control requirements of roll performance given in MIL-HDBK-1797. The document MIL-HDBK-1797 is a handbook that gives guidelines on aircraft handling; however, it is not a military standard. The actual military standard specifications document named MIL-SPEC-1797 is currently classified. From MIL-HBDK-1797, our hypersonic concept aircraft will fall into Class III, meaning heavy transport requiring low-to-medium maneuverability. For a Class III aircraft, the roll performance requirements are 300 in 1.5 seconds [25]. This report will detail the longitudinal control aspects. The lateral controllability will be covered by fellow S&C engineer, Carlos Carmona and directional control by Oscar Ariza.

4.4.1 Takeoff rotation

Many disciplines are involved for this critical condition. First, the P&T team determines the angle of attack at takeoff. The W&B team provides the C.G. location to the Structures team who determines the appropriate placement of landing gear so that the aft end does not strike the ground and damage any engine. This is determined by a ground clearance requirement. Notice, most commercial airplanes have an angled fuselage at the aft for the same purpose. For takeoff rotation, the location of the main landing gear is directly related to the most aft C.G. location.

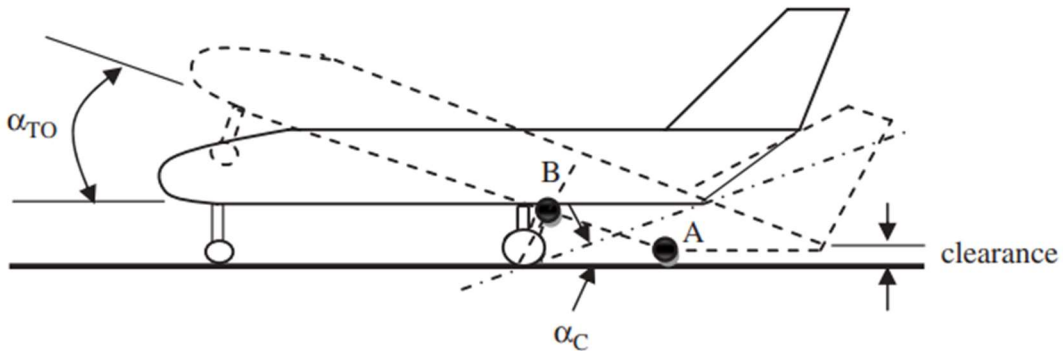


Fig. 27 Ground clearance required for takeoff rotation [28].

In terms of S&C, takeoff rotation is a longitudinal control requirement. The elevons must have enough control power to rotate the aircraft about the main landing gear such that the nose lifts up at 80% take-off speed. The methodology for takeoff rotation is adapted from reference [28] due to detailed steps given for the process. A more detailed Quasi-steady-state process is given by reference [61], however, it may be too complex to compute for the given time available. The elevon deflection needed to rotate the aircraft about the main landing gear is given by the following:

$$\delta_e = -\frac{C_{L\alpha}C_{m0} + C_{m\alpha}C_L}{C_{L\alpha}C_{m\delta_e} - C_{L\delta_e}C_{m\alpha}} \quad (3)$$

Note, most of the input comes from within S&C team and Aerodynamics team. A detailed procedure for locating the main landing gear position is given in the same reference. Here, the rotation point is about the main landing gear, and the initial acceleration has to have a value of 4-6 deg/s².

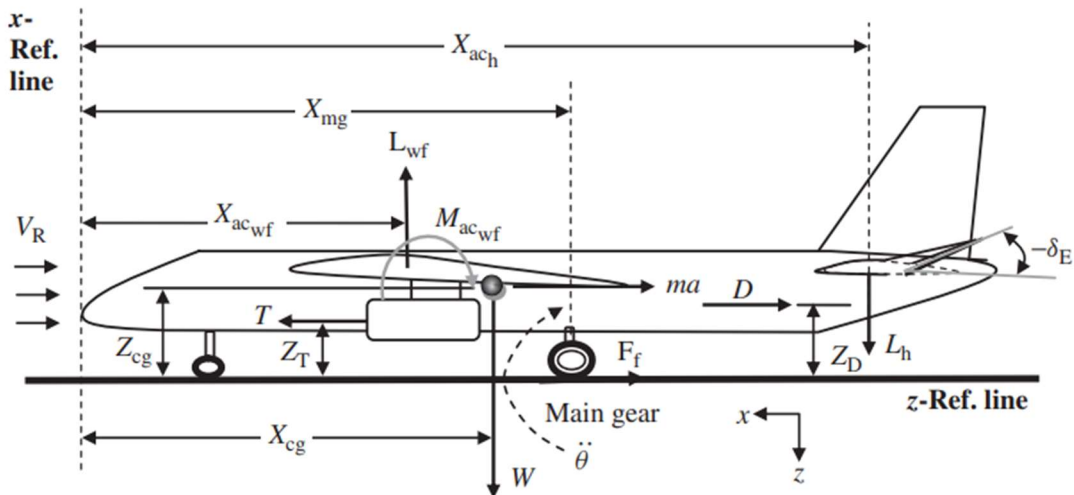


Fig. 28 Forces and moments during takeoff rotation [28]

	SENIOR DESIGN: MAE 4351 Project	Ref.: MAE 4351-001-2021 Date: 11. Aug. 2023 Name: Gayathri Kola Status: Complete
---	---	---

This requirement is for a tricycle landing gear arrangement. The overall takeoff rotation should not exceed 3-5 seconds for a large transport. The following gives the main forces and moments related to takeoff rotation. The moments about the C.G. location must be overcome by elevon deflection at takeoff rotation, given in the equation below.

$$\sum M_{cg} = I_{yy\ mg} \ddot{\theta} = -M_W + M_D - M_T + M_{Lwf} + M_{acwf} + M_{Lh} + M_a \quad (4)$$

The forces and distances associated with the moments are given in **Fig. 28**. As mentioned, the initial acceleration $\ddot{\theta}$ value for a large transport must be within 4-6 deg/s². The entire process is coded to find the maximum elevon deflection for takeoff rotation. The moment of inertia I_{yy} of the landing gear is an input from W&B team.

4.4.2 Trim drag

Trim drag is caused due to excessive force required to trim an aircraft. Usually, an overly stable aircraft flying at high speeds will experience large amounts of trim drag when pitch control effectors are used. One way to minimize this trim drag is by moving the neutral point forward, either closer to the aircraft C.G. or ahead of it. This destabilizes the aircraft enough that large control deflections producing trim drag are avoided. The procedure to estimate the elevon deflection angle is given in Eq. (5). A generic method to calculate trim drag is given below in Eq. (6) [25].

$$D_{trim} = \eta_T q_\infty S_T K_T C_{LT}^2 \quad (7)$$

The term C_{LT} is the lift coefficient of the tail. The trim drag must not be more than 10% of the total drag. If this is the case, moving the C.G. near the neutral point, or increasing the tail aspect ratio can help reduce trim drag. Increasing the control effector size can also reduce trim drag since less force will be needed for deflection.

4.4.3 Trim of tailless aircraft

Following are the elevon trim equations for a tailless aircraft, similar to the WB configuration being considered [25]. The following equations are for a load factor $n = 1$. A load factor of 1 represents straight and level flight, meaning lift on the body is equal to its weight.

$$0 = C_{M\ ac_w} - \frac{x_w}{\bar{c}} C_L + \frac{Tz_T}{q_\infty S_{ref} \bar{c}} \quad (8)$$

For a deflected elevon:

$$0 = \left(\frac{dC_{M\ ac_c}}{d\delta_e} \right) \delta_e - \frac{x_w}{\bar{c}} \left[\left(\frac{dC_L}{d\alpha} \right)_w \alpha + \left(\frac{dC_L}{d\delta_e} \right) \delta_e \right] + \frac{Tz_T}{q_\infty S_{ref} \bar{c}} \quad (9)$$

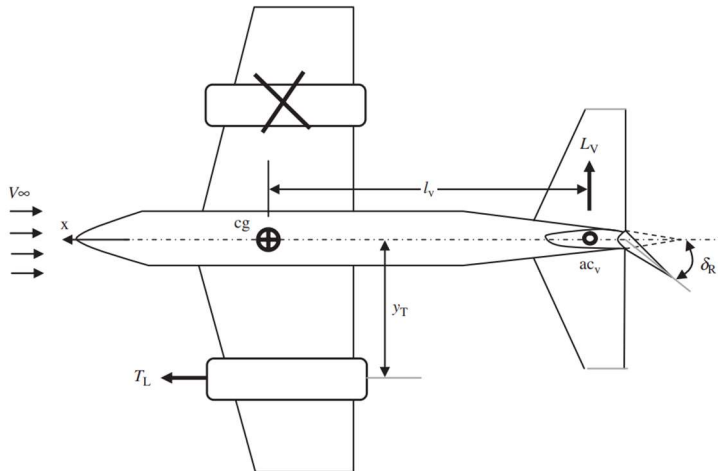
Can be re-written as:

$$\delta_e = \frac{\left(\frac{x_w}{\bar{c}} \right) \left(\frac{dC_L}{d\alpha} \right)_w \alpha - \left(\frac{Tz_T}{q_\infty S_{ref} \bar{c}} \right)}{-\left(\frac{x_w}{\bar{c}} \right) C_{L\delta} + C_{M\delta}} \quad (10)$$

The geometric parameters in the Eq. (11-12) are illustrated in Fig. 35.

4.4.4 Asymmetric thrust

One of the most critical conditions to size for occurs at takeoff when an engine fails. This critical condition is also known as One-Engine-Inoperative (OEI). However, if there are two engines on one side of the aircraft, the possibility of both engines failing must be considered as well. Another flight phase where OEI can be evident is in the case of inlet unstarts at cruise. This was most notable in SR-71 Blackbird's case where the SAS would also manage control movements in such small time spans. For such a case, knowing the maximum rudder or vertical tail deflection range is essential.


Fig. 29 Asymmetric thrust condition [28]

The maximum rudder deflection at OEI can be estimated using the following relation below in Eq. (13). The following assumptions can be made, first, the yawing moment bias C_{n_0} can be assumed to be zero for a symmetric aircraft. Then, the elevon deflection is assumed to be zero, along with sideslip angle β . If there are more than two engines on the aircraft, then the thrust for additional engines must be considered along with distance from fuselage centerline y_T .

$$\delta_r = \frac{T_L y_T}{-\bar{q} S_{ref} b C_{n\delta_r}} \quad (14)$$

Most parameters for this calculation come from the Propulsion, Geometry and S&C teams. A summary of all critical conditions to size for given below in **Fig. 30**.

Takeoff Rotation	Asymmetric Thrust (or OEI)
Flight phase: Takeoff	Flight phase: Takeoff, Cruise
Main Inputs: Geometry: z_t, S_{ref} Propulsion: Thrust S&C: $C_{m_0}, C_{L_1}, C_{L_0}, C_{m\delta_e}, C_{L\delta_e}$ Aerodynamics: $C_{L_{\alpha}}$	Main Inputs: Geometry: y_t, S_{ref}, b Propulsion: Thrust S&C: $C_{n\delta_r}$ Aerodynamics: $C_{L_{\alpha VT}}$
Analysis: Methodology: Conceptual Design, A Systems Engineering Approach, M. Sadraey, 2013.	Analysis: Methodology: Conceptual Design, A Systems Engineering Approach, M. Sadraey, 2013.
Outputs: Maximum elevon deflection angle δ_e	Outputs: Maximum rudder deflection angle δ_r
Trim Drag	Crosswind Landing
Flight phase: Cruise, Climb	Flight phase: Approach
Main Inputs: Geometry: z_t, S_{ref}, \bar{c} W&B: C.G. location Aerodynamics: Neutral point	Main Inputs: P&T: V_{TO} S&C: $C_{n\delta_r}, C_{n\beta}$ Aerodynamics: $C_{L_{\alpha VT}}$
Analysis: Methodology: Fundamentals of Aircraft and Airship Design, Nicolai & Carichner, 2010	Analysis: Methodology: Fundamentals of Aircraft and Airship Design, Nicolai & Carichner, 2010
Outputs: Trim drag at cruise, climb. Static Margin (SM)	Outputs: Maximum rudder deflection angle δ_r for a sideslip of $\beta = 11.5^\circ$

Fig. 30 Control surface sizing IDA for CE

4.4.5 Crosswind landings

There were two methods found for sizing for crosswind landings. A simple method was given in Nicolai and a more detailed method was obtained from reference [28]. The method given from Nicolai to size. Nicolai recommends a sideslip of $\beta = 11.5^\circ$ for the analysis. The crosswind condition is given by the following relation from Nicolai [25]:

$$C_n = 0 = C_{n\beta}\beta + C_{n\delta_r}\delta_r \quad (15)$$

4.5 Axis systems

This section presents the various axis systems involved in stability determination. The aircraft system generally used is the body axis which is fixed to the aircraft C.G. location with x-axis positive toward the nose, y-axis positive towards the right wing and z-axis positive towards the ground station on Earth. This axis system is fixed with the body of the aircraft.

The stability axis system is similar to the body axis system; however, it is independent on angle of attack. The stability axis system is rotated by right hand rule about the y-axis of body axis by some value of angle of attack as in Fig. 31 (a). A transformation matrix is used to move from stability frame to body frame using angle of attack.

Similarly, another axis system known as the wind axis is used for lateral stability. The wind axis is rotated by a sideslip angle β from the stability axis, as seen from top view.

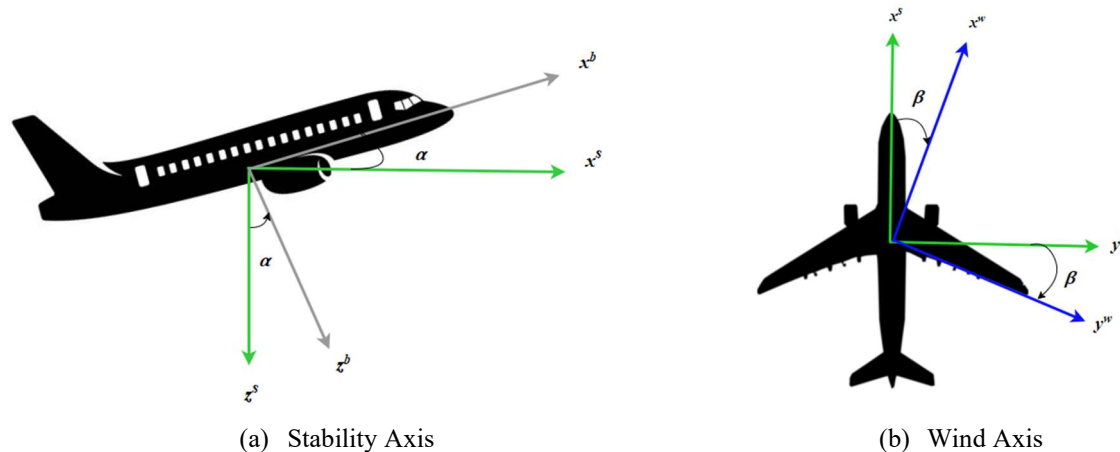


Fig. 31 Axis Systems with body frame

4.6 Static Stability

Static stability refers to the condition when an aircraft inherently returns to its equilibrium position when disturbed. This is also known as positive static stability when the aircraft returns to equilibrium after experiencing some decreasing oscillations. In the case of neutral static stability, the disturbance (such as wind) changes the attitude of the aircraft after which it stays on the same path. If the aircraft starts to deviate from the equilibrium position after a minor disturbance, the aircraft is said to have negative static stability, often undesirable for stability design.

Since our aircraft will be carrying passengers, it will be considered a transport aircraft. According to FAR 25, the document ascribing flying qualities for transport aircraft, the aircraft must have static stability in all directions:

“The airplane must be longitudinally, directionally, and laterally stable. In addition, the airplane must show suitable stability and control “feel” (static stability) in any condition normally encountered in service” [25].

The Fig. 32 gives an overview on static stability requirements in general. Static stability is measured by three common derivatives based on longitudinal, lateral, and directional sections. For longitudinal static stability, pitching moments as a function of angle of attack $C_{m\alpha}$ and static margin SM are of primary importance. For most aircraft, the lateral and directional movements are coupled; a yawing motion induced a rolling motion inherently since the aircraft must bank a little. They are influenced by the wind axis, hence a sideslip angle β is considered for lateral-directional moments. The sign conventions that assure stability are given in the Fig. 32 below. The primary objective is to have our aircraft statically stable. Lateral modes such as spin resistance and roll reversal will be omitted from our analysis.

Criterion	Description
Longitudinal $C_{m_\alpha} = -(SM)C_{L_\alpha} < 0$	When satisfied, any disturbance in pitch will result in a restoring pitching moment. This requirement may be relaxed to improve performance or maneuverability.
Directional $C_{n_\beta} > 0$	When satisfied, any disturbance in side-slip will result in a restoring yawing moment. Primarily effected by the vertical lifting surface.
$C_{l_\beta} < 0$	When satisfied, any disturbance in side-slip will result in a restoring rolling moment. Primarily effected by the dihedral effect.
Lateral (spin resistance and roll reversal) $C_{n_{\beta_{dyn}}} = C_{n_\beta} - C_{l_\beta} \frac{I_{zz}}{I_{xx}} \tan \alpha > 0$ $LCSP = C_{n_\beta} - C_{l_\beta} \frac{\frac{I_{zz}}{I_{xx}} \tan \alpha}{C_{l_\delta} \frac{LaCE}{LaCE}} > 0$	Provides an approximation for aircraft spin resistance during non-rolling maneuvers, no control inputs. Usually important for fighter and high-speed aircraft. Lateral Control Spin Parameter provides an approximation for roll reversal. Adverse yaw induced by the aileron combined with low directional stability can produce a natural roll reversal. Usually important for fighter and high-speed aircraft.

Fig. 32 Static stability requirements overview [35]

4.7 Dynamic Stability

In dynamic stability, the time, and oscillations of the aircraft before returning to the equilibrium state are considered. If an aircraft has positive dynamic stability, the aircraft return to equilibrium through a sequence of decreasing oscillations. For neutral dynamic stability, the aircraft will keep oscillating with the frequency until another disturbance occurs. For a negative dynamic stability, the aircraft will have increasing oscillations making it unstable. For an aircraft to have dynamic stability, it must first have positive static stability. Hence, static stability analysis is conducted first.

4.8 Longitudinal Stability

Longitudinal stability consists of assessing the pitching motion of an aircraft. To maintain a steady-level flight, the net moments along the longitudinal axis of an aircraft must be zero at a given angle of attack. If there is a positive pitching moment, it causes the aircraft to pitch up (nose up). If the moment is negative, it causes a nose down moment. Either of these moments, be it pitch up or down, are undesirable beyond a certain limit. After an aircraft crosses the sonic barrier ($M = 1$), the center of pressure (point where lift and drag forces act) also known as the neutral point shifts backward aft the center of gravity. This over-stabilizes an aircraft at high speeds prohibiting its maneuverability. If the aircraft were to solely rely on its pitch control effectors such as elevons to pitch up, the aircraft will experience large amounts of *trim drag*. Trim drag is the drag that occurs to trim an aircraft.

The most common and important longitudinal stability parameters are the following:

- Pitching moment as a function of angle of attack, c_{m_α}
- Static Margin (SM)

The static margin gives an assessment of the level of stability an aircraft has, it is calculated using the formula below:

$$SM = (\bar{X}_{np} - \bar{X}_{cg}) = -\frac{c_{m_\alpha}}{C_{L_\alpha}} \quad (16)$$

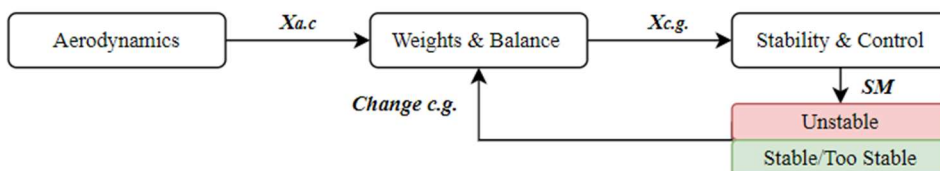


Fig. 33 Interactions between disciplines for longitudinal stability.

	SENIOR DESIGN: MAE 4351 Project	Ref.: MAE 4351-001-2021 Date: 11. Aug. 2023 Name: Gayathri Kola Status: Complete
---	---	---

Note, the location of neutral point and center of gravity must be normalized values. If the SM is negative, that means the aircraft is unstable and a positive value of SM indicates stability. A higher positive value of SM indicates that the vehicle might be overly stable. Most fighter aircraft are designed to have relaxed static stability, where their static margins are from 0 to -15% which allows them to maneuver easily. The Flight-Control-System (FCS) is used to automatically stabilize these aircraft, significantly reducing trim drag [30]. The aerodynamic center is calculated by the Aerodynamics team and given to the Weights & Balance (W&B) member. The W&B member will calculate the C.G location and provide it to S&C for SM calculations as seen in **Fig. 33**.

To estimate the pitching moment, the following relation can be used:

$$C_m = C_{m_0} - \frac{1}{c} C_{L\alpha} \alpha (x_{cp} - x_{cg}) \quad (17)$$

Where c_{m_0} is pitching moment independent of angle of attack. The relation above is valid for Mach number less than 5 [33]. Where the $C_{L\alpha}$ is the wing-body lift curve slope.

And the longitudinal stability derivative can be written as [25]:

$$C_{m\alpha} = -SM C_{L\alpha} \quad (18)$$

Table 6. Sign requirements for main stability derivatives [25].

Sub-section	Derivative	Derivative Name	Stable	Unstable
Longitudinal	$c_{m\alpha}$	Pitching moment as a function of angle of attack	Negative	Positive
Lateral	$c_{l\beta}$	Rolling moment due to side slip angle	Negative	Positive
Directional	$c_{n\beta}$	Yawing moment due to side slip angle	Positive	Negative

4.9 Methodology for Stability and Control derivatives

Now that there is some background given, the methodology used for calculating stability and control derivatives will be split into four different segments: subsonic, transonic, supersonic, and hypersonic Mach numbers. The following is the checklist for choosing a method to calculate stability derivatives:

- Wing-body configuration.
- Fewer geometric inputs.

This report will be covering the calculation of longitudinal stability derivatives. If time permits, dynamic stability will be assessed. The following is a helpful roadmap for static stability assessment.

Simplified trim equations of motion are given below from Eq. (19-20):

Longitudinal trim:

$$0 = C_{m_0} + C_{m\alpha}(\alpha) + C_{m\delta_e}(\delta_e) + C_{m\delta_r}(\delta_r) \quad (21)$$

Lateral trim:

$$0 = C_{l_0} + C_{l\beta}(\alpha) + C_{l\delta_e}(\delta_e) + C_{l\delta_r}(\delta_r) \quad (22)$$

Directional trim:

$$0 = C_{n_0} + C_{n\beta}(\alpha) + C_{n\delta_e}(\delta_e) + C_{n\delta_r}(\delta_r) \quad (23)$$

Please note that the derivatives due to stabilizer incidence have not been included in the equations above. Most of the derivatives can be found from Jan Roskam's design series within the subsonic regime. For supersonic and transonic regime, DATCOM methods are more applicable. A detailed overview is given in the Jan Roskam's design section.

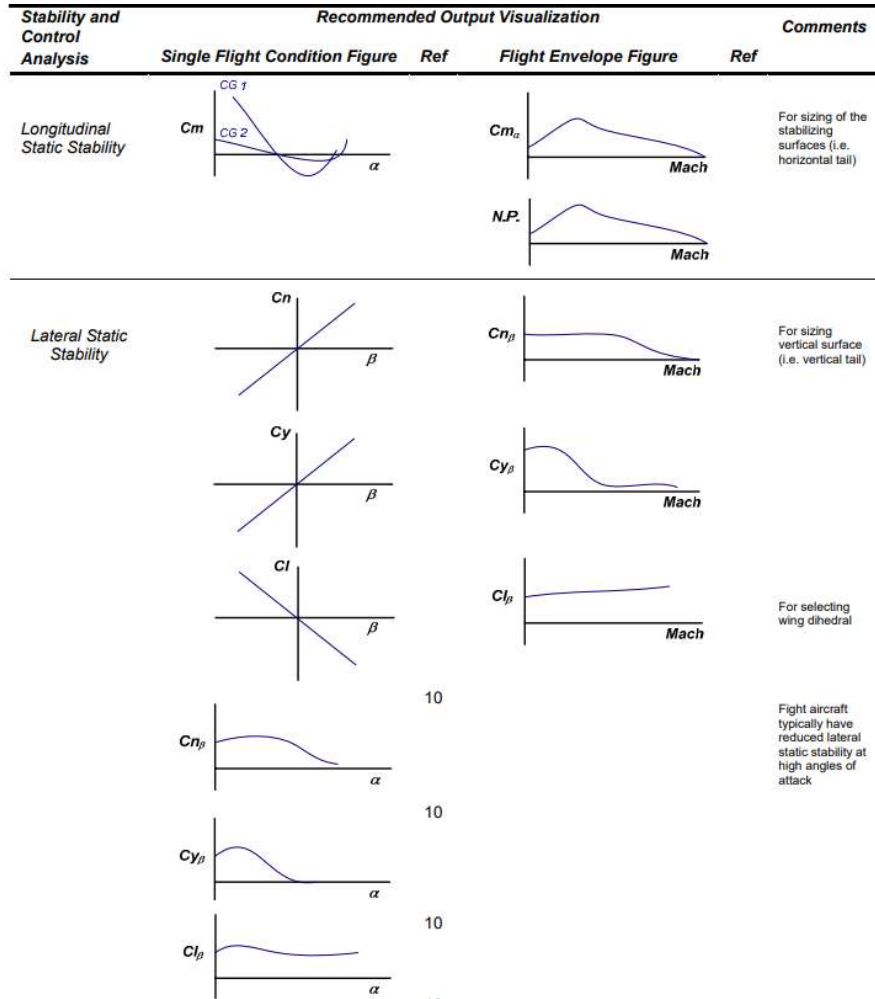


Fig. 34 Static stability assessment roadmap [35].

Chudoba, Cook Method – Trim Equations of Motion for Steady State Straight-line flight [62].

This paper gives a generic method to assess stability for symmetric and asymmetric aircraft. For stability assessment in conceptual design phase, a complete 6 DOF assessment is essential for characterizing a vehicle's stability. This analytical method allows for control power assessment in 6 DOF and allowing for trim analysis. There are two papers in this series – one covers steady state straight-line flight, and the other focuses on dynamic stability analysis involving turning flight, pull-up, and push over maneuvers [61]. For the dynamic analysis, perturbed EOMs are used instead of steady state EOMs. Due to the fully coupled 6 DOF analysis, there are 6 equations and multiple assumptions must be made to simplify the analysis. Following are 6 DOF steady state trim EOMs given:

$$0 = -mg \sin \theta + X_A + X_T \quad (24)$$

$$0 = mg \sin \phi \cos \theta + Y_A + Y_T \quad (25)$$

$$0 = mg \cos \theta \cos \phi + Z_A + Z_T \quad (26)$$

$$0 = L_A + L_T \quad (27)$$

$$0 = M_A + M_T \quad (28)$$

$$0 = N_A + N_T \quad (29)$$

Here, ϕ, θ, ψ are Euler angles denoting roll, pitch, and yaw. The variables L, M and N are external moments about the center of gravity. Meaning, rolling, pitching, and yawing moments. Finally, the variables X, Y , and Z are the resultant force components. The full description of equations is not mentioned here due to length. The equations follow these assumptions:

- The Earth is a flat surface and rests in the inertial space with rotational velocity ignored.
- Uses a body axis system with origin at the C.G. of the aircraft.
- The aircraft must be a rigid body, meaning the inertia matrix will be zero.
- Wind velocity is neglected.

The paper gives many critical condition cases where the controllability can be evaluated and adds the simplifying assumptions that can be made. For longitudinal stability, the following cases were suggested:

- Cruise trim drag utilizing aerodynamic control effectors – for symmetric thrust.
- Trim drag during straight sideslip – for symmetric thrust.
- Trim drag during OEI cruise – for asymmetric thrust.

Upon deliberation, it was decided amongst the team to first conduct a de-coupled stability analysis and if time permits, to move to a more complex analysis. If this method is chosen, methods for individual coefficients must be decided, and a MATLAB script will be written to perform the analysis. More detailed inputs from W&B and Propulsion team are required, specifically moments of inertia and thrust incidence angles. After collecting all methods for stability and control derivative coefficients at different speed regimes, the following assumptions were made to further simplify the equations of motions:

- Assuming thrust force acts only along x-axis of the aircraft. Hence,

$$T_{i_y} = T_{i_z} = 0; \phi_{T_i} = \psi_{T_i} = 0^\circ; T_i = T_{i_x} \quad (30)$$

- Additionally, all incidence angles are considered to be zero. This reduces the number of variables being solved for, reducing complexity.
- Lastly, only moment equations for roll, pitch and yaw are considered. No aerodynamic coefficients are used. Initially, this assumption was not made and required a lot more coefficients methods to be found. However, it was later realized that only three EOMs are needed to find the necessary control effector deflections throughout flight.
- The following equations were derived based on these assumptions made:

$$0 = [C_{l_0} + C_{l_\beta}(\beta) + C_{l_{\delta LaCE}}(\delta LaCE) + C_{l_{\delta DiCE}}(\delta DiCE)] qS_{ref} b \quad (31)$$

$$0 = [C_{m_0} + C_{m_\alpha}(\alpha) + C_{m_{\delta LoCE}}(\delta LoCE)] qS_{ref} b + n(T_i Z_T) \quad (32)$$

$$0 = [C_{n_0} + C_{n_\beta}(\beta) + C_{n_{\delta DiCE}}(\delta DiCE)] qS_{ref} b \quad (33)$$

To update angle of attack and sideslip angles, the following relations were re-solved for:

$$\alpha = \frac{-nT_i Z_T}{qS_{ref} b} \quad (34)$$

$$\beta = \frac{-C_{n_{\delta DiCE}}(\delta DiCE) - C_{n_0}}{C_{n_\beta}} \quad (35)$$

Nicolai – Pitching moments about C.G. [25]

For longitudinal derivatives, Nicolai gives a method to estimate pitching moments for a tailless aircraft, similar to the geometry our team is considering for CL. The axis system for the wing-body tailless aircraft is given in the Fig. 35. To calculate the pitching moments about the C.G. location, following relation can be used for a tailless aircraft:

$$C_{m,c,g.} = -C_L \frac{x_w}{\bar{c}} + C_D \frac{z}{\bar{c}} + C_{m,a.c.w} + \frac{T z_T}{q_\infty S_{ref} \bar{c}} - C_{m,c.g.Inlet} \quad (36)$$

Where, C_L and C_D need to be functions of Mach number M and angle of attack α . The Aerodynamics team can give MATLAB functions of the same. This resource is also being used for lateral rolling moment build-up by team member Carlos Carmona. A more general method for calculation of the coefficient in Eq. (37) is given in Raymer [30]. For a trimmed condition, the Eq. (38) is set to zero.

Similarly, to find the pitching moment as a function of angle attack $C_{m,\alpha}$, the following relation can be used. The $C_{m,\alpha}$ is important because it gives the angle of attack for trim condition. Additionally, if the term has constant values when the C.G. location is changed, the neutral point can be estimated, as in $C_{m,\alpha}$ will be zero.

$$C_{m,\alpha} = -\frac{x_w}{\bar{c}} m_w + C_{m,\alpha_I} \quad (39)$$

$$m_w = (C_{L,\alpha})_{WB} \quad (40)$$

$$C_{m,\alpha_I} \approx \frac{2\dot{m}_0 \beta l_i}{\rho V_\infty S_{ref} \bar{c}} \frac{d\beta}{d\alpha} \text{ (per radian)} \quad (41)$$

The exact geometric parameter definitions are illustrated in the Fig. 35 below. The last multiplier term in Eq. (42) can be assumed to be 1 for inlet placement beneath the wing. Most parameters are required from the Aerodynamics and Propulsion teams. A similar, a more geneneral method was found in Raymer, however, it seemed for applicable for traditional subsonic commerical aircraft present today with an aft tail. Hence, the method given in Nicolai was chosen for analysis.

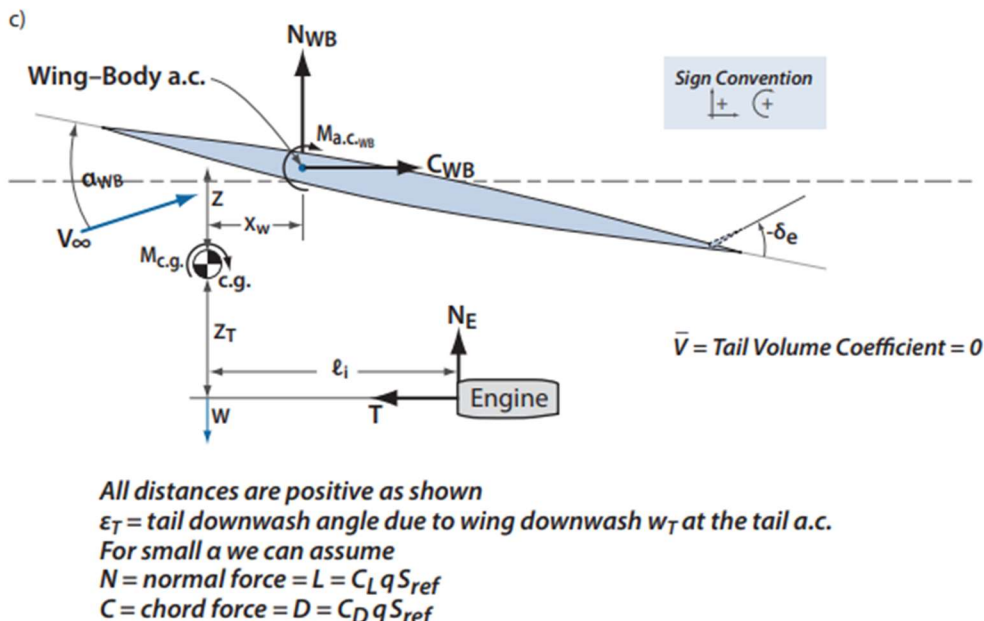


Fig. 35 Axis system and forces acting on a tailless wing-body [25]

Jan Roskam Design Series

As mentioned in the literature section, the Jan Roskam design texts give a simplified method to calculate many of the stability and control derivatives. The following table summarizes methods available for the derivatives involved.

Table 7. Stability and Control derivatives in Jan Roskam [20,38,63]

Derivative Symbol	Subsonic	Transonic	Supersonic	Hypersonic	Assumptions
Longitudinal Stability Derivatives					
Steady-state derivatives					
C_{L_1}	✓	✓	✓	✓	
C_{D_1}	✓	✓	✓	✓	
C_{M_1}	✓	✓	✓	✓	
$C_{T_{X_1}}$	✓	✓	✓	✓	
$C_{M_{T_1}}$	✓	✓	✓	✓	
Speed derivatives					
C_{L_u}	✓	✓	✓		
C_{D_u}	✓	✓	✓	✓	
C_{M_u}	✓	✓	✓	✓	
$C_{T_{X_u}}$	✓	✓	✓	✓	Gliders, RBCC = 0
$C_{M_{T_u}}$	✓	✓	✓	✓	
Angle of attack derivatives					
C_{L_α}	✓	✓	✓		
C_{D_α}	✓	✓	✓	✓	
C_{M_α}	✓	✓	✓	✓	
$C_{M_{T_\alpha}}$					
Rate of angle of attack derivatives					
$C_{L_{\dot{\alpha}}}$	✓				
$C_{D_{\dot{\alpha}}}$	0	0	0	0	Neglect
$C_{M_{\dot{\alpha}}}$	✓				
Lateral-Directional Stability Derivatives					
Sideslip derivatives					
C_{Y_β}	✓				
C_{l_β}	✓				
C_{n_β}	✓				
$C_{n_{T\beta}}$	✓				
Rate of sideslip derivatives					
$C_{Y_{\dot{\beta}}}$	✓				
$C_{l_{\dot{\beta}}}$	✓				
$C_{n_{\dot{\beta}}}$	✓				
Roll rate derivatives					
C_{Y_p}	✓				
C_{l_p}	✓				
C_{n_p}	✓				
Pitch rate derivatives					
C_{D_q}	✓				
C_{L_q}	✓				
C_{m_q}	✓				
Yaw rate derivatives					
C_{Y_r}	✓				
C_{l_r}	✓				
C_{n_r}	✓				
Control Derivatives					
Control: Elevator derivatives					
$C_{D_{\delta_e}}$	✓				
$C_{L_{\delta_e}}$	✓				
$C_{M_{\delta_e}}$	✓				
Control: Aileron derivatives					
$C_{Y_{\delta_a}}$	✓				

	SENIOR DESIGN: MAE 4351 Project	Ref.: MAE 4351-001-2021 Date: 11. Aug. 2023 Name: Gayathri Kola Status: Complete
---	---	---

$C_{l\delta_a}$ $C_{n\delta_a}$	✓ ✓
Control: Rudder derivatives	
$C_{r\delta_r}$ $C_{l\delta_r}$ $C_{n\delta_r}$	✓ ✓ ✓

As seen from the table above, most methodology available from this resource is applicable for subsonic regime, this is case for lateral and directional stability derivatives and control derivatives. Roskam recommends DATCOM for calculating lateral-directional derivatives for supersonic and hypersonic regimes. However, most methodology in DATCOM is complex so simplifications must be made before using the resource. Jan Roskam series also has methodology to calculate control derivatives for canards, differential stabilizers, and spoilers.

Jan Roskam Flight Dynamics – Pitching control derivatives [31]

This text gives formulas for the majority of control derivatives that can be used while evaluating trim conditions. The Eq. (43) gives the derivatives essential for calculating longitudinal trim. Notice, the pitching moment due to stabilizer incidence $C_{m_{i_h}}$ is being neglected here to simplify the analysis.

$$C_{m_0} \approx C_{m_{a,c}} + C_{L_0}(\bar{x}_{cg} - \bar{x}_{ac-e}) \quad (44)$$

$$C_{m_{\delta_e}} = -C_{L_\alpha}\eta_n \frac{S_e}{S_{ref}} (\bar{x}_{ac-e} - \bar{x}_{cg})\tau_e \quad (45)$$

Note, the pitching moment due to rudder deflection $C_{m_{\delta_r}}$ is neglected since its effect is negligible on longitudinal stability. The term C_{m_0} is often referred to as pitching moment bias, where the angle of attack and elevon deflection are zero. The term C_{L_0} is the lift coefficient at same assumptions. Since there is no aft tail, the dynamic pressure can be assumed to be the same at the elevons, thereby making the term η_h equal to 1. Finally, the term τ_e is the angle of attack effectiveness parameter of the elevon. These methods will be used in conjunction with Nicolai to estimate trim and control surface deflections needed at each flight phase.

4.10 Validation methods

Most verification data is available for Space Shuttle orbiter, SR-71 and XB-70. Following is the table listing all the resources with useful verification plots for S&C analysis.

Table 8. Stability and Control Verification Literature.

Aircraft	Year	Literature Name
SR-71	2012	SR-71 Flight Manual [52].
Space Shuttle	1975	Results of Investigations on a 0.010 scale 140A/B configuration space shuttle orbiter model 72-0 [64].
Space Shuttle	1974	Space Shuttle Orbiter and Subsystems [50].
XB-70	1973	Summary of stability and control characteristic of the XB-70 airplane [65].
XB-70	1973	Comparisons of predictions of the XB-70-1 longitudinal stability and control derivatives [66].

For method verification, this section will be focusing on verifying longitudinal and directional stability and control derivatives. The lateral stability and control derivative verification is being performed by S&C team member Carlos Carmona. The following is a roadmap, checklist for method verification for S&C. Stability and Control analysis is often highly dependent on vehicle geometry, hence some generic methods may produce very large errors. Additionally, some geometric parameters are not available with the vehicle data so must be assumed or estimated.

Table 9. Stability and Control Verification Road Map

Derivative Symbol	Subsonic	Supersonic	Hypersonic
C_{m_α}	Nicolai	✓	Nicolai

		XB-70		XB-70		
$C_{m\delta_e}$	Roskam, Systems	✓	Roskam, Systems	✓	Systems	✓
	SR-71		SR-71		Space Shuttle Orbiter	
$C_{n\beta}$	DATCOM	✓	DATCOM	✓	DATCOM	✓
	Space Shuttle Orbiter		Space Shuttle Orbiter		Space Shuttle Orbiter	
$C_{n\delta_r}$	Systems	✓	Systems	✓	Systems	✓
	Space Shuttle Orbiter		Space Shuttle Orbiter		Space Shuttle Orbiter	
$C_{l\beta}$	DATCOM	✓	DATCOM	✓	DATCOM	✓
	Space Shuttle Orbiter		Space Shuttle Orbiter		Space Shuttle Orbiter	
$C_{l\delta_e}$	Systems	✓	Systems	✓	Systems	✓
	Space Shuttle Orbiter		Space Shuttle Orbiter		Space Shuttle @ Descent	

Highlighted in grey in Table 9 are the verification vehicles used. Lateral and directional stability control derivatives verification will be presented in Carlos Carmona's report [67]. This table does not indicate the accuracy of any of the methods being verified. The method named "Systems" is reference [28].

4.10.1 Longitudinal Verification

The longitudinal method verification will be performed for stability derivative $C_{m\alpha}$ and control derivative $C_{m\delta_e}$. Since the control derivative is more dependent on lift coefficient and location of center of gravity, simplified methods will be used to validate for subsonic, supersonic, and hypersonic regimes.

Subsonic & Supersonic - $C_{m\alpha}$

For subsonic regime, methods presented in Nicolai were used since they are most applicable to a tailless aircraft rather than Roskam (Part VI) which is more generic. The verification vehicle used was XB-70 with dimensions given in the reference [66]. The following assumption was made for the verification:

- The moment due to inlet is zero since the inlet placement is right under the wing.
- The factor F has a value of 1.1 for a wing-body subsonic $C_{L\alpha}$. This is based on maximum fuselage diameter to wingspan ratio (d/b). The value of F was estimated from empirical chart given in Nicolai [25].
- The moment due to canard is ignored.
- For supersonic aerodynamic derivative $C_{L\alpha}$, supersonic linear theory & leading-edge suction method were included.

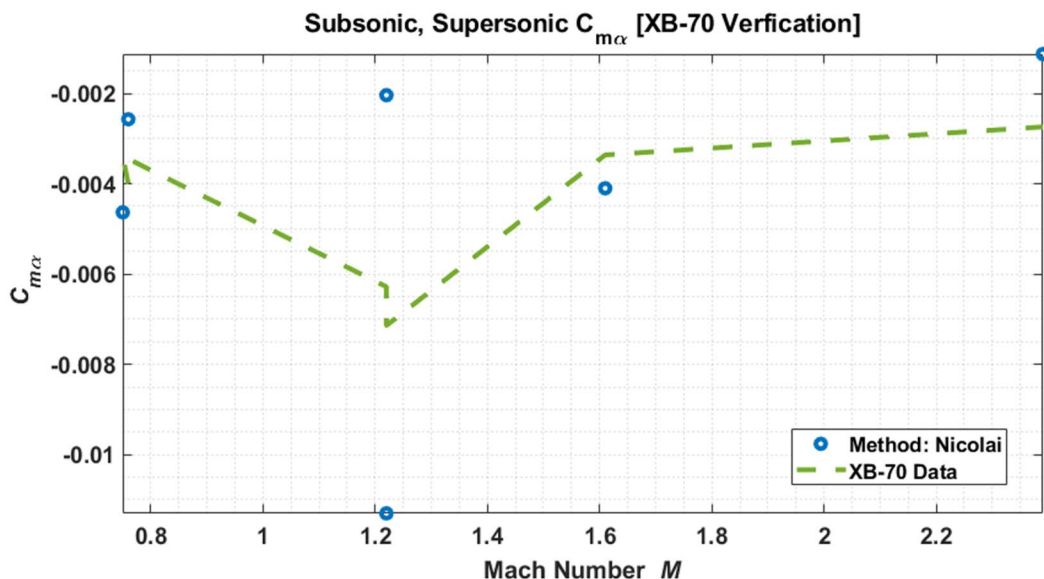


Fig. 36 Subsonic and supersonic pitching moment derivative verification attempt.

As seen from the **Fig. 36**, most of XB-70's data does not agree with Nicolai's method. However, this is due to the lack of some data such as neutral point locations for the specified flight regimes. Due to this, the neutral point was assumed to be fixed at 11.8 m from the nose based on given geometric data. Since the location of neutral point largely drives the method given in Nicolai, there is a large discrepancy seen in the supersonic/transonic region. For subsonic regimes, the method gives close results since there is less shift of neutral point. The data used from XB-70 is given in the **Fig. 37** below. For transonic region, additional methods must be used. Additionally, the data below used canard and elevon deflections at given Mach numbers, which was also neglected while using Nicolai's method.

	Case number					
	SC-1	SC-2	SC-3	SC-4	SC-6	SC-7
Flight number	63	63	64	75	81	68
Data time	0: 36: 49	1: 55: 57	0: 35: 30	2: 04: 0.5	1: 50: 26	1: 53: 23
M	0.76	0.75	1.22	1.22	1.61	2.39
h_p , m (ft)	4720 (15,500)	7650 (25,100)	9880 (32,400)	11,980 (39,300)	11,770 (38,600)	17,100 (56,100)
W, kg (lb)	2.179×10^5 (4.804×10^5)	1.541×10^5 (3.396×10^5)	1.921×10^5 (4.235×10^5)	1.622×10^5 (3.575×10^5)	1.871×10^5 (4.125×10^5)	1.747×10^5 (3.852×10^5)
Center of gravity, percent c_w	22.1	23.4	22.8	20.9	22.0	21.2
I_y , kg-m ² (slug-ft ²)	2.957×10^7 (2.181×10^7)	2.418×10^7 (1.783×10^7)	2.848×10^7 (2.100×10^7)	2.594×10^7 (1.913×10^7)	2.869×10^7 (2.116×10^7)	2.798×10^7 (2.063×10^7)
δ_T , deg	0	0	25	25	65	65
α , deg	4.5	4.4	3.7	4.7	3.2	3.7
δ_e , deg	3.8	2.6	10.9	6.7	10.2	4.6
δ_c , deg	2.36	2.58	1.18	1.73	1.26	2.54
a_n , g	1.0	1.0	1.0	1.0	1.0	1.0
Bypass door position, deg	Closed	Closed	1.00	1.00	3.50	5.00
Nose ramp position	Down	Down	Down	Down	Down	Down
V, m/sec (ft/sec)	244 (802)	232 (762)	362 (1191)	359 (1181)	474 (1559)	703 (2314)
\bar{q} , N/m ² (lb/ft ²)	22,645 (475)	14,745 (310)	27,675 (580)	20,300 (425)	36,535 (765)	34,855 (730)
C_L	0.1614	0.1748	0.1163	0.1325	0.0857	0.0841

Fig. 37 Flight test data for XB-70 used for verification [66].

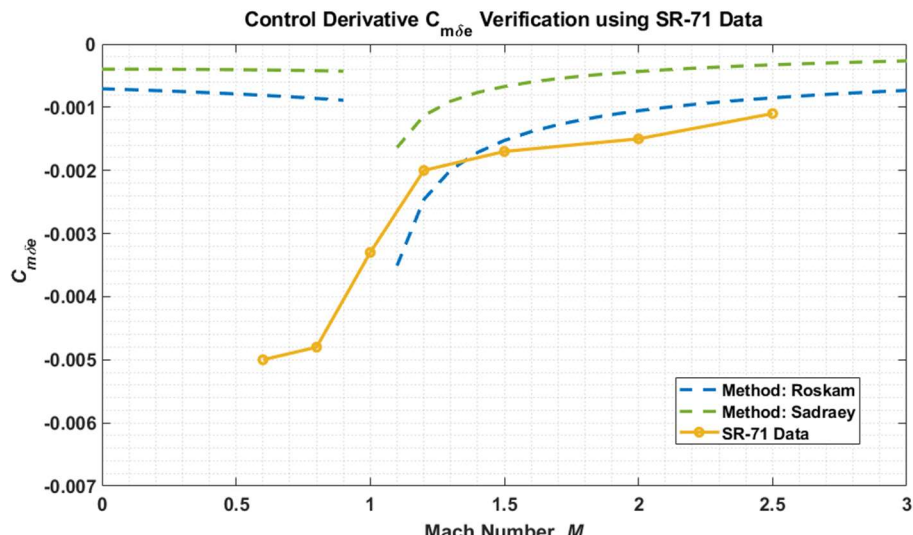
(1)	(2)	(3)	(4)	(5)	(6)	(7)	(8)
Table 4		Table 5			-----		
Case number	$(C_m)_w f_R$	$(\bar{C}_m)_R$ (1)	$(\frac{F}{R})_{(C_m)_w}$	$(\frac{F}{R})_{\bar{C}_m}$	$(\frac{F}{R})_{C_m}$	$(C_m)_R =$ $(2) + (3) \frac{1}{57.3}$ per deg	$(C_m)_F =$ $(2)(4) + (3)(5) \frac{1}{57.3} =$ $(6)(7)$, per deg
SC-1	-0.42680	0.19727	0.941	1.201	0.717	-0.00400	-0.00287
SC-2	-0.39157	.19706	.943	1.124	.760	-.00339	-.00258
SC-3	-.55483	.19476	.906	1.290	.700	-.00628	-.00439
SC-4	-.60661	.19731	.926	1.229	.780	-.00714	-.00557
SC-6	-.34879	.15627	1.019	1.284	.803	-.00336	-.00270
SC-7	-.26654	.10951	.990	1.141	.885	-.00274	-.00242

Fig. 38 XB-70 pitching moment derivative data for given Mach (Column 7) [66].

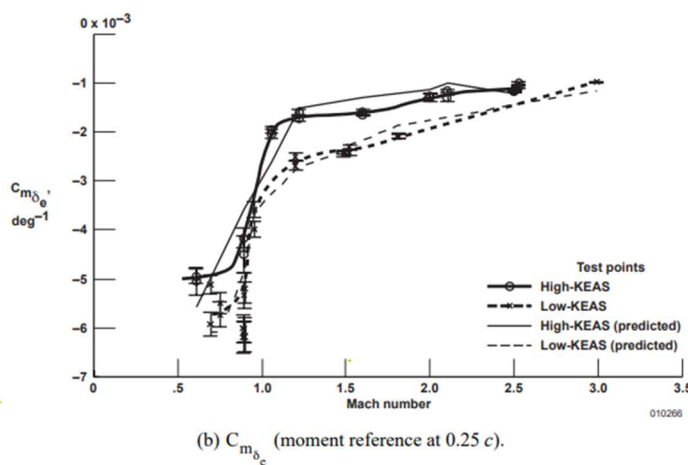
The method from Nicolai needs to be further verified since not enough data is available for XB-70 neutral point locations during flight. Additionally, our aircraft concept will not be having a canard, so Nicolai at least gives a good approximation for subsonic and supersonic. This method will be used until a better method is found that can be verified.

Subsonic, supersonic & hypersonic - $C_{m\delta_e}$

For this control derivative, there are two methods: a subsonic method given in Roskam, and a generic method given in the text by M. Sadraey. These methods will be extended to supersonic and hypersonic regimes since they are a function of aerodynamic coefficients. These coefficients can be obtained from respective teams as a function file for different speed regimes. For the current analysis, methods given in Nicolai were used to estimate the subsonic and supersonic $C_{L\alpha}$. As seen in **Fig. 40**, the subsonic portion of control derivative data is not available for the SR-71 experiment conducted by LASRE. Subsonic values for this method are too high.


Fig. 39 Elevon control derivative verification using SR-71 data

This could be due to the method used to calculate $C_{L\alpha}$. During CE, this term will be an input given to S&C team by the Aerodynamics team. The $C_{L\alpha}$ data was not available for this experiment, hence the method by Nicolai was added to the verification. The gap at Mach 1 in **Fig. 39** is due to the use of supersonic linear theory. According to the reference [21], the C.G. range was from $0.173c$ to $0.258c$ for the flight test data, where c is the mean aerodynamic chord of the aircraft. The main points were picked from **Fig. 40** for a given Mach number and plotted onto **Fig. 39** for comparison. The geometric data for SR-71 was taken from the online flight manual [52]. The exact data used is given in the code in the S&C Appendix . Based on the results above, both methods give a similar approximate result. Hence, Sadraey's method will be used for the calculation of this control derivative in subsonic & supersonic regime.


Fig. 40 Flight test results for baseline SR-71 configuration from LASRE [21].

To verify this elevon control derivative for hypersonic speeds, the data from Space Shuttle Orbiter is available. It is particularly applicable at descent phase when the aircraft is re-entering the atmosphere by glide flight. It is not the best available verification method, however, its WB configuration and glide to landing are being considered to be a useful comparison.

For this verification, code from Aerodynamics module was used to calculate $C_{L\alpha}$ at hypersonic regime since there was no data available for $C_{L\alpha}$. The angle of attack was varied, and the data was compared to the corresponding Mach number to obtain a plot for $C_{m\delta_e}$. The following are the assumptions/considerations:

- Mach number range from 4 – 10 was correlated.
- The wing root chord was needed for the analysis. It is assumed to be $\frac{3}{4}$ of the reference body length from **Fig. 41**. Elevon chord is assumed to be 5% of reference length.
- Total elevon area was used for volume coefficient calculation. The moment arm is assumed to be 20% of the reference length. All units are converted to SI units.
- The angle of attack, since it dependent on C_L calculation is varied from 5° to 40° , given in reference [68] for Mach number range of 1 – 10. Given in

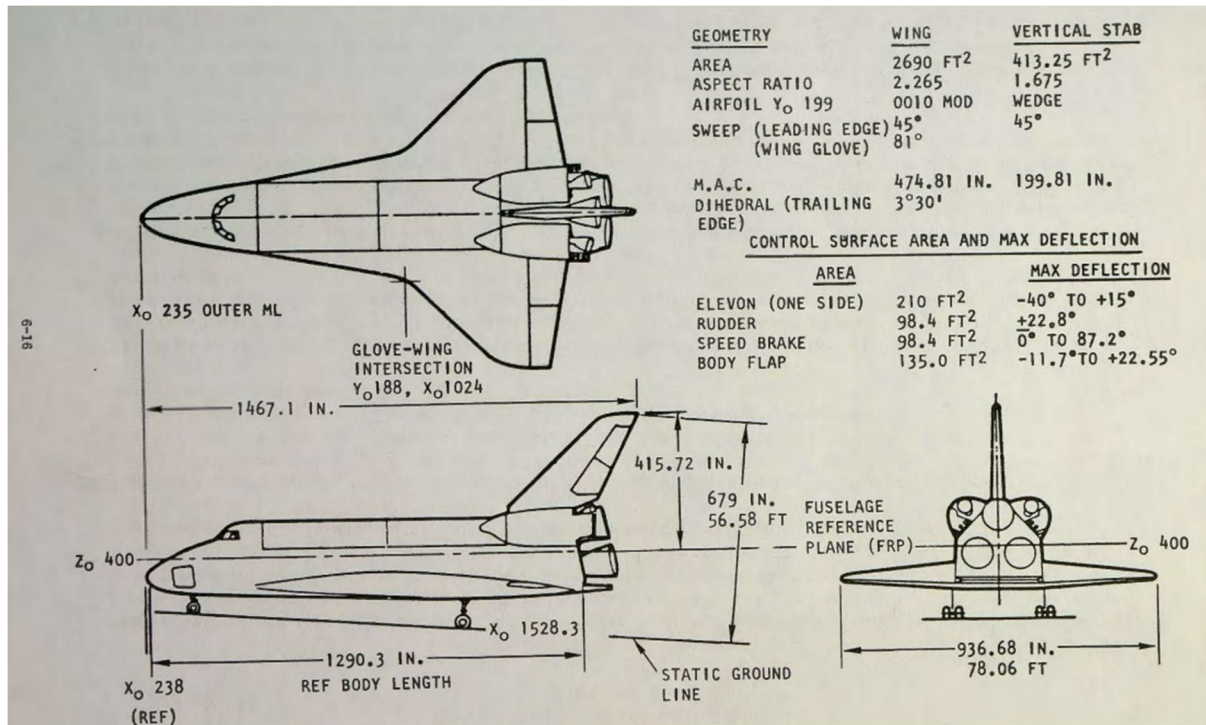


Fig. 41 Dimensions used for Space Shuttle Orbiter [50].

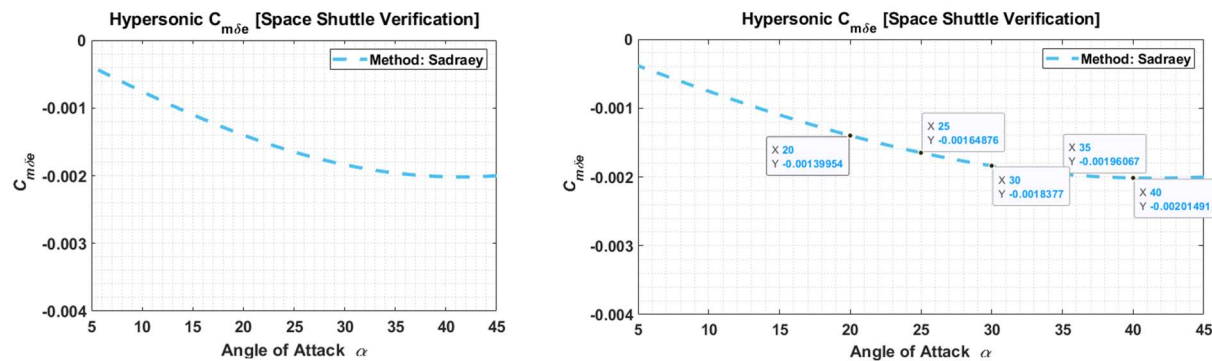


Fig. 42 Hypersonic elevon control derivative, same plots with chosen points for verification.

There was no analysis that directly related $C_{m_{\delta_e}}$ to Mach number. Hence, points were chosen from **Fig. 43 (b)** for the given Mach numbers and the angle of attack values at these Mach numbers were compared to **Fig. 43 (a)**, results are presented in Table 10. The following plots given in were used from reference [68] to find comparison points for relating the control derivative with Mach number range.

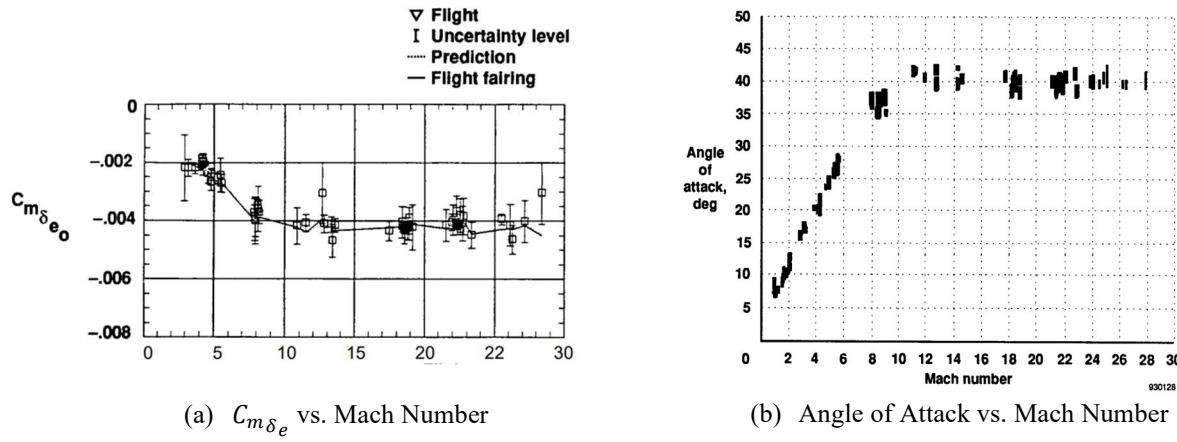


Fig. 43 Method verification plots used from Space Shuttle Orbiter data [68].

Table 10. Results from Space Shuttle hypersonic elevon control derivative [68].

Mach Number	α [°]	Sadarey $C_{m_{\delta_e}}$ [°]	Space Shuttle $\sim C_{m_{\delta_e}}$ [°]	% Error
10	40	-0.002198	-0.0040	45.05
8	35	-0.002139	-0.0040	46.53
6	30	-0.002005	-0.0030	33.17
5	25	-0.001798	-0.0025	28.08
4	20	-0.001527	-0.0020	23.65

As seen from Table 10, the error increases as the Mach number increases. Values for Space Shuttle data are approximate numbers extracted from **Fig. 43 (a)**. One reason for such high error is the use of C_L calculation from Aerodynamics module. This method uses Newtonian flat plate theory for very basic approximation of lift coefficient in hypersonic flow assuming a flat plate. Due to the generic nature of this method, which is mostly dependent on $C_{L\alpha}$, this method will be used for hypersonic regime.

4.10.2 Lateral and Directional Verification

The lateral and directional method verification was carried out by S&C team member Carlos Carmona [67]. The verification vehicle chosen is the Space Shuttle Orbiter during descent. The reason for choosing this aircraft for method verification is because the aircraft closely falls into the WB configuration category.

4.11 Sizing Results for S&C.

This portion of the report covers control surface sizing. This is a process that starts in Configuration Layout (CL) where the most suitable control surfaces are chosen to layout a vehicle design. Then, initial estimates of these control surfaces are made to be given to the Geometry team. During Configuration Evaluation (CE) phase, the sizes are checked to see if they can endure the most critical flight conditions. The author has chosen to combine the CL and CE section of this report to keep the flow of the design approach taken. Since both these phases were conducted almost simultaneously, it only makes sense to keep this section together. All 6 design points were chosen by the Synthesis team during week 8, and configuration layout was performed by all disciplines for single flow vehicles first. The following Table 11 and Table 12 are the single and dual flow path dimensions obtained from PS. During CL, the S&C team will be working with Geometry team members to provide initial control surface estimates for elevons & vertical tails. The code for initial estimates has been completed and provided in Appendix D. Only results for control surfaces and assumptions made are provided in this section.

Table 11. Results from PS for Single Flow Path design points [11,12,69]

Variable	units	Mach 5	Mach 7.5	Mach 10
TOGW	kg	119,587	148,864	2046,073
Spln	m ²	268.08	333.35	458.44
OWE	kg	39,488	48,422	65,261
OWE	kg	38,779	47,661	64,593
τ	-	0.059	0.052	0.043
KW	-	2.670	2.670	2.680
Swet	m ²	716.73	891.12	1,228.40
Vtot	m ³	258.98	316.49	422.07
Aircraft length	m	25.826	28.800	33.770
SD	m	6.920	7.720	9.050
Aircraft width	m	3.460	3.860	4.520
Total span	m	17.30	19.29	22.62
Span	m	13.84	15.43	18.90
Fuselage pln	m ²	89.36	111.12	152.81
Wing area	m ²	178.72	222.24	305.63
Aspect ratio	-	1.67	1.67	1.67
T/W	-	0.81	0.81	0.81
W/S	kg/m ²	499.04	499.04	499.04

Table 12. Results from PS for Dual Flow Path design points [11,12,69]

Variable	units	Mach 5	Mach 7.5	Mach 10
TOGW	kg	150,213.346	180,956.345	235,178.534
Spln	m ²	336.508	404.729	524.558
OWE	kg	51,570.490	58,574.275	75,313.900
OWE	kg	50,883.986	58,556.431	74,615.908
τ	-	0.052	0.046	0.041
KW	-	2.673	2.677	2.682
Swet	m ²	899.632	1083.352	1406.868
Vtot	m ³	320.994	374.546	492.576
Aircraft length	m	28.935	31.733	36.126
SD	m	7.753	8.503	9.680
Aircraft width	m	3.877	4.251	4.840
Total span	m	19.383	21.257	24.200
Span	m	15.506	17.006	19.360
Fuselage pln	m ²	112.169	134.910	174.853
Wing area	m ²	224.339	269.819	349.705
Aspect ratio	-	1.675	1.675	1.675
T/W	-	0.81	0.81	0.81
W/S	kg/m ²	446.388	447.105	448.337

The elevon and rudder design codes were completed using reference [28]. The logic used, inputs needed, requirements set, and outputs given to other teams are given below in Fig. 44.

The elevon sizing logic was modified since the W&B team member Noah Blakely notified us that the C.G. location cannot be moved at takeoff as the aircraft has full fuel. Hence, the C.G. location was fixed and a landing gear location range provided by Structures team member Jared Couldren was iterated to find feasible elevon deflection angles corresponding to a given elevon area [70].

With the given estimates from CL for vertical tails and elevons, the values were tested in the sizing process for the most critical conditions during flight. For elevons, this was during takeoff rotation and for vertical tails, three critical conditions were chosen to evaluate against:

- Multiple engines out from the fuselage centerline during takeoff
- Inlet unstarts during cruise. Here, the thrust is quite high from the ramjet and/or scramjets, so it is a check.
- Crosswind landings.

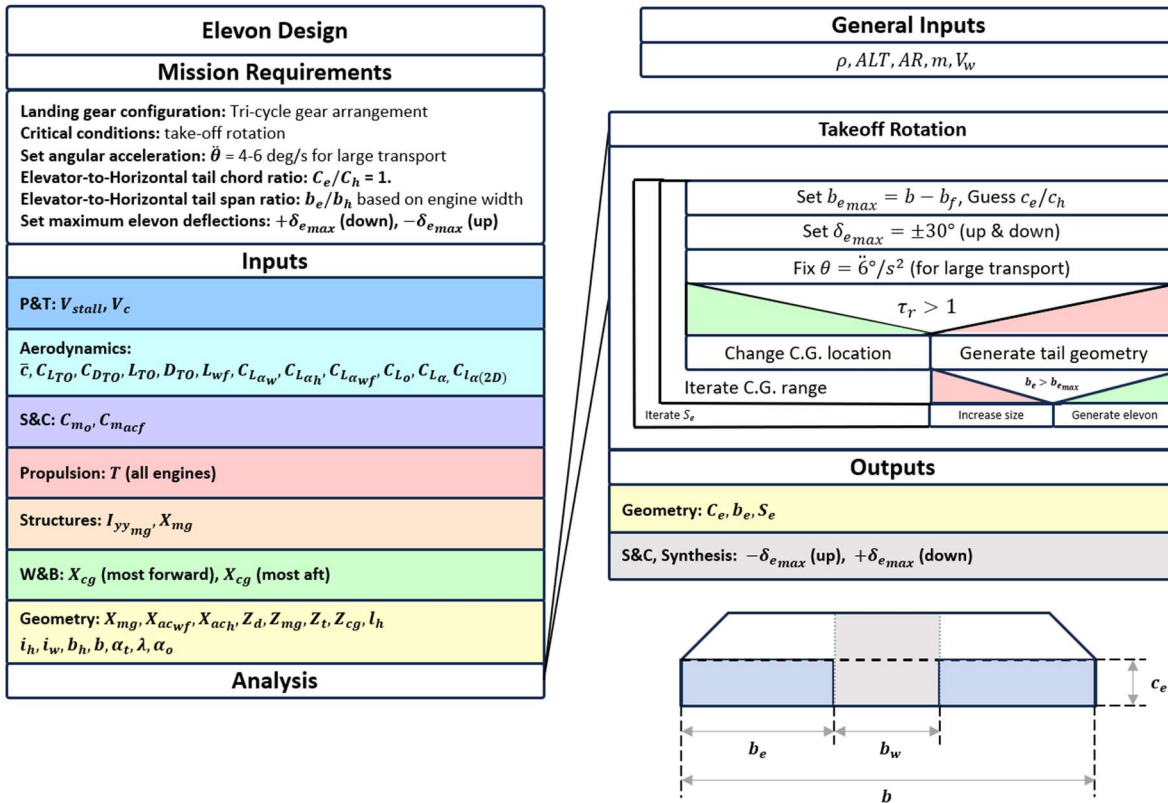


Fig. 44 Elevon design procedure [28].

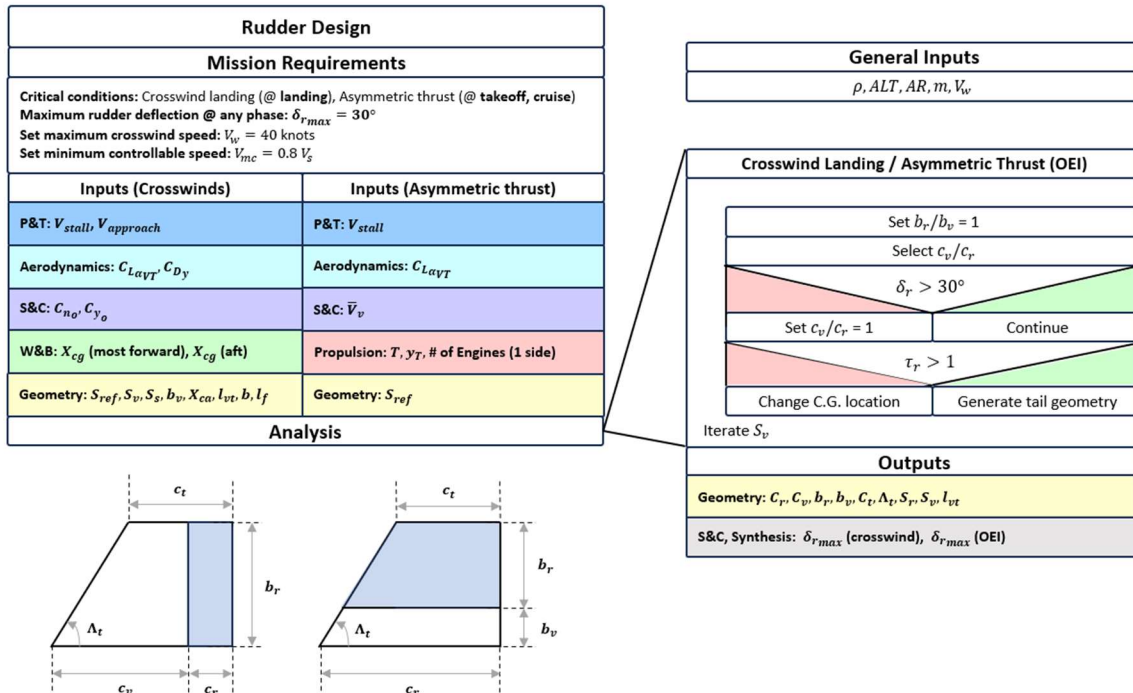


Fig. 45 Vertical tail and rudder design procedure [28].

4.11.1 Inputs obtained from other disciplines

For S&C, many inputs were given by other disciplines. This section gathers and presents all data given for analysis by the other disciplines. Firstly, all the CAD models shown throughout this section have been provided by Geometry team member Austin Prior [69]. With the CAD models obtained after CL, dimensions were extracted from the author as there were many specific lengths needed for elevon and rudder sizing. As of the report writing, the CAD model for single flow Mach 5.0, 7.5, and 10 as well as dual flow Mach 5.0 and 7.5 were provided to S&C. The Mach 10 design is being debated as the team is considering the vehicle to be infeasible.

The W&B team member Noah Blakely has provided C.G. locations for S&C given in Fig. 46Fig. 48 below. Due to issues with weight ratios provided by the P&T team, these locations were warned to be incorrect. However, due to time constraints, these initial values were used to generate outputs, as it is very difficult for S&C team to redo this for all vehicles by changing all inputs in a short notice.

TO	Component	CG Distance From Nose (m)	Weight (kg)	Moment (kg*m)
	Total Aircraft	14.55675512	117183.64	1705813.61
Climb S	Component	CG Distance From Nose (m)	Weight (kg)	Moment (kg*m)
f	Total Aircraft TOGW	14.3203661	113668.13	1627769.303
a	Total Aircraft TOGW	14.88603621	113668.13	1692067.968
Cruise S	Component	CG Distance From Nose (m)	Weight (kg)	Moment (kg*m)
f	Total Aircraft (Fore)	12.63895862	81866.95	1034713.051
a	Total Aircraft (Aft)	17.72259215	81866.95	1450894.646
Cruise E	Component	CG Distance From Nose (m)	Weight (kg)	Moment (kg*m)
f	Total Aircraft (Fore)	16.94100099	59876.02	718655.3273
a	Total Aircraft (Aft)	16.94100099	59876.50	1099047.422

Fig. 46 W&B C.G. location results for Mach 5.0 configurations, for single and dual flow [12].

Component	CG Distance From Nose (m)	Weight (kg)	Moment (kg*m)
Total Aircraft	16.01274658	153399.26	2456343.452
Component	CG Distance From Nose (m)	Weight (kg)	Moment (kg*m)
Total Aircraft TOGW	15.71314081	148797.28	2338072.623
Total Aircraft TOGW	16.33788308	148797.28	2431032.574
Component	CG Distance From Nose (m)	Weight (kg)	Moment (kg*m)
Total Aircraft (Fore)	15.06120548	139679.12	2103735.975
Total Aircraft (Aft)	17.04537266	139679.12	2380882.708
Component	CG Distance From Nose (m)	Weight (kg)	Moment (kg*m)
Total Aircraft (Fore)	19.2695301	53296.68	1027001.931
Total Aircraft (Aft)	19.2695301	53296.68	1027001.931

Fig. 47 W&B C.G. location results for Mach 7.5 configurations, for single and dual flow [12].

The single and dual flow paths are both to have the same C.G. location estimates, as informed by W&B team.

Component	CG Distance From Nose (m)	Weight (kg)	Moment (kg*m)
Total Aircraft	18.46771462	377538.12	6972266.26
Component	CG Distance From Nose (m)	Weight (kg)	Moment (kg*m)
Total Aircraft (Fore)	17.33124139	345351.93	5985377.731
Total Aircraft (Aft)	18.0747255	345351.93	6242141.406
Component	CG Distance From Nose (m)	Weight (kg)	Moment (kg*m)
Total Aircraft (Fore)	15.81810253	309928.33	4902478.035
Total Aircraft (Aft)	19.23765724	309928.33	5962294.903
Component	CG Distance From Nose (m)	Weight (kg)	Moment (kg*m)
Total Aircraft (Fore)	11.86824812	152701.69	1812301.499
Total Aircraft (Aft)	26.09801272	152701.69	3985210.548

Fig. 48 W&B C.G. location results for Mach 10.0 configurations, for single and dual flow [12].

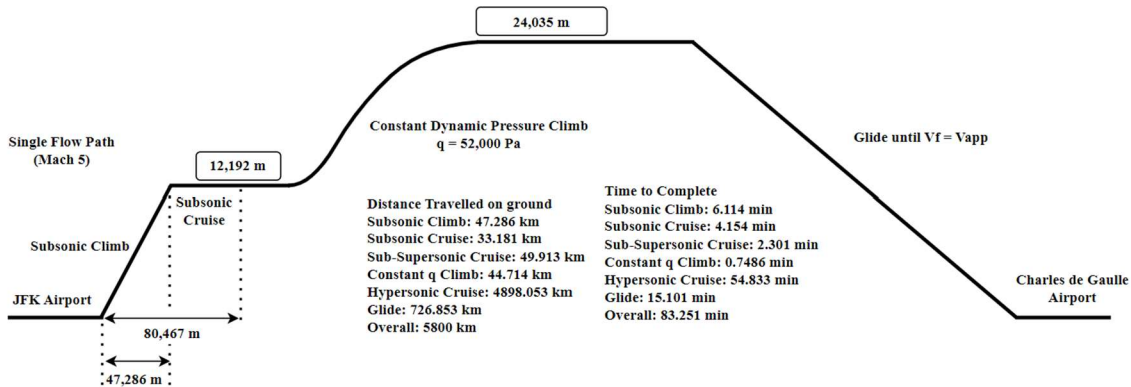
Landing gear location ranges were provided by Structures team member Jared Coultron [70]. As of the report writing, the ranges for single flow path vehicles were provided along with their corresponding landing gear heights, and moment of inertia of landing gear about principal y-axis. The values obtained are summarized in Table 13 below. Due to time constraints, landing gear locations for dual flow path vehicles were not provided by the Structures team, hence, the single flow ranges were used for dual flow path vehicles.

Table 13. Landing gear information provided by Structures team for single flow paths [70].

Parameter	Units	AX-105	AX-175	AX-110
Distance from C.G. to main gear, forward location	m	1.367	1.71	2.195
Distance from C.G. to main gear, aft location	m	2.38	2.98	3.82
Landing gear height	m	5.104	6.382	8.193
Moment of inertia about y-axis	kg/m ²	8335.9		
Landing gear mass	kg		3000	3000

The T&P team member Shiori Jo provided takeoff velocity, stall speed at takeoff, takeoff distance and approach speeds needed for takeoff and landing sizing conditions, given in **Fig. 49** [71]. Additionally, trajectories for all vehicles are in **Fig. 50****Fig. 55**.

Mach	Takeoff Velocity (m/s)	Stall Speed (m/s)	Takeoff Distance (m)	Approach Speed (m/s)	Landing Distance (m)
10	121.3586	86.6847	1685.488	112.69	2248.003
7.5	121.3586	86.6847	1685.744	112.69	2248.003
5	121.3586	86.6847	1686	112.69	2248.003

Fig. 49 P&T results needed for S&C sizing and evaluation [71].

Fig. 50 P&T trajectory results for Mach 5 single flow path [71].

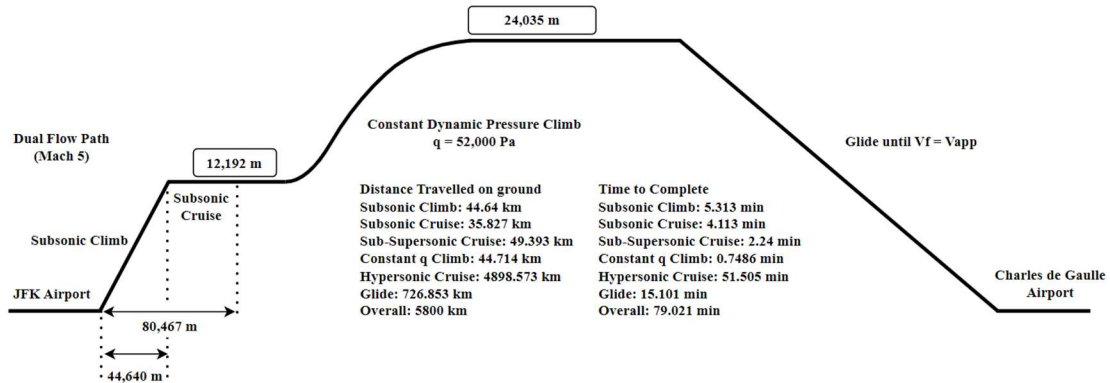


Fig. 51 P&T trajectory results for Mach 5 dual flow path [71].

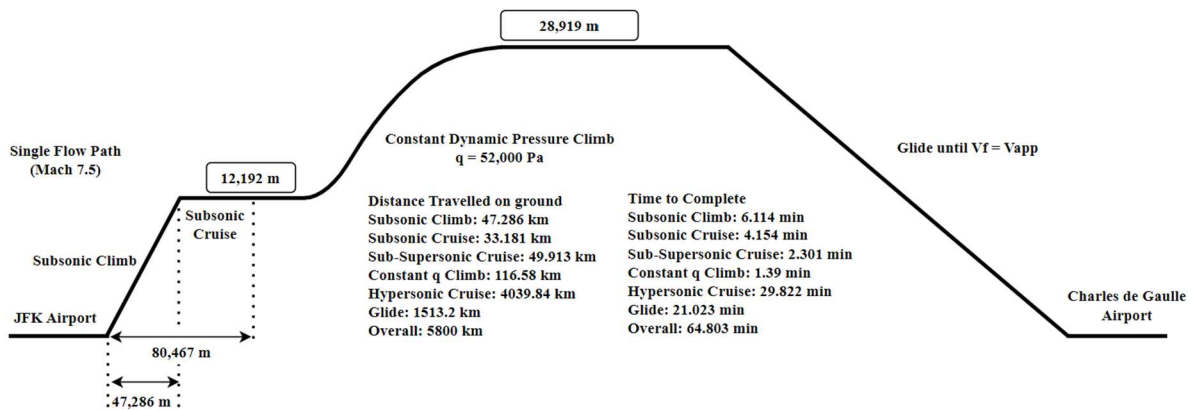


Fig. 52 P&T trajectory results for Mach 7.5 single flow path [71].

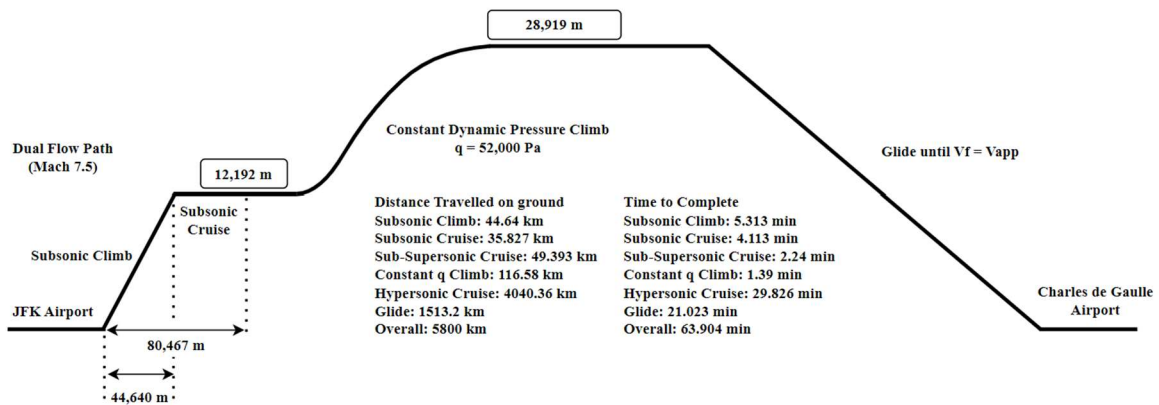


Fig. 53 P&T trajectory results for Mach 7.5 dual flow path [71].

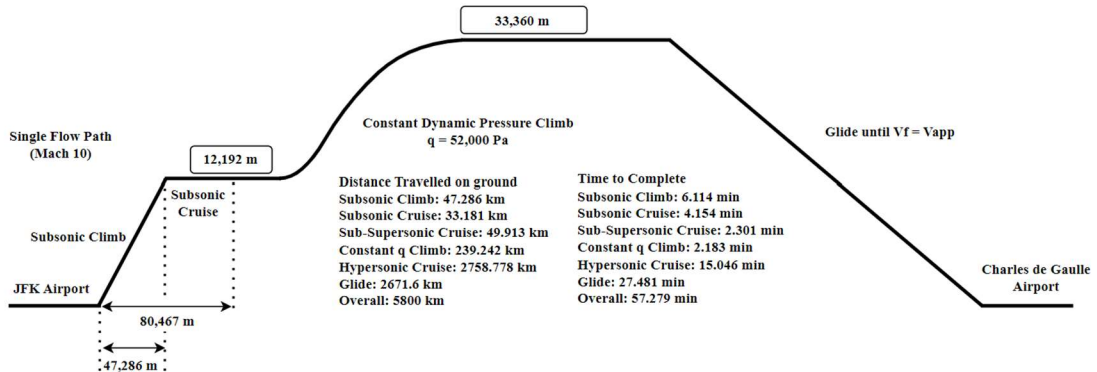


Fig. 54 P&T trajectory results for Mach 10.0 single flow path [71].

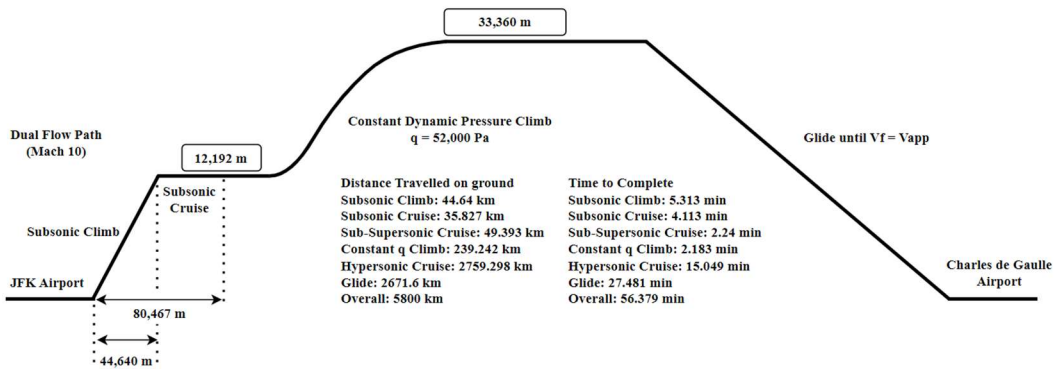


Fig. 55 P&T trajectory results for Mach 10.0 dual flow path [71].

The Propulsion team provided thrust at takeoff values for single and dual flow paths along with number of turbine engines being used. The tabulated outputs given by the Propulsion team are given in Appendix A. The Propulsion team has provided a number of ramjets and/or scramjets for all flow paths, however thrust values given are at cruise only. The values used thrust are the thrust required that equal to cruise drag is assumed for S&C analysis. For climbs, thrust was assumed to be 10% greater than the overall drag as excess thrust estimates were not provided to the Propulsion team. The values pertaining to S&C analysis are summarized in Table 14.

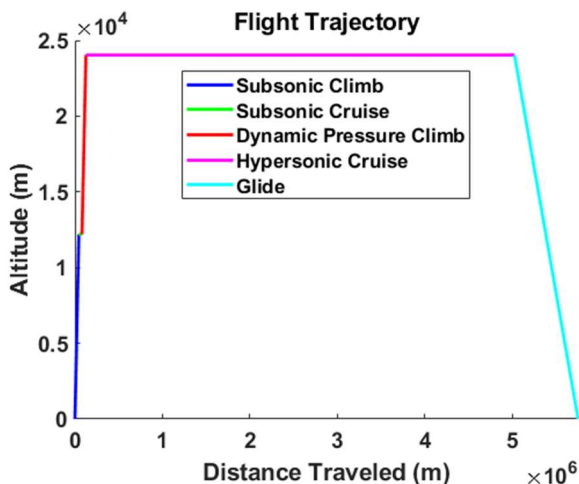


Fig. 56 Flight trajectory for distance travelled [72].

The flight trajectory for the distance travelled was provided by Aerodynamics team member Benjamin Jones [72]. This allows for visualizing the actual climb profiles for the vehicles. Additionally, angle of attacks for the whole mission profile were given. This allowed for easily guessing angle of attack angles for trim EOM analysis in Section 4.12.

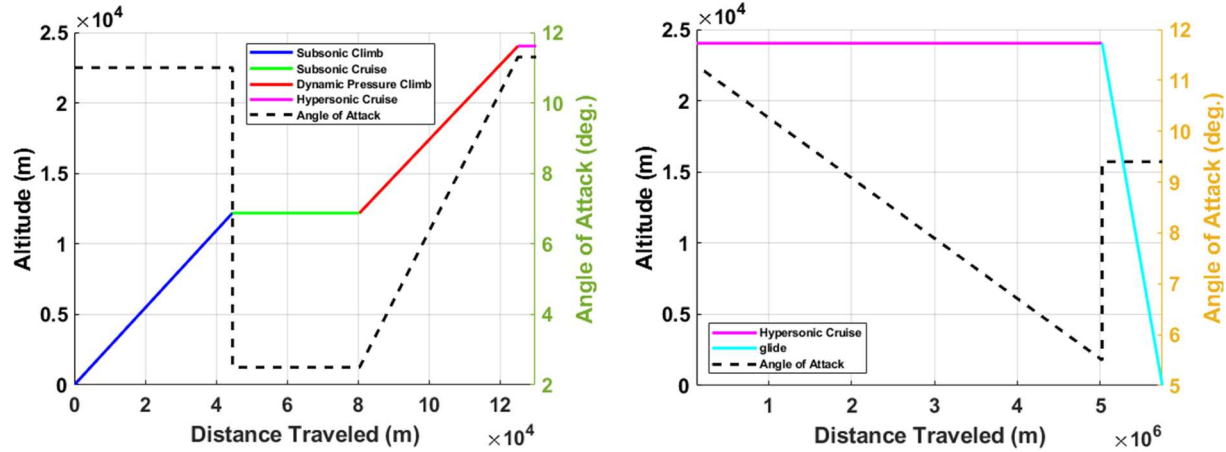


Fig. 57 Angle of attacks as a function of trajectory [72].

The subsonic and hypersonic lift curve slopes were provided by Aerodynamics team for Mach 5 configurations, given below in Fig. 58.

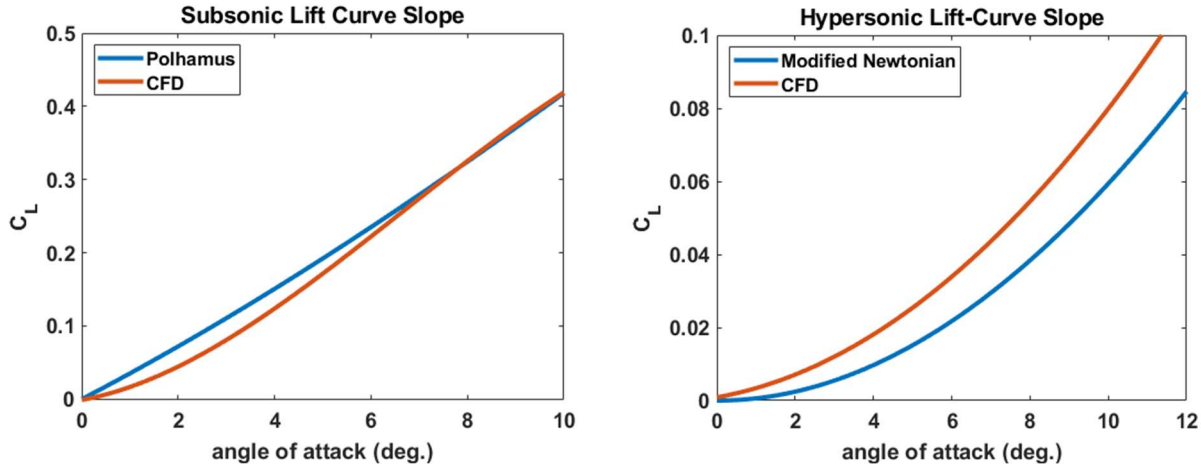


Fig. 58 Lift-curve-slope given for Mach 5 configuration [72].

Lastly, S&C team member Carlos Carmona provided with MATLAB functions for $C_{l\beta}$, $C_{n\beta}$, $C_{l\delta r}$, $C_{l\delta a}$, $C_{n\delta r}$ for all the speeds, from subsonic to hypersonic after verifying all the methods chosen. The MATLAB functions for longitudinal coefficients, $C_{m\alpha}$ and $C_{m\delta e}$ was written by the author for trim analysis and sizing conditions. Additionally, the Aerodynamics team was asked to provide MATLAB functions for lift and drag coefficients from subsonic to hypersonic speed regimes. These functions were incorporated into the trim analysis code. The following is the list of values used in Table 14.

Table 14. List of Dimensions Used.

Parameter	Units	AX-105	AX-175	AX-110	AX-205	AX-275
Initial Inputs						
mass	kg	119587	148864	206073	150213.346	180956.345

	SENIOR DESIGN: MAE 4351 Project	Ref.: MAE 4351-001-2021 Date: 11. Aug. 2023 Name: Gayathri Kola Status: Complete
---	--	---

AR	-	1.67	1.67	1.67	1.67	1.67
Sref	m ²	178.72	169.5	234.21	188.1	223.12
aoa @ TO	deg	11.1	12.4	11	11	11
lref	m ²	25.826	28.8	33.77	28.94	32.13
Cbar	m	16.667	18.586	21.66	18.6	20
CL	-	0.52	0.585	0.5866	0.515	0.641
CD	-	0.3519	0.35	0.3613	0.355	0.367
Claoa	-	2.65	2.70307	3.361	2.9985	3.0605
Claoah	-	2.389	2.65	3.361	2.9985	3.0605
No. of turbines	-	5	5	8	4	6
Thrust @ TO	kg	64977.57	94865.89	151785.4	75892.71	113839.1
Xmg1	m	16.5	17.72	20.665	16.5	17.72
Xmg2	m	18.3	19	22.29	18.3	19
Xcg	m	14.5	16.012	18.47	14.51	16.012
Neutral point	m	15.75	14.4	17.52	14.94	17.13
Zd	m	2.41	4.47	7.36	4.02	5.48
Zt	m	2.41	4.47	7.36	4.02	5.48
Zcg	m	5.104	6.38	8.193	5.104	6.38
LG height	m	5.104	6.382	8.193	5.104	6.382
LG mass or Iyy	kg	8339	1500	1500	8339	1500
theta_dot_dot	m/s ²	6	4	6	6	6
Cr	m	25	27.88	32.5	28	30
b	m	14.7	19.02	23.68	16.46	22.57
bf	m	4.49	5.4	6.07	5	6
Elevon area	m ²	30	15	35	35	40
Fuselage Volume	m ³	248.18	429.51	501.24	333.02	480.43
Vbar_h	-	0.2292	0.1056	0.1718	0.2935	0.2305
Vbar_v	-	0.0914	0.1172	0.0982	0.2098	0.1873
be/bw	-	0.6946	0.7161	0.7437	0.6962	0.7342

4.11.2 AX-110: Mach 10, Single Inlet

The first baseline configuration was chosen from the convergence results by the Synthesis team. The S&C team will be providing control surface dimensions to Geometry team during CL. The following are the design parameters in **Fig. 59** were given by the Synthesis team. Note, the first iteration results given in **Fig. 59** below have since changed. These new Mach 10 results for single flow path are given in Table 11.

Table 5 First iteration design point results

Variable	Value
TOGW	202740 kg
S _{pln}	452.1834
OEW	64789 kg
OWE	63843 kg
τ	0.034
K _W	2.6934
S _{wet}	1217.9 m ²
V _{tot}	326.927 m ³
Aircraft length	33.5417 m
S _Δ	8.9875 m
Aircraft width	4.4937 m
Total span (b _{air})	22.4687 m
Span (b)	17.975 m
Fuselage planform	150.7278 m ²
Visible wing area	301.4556 m ²
Aspect Ratio	1.6747
T/W	0.81

Fig. 59 AX-110 Design point results [11,12,69].

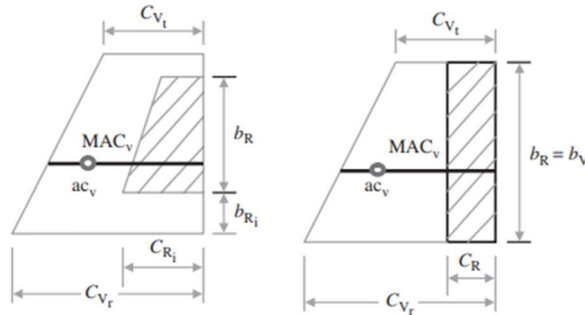


Fig. 60 Vertical tail geometry with rudder [28].

The geometry on the left features a swept rudder enclosed in vertical tail while the right has rectangular rudder. Currently, the rectangular rudder will be chosen for the analysis, in addition to the all-moving tails option. The following segment outlines the process taken by the S&C to outline control surfaces for our first baseline vehicle. While the generic tail volume coefficient method is available, S&C member Carlos Carmona found a more suitable method to estimate the coefficient with the use of NASA Flight Optimization Software (FLOPS). The method outlined in the document is more suitable for high-speed transport vehicles [73]. This method has produced relatively small errors and with this knowledge, the tail volume coefficients will be estimated using these methods [67]. With the tail volume coefficient and tail area results, the tail geometry will be generated using method provided by reference [28]. A simple code was written by the author that generates tail root chord, tip chord, thickness at root and tips, vertical tail span and rudder dimensions.

The AX-110 will have twin vertical tails. The reason for twin verticals comes down to having more roll stability at high speeds. Additionally, a single tail would be very large and has to be located on the aft end of fuselage centerline. This would place the single vertical tail in the fuselage wake region, which may inhibit control authority at high speeds. Two smaller tails placed at a distance from one another can easily avoid this issue, hence they are being used for this design and all other designs. The dihedral the twin tails is being undertaken by Carlos Carmona as a part of lateral stability analysis.

The control surface estimates have been completed and the following outputs were given to Geometry which will be modelled in week 8. These dimensions are based on the current aircraft geometry. Which is presented below as well. A few assumptions were made while calculating the dimensions for elevons and vertical tails:

- The vertical tail sweep is unknown currently; hence, it is assumed to have a value of 33 degrees. Taken from SR-71's dimensions.
- The vertical tail root chord has been assumed to be 25% of total aircraft length.

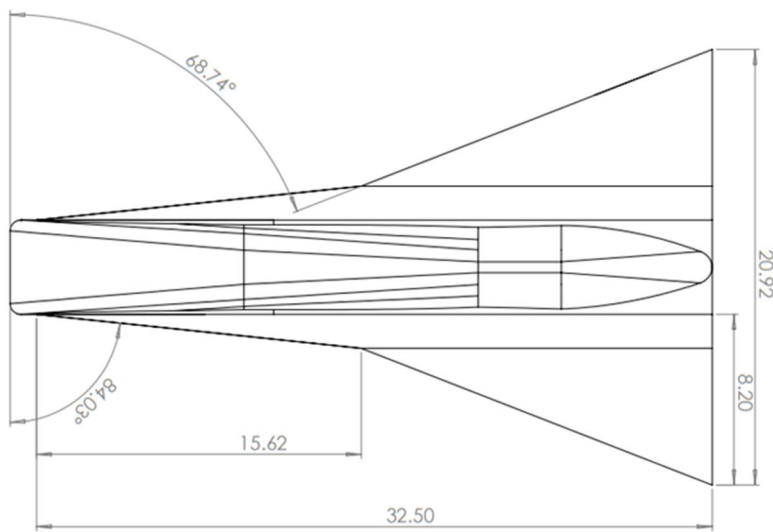


Fig. 61 AX-110 initial dimensions decided by Aerodynamics, Propulsion & Geometry [69].

```
=====1 ELEVON=====
Elevon Shape: Right Trapezoid
Elevon chord: Ce = 0.5420 [m]
Elevon span (on 1 side): be = 8.1977 [m]
Elevon area (single side): Sht = 4.3859 [m^2]

=====1 VERTICAL TAIL=====
Vertical Tail Shape: Right Trapezoid
Vertical Tail Sweep: SweepVT = 33.0000 [deg]
Vertical Tail Root chord (1 tail): Cvr = 8.1250 [m]
Vertical Tail tip chord (1 tail): Cvt = 5.9295 [m]
Vertical Tail height (1 tail): bh = 1.4258 [m]
Vertical Tail root thickness (bottom): tr = 0.2844 [m]
Vertical Tail tip thickness (top): tt = 0.2075 [m]
Vertical Tail area (single side): Svt = 10.0191 [m^2]
>>
```

Fig. 62 AX-110 initial control surface dimensions based on initial geometry [67].

Since the results were given to Geometry team member, the vertical tail height was visibly higher than anticipated. To negate this, the vertical tail's root chord length was increased to have better proportions. Additionally, with a shorter chord length, there was no tip chord for the set sweep angle of 33°. The geometry was modelled by Geometry team. An issue for elevons was that the chord length c_e was notably higher due to reduced wingspan. However, it is anticipated to change in CE when sizing for takeoff and cruise.

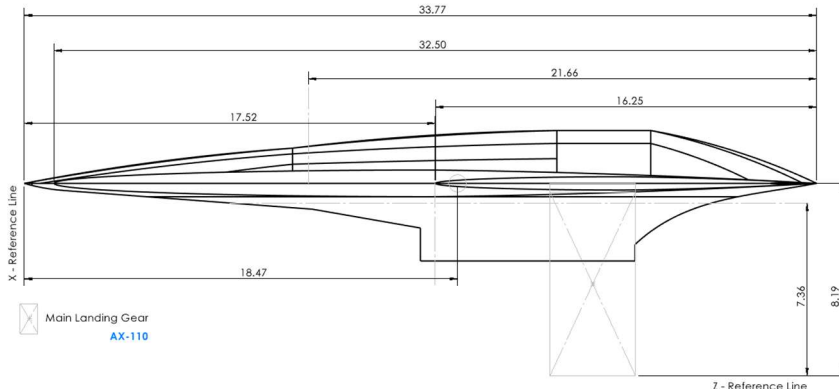
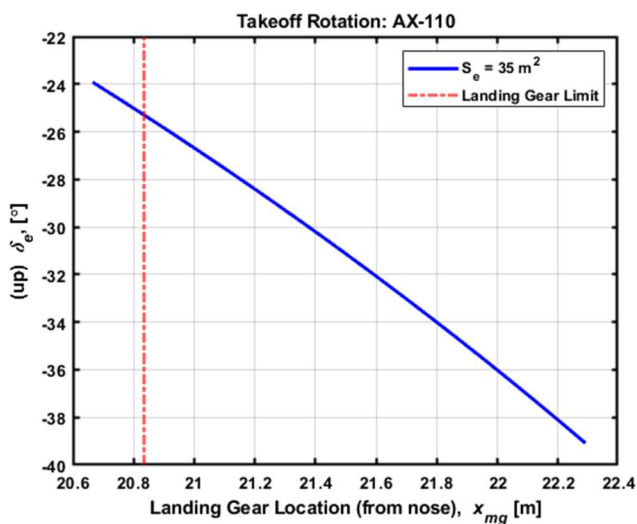


Fig. 63 AX-110 dimensions used for elevon sizing at takeoff [69].



```
AIRCRAFT NAME: AX-110

=====ELEVON @ TAKEOFF ROTATION=====
1 ELEVON AREA = 35.0000 [m^2]
1 ELEVON SPAN = 8.8050 [m]
ELEVON CHORD = 4.6989 [m]
C.G LOCATION FROM NOSE = 18.4700 [m]
A.C LOCATION FROM NOSE = 17.5200 [m]

For lesser than -25 deg elevon deflection:
LANDING GEAR LOCATION BEFORE = 20.8361 [m]
>>
```

Fig. 64 Sized elevons for CE of AX-110.

For vertical tail sizing, the engine-out scenario could not be performed on AX-110 as the aircraft features 4 stacked turbine engines on top of each other on one side as seen **Fig. 65**. Instead, the tails are only sized for inlet unstarts at cruise and the crosswind landing scenario.

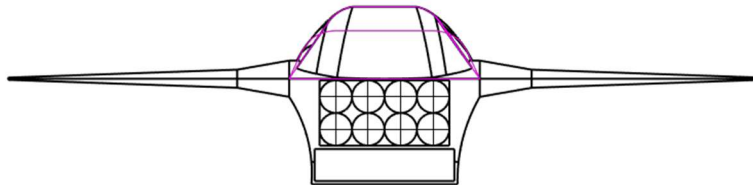


Fig. 65 Stacked turbines of AX-110 [69].

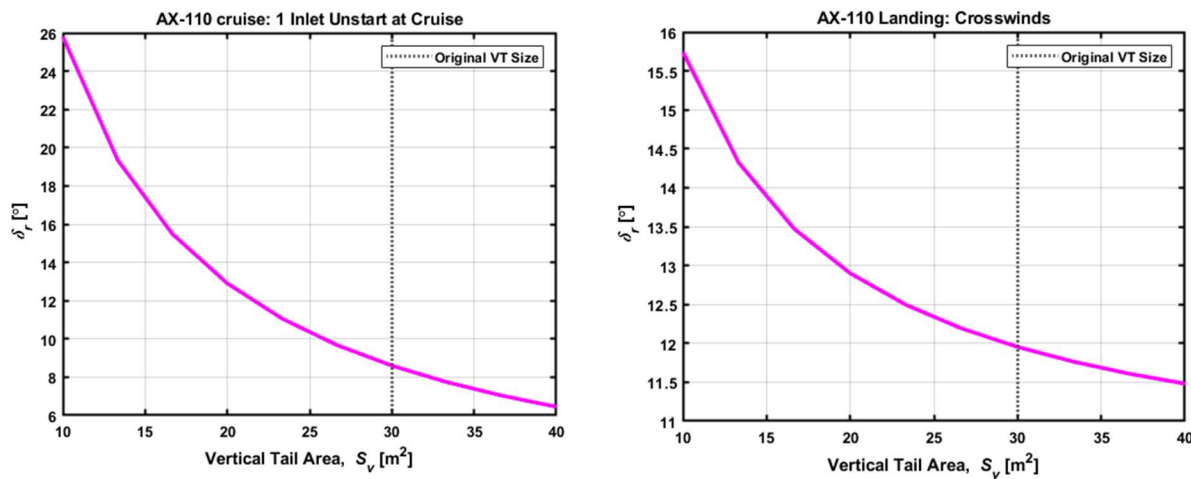


Fig. 66 AX-110 Vertical tail sizing results for inlet unstart and crosswind landing.

The vertical tail sizes will remain unchanged for AX-110 as they are not sized for takeoff engines out condition. With as many as 4 engines, it is anticipated that the CL sizes will be enough for control. For crosswind landing and inlet unstart at cruise, the rudder deflections needed are well below the 25° limit imposed.

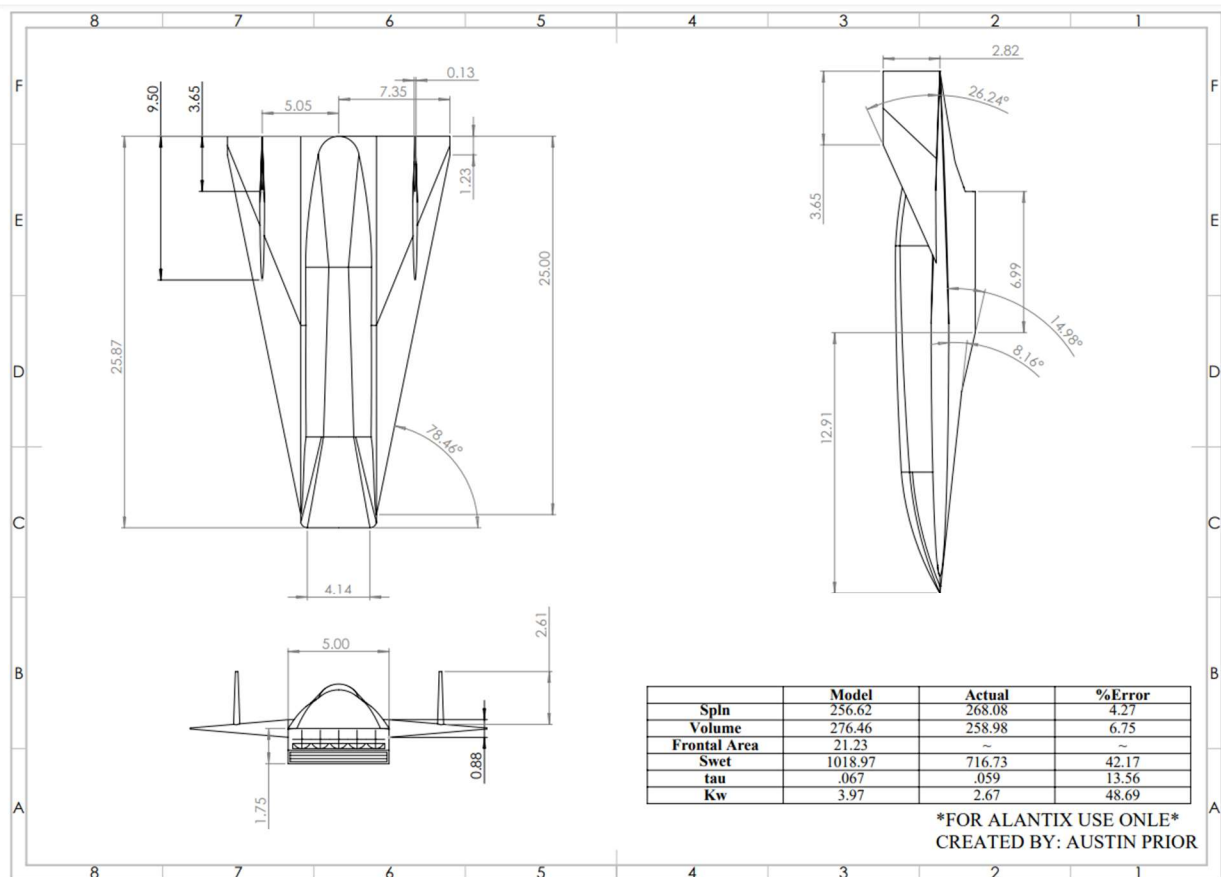
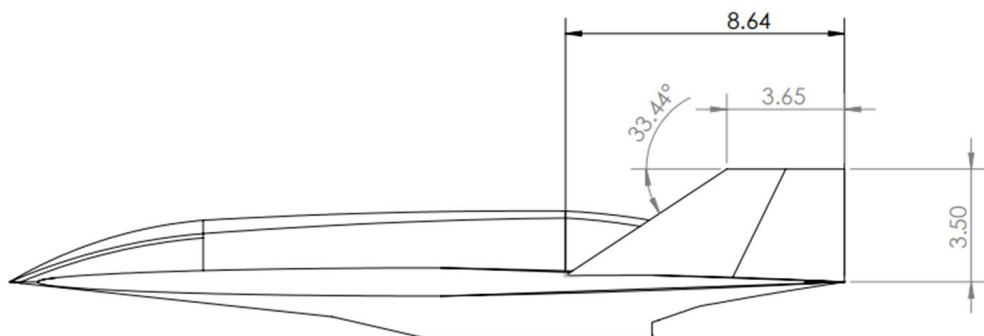
4.11.3 AX-105: Mach 5, Single Inlet

The following dimensions in **Fig. 68** were given by Geometry team member for Mach 5, single flow path design during CL. Based on the dimensions obtained, the initial control surface estimate code generated the control surface dimensions below. These initial areas and geometry will be used in the sizing code for CE.

```
=====1 ELEVON=====
Elevon Shape: Right Trapezoid
Elevon chord: Ce = 1.3012 [m]
Elevon span (on 1 side): be = 9.9130 [m]
Elevon area (single side): Sht = 12.7248 [m^2]

=====1 VERTICAL TAIL=====
Vertical Tail Shape: Right Trapezoid
Vertical Tail Sweep: SweepVT = 33.0000 [deg]
Vertical Tail Root chord (1 tail): Cvr = 9.0391 [m]
Vertical Tail tip chord (1 tail): Cvt = 3.6475 [m]
Vertical Tail height (1 tail): bh = 3.5013 [m]
Vertical Tail root thickness (bottom): tr = 0.3164 [m]
Vertical Tail tip thickness (top): tt = 0.1277 [m]
Vertical Tail area (single side): Svt = 22.2101 [m^2]
>>
```

Fig. 67 Control surface dimensions based on AX-105 geometry given [67].


Fig. 68 Mach 5, Single flow path dimensions from CL [69].

Fig. 69 Mach 5 AX-105 vertical tail geometry [67,69].

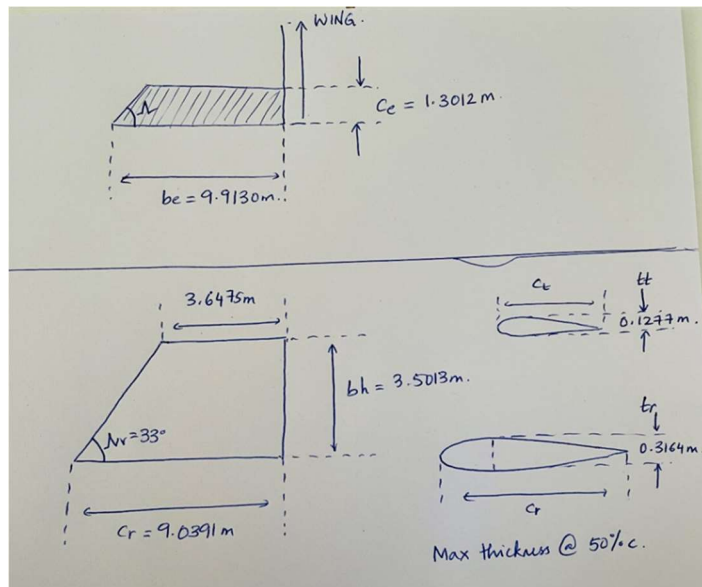


Fig. 70 Hand-drawn control surface definitions given to Geometry.

The **Fig. 68** has a different tail geometry since it was an initial drawing. The new CL dimensions for AX-105 are given in **Fig. 69** above. The initial vertical tail root chord length is assumed to be 30% of the reference aircraft length. This geometry will change based on take-off rotation sizing requirement.

The Mach 5 CAD model was obtained from Geometry team member, Austin Prior [69]. The following dimensions were extracted from the model for S&C's elevon sizing procedure. The definitions of the lengths shown below are given in **Fig. 71**. The most forward and aft C.G. locations were given by W&B team member, Noah Blakely [12] and given in **Fig. 46**. The landing gear was assumed to be located some distance aft the C.G. location for initial sizing. Once the location is obtained by the Structures team, the value will be modified, along with the heights.

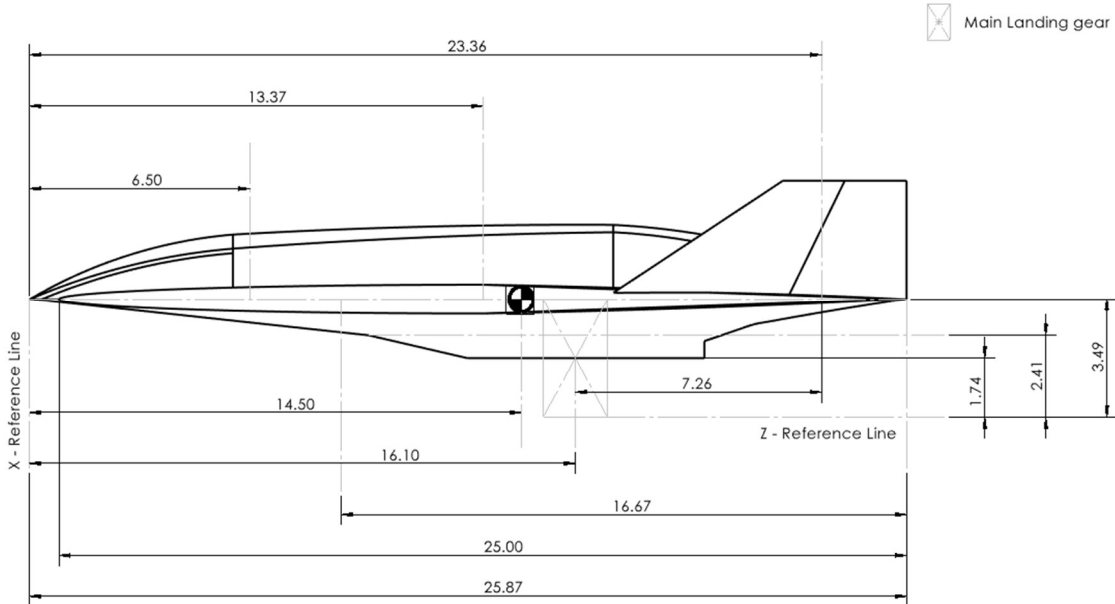


Fig. 71 AX-105 dimensions needed for elevon sizing at takeoff rotation [69].

The drag force is assumed to be acting directly opposite to the engine thrust as seen in **Fig. 72** below at takeoff.

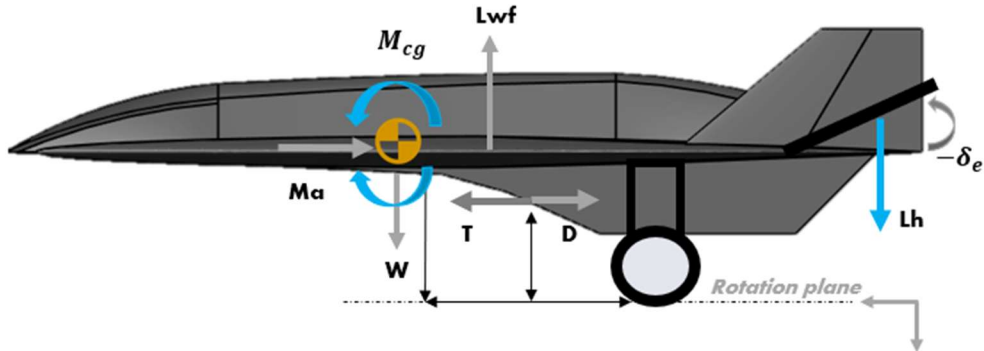


Fig. 72 Simplified moment diagram at takeoff rotation [69].

An angular acceleration value of $\ddot{\theta} = 6^\circ/s^2$ was assumed for all the takeoff rotation analysis based on M. Sadraey's database on similar aircraft weights. The aircraft chosen were within the 150,000 kg to 250,000 kg range.

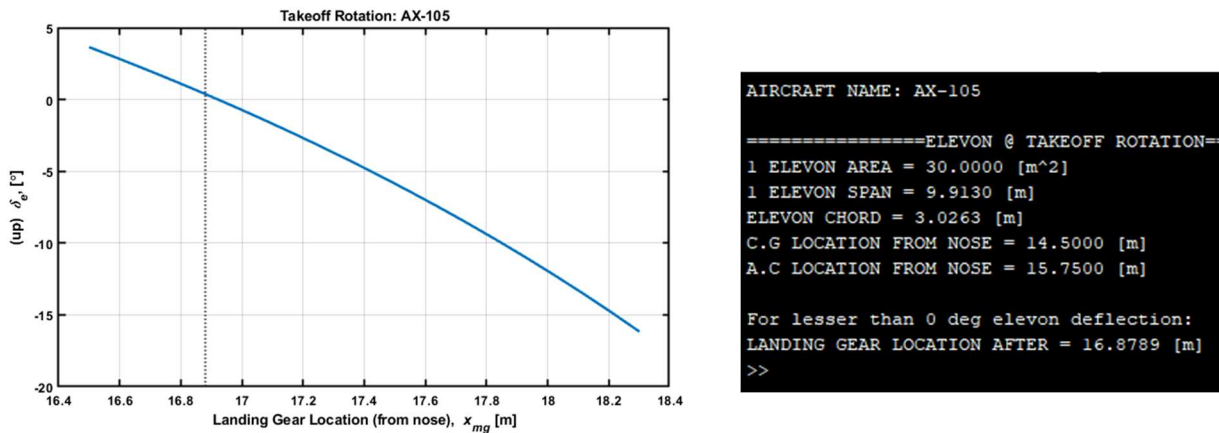


Fig. 73 AX-105 elevon sizing analysis at takeoff rotation – increased elevon size.

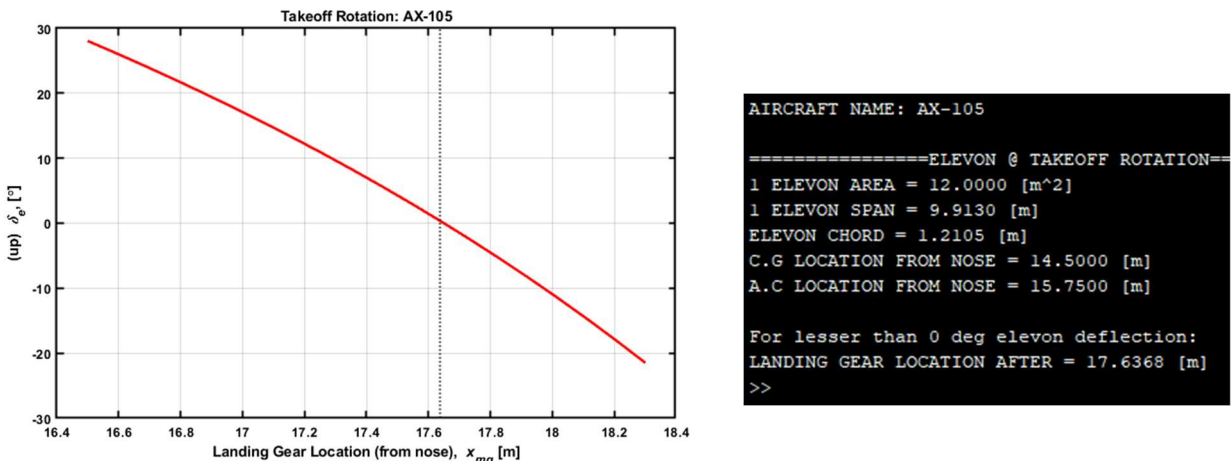


Fig. 74 AX-105 elevon sizing analysis at takeoff rotation – original CL elevon size.

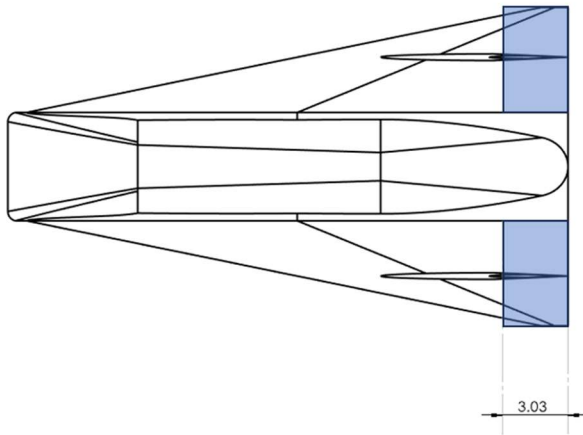


Fig. 75 New elevon size needed for AX-105 to takeoff with given landing gear configuration [69].

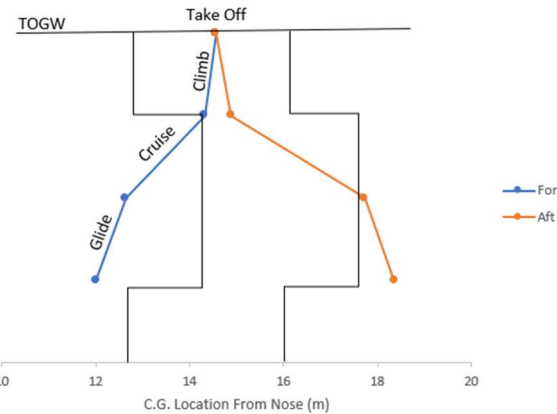


Fig. 76 The C.G. movement with example SM bounds provided by Noah Blakely [12].

The vertical tails were sized once all variables were obtained from all disciplines during week 9. For AX-105, the CL estimates yielded unusually large twin vertical tails. This size seemed to be redundant since it would create an equally large drag as a single vertical tail. While sizing these tails, our main goal in S&C was to reduce its overall size. Following the sizing logic presented in **Fig. 45**, the results below were obtained for engines out scenario.

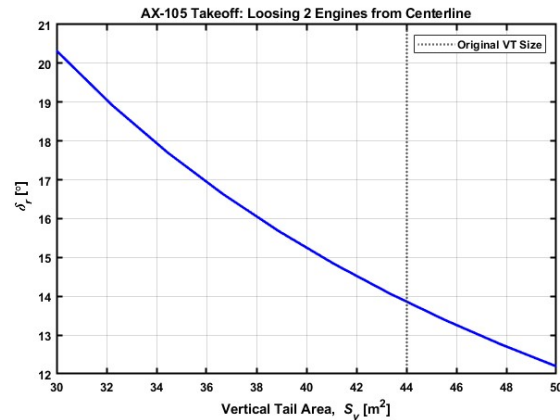
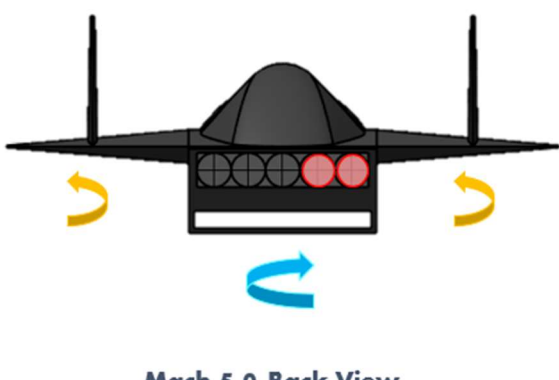


Fig. 77 AX-105 engines out during takeoff [69].

AX-105 has 5 turbine engines for takeoff. Of the five engines, two engines were considered to be lost during engines-out, the engine in the middle will not create any yawing moment as it lies on the axis of the fuselage centerline. The following diagram illustrates an engine failure situation. Given next to it is the corresponding rudder deflection needed for the CL estimated size. The goal is to keep rudder deflection angles less than 25° for structural safety. The rudder must deflect left in this case to create a counterclockwise moment to overcome the yawing moment due to engines lost.

Another phase this condition is checked for is at cruise. The thrust from the ramjets is very high, this can also create large yawing moments. For this vehicle, the Propulsion team informed that there will be two ramjets. The distances for ramjets from the fuselage centerline were extracted from the CAD models. A single inlet was assumed to unstart during cruise, assuming this did not initiate the second inlet to unstart as seen in **Fig. 78**. The results yielded significantly lower rudder deflection angles than takeoff.

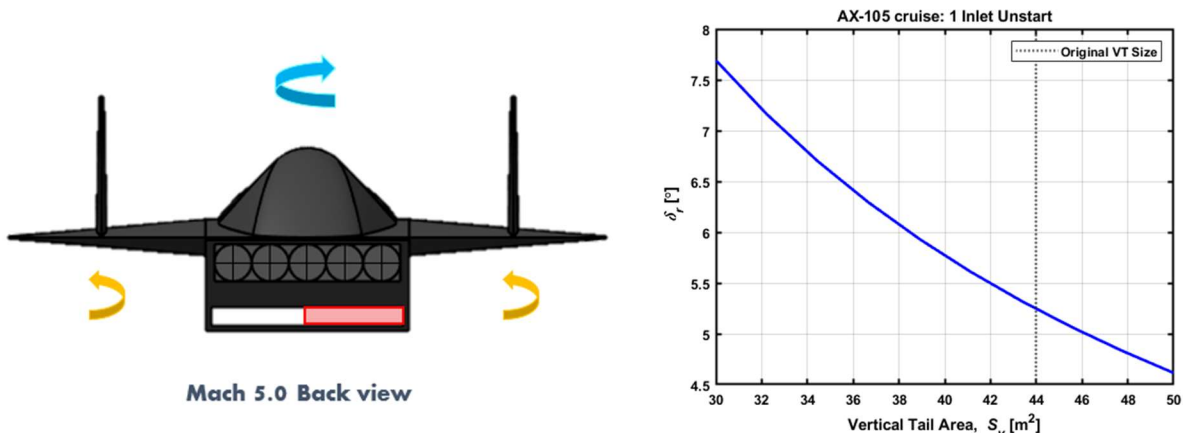


Fig. 78 AX-105 ramjet's inlet unstart at cruise [69].

The last condition checked for controllability as mentioned is at crosswind landing. Here, a crosswind speed of 40 knots was assumed for all configurations to reduce analysis time and maintain consistency. There are two directions the velocity is being approached from. One from the front of the aircraft, and the other from the crosswinds. This tilts the aircraft during landings making it harder to control the aircraft. Enough rudder deflection is needed to maintain control of the aircraft and overcome the sideslip angle created. The following is illustrated in **Fig. 79**.

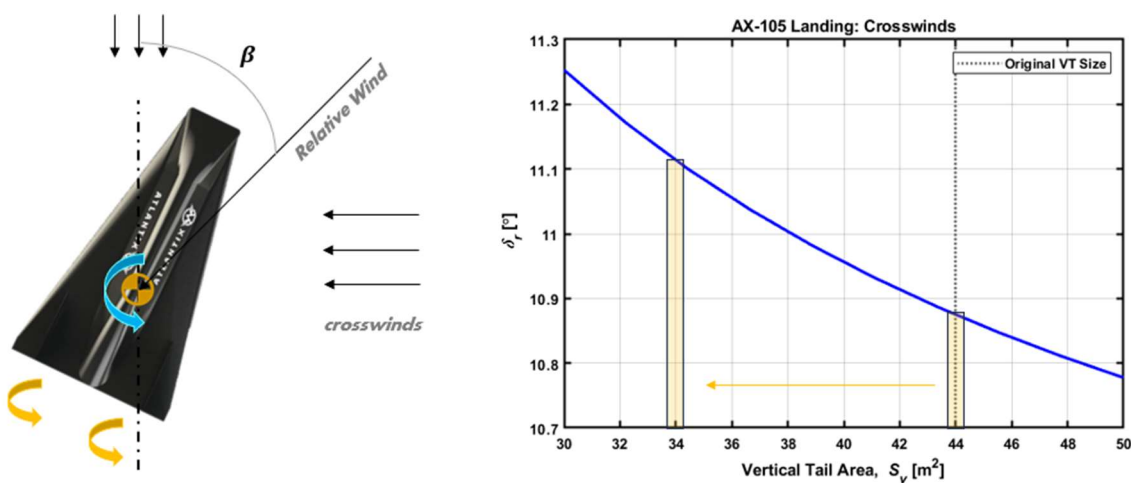


Fig. 79 AX-105 during crosswind landing conditions [69].

After analyzing all three sizing conditions for rudder deflections, it was apparent that takeoff had the highest control requirement than cruise or landing. Since our goal for this configuration was to reduce size, we decided to reduce it to

34m^2 . This of course had higher deflection angles, but it would significantly decrease the drag from an aerodynamics standpoint. This approach yielded in the following rudder design below in **Fig. 80**.

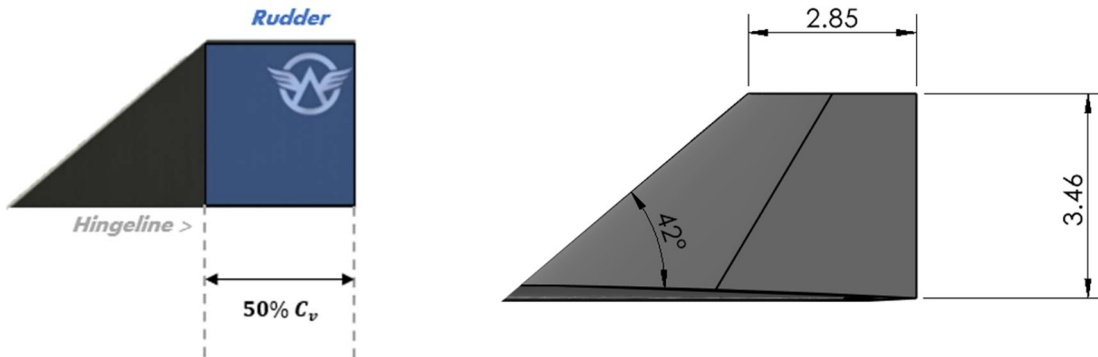


Fig. 80 Rudder and Vertical tail geometry for AX-105 [69].

The same approach was taken to size the remaining vehicles for the same sizing conditions. The illustrations will not be repeated, only the results obtained, and corresponding dimensions extracted will be showcased.

4.11.4 AX-175: Mach 7.5, Single Inlet

For the AX-175, the same approach was taken to size the control surfaces. First, the initial vehicle dimensions from CL were obtained from the Geometry team member as seen in **Fig. 81**. All these dimensions were entered into the initial control surface estimates code developed by Carlos Carmona and the author [67]. This generated the control surface estimates for CL as seen in **Fig. 82**. These initial estimates were used to check if the control power of elevons and rudders were enough during sizing in CE.

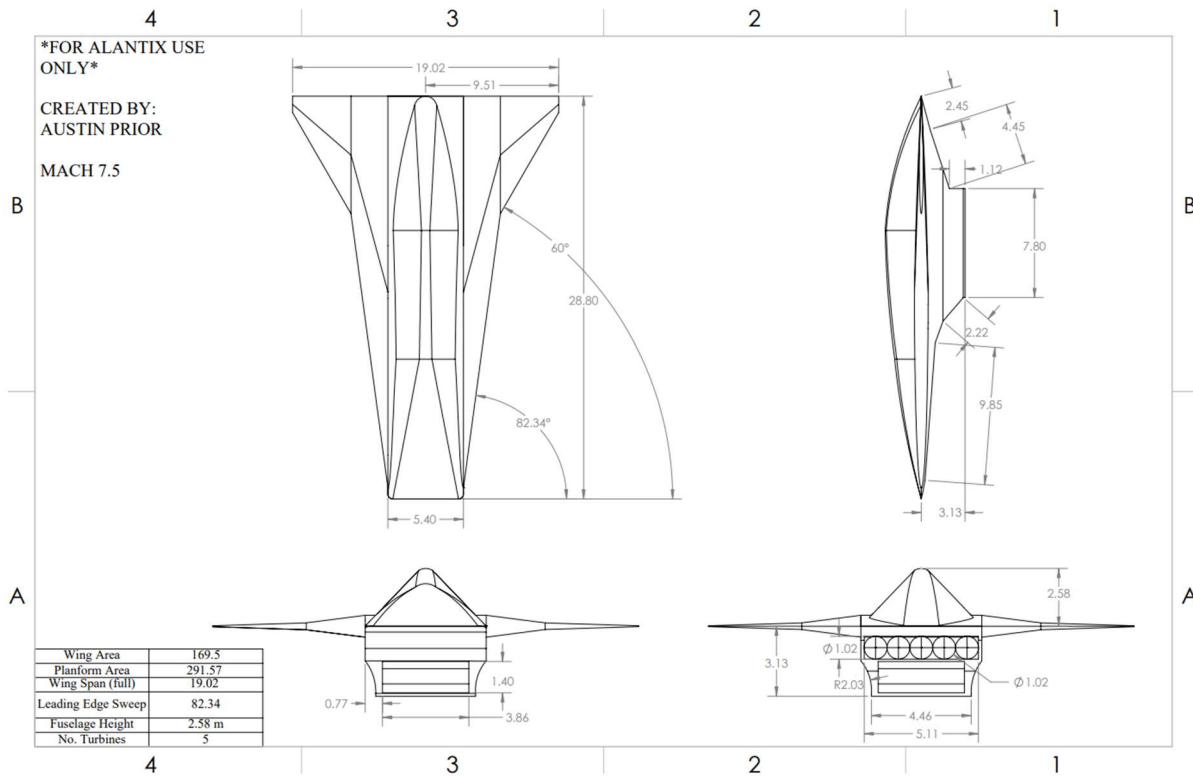


Fig. 81 Mach 7.5 AX-175 dimensions provided by Austin Prior [69].

```
=====1 ELEVON=====
Elevon Shape: Right Trapezoid
Elevon chord: Ce = 0.8569 [m]
Elevon span (on 1 side): be = 6.8100 [m]
Elevon area (single side): Sht = 5.6238 [m^2]

=====1 VERTICAL TAIL=====
Vertical Tail Shape: Right Trapezoid
Vertical Tail Sweep: SweepVT = 33.0000 [deg]
Vertical Tail Root chord (1 tail): Cvr = 6.3360 [m]
Vertical Tail tip chord (1 tail): Cvt = 2.4765 [m]
Vertical Tail height (1 tail): bh = 2.5064 [m]
Vertical Tail root thickness (bottom): tr = 0.2218 [m]
Vertical Tail tip thickness (top): tt = 0.0867 [m]
Vertical Tail area (single side): Svt = 11.0437 [m^2]
```

Fig. 82 Control surface dimensions provided to Geometry based on AX-175 dimensions.

The vertical tail chord length for AX-175 was assumed to be 22% of reference aircraft length. This is the distance from aircraft nose to end of the fuselage. The vertical tail sweep angle is again assumed to be 33° .

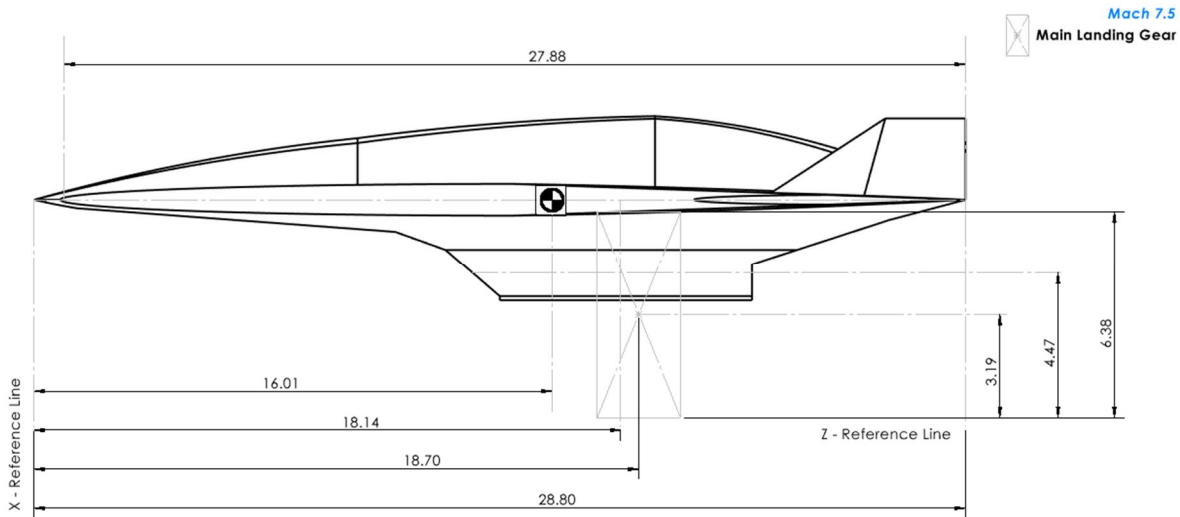
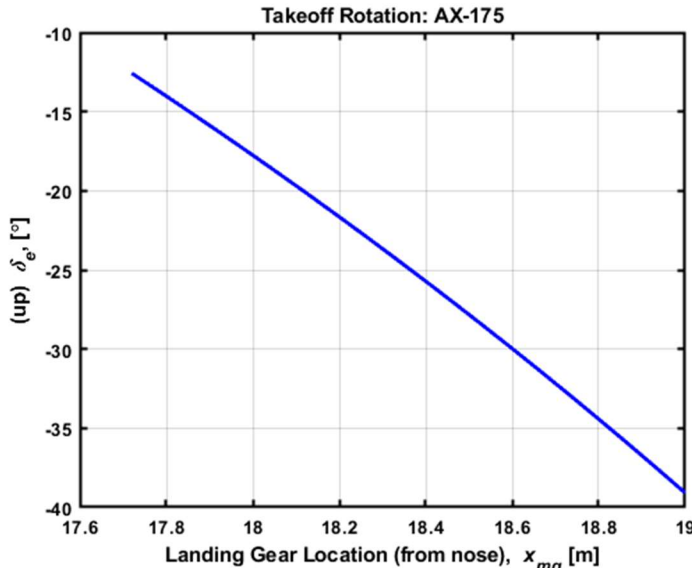


Fig. 83 AX-175 dimensions needed for elevon sizing at takeoff rotation [69].

The dimensions above were obtained from Geometry, W&B and Structures team. The location of the landing gear was given as an acceptable range allowable from C.G. location. Additionally, landing gear heights were provided for each configuration and their respective moments of inertia I_{yy} . The neutral point was obtained from the method given in Section 5.2.5. The C.G. location for takeoff was issued to be a fixed value due to full fuel weight. The thrust and drag vectors are assumed to be acting in the center of the engine entrance, but in opposite directions as seen in **Fig. 72**. The bottom of the landing gear wheel is assumed to be the point at which all the moments are summed about.

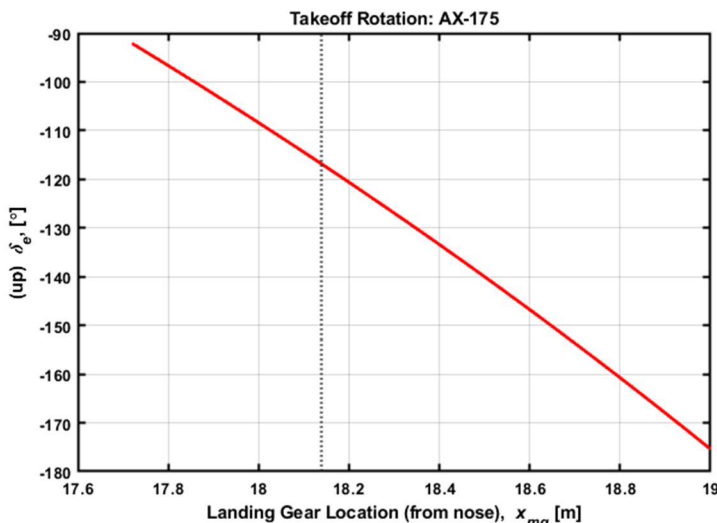
The following were the results obtained from the elevon sizing code for takeoff in **Fig. 84****Fig. 85**. The red line in the **Fig. 85** indicates the maximum elevon up deflection angle. Higher than this amount is not recommended. Hence, the landing gear must be placed more forward to reduce this deflection. To achieve smaller deflections, the elevon size had to be increased. The Fig. 85 gives the original CL estimates obtained from the control surface estimate method used – NASA FLOPS. This proved to be not enough area available, resulting in very high elevon deflection angles. Hence, there is no red line showing the cutoff, all deflections are unacceptable. The elevon size for AX-175 was increased by 10 times, this resulted in increased elevon chord and decently high elevon deflection angles, although acceptable.



```
AIRCRAFT NAME: AX-175
=====
=====ELEVON @ TAKEOFF ROTATION=====
1 ELEVON AREA = 15.0000 [m^2]
1 ELEVON SPAN = 6.8100 [m]
ELEVON CHORD = 2.4590 [m]
C.G LOCATION FROM NOSE = 16.0120 [m]
A.C LOCATION FROM NOSE = 14.4000 [m]

For lesser than -25 deg elevon deflection:
LANDING GEAR LOCATION BEFORE = [m]
```

Fig. 84 AX-175 elevon sizing analysis at takeoff rotation – increased elevon size.



```
AIRCRAFT NAME: AX-175
=====
=====ELEVON @ TAKEOFF ROTATION=====
1 ELEVON AREA = 5.6238 [m^2]
1 ELEVON SPAN = 6.8100 [m]
ELEVON CHORD = 0.4129 [m]
C.G LOCATION FROM NOSE = 16.0120 [m]
A.C LOCATION FROM NOSE = 18.1400 [m]

For lesser than -25 deg elevon deflection:
>>
```

Fig. 85 AX-175 elevon sizing analysis at takeoff rotation – original CL elevon size.

The elevons for AX-175 resulted in larger chord lengths, up to 15% of aircraft lengths. Although this allows for control during takeoff rotation, the placement of these elevons becomes a challenge. The vertical tails obstruct elevons control. The wingspan needs to be increased to accommodate elevons such that the vertical tails are not hindered. Due to the high elevon deflection angle needed for takeoff rotation, this design is not desirable. The Aerodynamics team was informed for the need to increase wingspan, however, with more basic calculations the wingspan needed appeared to significantly increase the aspect ratio of the vehicle. The AX-275 had the same issue as seen in Fig. 96.

The CL estimates of AX-175 were again used to size vertical tails for all three tail sizing conditions as seen in Fig. 86Fig. 87. The original CL sizes proved to be very small for controllability at two engine loss from centerline at takeoff. The opposite was the case for rudder sizes from AX-105 was seen for this vehicle. The vertical tail size proved to be too small. Size comparison graphs are given in the following Fig. 86Fig. 87. As seen in Fig. 86, the engines out at takeoff creates a high rudder deflection angle, greater than 25°. This is undesirable, and the size of the tails were increased. For this scenario, again 2 of the 5 turbine engines were considered lost at takeoff. Due to time constraints, the reduced sizes were given to the Geometry team member and directly used for stability assessment.

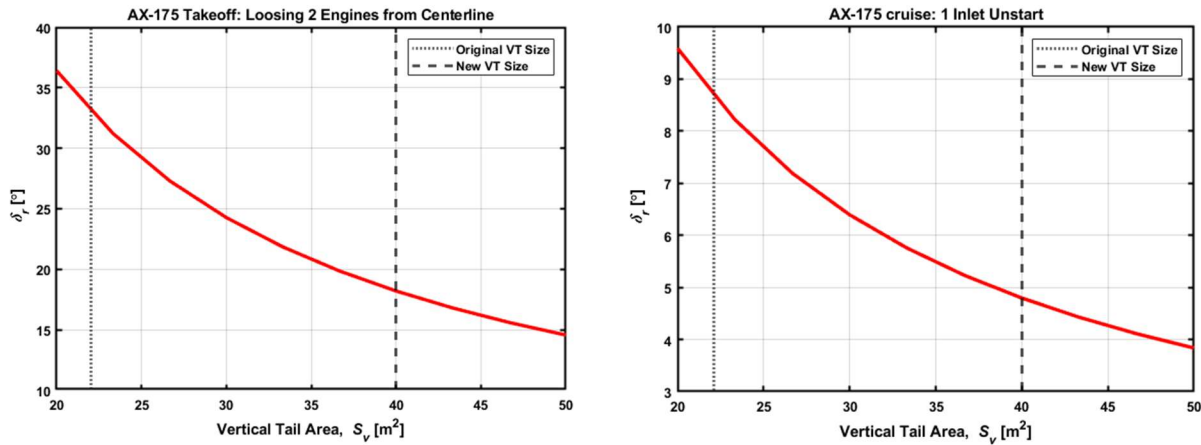


Fig. 86 CL and CE vertical tail sizes for AX-175 at takeoff and cruise.

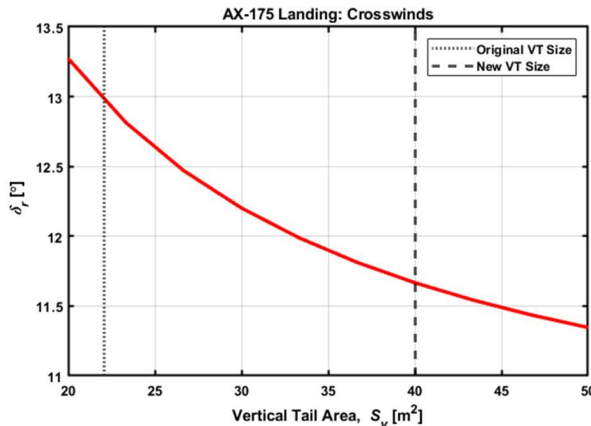


Fig. 87 CL and CE vertical tail sizes for AX-175 at crosswind landing.

4.11.5 AX-205, Mach 5.0, Dual Inlet

For the dual flow path vehicles, only Mach 5 and 7.5 configurations were given to the S&C team. Due to the same procedure used, the sections for AX-205 and AX-275 are predominantly only show the sizing process procedure and results through the following images below.

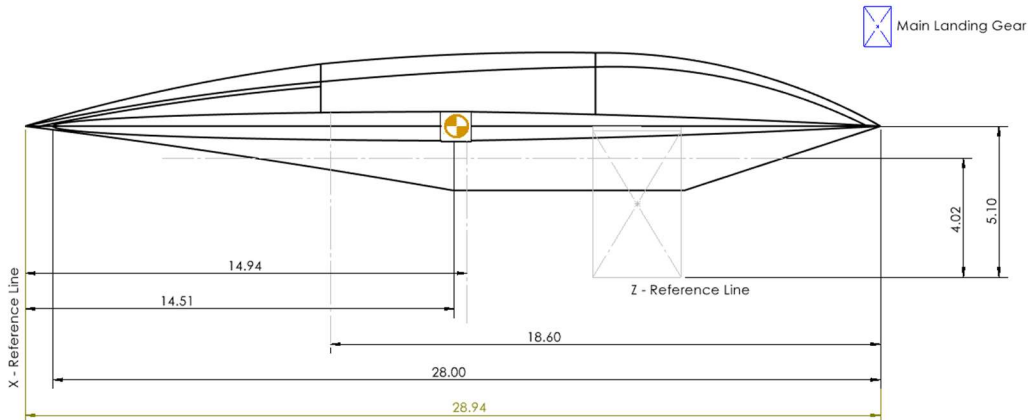


Fig. 88 AX-205 dimensions used from CAD models [69].

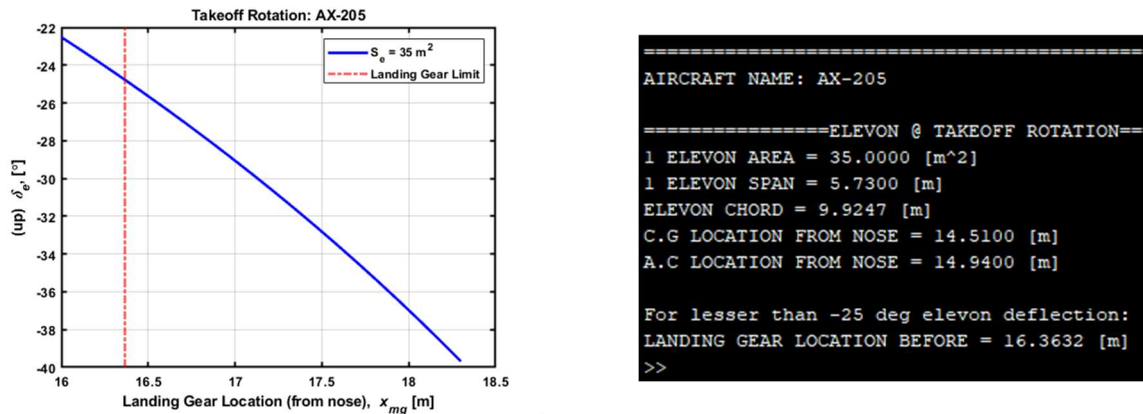


Fig. 89 Sized AX-205 elevons for takeoff rotation.

```
PLANE: AX-205
===== 1 ELEVON =====
Elevon Shape: Right Trapezoid
Elevon chord: Ce = 7.0135 [m]
Elevon span (on 1 side): be = 5.7300 [m]
Elevon area (single side): Sht = 35.0000 [m2]

Minimum Elevon span needed (on 1 side): be_new = 9.9807 [m]
Original Elevon span (on 1 side): be_old = 5.7300 [m]
FULL wingspan needed: bspan_new = 24.9615 [m]
New Elevon chord: Ce_new = 3.5068 [m]
>> |
```

Fig. 90 Re-sized elevons for AX-205 after reducing elevon chord lengths.

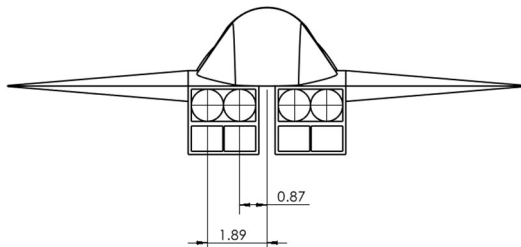


Fig. 91 AX-205 Dimensions used for engines-out [69].

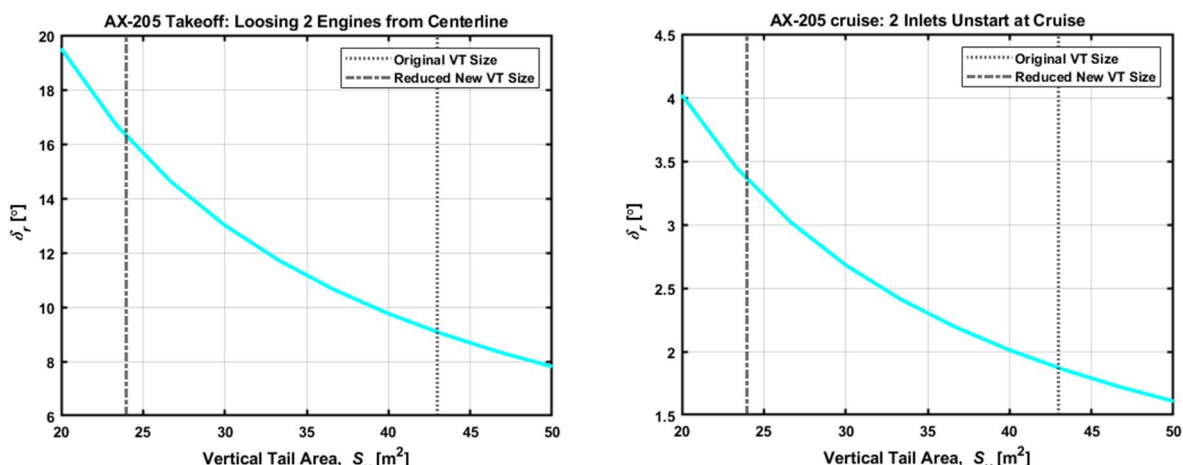


Fig. 92 Vertical tail sizing results for AX-205 at takeoff and cruise.

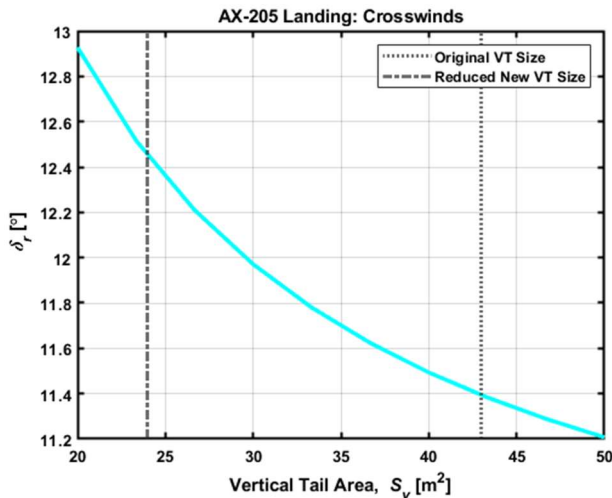


Fig. 93 Vertical tail sizing results for AX-205 at landing.

The main takeaway from the AX-205 control surface sizing results is that the elevon sizes were significantly increased. With this increase in size, the resultant elevon chord length was long again, and the wing needed to be resized. Due to time constraints, the new elevon size was directly used for stability assessment as resizing the wing would restart the sizing process for all other disciplines.

The vertical tails for AX-205 however, were sized down. At cruise, two ramjets were considered to unstart and at takeoff, two turbines were considered lost. This vehicle had the highest control requirement at takeoff phase, and with the new sizes, the stability was assessed directly.

4.11.6 AX-275, Mach 7.5, Dual Inlet

For the dual flow path vehicles, only Mach 5 and 7.5 configurations were given to the S&C team. Due to the same procedure used, the sections for AX-205 and AX-275 are predominantly only show the sizing process procedure and results through the following images below. Note for the reader, the landing gear ranges used for sizing elevons for dual flow are the same as single flow. The aircrafts for single and dual flow paths have approximately the same length, which is why the author made the assumption due to unavailability of time and inputs. The maximum elevon deflection is kept at 25° for all dual flow paths as well.

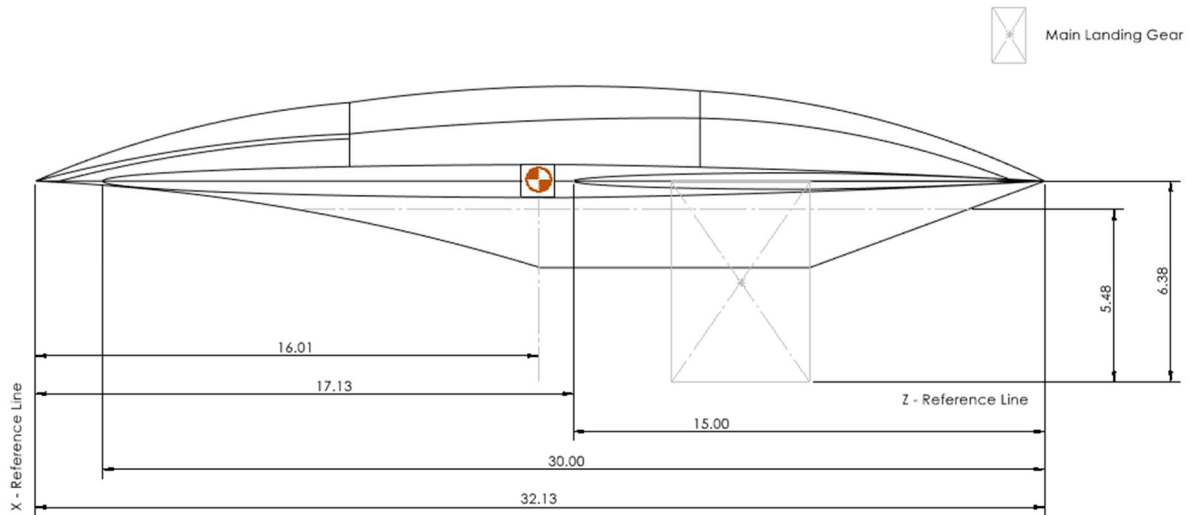
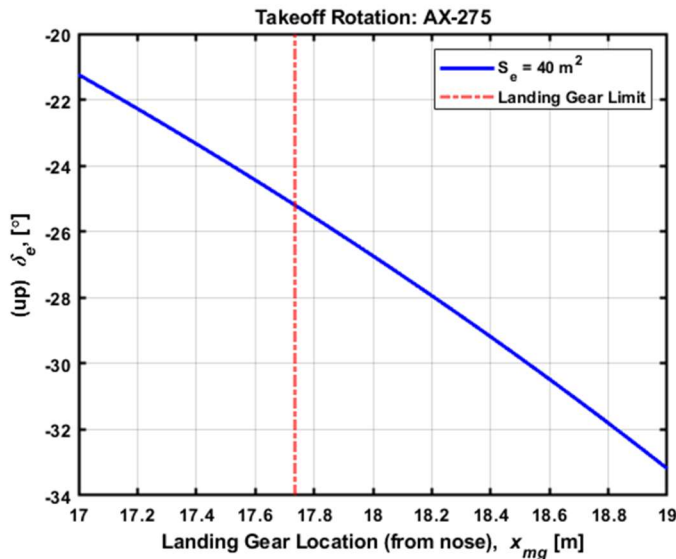


Fig. 94 AX-275 dimensions used from CAD models [69].



```

=====
AIRCRAFT NAME: AX-275

=====ELEVON @ TAKEOFF ROTATION=====
1 ELEVON AREA = 40.0000 [m^2]
1 ELEVON SPAN = 8.2850 [m]
ELEVON CHORD = 6.1428 [m]
C.G LOCATION FROM NOSE = 16.0120 [m]
A.C LOCATION FROM NOSE = 17.1300 [m]

For lesser than -25 deg elevon deflection:
LANDING GEAR LOCATION BEFORE = 17.7368 [m]
>>

```

Fig. 95 Sized elevons for AX-275 at takeoff rotation.

```

=====
1 ELEVON
=====
Elevon Shape: Right Trapezoid
Elevon chord: Ce = 5.8149 [m]
Elevon span (on 1 side): be = 8.2850 [m]
Elevon area (single side): Sht = 40.0000 [m^2]

Minimum Elevon span needed (on 1 side): be_new = 13.7577 [m]
Original Elevon span (on 1 side): be_old = 8.2850 [m]
FULL wingspan needed: bspan_new = 33.5154 [m]
New Elevon chord: Ce_new = 2.9075 [m]
>>

```

Fig. 96 Resize needed for AX-275 wings to accommodate shorter elevon chord lengths.

The wing must be resized for AX-275 to accommodate elevons and reduce elevon chord length again. The new span needed is higher than AX-275's aircraft length at 32.13 m.

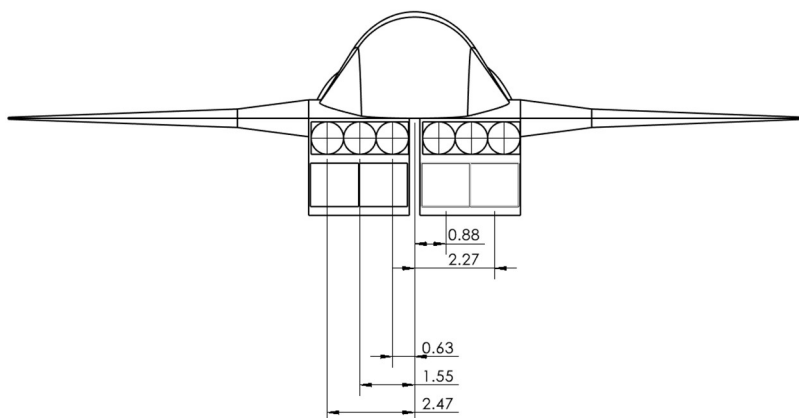


Fig. 97 AX-275 Dimensions used for engines-out [69].

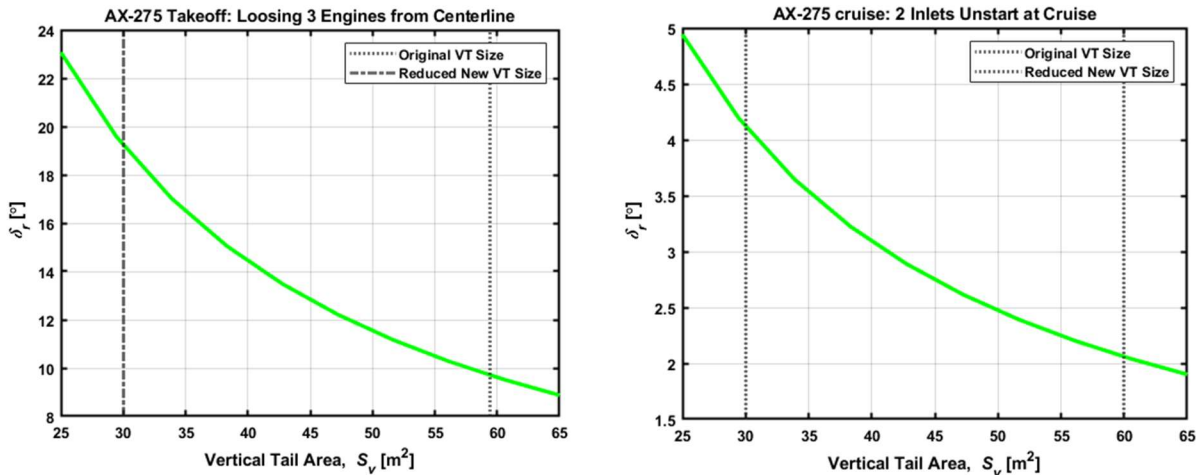


Fig. 98 Rudder sizing results for AX-275 at takeoff and cruise.

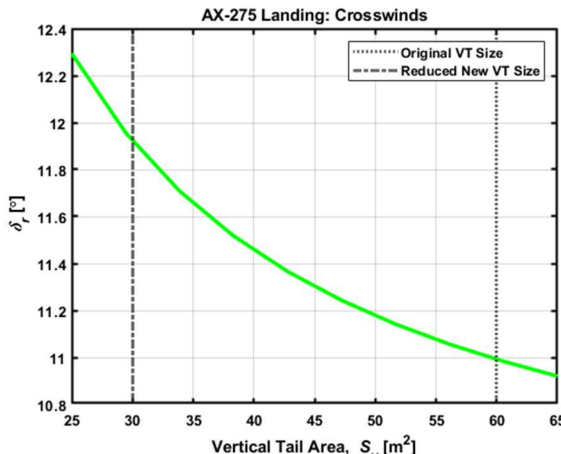


Fig. 99 Rudder sizing results for AX-275 at crosswind landing.

For the AX-275, the elevons size had to be increased, similar to all our aircrafts from initial CL estimates. For the rudder, the tails could be reduced in size as the AX-275 had the highest estimated vertical tail size from CL. This was significantly reduced, by half, as new tail area indicate that they have sufficient control in all three critical conditions.

In conclusion from the CL and CE sizing process, the key issue is that elevon sizes needed for control are very high during takeoff rotation. This means that the wings need to be resized, increase in wingspan to reduce the chord length of the elevon. Elevon chord lengths produced are as high as 40% of the total aircraft length, making it not feasible.

4.11.7 CL and CE Sizing Results Summary

The following segment summarizes the results obtained from CL and CE in a concise manner. The Table 15 shows the CL estimates from all CL inputs. The Table 16 shows the CE results, a summarization of Section 4.11 above.

Table 15. Configuration Layout (CL) Results for S&C Control Surface Estimates

Parameter	Units	AX-105	AX-175	AX-110	AX-205	AX-275
Initial Inputs						
% chord of lref	-	35%	24%	22%	28%	25%
Wing area	m^2	215.43	169.5	234.21	188.1	223.12
Wingspan	m	14.7	19.02	23.68	16.46	22.57



Aircraft length	m	25.83	28.8	33.77	28.94	32.13
Max fuselage width	m	4.5247	5.11	6.07	5	6
LE sweep	deg	78.46	82.34	84.26	78.09	82.34
Second Sweep	deg	-	60	63.17	-	64.19
Fuselage height	m	1.75	2.58	2.25	2.48	2.87
No. of Engines (trb + rj/sj)	-	5+2	5+3	8+3	4+4	6+4
SHT (all)	m^2	25.4496	11.2476	8.4422	17.6648	11.3078
SVT (all)	m^2	44.4202	22.0874	30.6714	43.3778	59.4544
Results (singles)						
Elevon Shape	-	trapezoid	trapezoid	trapezoid	trapezoid	trapezoid
Elevon Chord	m	1.3012	0.8569	0.4842	1.5878	0.6966
Elevon Span	m	9.913	6.81	8.84	5.73	8.285
Elevon area	m^2	12.7248	5.6238	4.2211	8.8324	5.6539
Vertical tail shape		trapezoid	trapezoid	trapezoid	trapezoid	trapezoid
Tail Sweep angle	deg	33	33	33	40	60
Tail root chord	m	9.0391	6.336	7.4294	8.1032	8.0325
Tail tip chord	m	3.6375	2.4765	2.8225	3.7371	5.495
Tail height	m	3.5013	2.5064	2.9918	3.6636	4.3951
Tail root thickness	m	0.3164	0.2218	0.26	0.2836	0.2811
Tail tip thickness	m	0.1277	0.0867	0.0988	0.1308	0.1923
Tail area	m^2	22.2101	11.0437	15.3357	21.6889	29.7272

Table 16. Configuration Evaluation (CE) Results for S&C Control Surface Sizes.

Parameter	Units	AX-105	AX-175	AX-110	AX-205	AX-275
Initial Inputs						
Max Elevon deflection at Takeoff Rotation	deg	-25	-25	-25	-25	-25
Max Rudder deflection, engine loss at takeoff	deg	18	17.5	N/A	16	19
Max Rudder deflection, cruise inlet unstarts	deg	6.75	4.7	9	3.4	4.2
Max Rudder deflection, crosswind landings	deg	11.13	11.7	12	12.5	11.9
Results (singles)						
Elevon Shape	-	trapezoid	trapezoid	trapezoid	trapezoid	trapezoid
Elevon Chord	m	3.6553	2.459	4.6989	3.5068	2.9075
Elevon Span	m	8.2073	6.81	8.805	9.9807	13.7577
Elevon area	m^2	30	15	35	35	40
Vertical tail shape		trapezoid	trapezoid	trapezoid	trapezoid	trapezoid
Tail Sweep angle	deg	40	45	33	33	32
Tail root chord	m	6.9741	6.912	7.4294	6.3668	7.0664
Tail tip chord	m	2.8493	2.7885	2.8225	1.8919	1.3871
Tail height	m	3.4611	4.1235	2.9918	2.906	3.5488
Tail root thickness	m	0.2441	0.2419	0.26	0.2228	0.2473
Tail tip thickness	m	0.0997	0.0976	0.0988	0.0662	0.0485
Tail area	m^2	17	20	15	12	15
Rudder area	m^2	12.069	14.251	11.114	9.251	12.539
Rudder chord	m	3.487	3.456	3.7147	3.1834	3.5332
		decreased size		increased size		highest requirement

4.12 Aircraft trim analysis

Initially, the S&C team was aiming to perform a complete trim analysis for the configurations. However, due to sizing constraints, lack of inputs from disciplines for different flight phases, and the time taken to troubleshoot the trim code, the analysis was performed for AX-105 at takeoff and hypersonic cruise only. Instead, a complete stability assessment was performed with all the available initial inputs to showcase results. The AX-105 trim results are given in Section 4.12.2. Below, the initial code test results are presented.

4.12.1 Initial code test results

The aircraft trim code is being troubleshooted. Currently, all stability and control derivative functions must be integrated into code. Some functions were coded into the main script while other functions were being verified. The code was tested to see if it functioned properly, however, minor errors need to be fixed to move forward. Currently, some of the functions have assumed values, due to which there are large discrepancies in values. However, the results are presented below as initial trial results. The code is expected to be completed after week 8. Since the stability and control derivatives are verified, this method solves for elevon pitch and roll trim angles and rudder trim angles. No change in values indicates that the functions need to be added to the main code.

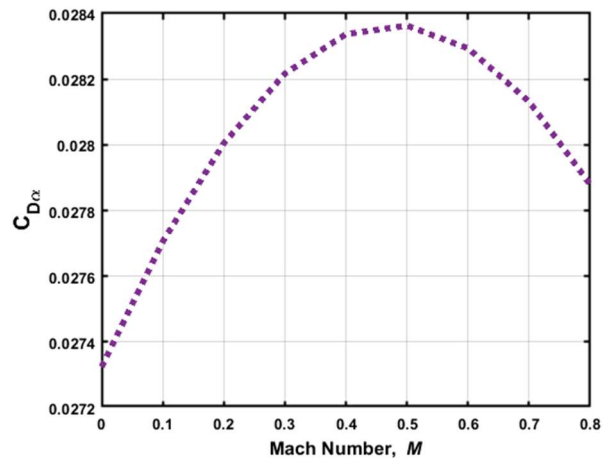
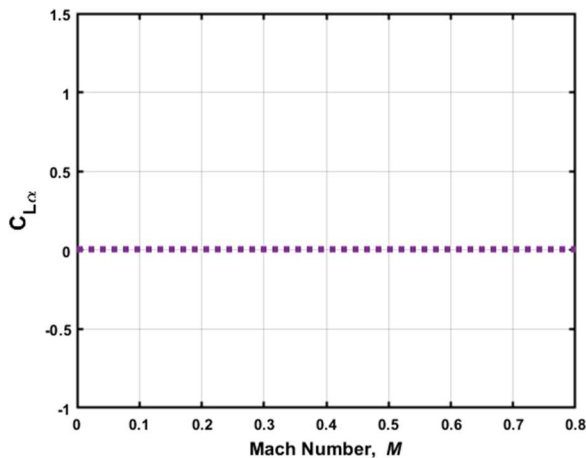


Fig. 100 Initial trim code results.

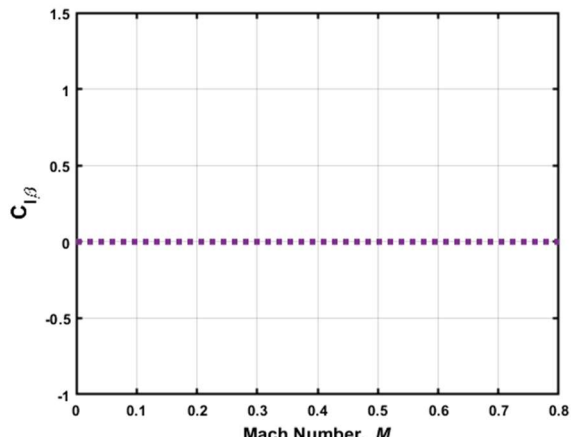
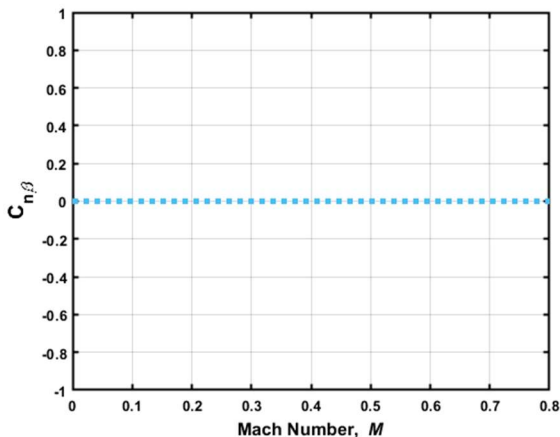


Fig. 101 Initial trim code results.

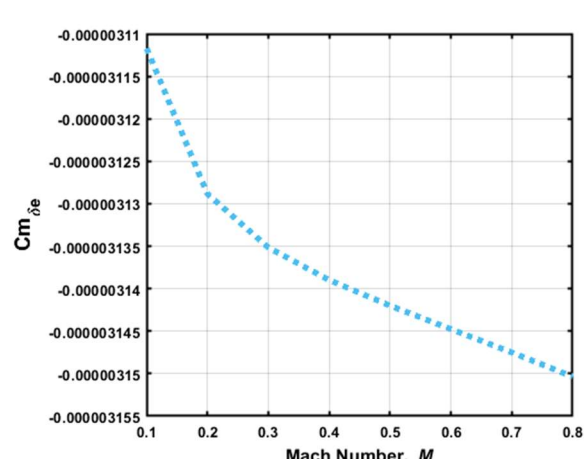
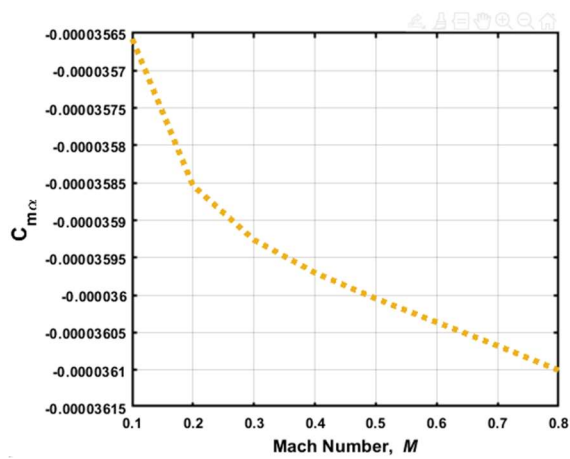


Fig. 102 Initial trim code results.

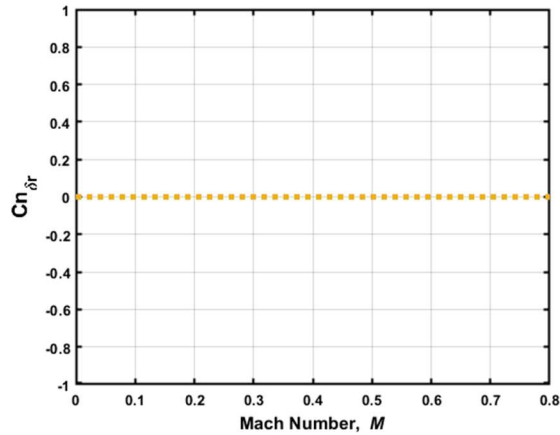
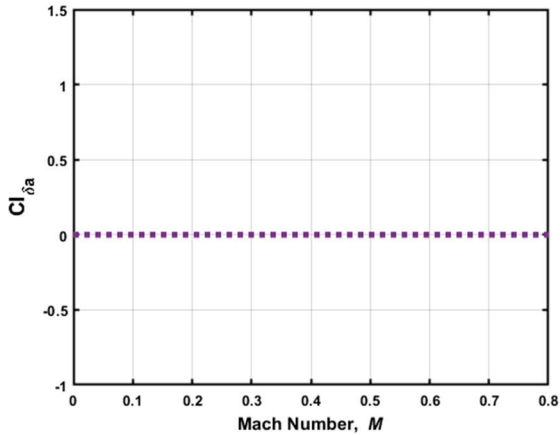


Fig. 103 Initial trim code results.

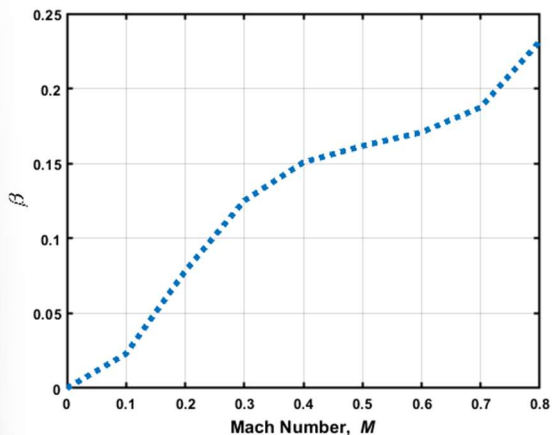
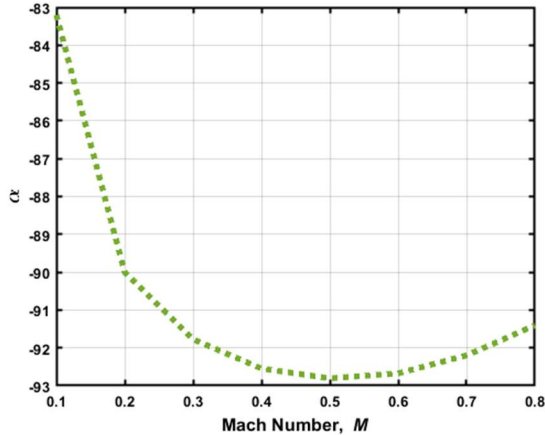


Fig. 104 Initial trim code results.

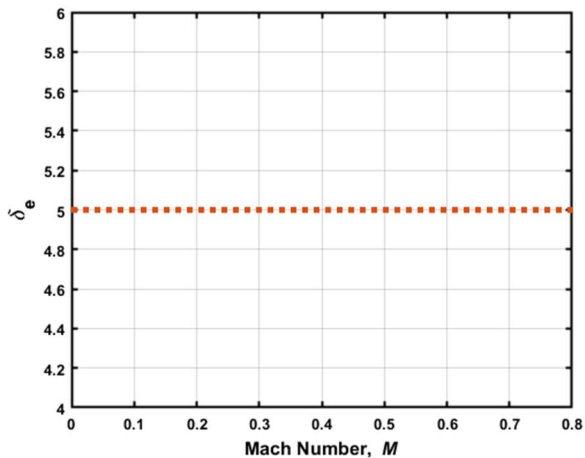
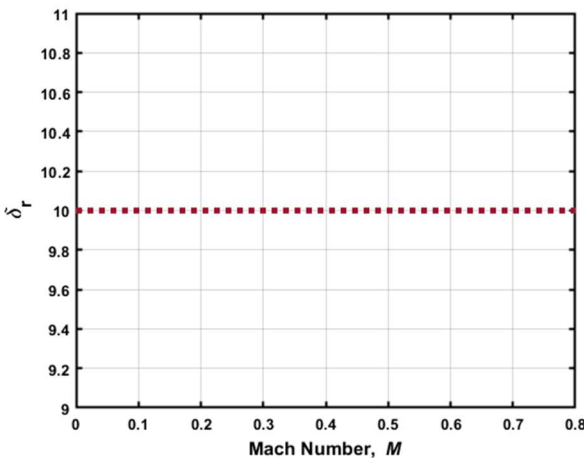


Fig. 105 Initial trim code results.

As seen from above, the issue is that the code is not changing its guesses, it has just generated initial guesses as a function of Mach number. This could be due to the definition of equations of motion in the trim code. This has to be rectified so the code can generate correct plots just by changing inputs in the G structure (General Inputs).

4.12.2 Trim – AX-105

The following are the initial results for trim analysis. Modifications were made to the trim code to make it simpler; this may have led to inconsistent results. Some of the axes have the same numbers, this is due the numbers being too small, and a decimal limit placed in the plotting commands to avoid cluttered graphs. The issue for high values in some coefficient charts could be because the angles of attacks were not updating with each iteration. In the previous trim code, there was a segment that specifically updated these values. However, this over-complicated the code and results, hence they were removed and only 3 trim EOMs were used instead. The numerical solvers were also changed from ode45 to fsolve function in MATLAB as ode45 is for a time-based analysis. Since our analysis was for a steady-state analysis, the time variable was not necessary. The function fsolve works by using variable numbers until the trim equations yield a zero value for several iterations. Once this condition is met, these guesses are stored in the results variable. The resultant guesses are angle of attack, sideslip angle, elevon deflection angle (δ_{LoCE}), aileron or roll deflection angle (δ_{LaCE}) and rudder deflection angle (δ_{DiCE}). As mentioned before, the constant dynamic pressure climb C.G. locations were not given by the W&B team as it based on trajectory, hence, the analysis for this phase will be omitted. Only results for takeoff, and hypersonic cruise are presented in these sections as thrust values were not provided for other phases at the time of the report writing.

The control surface deflections are given below for takeoff and hyperonic cruise of AX-105.

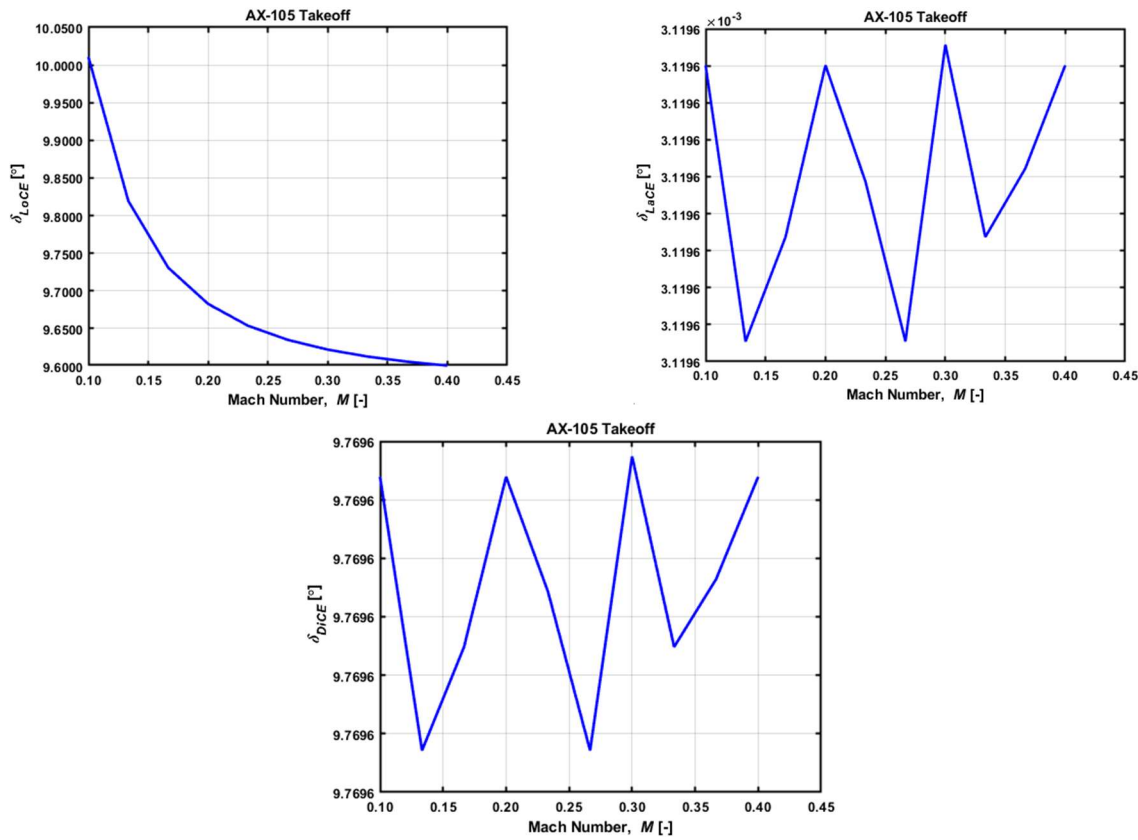


Fig. 106 Takeoff trim results for AX-105.

Hypersonic Cruise

The following were the initial guesses used for this phase:

- Angle of attack is 3.5 deg.
- Sideslip angle is 0 deg.
- The longitudinal control surface effector angle is 5 deg.
- The lateral control surface effector angle is 5 deg.
- The directional control surface effector angle is 5 deg.

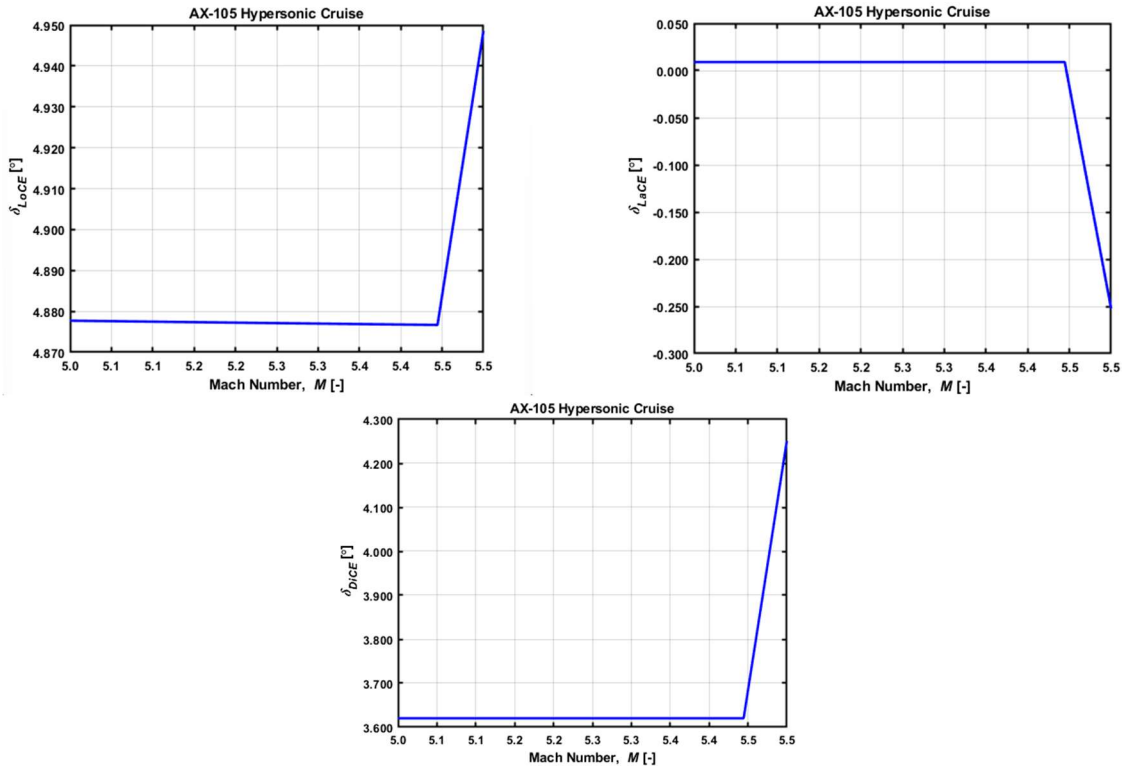


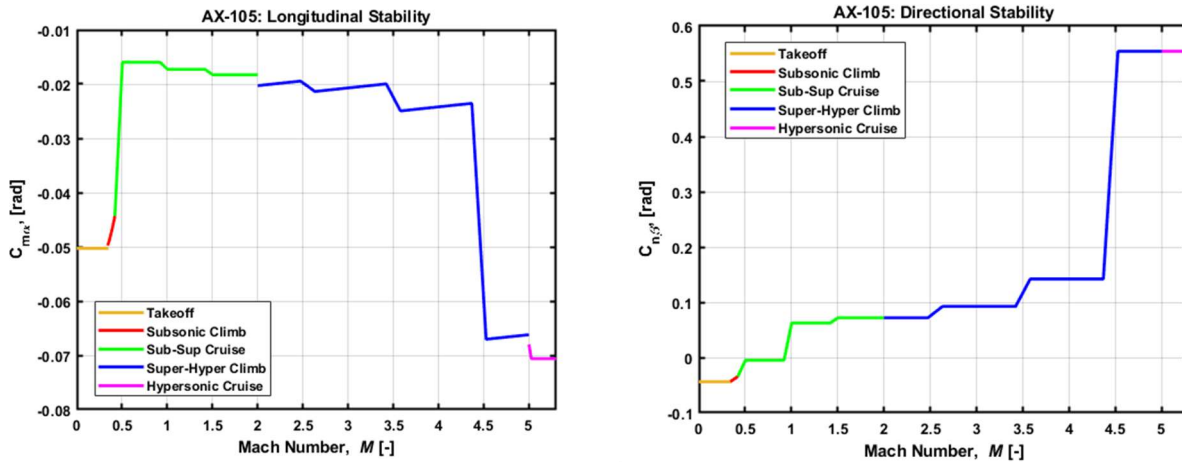
Fig. 107 Hypersonic cruise trim results for AX-105.

Only trim analysis for the Mach 5 single flow path could be conducted due to unavailability of inputs, time and code errors. However, stability derivatives are assessed for all 5 available configurations.

4.13 Stability Results

The following section covers stability assessment for 5 of 6 vehicle configurations. The Mach 10 dual flow path configuration has been declared infeasible, a dead horse by team Atlantix, and therefore, was not created.

4.13.1 Stability – AX-105



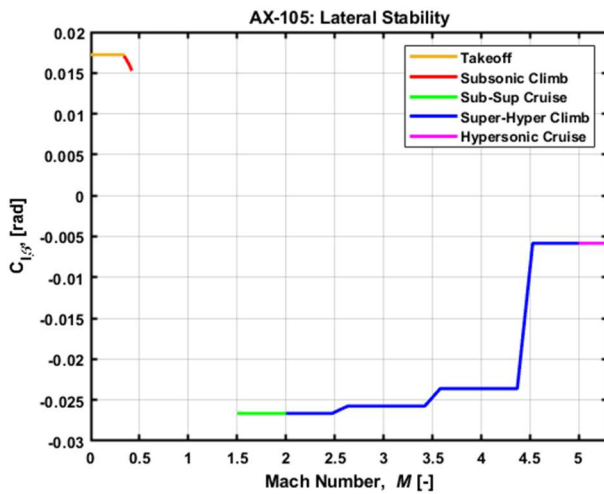


Fig. 108 Stability results as a function of Mach number for AX-105.

4.13.2 Stability – AX-175

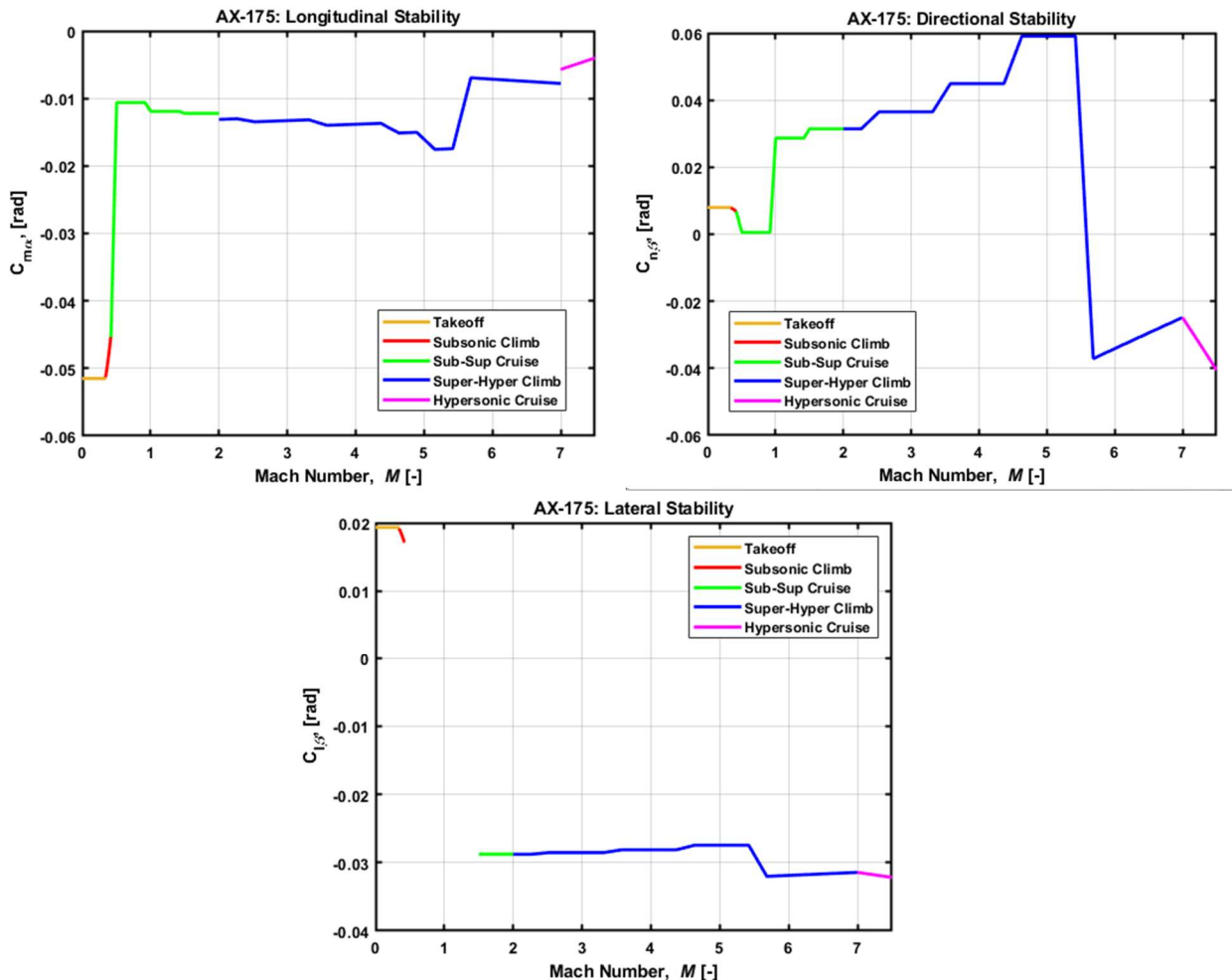


Fig. 109 Stability results as a function of Mach number for AX-175.

4.13.3 Stability – AX-110

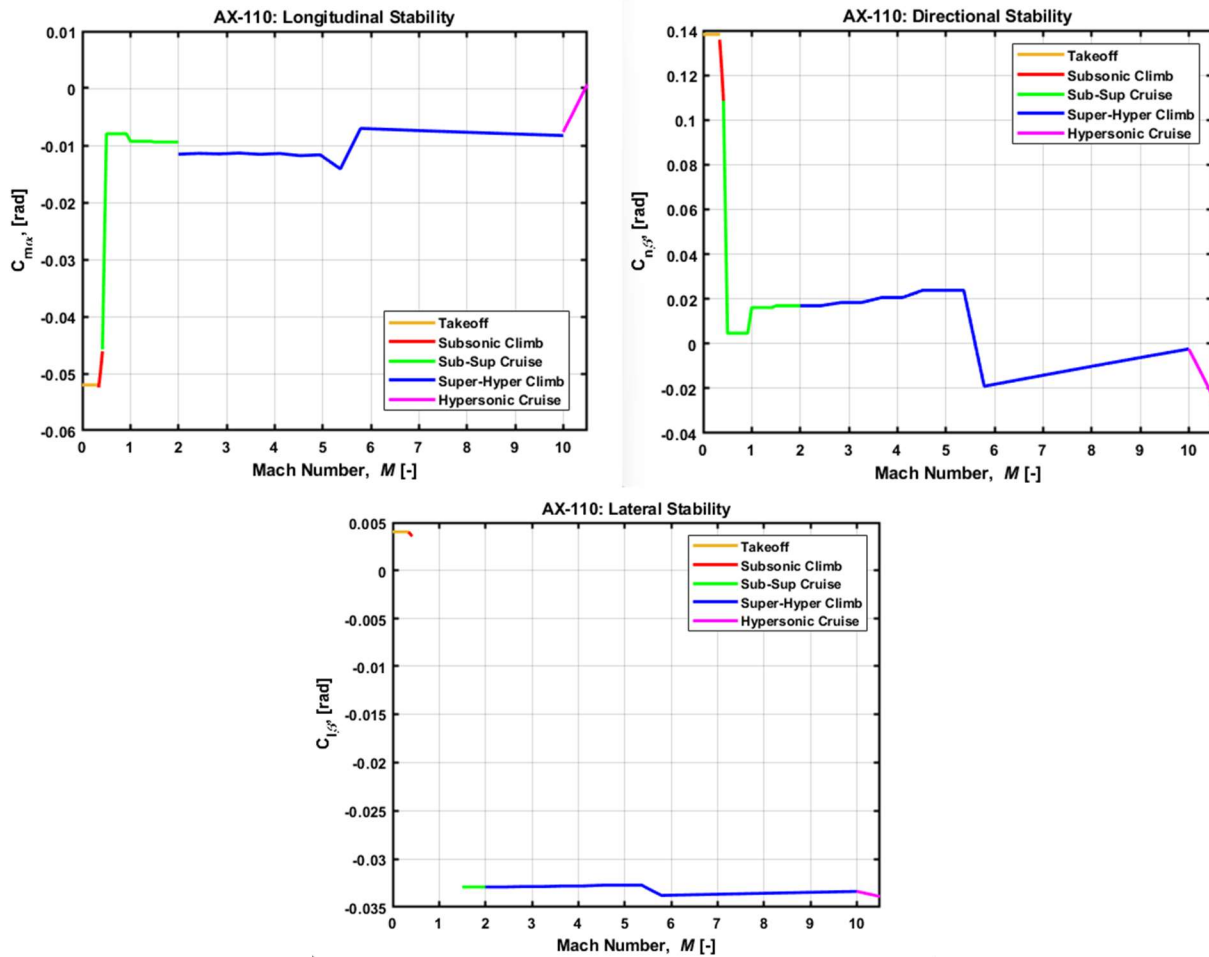
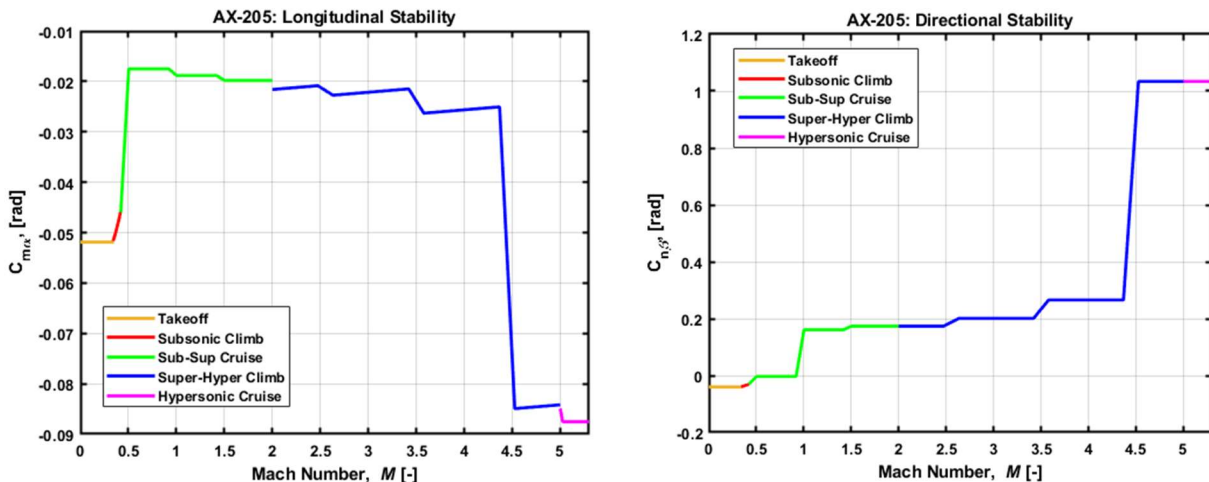


Fig. 110 Stability results as a function of Mach number for AX-110.

4.13.4 Stability – AX-205



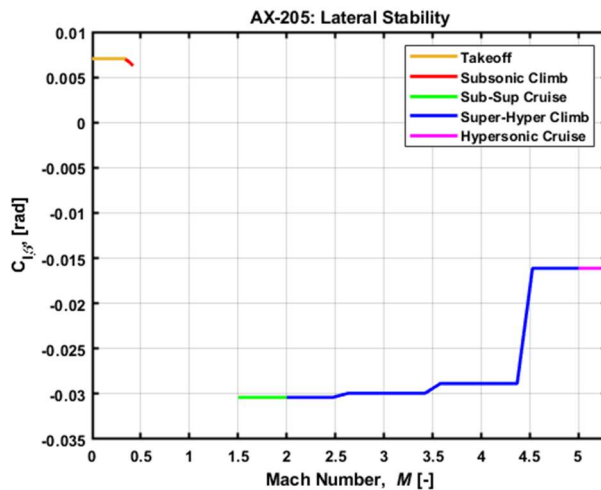


Fig. 111 Stability results as a function of Mach number for AX-205.

4.13.5 Stability – AX-275

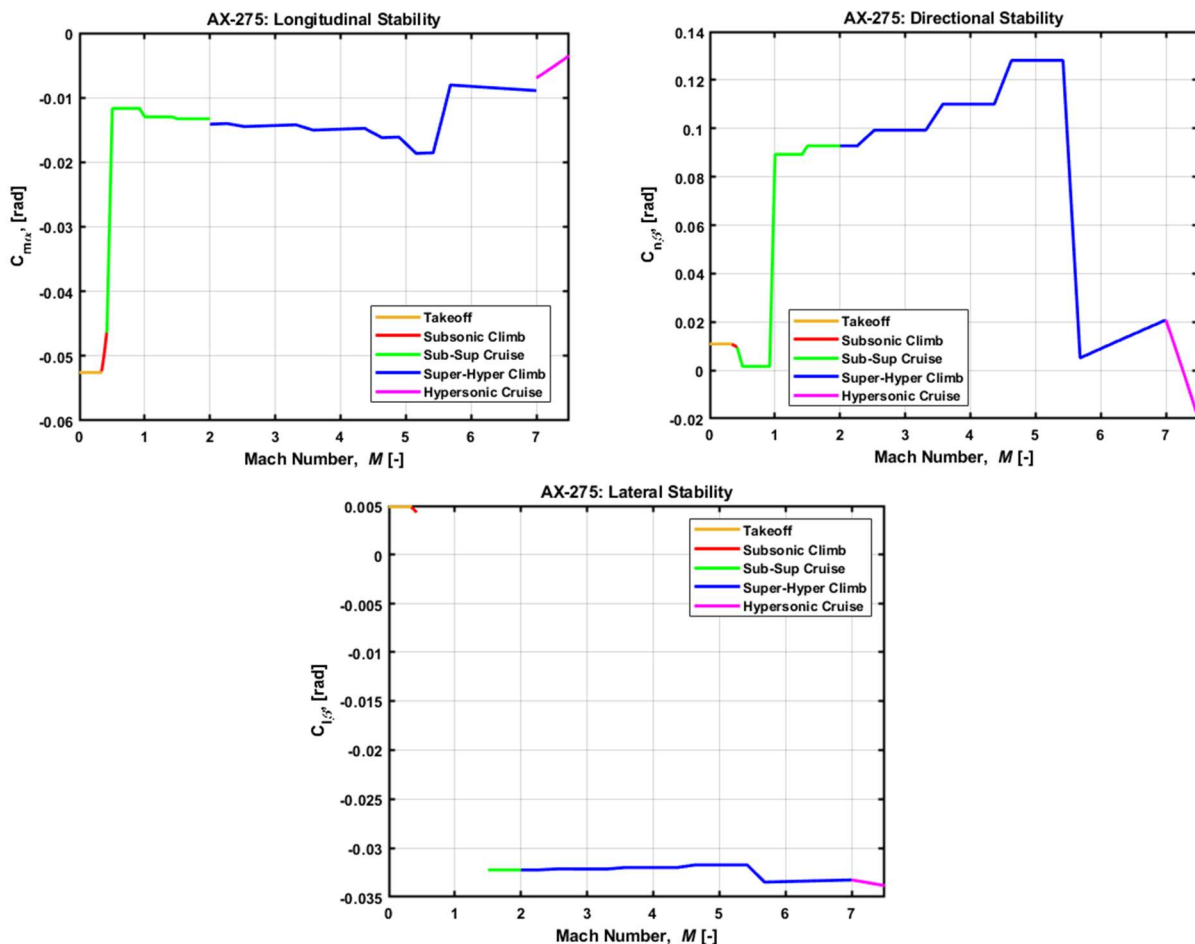


Fig. 112 Stability results as a function of Mach number for AX-275.

4.13.6 Stability CE Results Summary

The following in Table 13 shows a summary of the main stability derivatives throughout flight, up to cruise. The letters “Y” equates to “Yes” for stability and “N” for “No” if unstable. The corresponding cells are highlighted in red and green colors for visualizing.

Table 17. Stability Results Summary for Assessed Configurations.

Phase	AX-105			AX-175			AX-110			AX-205			AX-275		
	C_{m_α}	C_{l_β}	C_{n_β}												
Takeoff	Y	N	N	Y	N	Y	Y	N	Y	Y	N	N	Y	N	Y
Subsonic Climb	Y	N	N	Y	N	Y	Y	N	Y	Y	N	N	Y	N	Y
Sub-Sup Cruise	Y	N	Y	Y	N	Y	Y	N	Y	Y	N	Y	Y	N	Y
Sup-Hyp Climb	Y	Y	Y	Y	Y	N	Y	Y	N	Y	Y	Y	Y	Y	Y
Hypersonic cruise	Y	Y	Y	Y	Y	N	N	Y	N	Y	Y	Y	Y	Y	N

As seen from the Table 13 above, the aircrafts are not stable in roll at subsonic and supersonic speeds. As explained in the previous section, there was a glitch when C_{l_β} subsonic portion of the code. This caused results to not appear in the plots around the transonic region. Additionally, for some vehicles, the directional stability decreased with an increase in Mach number. This is expected since control effectors are less responsive with a gain in altitude. Overall, the roll stability can be improved by adding dihedral to the twin vertical tails. The C.G. locations for Mach 10 flight has to be moved forward during hypersonic cruise as it appears to destabilize in pitch. For additional directional stability, dropped wings can be added to keep the aircraft from yawing during flight. The changes to the design could be a starting point for future work.

5 Aerodynamics

Aerodynamics is one of the primary disciplines in aircraft design. The flow of air around an aircraft determines how it will fly. For that reason, understanding the key concepts such as how lift is generated, where drag is beneficial and where it is unnecessary can help with better, efficient designs. Lift is the byproduct of uneven pressure distribution on an aircraft.

5.1 Background

5.1.1 Hypersonic Aerodynamics

One of the most common misconceptions that author John D. Anderson discusses in the book “Fundamentals of Aerodynamics” is that flow becomes hypersonic at Mach 5. For most aircraft, crossing the sound barrier at Mach 1, the aircraft must overcome significant drag buildup. The drag increases exponentially at the sonic limit, and to counter this various design features can be incorporated to reduce that drastic increment. The region of Mach 0.8 to 1.2, transonic speeds, the aircraft experiences shock wave induced flow separation that severely alters the aerodynamic characteristics of the design. To reduce this, the critical Mach number of the aircraft must be increased to delay flow separation on the wings. This can be done by decreasing wing thickness ratio (t/c), increasing leading edge sweep angle of the wing, decreasing aspect ratio or using a supercritical airfoil [25].

Intuitively, having rectangular wings at hypersonic speeds does not seem feasible. The drag will be significantly high, and due to the heat, there are potential safety concerns. The key term is having a low aspect ratio. Additionally, the vehicle cannot be very heavy since at hypersonic speeds the aircraft will be flying at high altitude where the air is less dense. At the same time, the airframe must be strong enough to withstand the extremely high temperatures and keep the passengers cool inside.

At hypersonic speeds, the aerodynamics of the aircraft significantly changes since there is another variable that has to be taken into account: temperature. John Anderson illustrates this by giving the example of a blunt body during re-entry into Earth’s atmosphere at Mach 36. The blunt bottom causes a bow shock wave, with the temperature behind the normal portion of bow shock reaching up to 65,248 K (approximately 65,000 °C). The air must be assumed to be calorically perfect for this case. However, at such high temperatures, the density is not constant due to chemical reactions, and the air is not considered calorically perfect anymore (specific heat γ keeps changing). So the actual

temperature is approximately around 11,000 K (or around 10,700 °C). Around 9000 K, the Nitrogen and Oxygen molecules would have both dissociated into ions; the resulting shock layer will be partly ionized plasma [37].

The density is no longer stable, its changing due to boundary layer formation and its interaction with the surface of the aircraft. This viscous phenomenon increases skin friction drag. Additionally, there are shock waves that form at sharp edges of the aircraft such as the nose cone, inlets, vertical tails, etc. This creates wave drag. It must be taken into account to estimate drag for supersonic and hypersonic speeds.

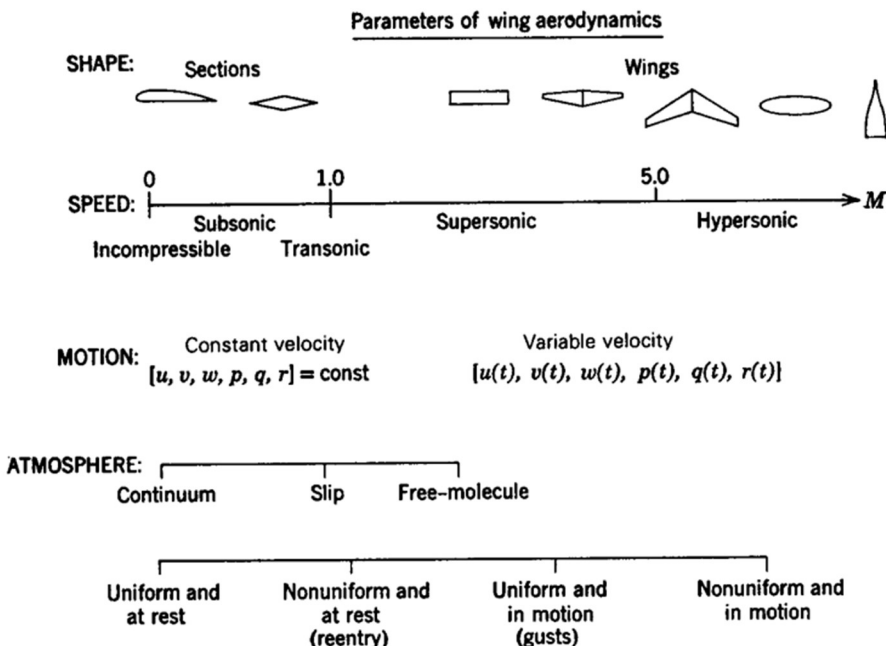


Fig. 113 Spectrum of aerodynamic issues to address [74].

5.1.2 Hypersonic Convergence and Aerodynamics

This portion will explain the role of the Aerodynamics team within the Synthesis convergence methodology to be adopted. A brief review of the Hypersonic Convergence methodology is given in section 3.1. To start the PS process, an estimate for the maximum lift-to-drag ratio must be known of a given aircraft. Since our aircraft will be a hypersonic, wing-body configuration with an air-breathing propulsion system, looking into similar aircraft can give an approximate for starters.

For the PS phase, the Kuchemann relation can be used to estimate the lift-to drag ratio as seen below [41].

$$\left(\frac{L}{D}\right)_{max} = \frac{A}{M}(M + B) = \frac{4}{M}(M + 3) \quad (46)$$

Where constant A and B are taken to for future state-of-the-art (SoA) aircraft. Hence, as given in the text by Czysz, P, the constants are A = 4 and B = 3 as seen in the Eq. (47). To calculate the zero-life drag coefficient, the following relation can be used for initial estimates:

$$\beta C_D = 0.05772 \cdot e^{0.4076} \quad (48)$$

Where,

$$\beta = \sqrt{M^2 - 1} \quad (49)$$

So, for the three conceptual vehicles of Mach numbers 5, 7.5 and 10, the following are the initial estimates to be given to the Synthesis team.

Table 18. Concept vehicles aerodynamic estimates for PS phase.

Vehicle Mach, M	Constant A	Constant B	β	$(L/D)_{max}$	C_{D_0}
5.0	4	3	4.89	6.4	0.01771
7.5	4	3	7.43	5.6	0.01167
10.0	4	3	9.95	5.2	0.00872

5.1.3 Wings for hypersonic aircraft

Highly swept wings are suitable for high-speed flight. Intuitively, swept wings are less likely to obstruct airflow than rectangular wings. Hence, a hypersonic Spirit of St. Louis with rectangular wings is not feasible from an aerodynamics standpoint. The goal with the concept of hypersonic Spirit of St. Louis is to maximize range. By using highly swept wings such as the delta wings, the goal for Aerodynamics is to minimize drag at hypersonic speeds. The following are many variations of delta wings in Fig. 114.

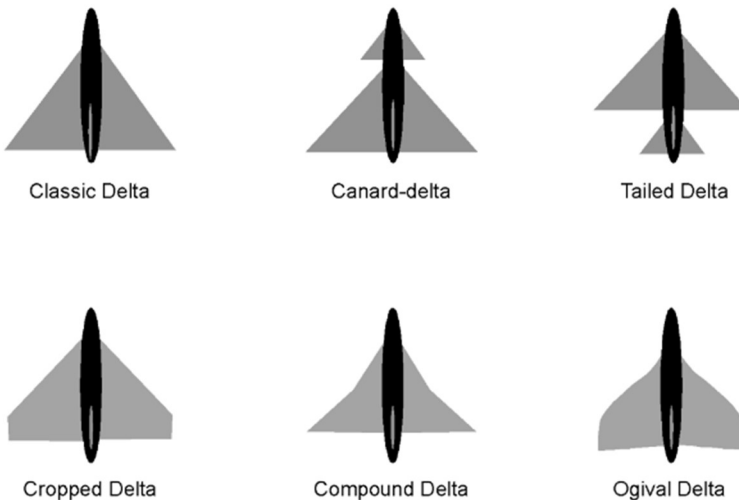


Fig. 114 Common types of delta wings [75]

One of the main reasons to have a canard is to destabilize the aircraft, which is much needed since the neutral point shifts backward. Supersonic aircraft such as the experimental plane by NASA – the XB-70 Valkyrie had a canard with trim capability. The Russian supersonic transport Tupolev TU-144 featured retractable canards. The compound delta wings, also known as double delta, aid in generating strong free vortices along the wing intersection allowing for low-speed efficiency. The Ogive wing has a similar effect to the double delta wings. Most supersonic transports have an extended fuselage where the vertical tail is placed. A tailed delta wing might not be suitable for controllability since strong downwash at high-speed may render the tail end useless. Cropped delta wing has the benefit of low induced drag due to trailing edge vortices. A wing-body aircraft typically has a higher aspect ratio than an All-body aircraft, which increases viscous drag known as parasite drag. The term is a culmination of skin friction drag, wave drag, interference drag, pressure drag (form drag), miscellaneous drag, etc. The high drag may create thick boundary layers, where viscous interaction phenomena take place, specifically in hypersonic flow. Therefore, the aircraft must have strong airframe material and TPS to safeguard its passengers. The Concorde, TU-144, XB-70 are good examples of delta wing variations, although they are built for supersonic speeds. The Hermeus Halcyon has similarities between the space shuttle orbiter and XB-70 with its drooped wings and wing geometry.

For additional lift, devices like Leading Edge Extensions (LEX), fuselage strakes can be incorporated into the wing, provided they are able to withstand hypersonic heating. These devices can create tiny free vortices that propel energized air through suction on a boundary layer. This can prevent boundary layer separation.

5.1.4 Shape of the Nose

The shape of the nose determines the type of shock wave the aircraft will encounter during flight. Oblique shock waves are weaker in nature. The flow after the shock is supersonic. Normal shock waves are very strong, leading to subsonic flow after. Normal shock waves are used in engine intakes to slow the flow from supersonic to subsonic as the air flows to the combustor. Typically, engines need to be placed within the Mach cone produced by a sharp nose. If placed outside the cone, the flow may interfere with flow at engine intakes.

The leading-edge shape of the aircraft has significant effects on the airflow around the body. It becomes important to explore the types of noses suitable for hypersonic travel. Sharp cone noses reveal an oblique shock wave, blunt noses as in the case of X-43A (AB configuration) yield a bow shock.

The X-43A has a spatula nose geometry, similar to one chosen for our concept hypersonic plane during PS phase. A spatula nose is primarily beneficial for propulsion integration. With a more flatter nose, the airframe has increased wingspan to accommodate either a larger engine or higher number of engines. Additionally, the bow shock wave created at the nose at high speeds has its own benefits.

5.2 Methodology for Aerodynamics in PS

5.2.1 Lift

The lift generated by a delta wing will be non-linear due to crossflow and formation of free vortices at the upper edges of the wing. The crossflow is the spanwise flow of air. The velocity component for crossflow increases in the spanwise direction leading to flow separation near wing tips at high speeds. Thus, for low aspect ratio (AR) bodies such as a delta wing, it becomes important to account for the non-linearity of lift. Following in the Fig. 115 below is the flow pattern for the slender bodies.

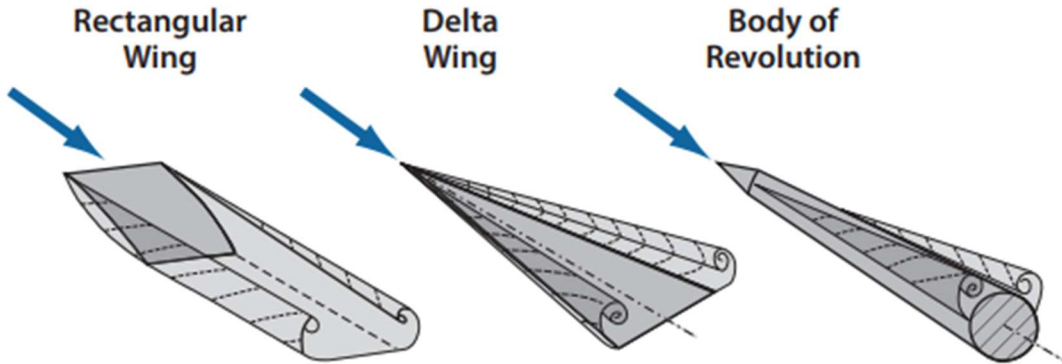


Fig. 115 Lift formation due to free vortices on various aircraft bodies [25].

Nicolai's method – CL max

Following the information presented, the methodology given below can be used to estimate the lift coefficient for subsonic, slender bodies of low aspect ratios [25]:

$$\frac{dC_L}{d\alpha} = C_{L\alpha} = \frac{2\pi AR}{2 + \sqrt{4 + AR^2\beta^2(1 + \left[\left(\frac{\tan^2 \Lambda_{LE}}{\beta^2} \right) \right])}} \quad (50)$$

Where,

$$\beta = \sqrt{1 - M^2} \quad (51)$$

The non-linear lift coefficient will be:

$$C_L = \left(\frac{dC_L}{d\alpha} \right)_{\alpha=0} \alpha + C_1 \alpha^2 \quad (52)$$

To obtain the coefficient C_1 , the following chart can be used once AR is known, specifically for a delta planform. The pitching moment can also be estimated in similar fashion for an estimate during PS phase.

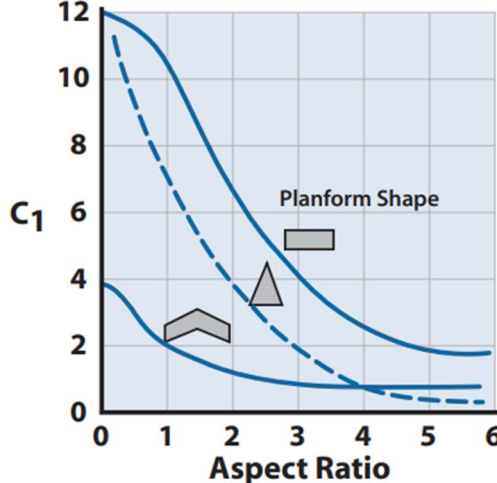


Fig. 116 Chart for determining constant for non-linear lift coefficient [25].

This method by Nicolai was tested to obtain $C_{L_{max}}$, details are presented in Section 5.4. The lift-curve-slope C_{L_α} was calculated first, then the angle of attack was varied while extracting constants from Fig. 116 for delta wing. Aspect ratios ranging from 1.5 to 3.0 were chosen. This resulted in a non-linear plot, however, there is no indication of stalling. Usually, predicting stall point using analytical models is difficult, wind tunnel tests give a much more accurate depiction of flow behavior. Another option can be to select a maximum angle of attack α_{max} , to find the corresponding maximum lift coefficient. Another method from Raymer was also considered and given below.

For a generic estimate of the lift-curve-slope C_{L_α} during the PS phase, the following approximating for wing-body configuration can also be used, outlined in Roskam [76]. However, the author will be using Nicolai's method since it is more applicable to delta planforms.

$$\left(\frac{dC_L}{d\alpha} \right)_{WB} = \left[1 + \frac{1}{4} \left(\frac{d}{b} \right) - \frac{1}{40} \left(\frac{d}{b} \right)^2 \right] \left(\frac{dC_L}{d\alpha} \right)_w \quad (53)$$

To compare the results, similar transport and high-speed WB aircraft are chosen. The Synthesis team has provided an initial aircraft weight of 500,000 lb. Following in the table below are chosen aircraft and their geometric features.

Table 19. Aircraft with similar TOGW as our conceptual vehicles

Aircraft Name	TOGW [lb]	Δ_{LE} [deg]	Δ_{ND} [deg]	AR
Concorde	408,010			1.85
TU-144	456,357	76.00	57.00	1.66
XB-70	542,000	65.57	-	1.75
Sanger 2	559,000	83.00	67.00	2.40
Space Shuttle Orbiter	242,508	81.00	45.00	2.27

Raymer's method – CL max [30]

The text also provides a way to estimate $C_{L_{max}}$ for low aspect ratio wings. The difference from the method above is that Raymer recommends estimating this value assuming maximum lift at takeoff occurs at Mach 0.5. There is no

clear explanation for why this speed was chosen. Two leading edge sweep angles were chosen based on a study done by NASA in 1966 for low-speed delta and double delta wings. It was concluded that the strake portion of a double delta wing increased the strength of vortices over the wing [77]. Following assumptions were made to test the method:

- No taper delta wings ($\lambda = 0$)
- Mach number = 0.5
- Low aspect ratio
- Two leading edge sweep angles: $\Lambda_{LE} = 75^\circ$ and $\Lambda_{LE} = 62^\circ$

Upon choosing the necessary variables, the maximum low aspect ratio was determined:

$$AR \leq \frac{3}{(C_1 + 1)(\cos \Lambda_{LE})} \quad (54)$$

The constant C_1 is a function of taper ratio, must be determined empirically. From the empirical charts, C_1 will be zero. Using additional empirical charts given for this process, C_{Lmax} and α_{max} are estimated.

$$\text{term 1} = (C_1 + 1) \frac{AR}{\sqrt{1 - M^2}} \cos \Lambda_{LE} \quad (55)$$

$$\text{term 2} = (C_2 + 1) AR \tan \Lambda_{LE} \quad (56)$$

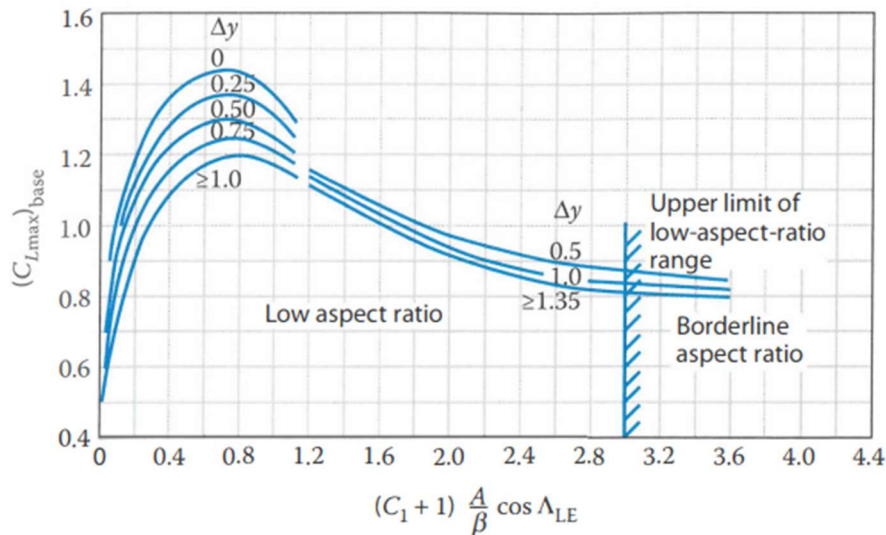
The maximum lift coefficient is given by:

$$C_{Lmax} = (C_{Lmax})_{base} + \Delta C_{Lmax} \quad (57)$$

And its corresponding maximum angle of attack is given by:

$$\alpha_{C_{Lmax}} = (\alpha_{C_{Lmax}})_{base} + \Delta \alpha_{C_{Lmax}} \quad (58)$$

Here, the first term of Eq. (59-60) can be found using the empirical charts given below:



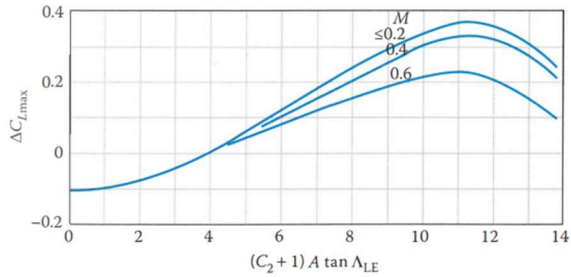


Fig. 117 Empirical charts to estimate maximum lift coefficient [30]

Following was the data produced from this process in the Table 20. The term Δy is the leading-edge slenderness parameter. For this analysis, a value of 11.8 t/c for a biconvex airfoil was chosen, with a thickness-to-chord ratio (t/c) of 0.05. This gives the term $\Delta y = 0.56$.

Table 20. Data using Raymer's method for subsonic maximum lift coefficient [78].

Leading edge sweep angles Λ_{LE} [deg]	AR	Term 1	Term 2	$(C_{Lmax})_{base}$	ΔC_{Lmax}	C_{Lmax}	$(\alpha_{C_{Lmax}})_{base}$	$\Delta \alpha_{C_{Lmax}}$	α_{max}
62	4.45	3.46	-4.88	0.85	-0.1	0.75	22	-10	12
63	3.04	3.46	0.52	0.85	-0.1	0.75	22	-8	14
70	4.74	3.46	5.79	0.85	0.1	0.95	22	-10	12
75	3.25	3.46	-1.37	0.85	-0.1	0.75	22	-10	12

As seen in the table above, there is no clear trend seen amongst the values obtained. The angles were converted to radians before using the equations. Although, the maximum lift coefficient and angle of attack fall in the right ballpark values. For a known airfoil, the 2D lift-curve-slope can be obtained from which a 2D maximum lift coefficient C_{lmax} can be estimated. From that, for moderate sweep angles the following can be used:

$$C_{Lmax} = 0.9 C_{lmax} \cos \Lambda_{0.25c} \quad (61)$$

HYFAC method – Supersonic $C_{L\alpha}$

The supersonic lift-curve-slope can be estimated from the following correlation for delta planforms of a WB configuration. This chart is obtained from HYFAC document where it gives lift estimation method for hypersonic vehicle concepts. Most of these vehicles are Hydrogen fuel based. For a double-delta wing, an effective leading-edge angle must be calculated to obtain the $C_{L\alpha}$. The geometric parameters needed are provided in the chart, are the inputs needed from Geometry team.

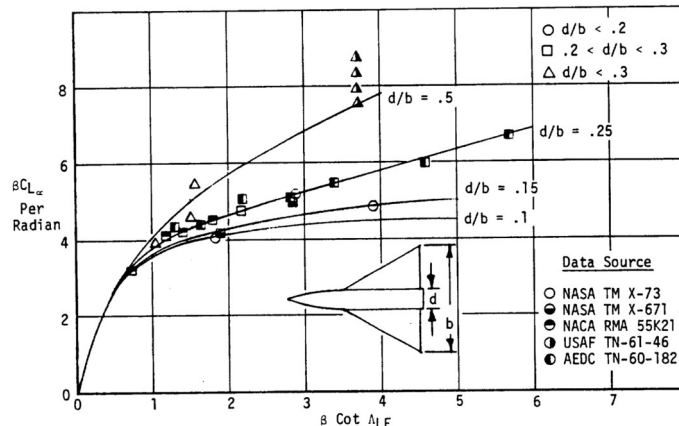


Fig. 118 Correlation for supersonic lift-curve-slope of delta wing-body configuration [13].

	SENIOR DESIGN: MAE 4351 Project	Ref.: MAE 4351-001-2021 Date: 11. Aug. 2023 Name: Gayathri Kola Status: Complete
---	---	---

5.2.2 Drag: Induced Drag and Wave Drag

For the drag build-up, many analytical and empirical methods can be used to give the Synthesis & Performance teams with approximate values. General analytical methods for wave drag coefficients may have large errors since wave drag depends on shock waves produced at different Mach numbers. This is dependent on the aircraft geometry for which higher fidelity methods can be used for accuracy. For PS, these coefficients are heavily based on empirical estimates.

The total drag of an aircraft can be calculated by the following relation:

$$C_{D_{total}} = C_{D_0} + L' C_L^2 \quad (62)$$

The first term C_{D_0} is known as the zero lift drag coefficient. It accounts for all the viscous effects of drag including skin friction drag, pressure drag, wave drag, base drag, interference drag, and engine drag. The second term accounts for drag due to lift, an inviscid phenomenon.

HYFAC method – Drag Coefficient at subsonic speeds [13]

A method to estimate skin friction drag is given in HYFAC [13]. This is the Von Karman-Schoenherr equation which assumes incompressible flow along a smooth flat plate. For temperature conditions less than Mach 5.0, adiabatic gas condition is assumed.

$$\log 10 (R_N C_F) = \frac{0.242}{\sqrt{C_F}} \quad (63)$$

To account for the thickness of the body at subsonic speeds, relations for the ratio between the wing and flat plate are given. The same is done for the body of the aircraft using the following relations below:

$$\frac{C_{F_{Body}}}{C_{F_{Flat\ plate}}} = 1 + 1.5 \left(\frac{d}{l} \right)^{\frac{3}{2}} + 7 \left(\frac{d}{l} \right)^3 \quad (64)$$

$$\frac{C_{F_{Wing}}}{C_{F_{flat\ plate}}} = 1 + 2 \left(\frac{t}{c} \right) + 60 \left(\frac{t}{c} \right)^4 \quad (65)$$

Here, the skin friction coefficient for the body takes body diameter and length into account. For the wing, the ratio of thickness and chord are used. These correction factors are not applicable for supersonic speeds.

P. Czysz and HYFAC methods – Subsonic/Supersonic Induced Drag Factor [13]

The drag and drag polar estimations are split into three speed regimes: subsonic, transonic, supersonic/hypersonic. The methods for drag polars are summarized in Gary Coleman's thesis paper [39]. These empirical methods are pulled from different sources namely HYFAC reports and "Hypersonic Convergence" publication by Paul Czysz. These methods given below are applicable to both WB and BB configurations. These methods are specifically for hypersonic cruise vehicles, which is a bonus.

For the subsonic drag polar of a highly swept WB planform, empirical relations are used to estimate the maximum L/D and induced drag factor L' . The induced drag factor can be found using the equation below [39]. These are just used for baseline estimates for PS phase.

$$L' = \frac{1}{4C_{D_0} \left(\frac{L}{D} \right)^2} \quad (66)$$

For the supersonic/hypersonic drag polar of WB or BB configuration, the same method above can be used for Mach numbers up to 12. The thesis gives empirical relations for Mach numbers 2, 5, 12. For our case of Mach numbers 7.5 and 10, the empirical data can be interpolated to estimate the maximum L/D for a given slenderness ratio. The Synthesis team has requested equations that directly relate to geometric changes which could be integrated into the convergence code instead of empirical relations.

Add cleaner empirical charts.

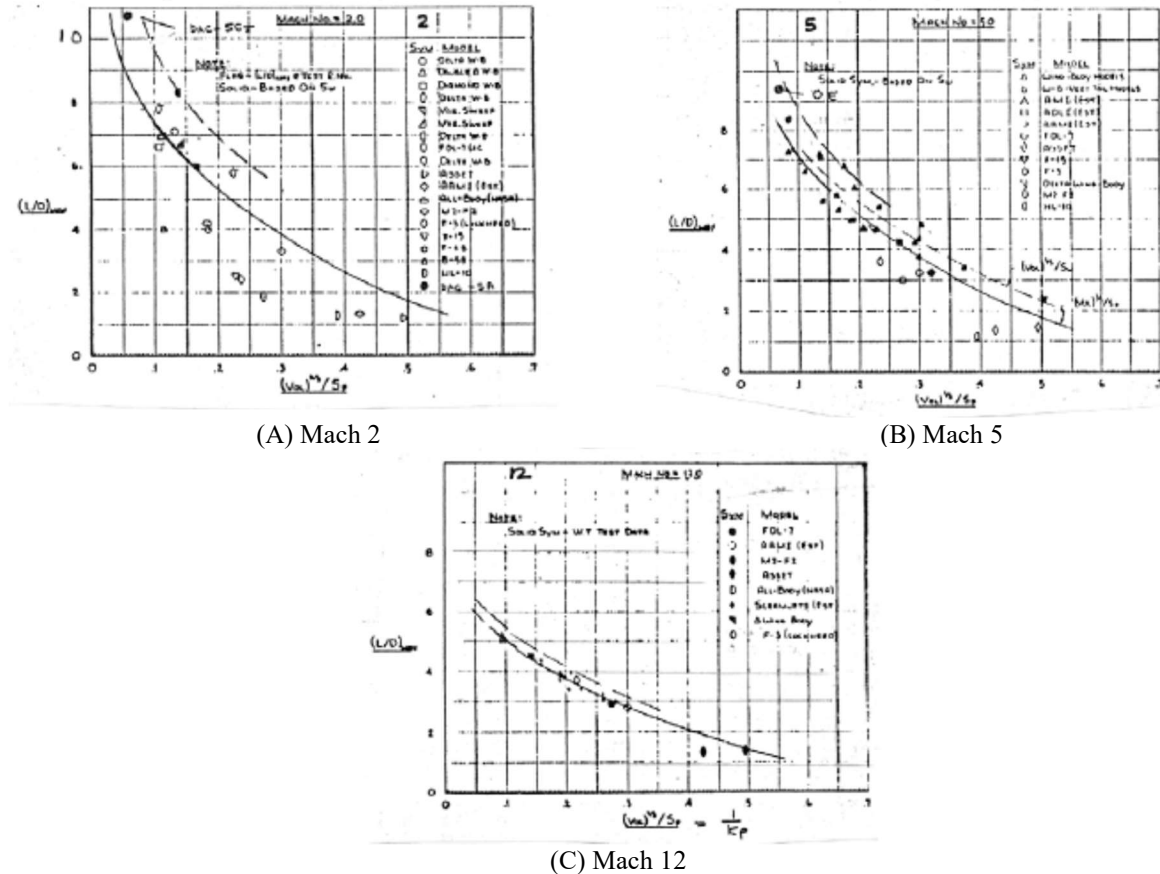


Fig. 119 Lift-to-drag relations for Mach numbers 2, 5 and 12 [39].

Coleman's thesis – Transonic/Supersonic Wave Drag Coefficient [39]

A method to estimate wave drag at transonic regime (transonic drag rise) is also given in the thesis. This method applies to highly swept WB and BB planforms. This correlation is made based on the aircraft's frontal area S_{front} . This method is applicable to speeds up to Mach 2.0 and requires frontal area and total aircraft length as inputs. There are two criteria for estimating the wave drag:

1. If $S_{front}/L^2 < 0.015$, the wave drag coefficient is:

$$(C_{Dwave})_{max} = \frac{S_{front}}{S_{pln}} \left[1.3862 \left(\frac{S_{front}}{L^2} \right) + 0.067 \right] \quad (67)$$

2. If $S_{front}/L^2 > 0.015$, the wave drag coefficient is:

$$(C_{Dwave})_{max} = \frac{S_{front}}{S_{pln}} \left[0.9536 \left(\frac{S_{front}}{L^2} \right)^3 - 1.916 \left(\frac{S_{front}}{L^2} \right)^2 + 1.3651 \left(\frac{S_{front}}{L^2} \right) + 0.1119 \right] \quad (68)$$

The question then becomes, what is the limit for maximum wave drag at transonic, supersonic, and hypersonic speeds.

Aprovitola, et. al Method – Supersonic Wave Drag [79]

The wave drag for the supersonic regime can be estimated using the Sears-Hack body concept. This method is used to minimize drag at high-speed flight. This method was used for Concorde aerodynamic analysis [79].

$$C_{D_w} = \frac{24V}{L^3} \frac{S_{max}}{S_{ref}} = \frac{9\pi^2}{2} \left(\frac{R_{max}}{L} \right) \frac{S_{max}}{S_{ref}} = \frac{4.69}{4} \left[\left(\frac{R_{max}}{2l_N} \right)^2 + \left(\frac{R_{max}}{2l_T} \right)^2 \right] \frac{S_{max}}{S_{ref}} \quad (69)$$

Here, the parameter S_{ref} is the reference area, also known as the planform area S_{pln} . The R_{max} is the maximum body radius, S_{max} is the maximum cross-sectional area also known as the frontal area S_{front} used in our convergence logic. The variables l_N and l_T are the nose and tail lengths as illustrated in the Fig. 120 below. Lastly, L is the entire body length. While the exact dimensions were not found, Tupolev TU-144 data was obtained from [49].

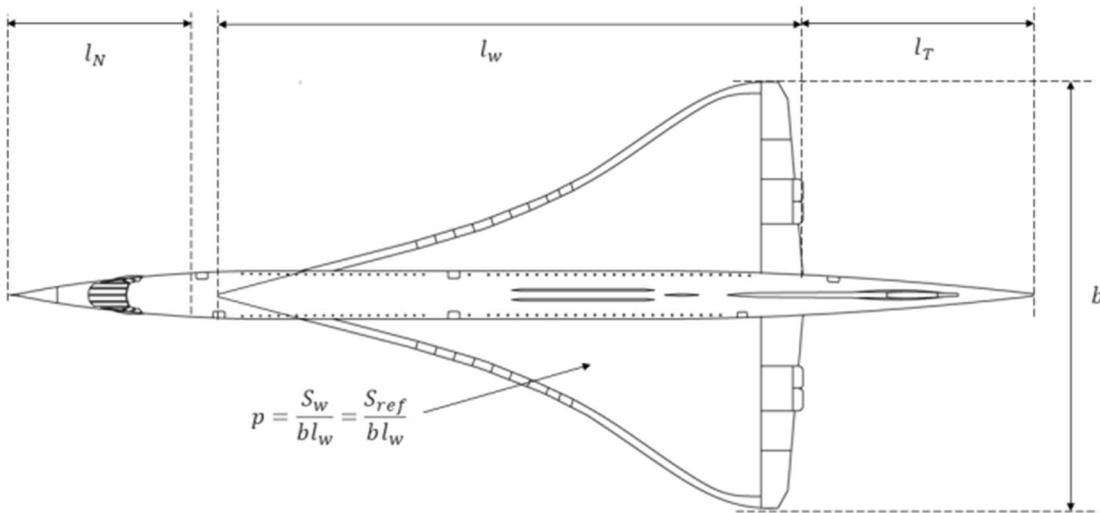


Fig. 120 Concorde aerodynamic analysis geometric parameters [79].

Raymer's method – Supersonic skin friction and wave drag coefficient [30]

Raymer gives a method for estimating supersonic parasite drag. For supersonic speeds, the wave drag becomes a lot dominant due to shock wave formation. First, a method to estimate skin friction drag is presented, followed by the area-ruled method for wave drag. Area ruling is a method to strategically allocate volume between wing and fuselage with an aim to minimize wave drag during transonic and supersonic speeds. Most area-ruled aircraft have tapered fuselage towards the end and the subsequent area is filled by the wing. The buildup of all component areas from the nose up to the end must give a Sears-Hack distribution. Note, no aircraft will have a perfect Sears-Hack distribution. The goal is to arrange components in such a way that there are no significant spikes in the area distribution. An area-ruled aircraft may be more efficient at certain Mach numbers than all.

The parasite drag is a culmination for all viscous drags experienced by the aircraft. At certain speeds, certain combinations of drag are more dominant than others. Parasite drag typically increases with speed. To estimate parasite drag, the following relation can be used:

$$C_{D_0} = C_{D_f} + C_{D_w} + C_{D_{misc}} + C_{D_{L&P}} \quad (70)$$

The last two terms of miscellaneous drag and leakage & protuberance drag are neglected for PS estimates. Only the wave drag coefficient and skin friction drag coefficient are estimated for the parasite drag portion.

	SENIOR DESIGN: MAE 4351 Project	Ref.: MAE 4351-001-2021 Date: 11. Aug. 2023 Name: Gayathri Kola Status: Complete
---	---	---

To estimate the skin friction drag for supersonic regime, turbulent flow is considered, and includes a Mach number correction. The same method is also presented in Nicolai [25].

$$C_f = \frac{0.455}{(\log_{10} R)^{2.58} (1 + 0.144M^2)^{0.65}} \quad (71)$$

The Reynold number cutoff from the Eq. (72) above is given by the following relation for supersonic or transonic regimes:

$$R = 44.62 \left(\frac{l}{k} \right)^{1.053} M^{1.16} \quad (73)$$

Where k is the skin roughness factor and l is the characteristic length of the body, meaning from nose to aircraft end. For our analysis, the skin roughness value was assumed to be 0.0000133 ft^2 for production sheet metal.

$$\left(\frac{D}{q} \right)_{wave-SH} = \frac{9\pi}{2} \left(\frac{S_{front}}{l} \right)^2 \quad (74)$$

Notice that equation above does not directly give the wave drag coefficient for a Sears-Hack distribution.

$$\left(\frac{D}{q} \right)_{wave} = E_{WD} \left[1 - 0.2(M - 1.2)^{0.57} \left(1 - \frac{\pi \Lambda_{LE-deg}^{0.77}}{100} \right) \right] \left(\frac{D}{q} \right)_{wave-SH} \quad (75)$$

Note, the terms above are not the actual drag coefficient. In fact, the Eq. (76) above must be divided by planform area to obtain correct values.

Leading Edge Suction Method – Supersonic Induced Drag Factor [30]

There are two methods presented in Raymer to estimate the induced drag factor for supersonic regimes. One is a function of Mach number and leading-edge sweep angle Λ_{LE} , and the other is simply the inverse of $C_{L\alpha}$. Raymer recommends using the second method for more accuracy; it's based on the leading-edge suction method. The relation below can be used for a quick estimate of K :

$$K = \frac{AR(M^2 - 1) \cos \Lambda_{LE}}{(4AR\sqrt{M^2 - 1}) - 2} \quad (77)$$

$$K = \frac{\alpha C_L}{C_L^2} = \frac{\alpha}{C_L} = \frac{1}{C_{L\alpha}} \quad (78)$$

5.2.3 Lift-to-Drag Ratio

The lift-to-drag ratio also known as the “aerodynamic efficiency” is the simple ratio of overall lift and drag for a given speed. The following is the relation:

$$\frac{L}{D} = \frac{C_L}{C_D} \quad (79)$$

This ratio can also be estimated using empirical relations given in Fig. 119 with interpolated values for Mach numbers in between for the PS phase.

	SENIOR DESIGN: MAE 4351 Project	Ref.: MAE 4351-001-2021 Date: 11. Aug. 2023 Name: Gayathri Kola Status: Complete
---	---	---

Additionally, some analytical methods to calculate L/D are given in the book “Hypersonic Flow” by Maurice Rasmussen. These pertain to a caret waveraider, wedge-derived waveraider and general cone derived waveraider. There are methods to estimate base drag, wave drag, skin friction drag for supersonic and hypersonic flow. However, these seemed more applicable for All-Body designs. If any of these geometries are considered in the future, these will be applicable.

Newtonian flat plate theory – Hypersonic L/D estimation [75]

The following was used from Newtonian flat plate theory for hypersonic flow to estimate lift and drag coefficients as well as the aerodynamic coefficient.

$$C_L = 2 \sin^2 \alpha \cos \alpha \quad (80)$$

$$C_D = 2 \sin^3 \alpha \quad (81)$$

$$\frac{C_L}{C_D} = \frac{2 \sin^2 \alpha \cos \alpha}{2 \sin^3 \alpha} = \frac{\cos \alpha}{\sin \alpha} = \cot \alpha \quad (82)$$

Hypersonic flow – Maurice Rasmussen [46]

Dependent on the type of body chosen caret waveraider, general cone waveraider, wedge-derived waveraider. It is applicable for lifting bodies (AB configurations). However, the estimation process requires a lot more input and may be more tedious for PS logic.

5.2.4 Oswald efficiency factor e :

A simple method to estimate the Oswald efficiency factor is given by the following relation [80]:

$$\left(\frac{L}{D}\right)_{max} = \frac{1}{2} \sqrt{\frac{\pi e A R}{C_{D_0}}} \quad (83)$$

The equation above can be re-arranged for e :

$$e = \frac{4 C_{D_0}}{\pi A R} \left(\frac{L}{D}\right)_{max}^2 \quad (84)$$

Alternative methods are given in Raymer and reference [80], however, this variable is no longer required by the P&T team.

5.2.5 Aerodynamic center

Raymer Method [30]

For the Aerodynamics team, the author will mainly focus on aerodynamic center calculations during CL and CE phase. The aerodynamic center, also known as neutral point, becomes essential for static margin calculations to assess how stable the aircraft is. The current method being considered is given in Raymer [30] and given below:

$$x_{np} = \frac{C_{L_\alpha} \bar{x}_{acw} - C_{m_{\alpha fus}} + \eta_h \frac{S_e}{S_w} C_{L_{\alpha e}} \frac{\partial \alpha_h}{\partial \alpha} \bar{x}_{ach} + \frac{F_{p_\alpha}}{q S_w} \frac{\partial \alpha_p}{\partial \alpha} \bar{x}_p}{C_{L_\alpha} + \eta_h \frac{S_e}{S_w} C_{L_{\alpha h}} \frac{\partial \alpha_h}{\partial \alpha} + \frac{F_{p_\alpha}}{q S_w} \frac{\partial \alpha_p}{\partial \alpha}} \quad (85)$$

Most of the derivative terms in the Eq. (86) above are given in empirical relations. Majority of inputs come from Geometry and from within Aerodynamics team. While this method can be used, other directly codable methods are needed that give similar results.

DATCOM Method [29]

Another neutral point method was chosen other than Raymer since the results obtained were not good. The method from DATCOM was tested with SR-71 data, and showed good agreement with the shift in aerodynamic center.

For subsonic speeds, the lift-curve slope must be known in order to determine the neutral point location. DATCOM provides an analytical equation that can be used to calculate $C_{L\alpha}$. The same equation has been given in Eq. (87) to calculate subsonic lift coefficient from Nicolai [25] seen in **Fig. 121**. The method presented below assume a non-straight tapered wing, typically for double delta or cranked wings.

$$\frac{x_{a.c.}}{c_r} = \frac{(C_{L\alpha})_i S_i \left(\frac{x_{a.c.}}{c_r} \right)_i + (C_{L\alpha})'_o S'_o \frac{(x_{a.c.})'_o}{c_{r_i}}}{(C_{L\alpha})_i S_i + (C_{L\alpha})'_o S'_o} \quad (88)$$

Here, the subscripts i and o represent inner and outer wing segments, mainly corresponding to double-delta wings. However, for single delta planforms, only the inner wing must be considered making the outer wing terms zero. The subsonic $C_{L\alpha}$ must be determined from Fig or Eq. (89). The next term involving $x_{a.c.}$ and c_r can be determined from Fig. for both subsonic and supersonic speeds. Only the taper ratio of $\lambda = 0$ is presented here since our wings are designed as such. Additionally for verification, first an average value corresponding to the lines in **Fig. 122** were used. However, to improve the method, the empirical charts used from DATCOM were trend-fitted to the best accuracy possible. These plots are given from **Fig. 123** to **Fig. 131**. Upon using these functions for re-testing the verification, this proved to be less accurate. The neutral point shifts for subsonic and supersonic regimes yielded higher values. However, due to the nature of these trendlines being easier to add in code than manually enter each empirical value for each iteration, the trendlines will be used. For subsonic regime only, an average calculated value will be inputted instead of a trendline equation since it had the most deviation from verification data.

SUBSONIC SPEEDS

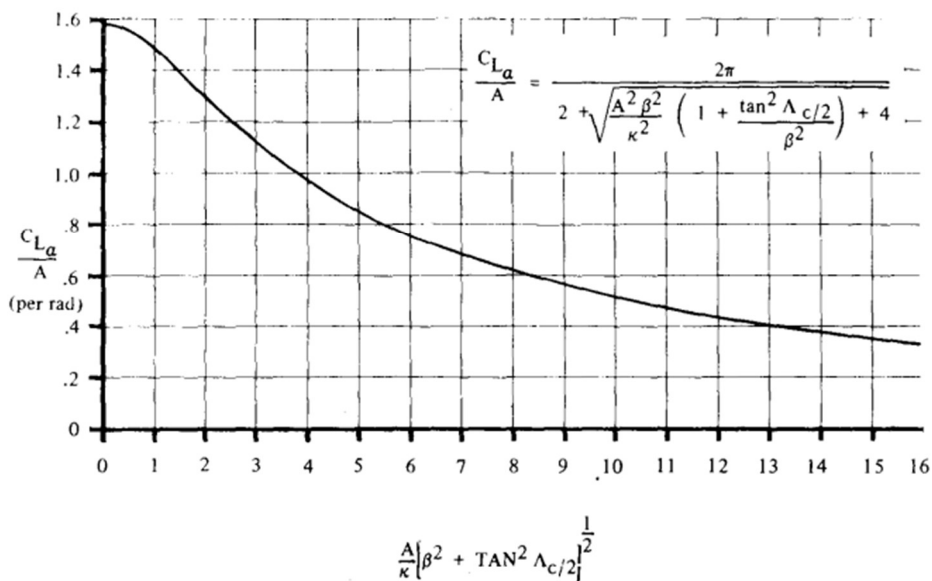


Fig. 121 DATCOM Subsonic lift curve slope [29].

For the empirical chart in **Fig. 122**, and trendline graphs, the first and last terms of x-axis are chosen for subsonic and supersonic regimes. These terms are particularly chosen for trendline equations due to the linear nature of these lines. The trendlines are made and their equations are added into a MATLAB function file that will output these terms based on inputs such as Mach number, leading edge sweep angle, root chord and aspect ratio. To improve the accuracy, each term has a 15 digits decimal extension, meaning 15 decimals has been included in the code.

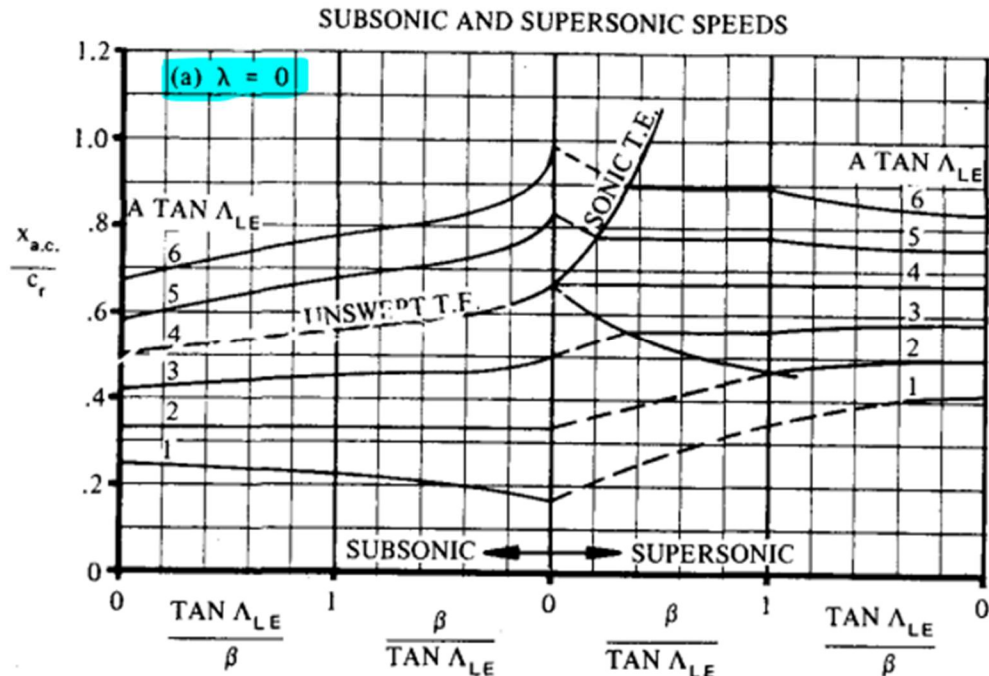


Fig. 122 DATCOM empirical relations for subsonic, supersonic aerodynamic center calculation [29].

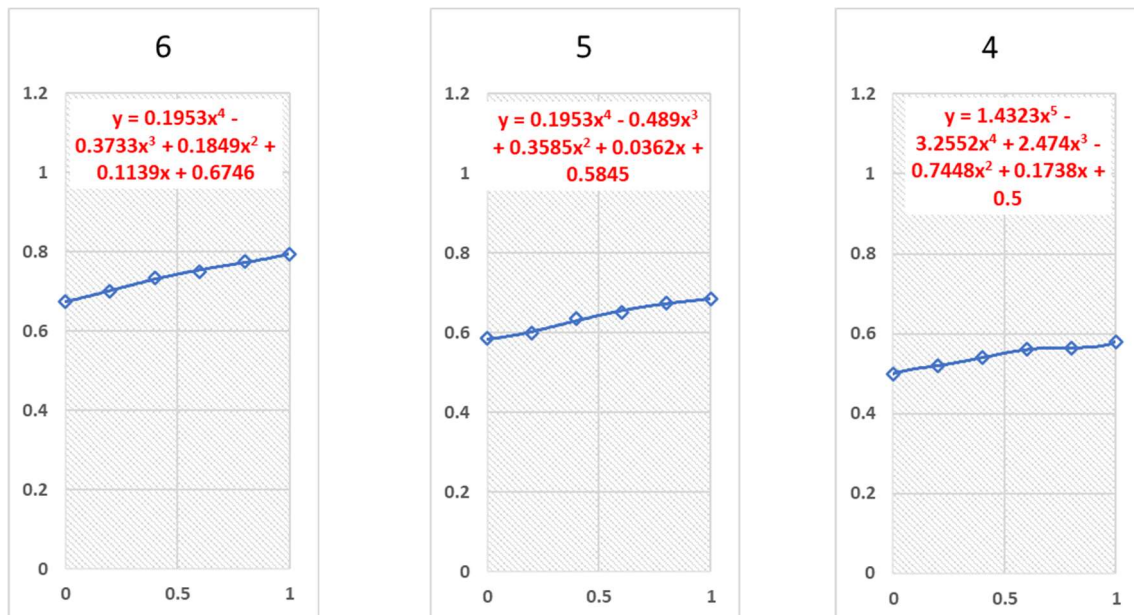
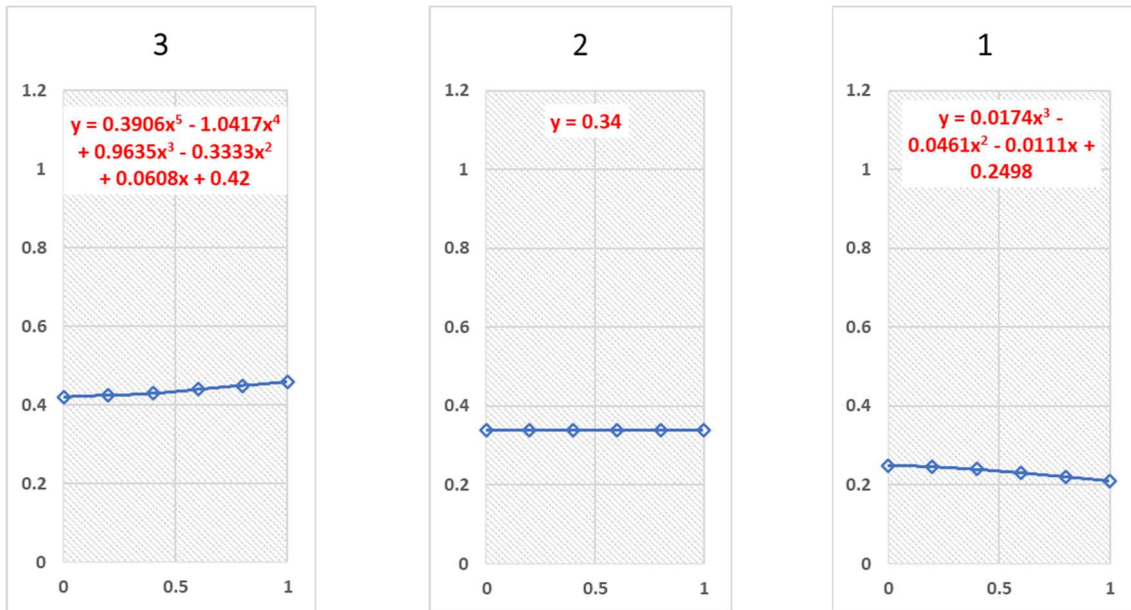
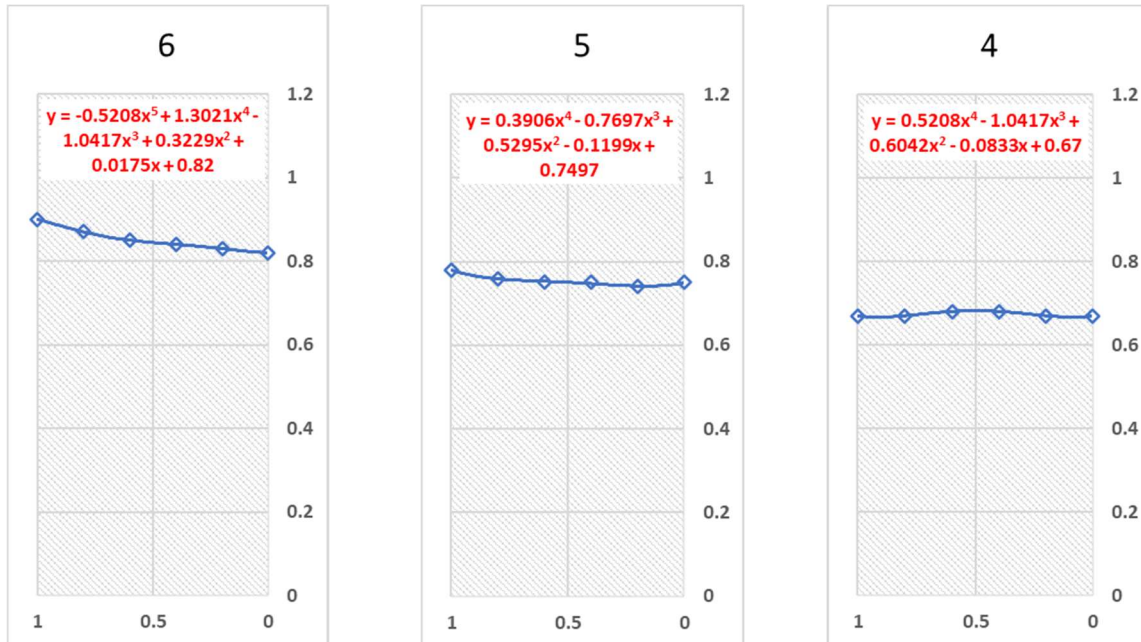


Fig. 123 Trendlines for subsonic DATCOM aerodynamic center empirical method.


Fig. 124 Trendlines for subsonic DATCOM aerodynamic center empirical method.

Fig. 125 Trendlines for supersonic DATCOM aerodynamic center empirical method.

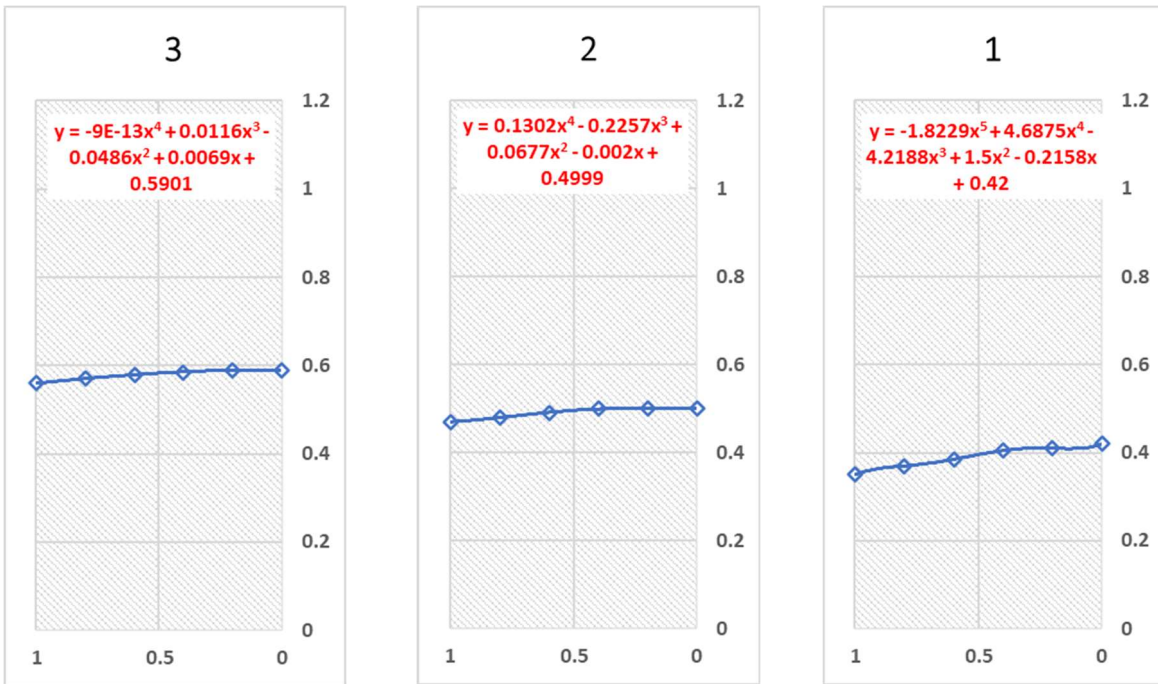


Fig. 126 Trendlines for supersonic DATCOM aerodynamic center empirical method.

For supersonic speeds, the normal force slope is considered instead of the $C_{L\alpha}$. Then, the following relation used for the calculation of neutral point.

$$\frac{X_{a.c.}}{c_r} = \frac{(C_{N\alpha})_i S_i \left(\frac{x_{a.c.}}{c_r} \right)_i + (C_{N\alpha})'_o S'_o \left(\frac{x_{a.c.}}{c_r} \right)'_o}{(C_{N\alpha})_i S_i + (C_{N\alpha})'_o S'_o} \quad (90)$$

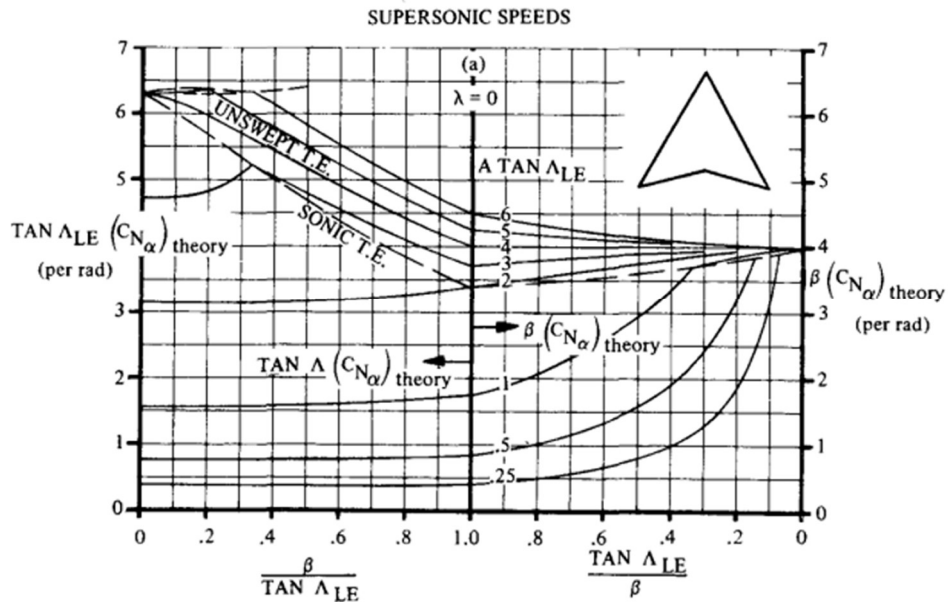


Fig. 127 Fig. 128 DATCOM empirical relations for supersonic normal force slope [29].

All subscripts are the same as for subsonic method, and supersonic $C_{N\alpha}$ can be estimated from Fig. below for non-straight, zero taper, delta or double delta wings. For coding purposes, these values will be an approximated average of the values.

For the Fig above, trendlines were created using EXCEL of the side ride. The following graphs below show the trend fitted graphs, which were used for coding into the neutral point code. The numbers 0.25 – 6 correspond to the numbers labelled on the lines in Fig. These trendline equations are made in a single MATLAB function that outputs the value based on the input. These plots are also used for $C_{l\beta}$ method from DATCOM used by Carlos Carmona [67].

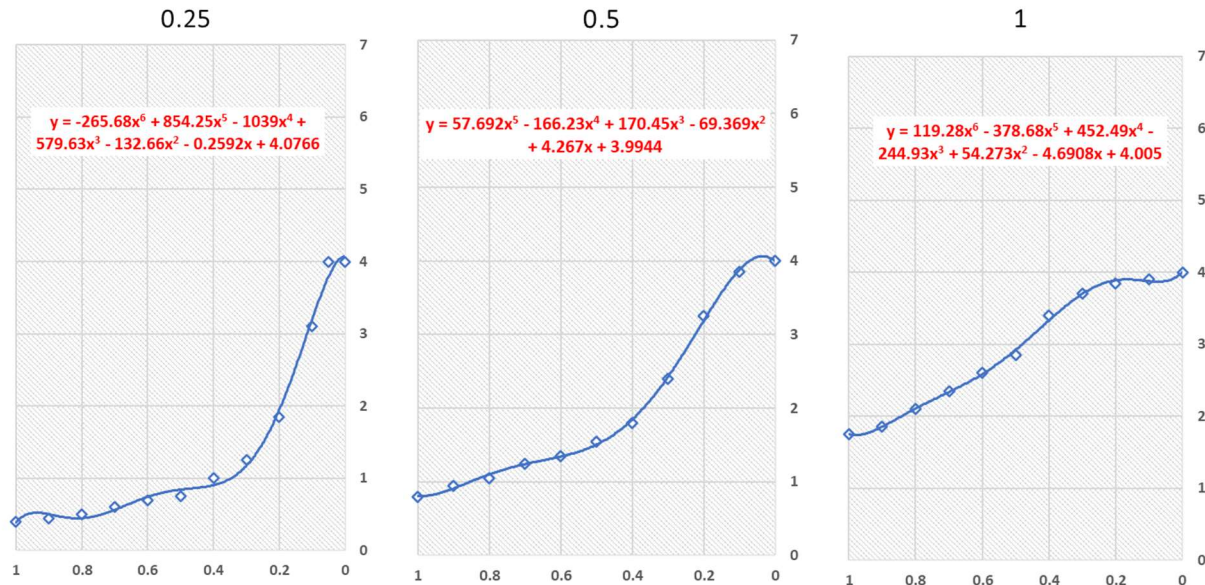


Fig. 129 Trend fitted graphs from DATCOM supersonic plots.

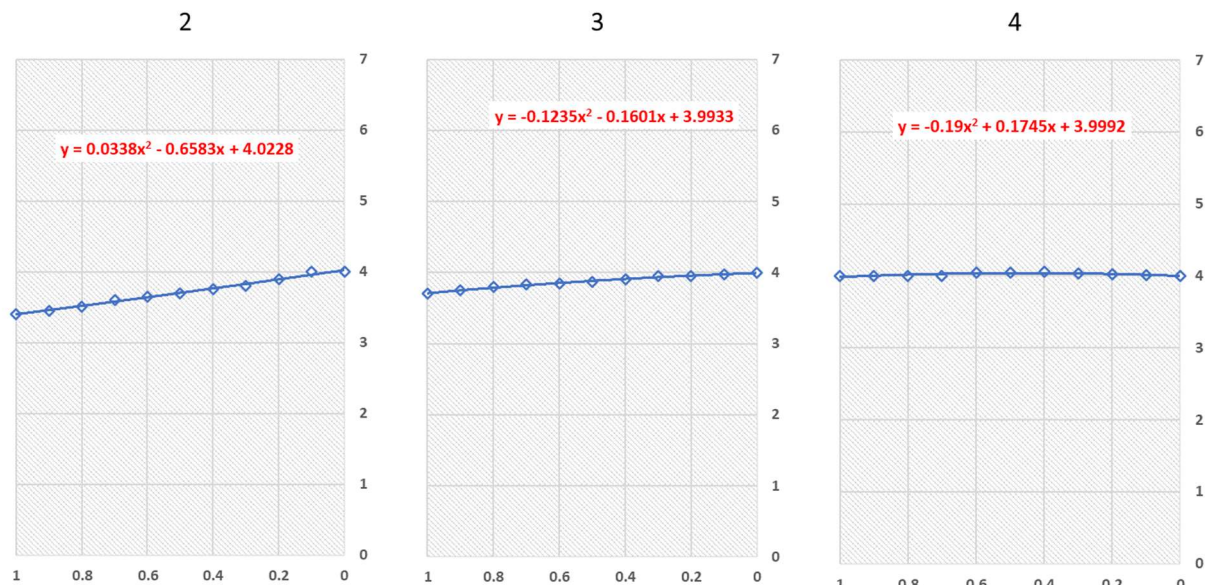


Fig. 130 Trend fitted graphs from DATCOM supersonic plots.

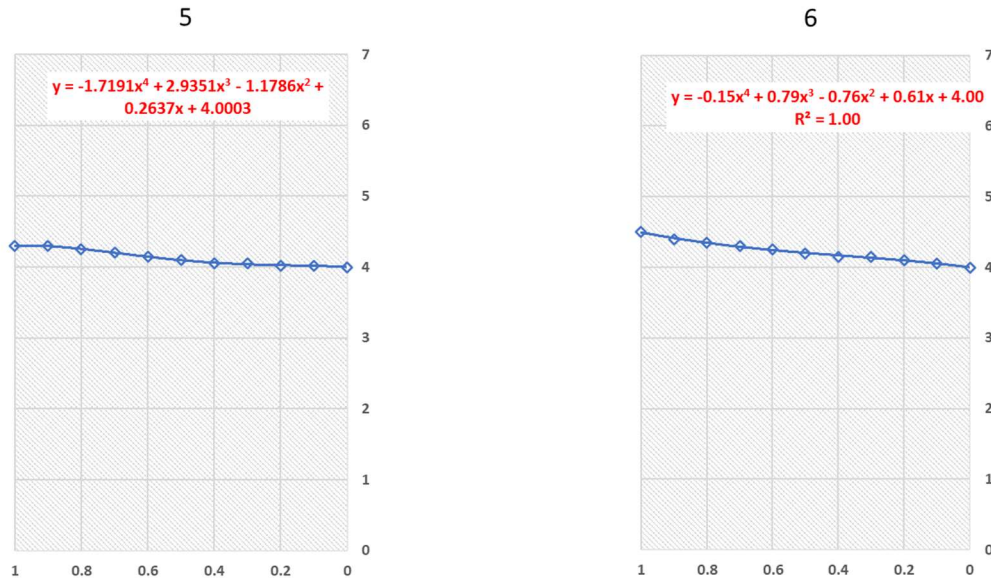


Fig. 131 Trend fitted graphs from DATCOM supersonic plots.

5.2.6 Mission Profile for PS

The mission profile has been generated by the Synthesis and P&T team. The altitude conditions have been checked by the Propulsion team. It has been decided amongst other competing teams to have JFK airport (New York) as the takeoff point and landing airport would Charles de Gaulle (Paris). There are three speed regimes with two vehicles designed for each: with single and double flow paths to engine intakes. For PS phase, there will be an ascent, cruise, and descent mission segments. One of the concerns raised was the single climb portion of the mission with no division for transonic region. This is a simplified trajectory specific to PS phase for gross sizing estimates. A detailed trajectory will be produced by P&T team in the CE phase.

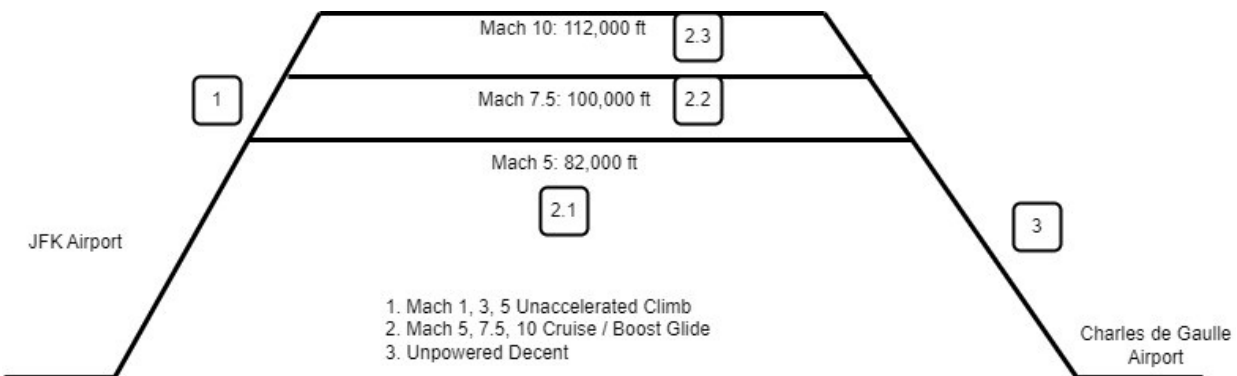


Fig. 132 Mission profile chosen for PS phase created by Noah Blakely [12].

5.3 Methodology for CL and CE

Once the aircraft geometry is defined, the lift and drag coefficients can be approximated using Oblique Shock Wave and Prandtl-Meyer Expansion wave theories. For X-43A Hyper X, an aerodynamic study was performed by *Universitat Politècnica de Catalunya* (Barcelona, Spain) by employing both analytical and Computational Fluid Dynamics (CFD) models. The study was evaluated for Mach 7 flight at 98,425 ft (30 km). For the analytical portion, several assumptions were made including steady state flow, neglecting viscous and heat transfer effects, assuming air as a calorically perfect gas. For the CFD portion, a tool named OpenFOAM was used to perform a more accurate analysis incorporating the thrust from the scramjet engine [81]. OpenFOAM is a free CFD software that is capable of

solving complex fluid flow scenarios [82]. OpenVSP is another tool that is capable of solving for aerodynamic forces within the module VSPAero [83]. Based on the geometry, either of these methods can be employed using CL and CE phase for a more sophisticated analysis.

5.4 Validation methods

This section serves to present method verification and the results obtained for aspects that are verifiable. Methods are compared with existing data, dimensions available for similar aircraft to assess the percent error between actual and method values.

Nicolai's method verification – lift curve slope for delta wings

This method was presented in section 5.2.1, and the produce was tested for varying angle of attack to hopefully obtain a maximum lift coefficient and stall region since the method was for non-linear calculations. Three aspect ratios were chosen that fall within the range similar aircraft given in Table 19. However, as seen in the **Fig. 133** below, there is no stall point. The lift coefficient values appear to be quite lower for the corresponding aspect ratio. This may not be the best method applicable for our use.

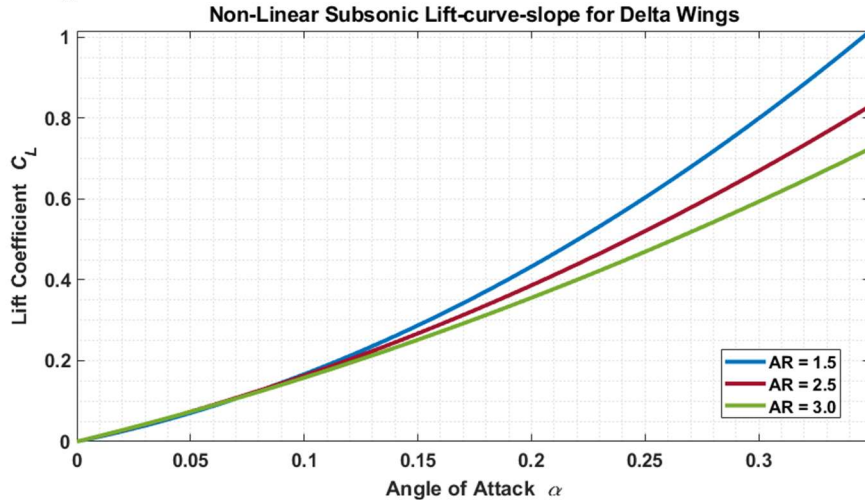


Fig. 133 Subsonic lift-curve-slope of Nicolai's method.

Raymer's method verification – supersonic zero-lift drag coefficient.

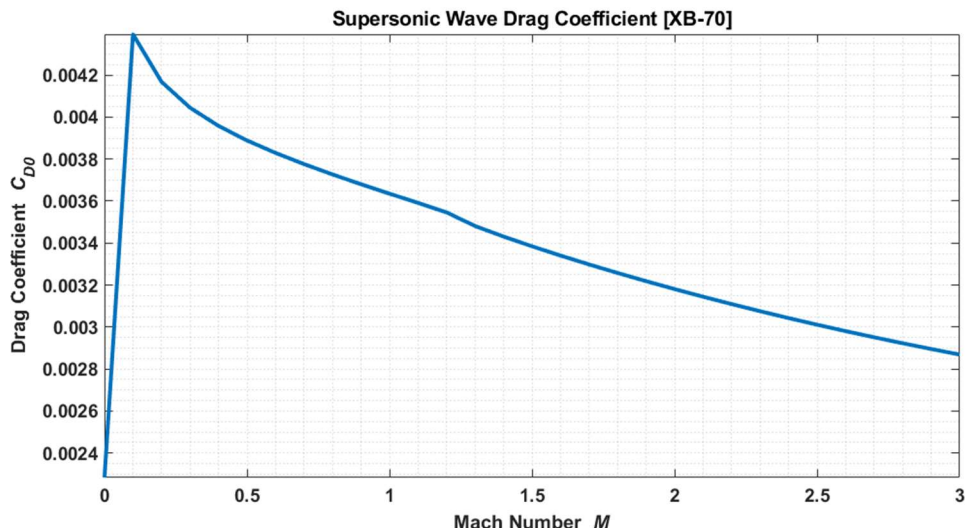


Fig. 134 XB-70 parasite drag test using Raymer's method.

	SENIOR DESIGN: MAE 4351 Project	Ref.: MAE 4351-001-2021 Date: 11. Aug. 2023 Name: Gayathri Kola Status: Complete
---	--	---

The parasite drag coefficient was tested using the method given in Raymer. When compared with the Fig. 135, the method given in Raymer does not agree. The C_{D_0} range is higher, around 0.005 for the XB-70. Additionally, unlike the Fig. 134, the parasite drag correctly increases around Mach 1, at the sonic speed. With the method given in Raymer, this spike occurs rather early, which is not correct. The geometric data for XB-70 was extracted from NASA technical report [78]. The following was the data used from the report, given in Table 21. Alternative methods need to be tested for this estimation. A reason for the low values, is the supersonic wave drag efficiency factor E_{WD} . Raymer recommends a range from 1.8 to 2.2 for supersonic transport aircraft. For the plot above, a value of 1.8 was used. But increasing the value up to 2.2 does not bring a significant change either. A higher value for frontal area would increase the parasite drag. Only the fuselage frontal area was used for calculations. The XB-70's engines are also a large part of the frontal geometric area; this was neglected in the analysis. Which could be the reason for low parasite drag numbers.

Table 21. The XB-70 data used for parasite drag verification [78].

Parameter	Symbol	Value	Units
Frontal Area	S_{front}	106	inches
Fuselage Length	l	189	ft
Planform Area	S_{pln}	1184	ft
Leading edge sweep angle	Λ_{LE}	65	degrees
Mach number	M	0 – 3	-

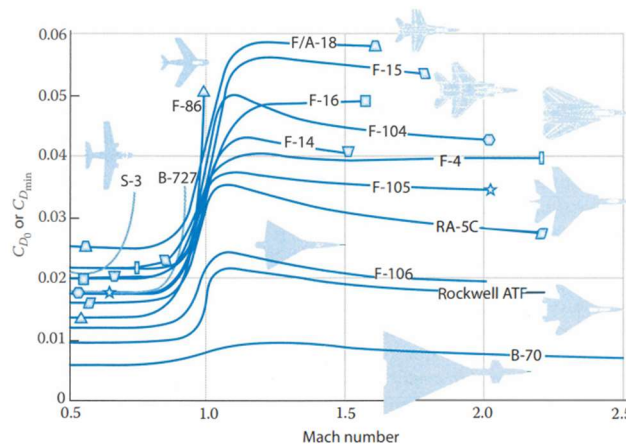


Fig. 135 Zero-lift drag coefficient verification of XB-70 [Raymer].

5.4.1 Neutral point

The methodology given in Raymer was used for neutral point calculations. However, this has yielded large values when verification was attempted. The cause of this could be because some of x-distance measurements have not been clearly specified in the text. In some places it was mentioned that these measurements are normalized with the mean wing chord, but specifics were not given. The code needs to be rechecked and verified. Due to a lack of data, available dimensions for supersonic planes were gathered and given in Table 22. The SR-71 dimensions were used.

Table 22. Verification data for neutral point methodology [49,78,84].

Parameter	Units	XB-70	SR-71	TU-144	Concorde
Subsonic C_{L_a}	1/rad				
Wing airfoil					
Wing MAC	m	23.94	12.19	23.29	
MAC	m	23.94	12.19	23.29	
Elevon area (all)	m^2	61.88	9.54		32.00
Wing area	m^2	585.07	166.76	506.97	358.25
Elevon C_{L_a}	1/rad				
Elevon airfoil					

X_{ace}	m	54.66		
X_p	m			
Forward limit for C.G, X_{cg}	m	4.55	26.27	
Aft limit for C.G, X_{cg}	m	5.98	27.59	
Engine mass flow rate, \dot{m}	kg/s			
Root chord, C_r	m	35.89	18.29	31.87
Fuselage length, l_{ref}	m	57.61	32.61	65.68
Fuselage width, w_f	m	2.54	1.52	3.50
Inlet capture area (both)	m^2	7.22	20.00	2.88

DATCOM Method – Neutral Point

Due to the inconsistency the method above, the method from DATCOM outlined in Section 5.2.5 was used. The method is compared against SR-71 data for subsonic & supersonic regimes. For hypersonic regime, the neutral point method that DATCOM describes is essentially that it moves to aircraft centroid at high Mach numbers. The method was extended to hypersonic speeds beyond Mach 3, however, there is not enough data to verify for this for SR-71. Below in Fig. 136 is the comparison against SR-71 neutral point data. Note, the effects of chine have not been added for this analysis. The method shows good agreement of the neutral point shift for up till Mach 3.

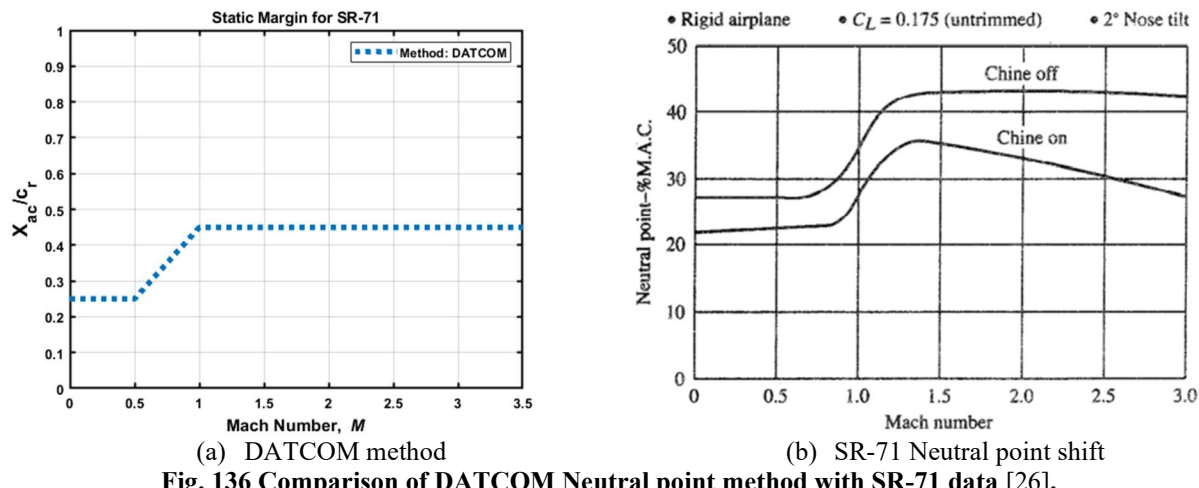


Fig. 136 Comparison of DATCOM Neutral point method with SR-71 data [26].

Extending the supersonic method up to Mach 10 gives the following results using SR-71 data. For the hypersonic case, the neutral point is assumed to have moved up to centroid of the aircraft at 50%.

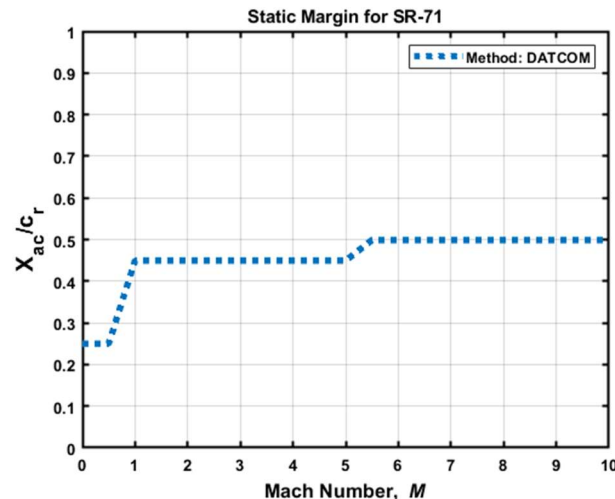


Fig. 137 DATCOM method extended to hypersonic speeds using SR-71 data [29]

However, using regression analysis functions has yielded less accurate plots as seen in **Fig. 138**. The subsonic neutral point values are much higher than the original values. Additionally, for supersonic speeds, the neutral shift is higher than normal at 60% MAC. However, since the functions have already been made, they will be utilized when evaluating neutral point shift at supersonic and hypersonic speeds.

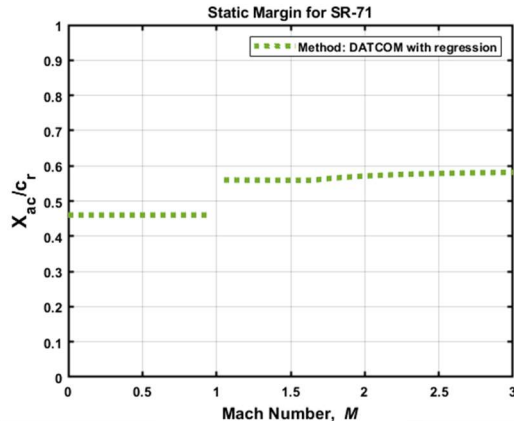


Fig. 138 SR-71 method verification of DATCOM's neutral point method using regression.

5.5 Results and Discussion for Aerodynamics

The following section presents the neutral point movement results obtained from the configured vehicles. Overall, approximations were made for hypersonic method, as the supersonic method of DATCOM was extended to higher speeds. A MATLAB function was made and directly included in the Stability and Control code. The lack of curvature was due to average values being used within the method as regression analysis resulted in large errors.

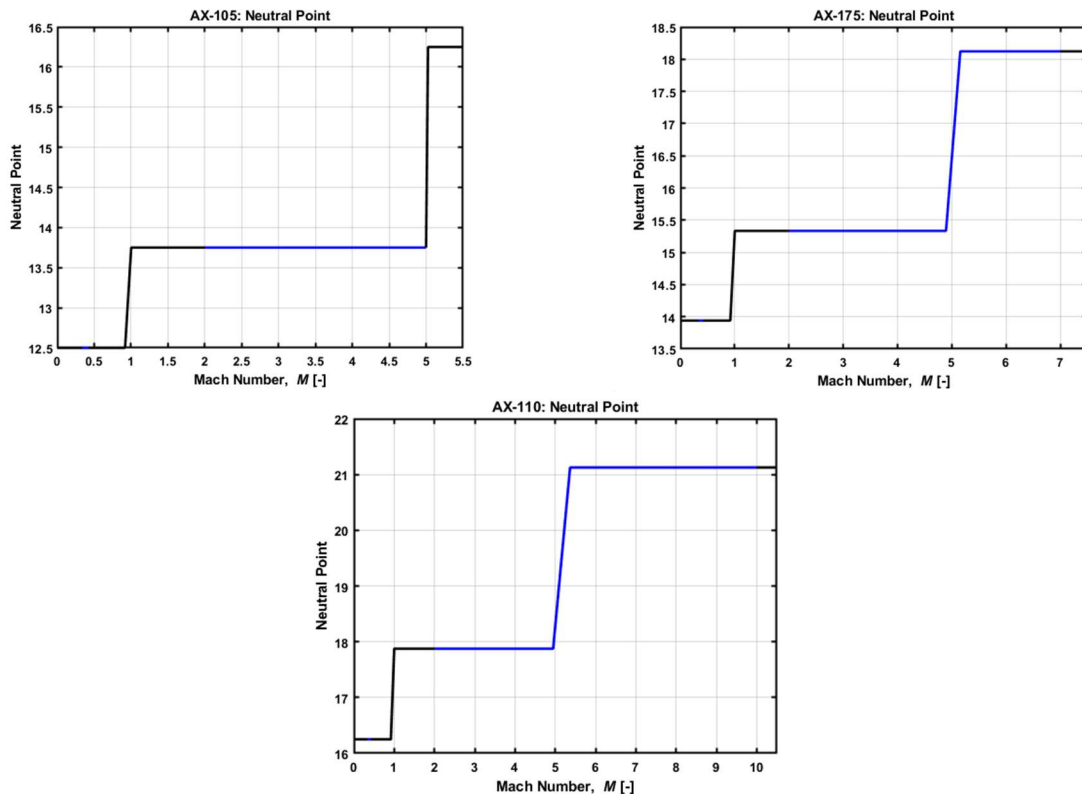


Fig. 139 Neutral point movement for single flow path vehicles.

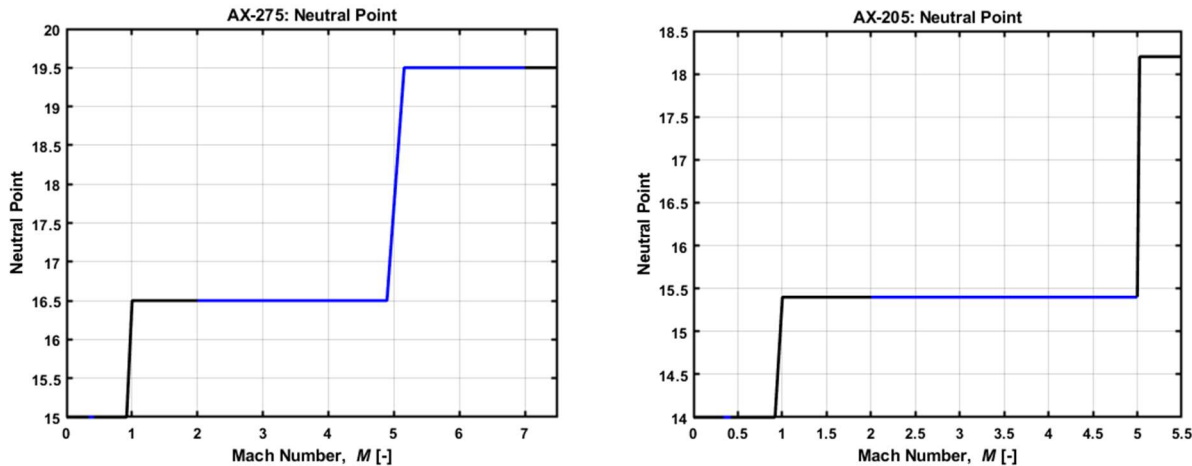


Fig. 140 Neutral point movement for dual flow path vehicles.

The blue lines in the plots above indicate the supersonic to hypersonic climbs, and the black lines indicate the subsonic and hypersonic cruise portions of the mission. Future work would include using sophisticated methods to define the neutral points based on wing geometry and simulations. It is very difficult to estimate this variable with analytical methods as they are time-consuming and slightly inaccurate.

6 Conclusions

From the literature review process, understanding was built for stability and control and aerodynamics. All relevant literature were gathered and listed in the literature review section. As weeks progress, background knowledge was built on hypersonic flight, from both an aerodynamics, and stability and control standpoint. Knowledge was build on the fact the hypersonic flow does not necessarily start at Mach 5 and control surfaces are less effective with increase in altitude. For S&C, various kinds of control surfaces were explored and justifications for suitable scenarios to use them were discussed.

The S&C team started the methodology search with segregating necessary coefficients for stability and control analysis. Important sizing conditions were chosen after researching what is most necessary for a transport aircraft with a WB configuration. Initially, Jan Roskam design texts were used for subsonic coefficients and EOM buildup. After careful consideration of the main priority being hypersonic flight, DATCOM and M. Sadraey methods were utilized. This further simplified the number of methods needed for S&C team. Due to a team member dropping out in the S&C team, the lateral and directional stability method search and verification was undertaken by Carlos Carmona while the author of this report focused on longitudinal portion and trim method buildup.

The verification process included 18 methods to be verified based on coefficients and speed regime. The method verification was conducted using XB-70, SR-71, and Space Shuttle Orbiter during descent data. The hypersonic stability coefficient was unable to be verified due to unavailability of Space Shuttle Orbiter neutral point data. The method involved neutral point and C.G. locations to be known variables. However, after comparing other methods, the same equations were mentioned with slightly different variables. Hence, the DATCOM method was used. The errors obtained from the remaining verifications ranged from 20% to 45%. The high error can be attributed many factors. Space Shuttle Orbiter, which was the only WB configuration vehicle to have extensive hypersonic data, is still a rocket powered vehicle. During the glide phase, the aircraft has almost no thrust, hence it was the best phase data to compare our methodologies with. This means the verification is weak during the cruise phase, and our vehicles have high cruise time, up to 60 minutes. There is not much publicly available data on hypersonic stability research for such lengthly amounts of time. Most hypersonic flight data from X-15 and X-43A are constrained to approximately 2 minutes. The best way for quickly verify our methods to the best possible accuracy would be to use CFD. However, our approach to verification was only analytical, and flight data comparisons.

With the method verification performed, generic sizing method were used with verified coefficient methodologies. The sizing results for elevons yielded in need for increased elevon size from CL results and considerably high elevon

	SENIOR DESIGN: MAE 4351 Project	Ref.: MAE 4351-001-2021 Date: 11. Aug. 2023 Name: Gayathri Kola Status: Complete
---	---	---

deflection angles even with increased sizes, upto -25 degrees. Additionally, most of our vehicles need to have resized wings as a future work. The increased elevon sizes resulted large elevon chord length, some as high as 40% of aircraft length. This is very undesirable. However, these new sized values were used for stability assessment directly due to time constraints associated with resizing the wings and iterating through CL and CE again. This explains why we do not see HTHL hypersonic aircraft. These vehicles need to have high aspect ratios to get off the ground but very low aspect ratio to travel at hypersonic speeds. The vertical tail sizes from CL results were higher than needed for two vertical tails. Hence, for some vehicles the vertical tail sizes were decreased after checking for controllability in engines out scenario, inlet unstarts at cruise and crosswind landing of 40 knots.

The stability results show that the vehicles are very longitudinally stable due to airfoil structure and the maximum thickness according at half-chord. This keeps the neutral point very far back from the initial phases, and progresses to be more stable as speed increases. However, the lateral stability takes a huge hit, especially in the subsonic regime. This could also be due an error in the code itself. If this is ignored, the roll stability can be increased by having wing and tail dihedral. However, the increases drag and also impacts longitudinal and directional stability as a consequence. Overall, many design improvements can be made to increase both stability and controllability.

The Mach 10 dual flow path was deemed to be infeasible by the Propulsion discipline, hence a configuration was not made. The reasoning made was that the combustion temperature within the scramjet engines reach upto 6,000 K, thereby heating up the aircraft surface temperature leading to dangerous aerothermal effects. Additionally, the Propulsion team informed that the dual flow path vehicles cannot make it through climb phases without having a variable geometry inlet or spillage. Both of which are again dangerous from a safety standpoint. Additionally, it is the personal opinion of the author that building a hypersonic transport vehicle from conventional technology and Kerosene based fuel will leave terrible impacts for the environment. If this vehicle were to exist, we really need to reimagine the propulsion system and use a different type of fuel. Not necessarily fossil fuels. From a cost standpoint, these vehicles will be very unreasonably expensive, instead, the cost could be put toward developing a different type of propulsion system all together in order to make it feasible.

7 Historical Development

The following section will be dedicated to weekly progress: work that was done and then work that needs to be completed for the following week.

7.1 Week 1

The first week was spent gathering literature suitable for each discipline and material pertaining to hypersonic aircraft after the project was launched. The basics of hypersonic aerodynamics were reviewed and understood from previous course texts. For Stability and Control, resources other than DATCOM that can be applied for hypersonic aircraft were searched. Time was spent on looking into project aircrafts such as the Spirit of St. Louis, Gulfstream G700, SR-71, Quarterhorse, Darkhorse, Halcyon, and X-43A. The team meeting included basic communication setup and expectations for weekly meeting presentations. The author will be keeping track of minutes of meetings and producing written summaries for the team at the end of each meeting. The next week's goal is to identify important parameters for Aerodynamics and Stability and Control that can aid in Parametric Sizing process.

7.2 Week 2

The Stability and Control team decided to split responsibilities by topic: longitudinal, lateral, and directional stability and control. The author will be focusing on longitudinal stability and control. The week was spent gathering methodology for longitudinal Stability/Control for CL and CE as well as understanding the issues emerging at hypersonic speeds. The Aerodynamics team decided to look into methods for calculating wing geometry parameters needed and for coming up with a list of similar aircraft and their geometries for reference.

Next week, the goal is to write MATLAB scripts to build on the collected methodology.

7.3 Week 3

The week was spent understanding hypersonic aerodynamics and gathering suitable methodology for PS phase. The Synthesis and Performance team have given Aerodynamics team with the inputs required: CL at takeoff, subsonic CD, supersonic CD, hypersonic CD, maximum subsonic lift coefficient, L/D and Oswald Efficiency factor. Aircraft within similar weight class were gathered for method verification. The Synthesis team had requested analytical

	SENIOR DESIGN: MAE 4351 Project	Ref.: MAE 4351-001-2021 Date: 11. Aug. 2023 Name: Gayathri Kola Status: Complete
---	---	---

equations for the inputs required to code into convergence logic. However, upon further research it appears that the accurate calculation of supersonic, hypersonic wave drag requires higher fidelity software. Since the current geometry is a spatula double delta wing, it was difficult to find equations for the same. Empirical relations for WB delta wing with double delta estimation techniques were easier to find. Hence, it appears best to use empirical estimates for PS. Various design features were studied, however, there was less time to write about them. It will be included in the next report.

For Stability and Control, the majority of data was found for control surfaces of the chosen WB aircraft. Less lucky with AB aircraft. The volume coefficients have to be calculated and a database needs to be made to include in code. For next week, methodology for supersonic and hypersonic pitching moment calculation needs to be found and method verification must be done.

7.4 Week 4

The week was spent gathering methodology for Aerodynamics team. The initial plan was to find methodology for all parameters related to hypersonic flight by all three team members to compare the assumptions. However, later in the week, the author focused on supersonic drag build up, calculation and verification to add to Aerodynamics module in Synthesis convergence code. Three simple estimation methods were found, of which the author decided to go with the method given in Raymer since the inputs were simpler to obtain from Geometry module.

7.5 Week 5

The midterm week was spent gathering and organizing control sizing methodology and identifying useful methods for critical conditions in S&C. Verification literature was gathered and organized based on aircraft type. Additionally, methodology for calculating many stability and control derivatives was found in Roskam's design text and the method is being implemented in code. The code is currently under works, being written with expected completion after week 6. Control surfaces and geometries were explored by the author, however, not much information was found on elevon geometries. Geometries for vertical tail have been found. For control surface sizing code, all the methodologies have been identified, the code must be written and tested.

For Aerodynamics, additional methods for neutral point calculations were looked at, however, the author will be continuing with the method presented in Raymer unless another method is found.

7.6 Week 6

The week was spent developing design codes for S&C team. Additionally, trim conditions codes are also being developed. Initially, the method given in Roskam (VI-VII) was being used. However, upon further deliberation, coding a generic trim method seemed more effective considering time constraints. This code is expected to be completed early next week. Verification for longitudinal & lateral was completed for the most part. The directional verification is expected to be completed by next week. Some methods have yielded large errors due to lack of data or overly simplified assumptions. These methods will be used unless a better method is found.

7.7 Week 7-10

The weeks were spent completing verifications, building sizing codes, trim codes, neutral point codes, and stability codes. All focus was put to complete configuration layout and control sizing before the final presentation. There were issues with how the trim code was updating the angle of attack and sideslip angles. A simpler code was made with 3 EOMs instead. This worked, however, the S&C team focused more on finishing sizing for all five CL models and producing stability results first. The past few weeks were a blur due to many things being completed simultaneously and sent to the S&C team.

8 ABET Accreditation

The following section outlines how educational objectives of the ABET accreditation have been achieved throughout the semester for outcomes listed below. The outcomes and/or key assignments are described below.

8.1 Outcome 2

"An ability to apply engineering design to produce solutions that meet specified needs with consideration of public health, safety, and welfare, as well as global, cultural, social, environmental, and economic factors."

	SENIOR DESIGN: MAE 4351 Project	Ref.: MAE 4351-001-2021 Date: 11. Aug. 2023 Name: Gayathri Kola Status: Complete
---	---	---

1. Accomplish

The requirements for outcome 2 will be addressed to accomplish the team project deliverables. Each team split into multiple disciplines, each focusing on specific aspects of aircraft design. The team's interconnectivity is decided by the Synthesis team that starts with grossly estimating the size of the vehicles. The Synthesis team designates the flow of important parameters needed by each discipline. In order to do this, a project timeline is made, that estimates the time required to complete each phase of the conceptual design process. Each discipline also estimates a timeline based on time required for literature review, deciding, and testing methodology, completing method verification, and showing results. For literature review, many articles were requested from the UTA's Inter-Library Loan service to learn aspects of Hypersonic flows. Weekly meetings are conducted where the team gathers at a decided time and discusses progress made, issues, and solutions. Any questions on how to accomplish the tasks are directed to the class's teaching assistants and the professor.

2. Demonstrate

To demonstrate the outcome 2, weekly reports are produced that document our progress. Throughout the semester, a detailed literature review is performed, and key findings are addressed in the reports. Through the process of literature review, many solutions are learned that have been applied in the past for similar problems. One such discussion that pertains to outcome 2 can be explained by the need for stability assessment in aircraft design. Making a marketable design that has high performance is useful, however, for safety considerations, the stability and controllability of the design must be assessed to prove its feasibility. For the consideration of public health, the trajectory team has chosen a mission profile that is closer to the ocean to reduce noise problems for the public. The fuel required is Kerosene, a more economic option for the aircraft industry. The global, cultural, and economic factors are addressed by the costs team. The final deliverables for Outcome 2 are the final report, a final presentation, 3D solution spaces, 3D printed models of all feasible configurations, and a final poster. The team works together to determine if a design is feasible. Each team contributes to some aspect of the final deliverable, if not directly physical, then the team would be involved in assessing its feasibility. To make a design feasible, different solutions are explored and tested. If improvements are the outcome of the analysis, they are chosen as a possible solution.

3. Key Assignment

The important assignments of Outcome 2 are the midterm report, midterm presentation, final presentation, and final report. There is a high emphasis on these assignments throughout the semester, where the progress reports capture the lead up to the main assignments. The midterm and final report discuss in detail the deliverables in Demonstrate section of Outcome 2.

8.2 Outcome 3

"An ability to communicate effectively with a range of audiences."

1. Accomplish

The Outcome 3 is accomplished by producing a final report and giving a final presentation in presence of the other competing teams, course professor, teaching assistants and other faculty during the final week. The weekly reports are produced to document the progress. The final report is organized into different segments to clearly convey the concepts being talked about; relevant background information is needed to showcase results obtained. The midterm report discusses the progress made up to the midpoint in the semester and gives necessary plans of action to complete tasks outlined.

2. Demonstrate

The Outcome 2 can be demonstrated by completing the necessary weekly reports, midterm and final reports and the presentation outlined in Accomplish section. The midterm and final presentation are a less-detailed communication format where we explain our progress, insights, and results in a clear and concise manner so that a variety of audiences can understand. The reports on the other hand are more detailed, discussing intricate aspects that may not be common knowledge, explaining the approach taken and findings to a more informed reader of aircraft design.

3. Key Assignment

The important assignments of Outcome 3 are the midterm report, midterm presentation, final presentation, and final report. There is a high emphasis on these assignments throughout the semester, where the progress reports capture the

	SENIOR DESIGN: MAE 4351 Project	Ref.: MAE 4351-001-2021 Date: 11. Aug. 2023 Name: Gayathri Kola Status: Complete
---	---	---

lead up to the main assignments. The midterm and final report discuss in detail the deliverables in Demonstrate section of Outcome 3.

8.3 Outcome 4

"An ability to recognize ethical and professional responsibilities in engineering situations and make informed judgments, which must consider the impact of engineering solutions in global, economic, environmental, and societal contexts."

1. Accomplish

Design decisions made throughout the semester have involved safety and the ethical responsibility of aircraft design. One such case is for the chosen trajectory as given by the Performance & Trajectory discipline. The trajectory layout considers the implications of the sonic booms that are generated from an aircraft as it goes supersonic. This is not acceptable by regulations over land, and the aircraft must only go supersonic over oceans. Hence, the trajectory for supersonic travel is not over land, additionally, it helps that our aircraft has a trans-Atlantic route. Another consideration was made during the control surface design process. There were two choices. The first option was to have a single vertical tail and second was to distribute that area into equally small twin tails placed at a distance from one another. This significantly increases lateral stability during high-speed flight. Having a single vertical tail would have inhibited the flow of air from the fuselage, where a wake region would be created. This increases heat above the aircraft cabin, having a higher load on the thermal regulation systems.

2. Demonstrate

The Stability and Control segment of this report especially pertains to the considerations of safety and reliability. The aircraft must be designed and assessed from a stability standpoint to see if the aircraft will complete this mission requirements smoothly. This is demonstrated by extensive literature review on suitable control surfaces for hypersonic flight, and aircraft design. If the stability is lacking in any area of the mission, these segments are identified and listed to understand the weak points of the design and possibly come up with solutions to negate these issues. In terms of the economic and environmental impacts of the hypersonic aircraft concept with Kerosene-based fuel type, the downsides are discussed in the conclusion segment of this report.

3. Key Assignment

The weekly progress reports are presented to systematically document these responsibilities in engineering solutions and make informed decisions.

8.4 Outcome 5

An ability to function effectively on a team whose members together provide leadership, create a collaborative and inclusive environment, establish goals, plan tasks, and meet objectives.

1. Accomplish

The Outcome 5 is accomplished by having the class divided into three competing teams designing with same goal, but using different configuration baselines – Wing-body, Blended-Body and All-Body. Each team is split into nine sub-disciplines, focusing on different aspects of aircraft conceptual design process. The team consists of a Chief Engineer, overseeing all the requirements and deliverables at all stages. Each sub-discipline consists of a discipline lead tasked with leadership, organizing discipline meetings, objectives, and plan of action of the respective discipline. All team members choose two sub-disciplines and choose a primary discipline within the two. The team members perform individual literature reviews and sort methodology, verifications needed for producing results. These are explained in weekly reports.

2. Demonstrate

Each week, the team meets together to outline all the tasks needed to be completed and learn about the overall progress of the team as well as learn about any design challenges any of the disciplines are facing. Ideas are discussed for the best approachable solution and implemented throughout the week. The flow of the disciplines tasks is segregated by the Synthesis discipline on a multidisciplinary level. ‘Burning Slides’ were made to showcase the team’s progress and sent to the professor and teaching assistants. Feedback was given by the teaching assistants on our presentation and later implemented by the team for future assignments.

	SENIOR DESIGN: MAE 4351 Project	Ref.: MAE 4351-001-2021 Date: 11. Aug. 2023 Name: Gayathri Kola Status: Complete
---	---	---

Within the Stability and Control discipline, the team met after team's weekly meetings (twice a week) to discuss about the methods found, logic for control surface sizing, suitable verification available and tasks to be completed. Any useful resources found were shared amongst team members to help speed up discipline's progress.

3. Key Assignment

The class requires the students to work in teams for the project. Teams are decided amongst students and the Chief Engineer for the team is picked by the members. Each team must respond to a request for proposal (RFP) and must form a pseudo engineering design company. The project is for the entirety of the semester, and the managerial tasks are divided by the Chief Engineer with the help of the Synthesis discipline members. The team members are responsible for individual disciplines chosen and the literature review process. The disciplines must communicate amongst one another, set constraints, and work to mitigate issues as they arise. All the members are required to write weekly reports, midterm, and final reports, giving more background on structure and process taken to work on a design solution from their disciplinary perspectives.

8.5 Outcome 7

An ability to acquire and apply new knowledge as needed, using appropriate learning strategies.

1. Accomplish

The first week of the semester is exclusively dedicated to project introduction and beginning a broad literature review and gathering all available resources on a particular topic. These resources are listed within the weekly reports and updated with new references. The literature review starts by first searching for similar missions, aircraft, programs performed in the past and their conclusions. Then, present day programs are screened, and knowledge is built up. Lastly, any information on future programs is learned and their goals, missions and importance are understood. This was done by looking into Space Shuttle, supersonic aircraft, and past hypersonic programs. The current and future programs discussed are from Hermeus vehicles, the Quarterhorse and Halycon. Multiple tables in this report compare data of past, present vehicles to build a Data-Base, and Knowledge-Base approach to the literature review.

2. Demonstrate

The Outcome 7 ways to demonstrate are described in the Accomplish section. This application of new knowledge is demonstrated by documenting findings, literature resources and references in an organized manner in the weekly reports. The Literature Review section of this report lists the important and preliminary resources gathered for learning new material. One strategy to learning and applying new knowledge comes from gathering relevant methodologies for a particular analysis and verifying it with existing data whenever available. This ensures that the student is going in the right direction when a new challenge comes up. This was demonstrated by performing method verification for stability derivatives before using the method in a generic methodology build up.

3. Key Assignment

The major assignment for Outcome 7 are the weekly reports, midterm report and final report that document their overall DB and KB build up process.

Appendix

Appendix A

This appendix serves to give additional information on matters pertaining to Stability & Control and Aerodynamics disciplines.

$\frac{x_{a.c.}}{c_r}$	(calculations based on exposed wing geometry)
1.	Single wing with body (i.e., no cruciform or other multipanel arrangements)
2.	$M \leq 0.6$; however, if swept wing with $t/c \leq 0.04$, application to higher Mach numbers is acceptable
3.	Linear-lift range
C_{L_α}	
4.	$(\text{Body diameter})/(\text{wing span}) \leq 0.8$
5.	No curved planforms
6.	Bodies of revolution
7.	Slender-body theory
8.	$M \leq 0.8$, $t/c \leq 0.1$, if swept wing with round LE

$\frac{x_{a.c.}}{c_r}$	(calculations based on exposed wing geometry)
1.	Straight-tapered wings
2.	Single wing with body (i.e., no cruciform or other multipanel arrangements)
3.	Symmetric airfoils of conventional thickness distribution
4.	Linear-lift range
C_{L_α}	
5.	Bodies of revolution
6.	Slender-body theory
7.	$\alpha = 0$

(a) Subsonic

(b) Transonic

$\frac{x_{a.c.}}{c_r}$	(calculations based on exposed wing geometry)
1.	Single wing with body (i.e., no cruciform or other multipanel arrangements)
2.	Linear-lift range

C_{N_α}	
3.	Breaks in LE and TE at same spanwise station
4.	Bodies of revolution
5.	Slender-body theory
6.	$M \geq 1.4$ for straight-tapered wings
7.	$1.2 \leq M \leq 3$ for composite wings
8.	$1.0 \leq M \leq 3$ for curved planforms

(c) Supersonic

Fig. 141 Assumptions to calculate pitching moment as a function of angle of attack from DATCOM [29]

Following has been removed from the methodology in the Stability and Control section:

DATCOM method at subsonic speeds:

The method to calculate pitching moments at subsonic speeds for a wing body configuration is given in DATCOM [29]. The method given below is the same for *supersonic* and *transonic* regimes as well, however, the assumptions differ. The assumptions are given in the Appendix A. According to DATCOM, this method is applicable to the wing body configuration of a conical body mounted on a delta wing as seen in Fig. below. This method utilizes slender body theory, its limitations are that it does not apply to wings with sweptback trailing edges [29].

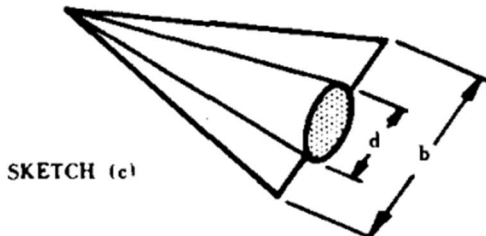


Fig. 142 Specific wing-body geometry for calculating 3D lift-curve slope of the wing [29].

$$C_{m\alpha} = \left(n - \frac{x_{a.c.}}{c_r} \right) \frac{c_r}{c} C_{L\alpha} \quad (91)$$

The parameters given in the Eq. (92) are shown in Fig below.

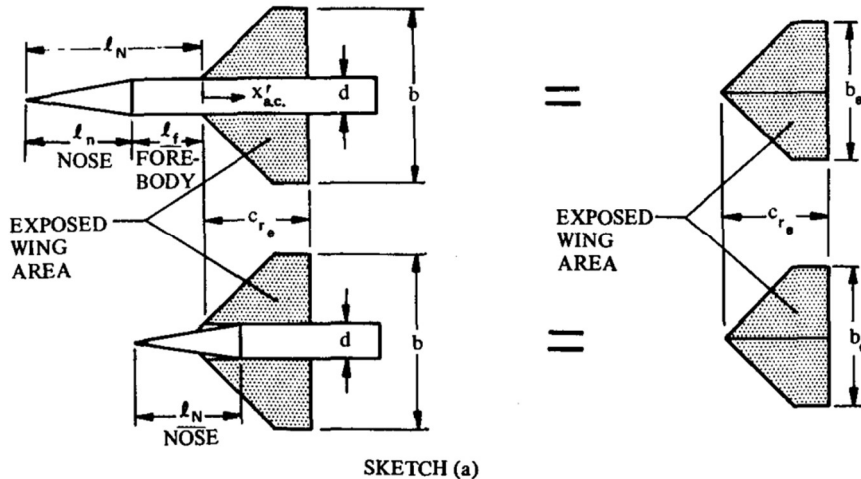


Fig. 143 Wing geometry parameter definitions [29].

Here, the 3D lift-curve slope for WB configuration is calculated by the following relation:

$$(C_{L\alpha})_{WB} = K_{(WB)} (C_{L\alpha})_W \quad (93)$$

Where $K_{(WB)}$ can be estimated from the following Fig. below. It requires the diameter of the body and wingspan.

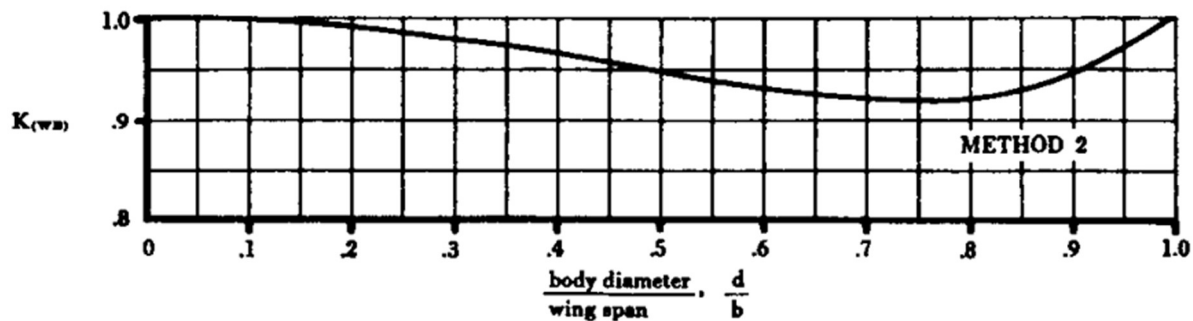


FIGURE 4.3.1.2-12c LIFT RATIO FOR METHOD 2

Fig. 144 Method to find lift ratio for estimating pitching moments [29].

To find the subsonic $(C_{L\alpha})_W$ for just the wing, the following relation must be used for a double-delta wing. There are methods available for Ogee and Gothic wings as well. The distinction in geometry is seen below in Fig.

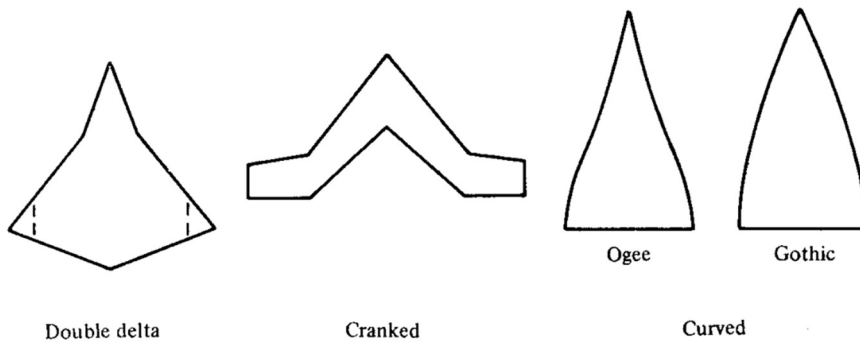


Fig. 145 Wing geometries presented to estimate the lift-curve slope [29].

As per the needs of the Aerodynamics team, any of these geometries can be chosen. Since the lift-curve slope is an output given by the Aerodynamics team, this portion will be further discussed in the section 5 once the geometry is chosen. It appears that it would be best to find the lift-curve slopes using a higher fidelity software such as OpenVSP once the geometry is known. The method laid out in DATCOM is time intensive.

The following are initial neutral point results obtained from using the methods provided in Raymer as seen in **Fig. 146** **Fig. 148**. These are placed in the Appendix as the results are not correct.

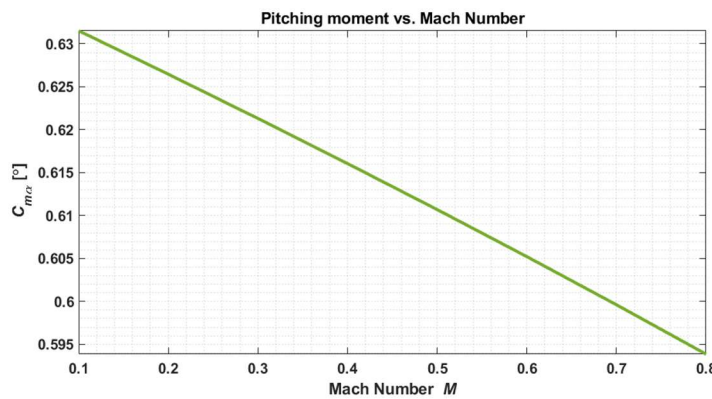


Fig. 146 Pitching moment as a function of angle of attack for subsonic speed.

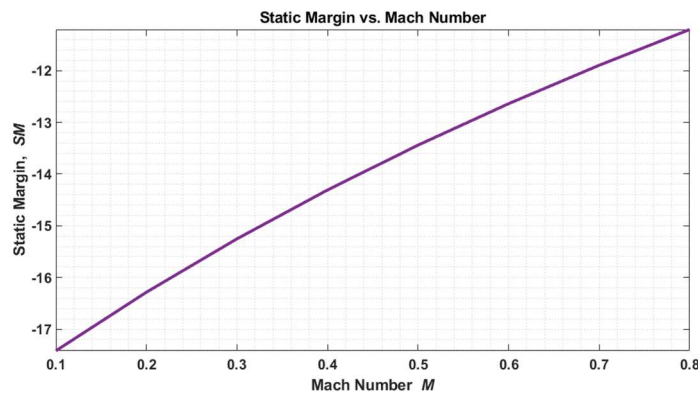
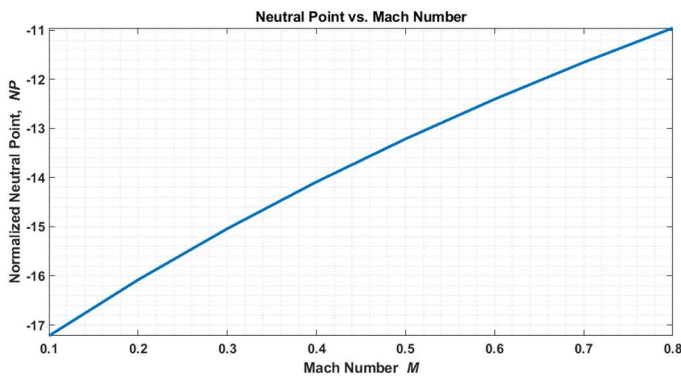
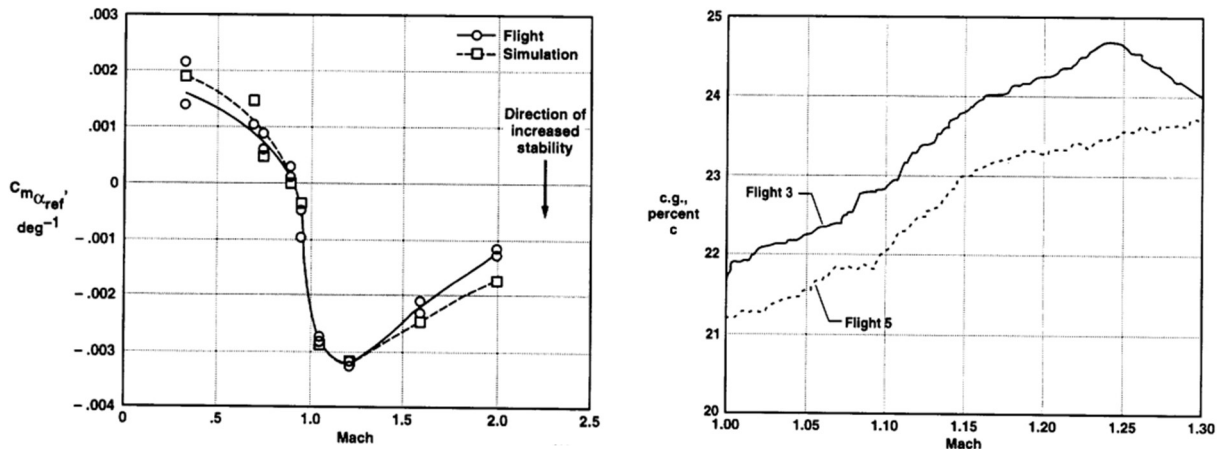


Fig. 147 Static margin change for subsonic speed.


Fig. 148 Neutral point shift for subsonic speed.

The pitching moment derivative verification data comes from NASA's LASRE experiment mentioned in Section 4.10. The data used for pitching moment derivative verification is given below in **Fig. 149**. The LASRE report mentions that the C.G. range evaluated for was from $0.19c$ to $0.24c$. Where c is the reference mean chord, which is 37.7 ft [21].


Fig. 149 NASA LASRE verification data for pitching moment derivative [21].

Appendix B

This appendix serves to give method summary cards chosen or considered at a certain phase in the design process.

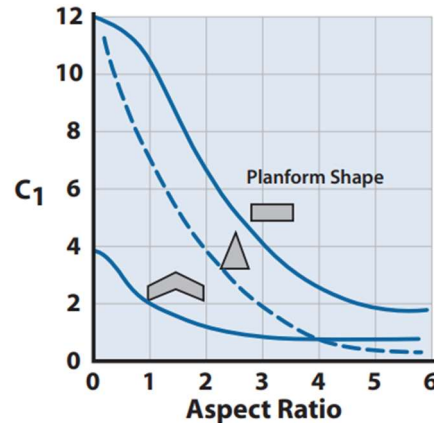
AERODYNAMICS

Method Overview					
Discipline	Design Phase	Method Title	Author(s)		
Aerodynamics	Parametric Sizing (PS)	Subsonic lift-curve-slope for delta wings. Subsonic lift coefficient for delta wings.	Nicolai		
Reference:					
Nicolai, L. M., and Carichner, G. E. <i>Fundamentals of Aircraft and Airship Design</i> . Volume I AIAA 2010					
Brief Description:					
Lift-curve-slope $C_{L\alpha}$ calculation for subsonic, Low AR, delta wings with a non-linear lift correction. The constant C_1 is estimated from the chart given below.					
Assumptions		Applicability			
<ul style="list-style-type: none"> • Subsonic • Delta wing, planform • Low aspect ratio (AR) • Non-linear lift 		Subsonic regimes only.			
Execution of Method					
Input					

Mach number M , leading edge sweep angle Λ_{LE} , aspect ratio AR , angle of attack α

Analysis Description

1. $\beta = \sqrt{1 - M^2}$
2. $\frac{dC_L}{d\alpha} = C_{L\alpha} = \frac{2\pi AR}{2 + \sqrt{4 + AR^2\beta^2(1 + \left[\frac{(\tan^2 \Lambda_{LE})}{\beta^2} \right])}}$
3. Chart: delta planform
4. $C_L = \left(\frac{dC_L}{d\alpha} \right)_{\alpha=0} \alpha + C_1 \alpha^2$



Output

 $C_{L\alpha}, C_L$

Experience

Accuracy
 Best for delta planforms

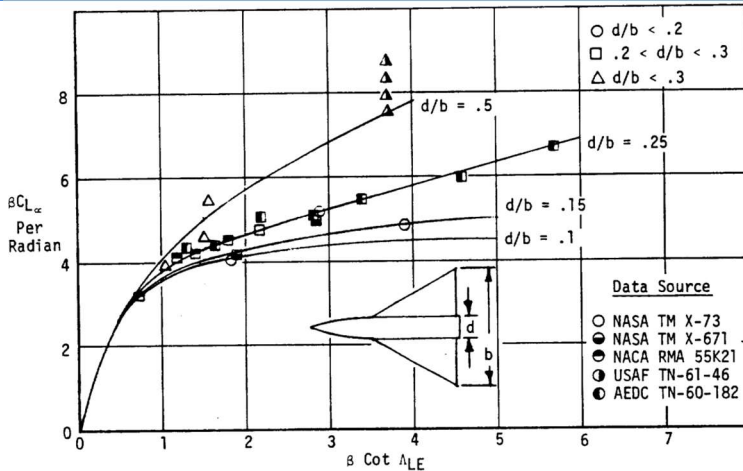
Time to Calculate
 Fast

General Comments
 Estimate for PS only.

Template adapted from Gary Coleman's thesis

Method Overview						
Discipline Aerodynamics	Design Phase Parametric Sizing (PS)	Method Title Supersonic lift-curve-slope: Delta wings of WB Configuration	Author(s) HYFAC			
Reference: HYFAC						
Brief Description: Lift-curve-slope $C_{L\alpha}$ calculation for supersonic, WB delta wings. For a double-delta wing, an effective leading edge sweep angle must be used.						
Assumptions			Applicability Supersonic regimes. Delta wing & Double-Delta wings.			
Execution of Method						
Input Mach number M , leading edge sweep angle Λ_{LE} or effective leading edge sweep angle Λ_{EFF} (double delta), wingspan b , fuselage diameter d						
Analysis Description						

1. $\beta = \sqrt{1 - M^2}$
2. Ratio: d/b
3. Calculate $\beta \cot \Lambda_{LE}$
4. Chart correlation for $C_{L\alpha}$
5. Don't forget to divide by β


Output
 $C_{L\alpha}$ (supersonic)

Experience
Accuracy

Best for delta planforms. Can be used for double-delta planforms

Time to Calculate

Fast

General Comments

Estimate for PS only.

Template adapted from Gary Coleman's thesis

Method Overview						
Discipline	Design Phase	Method Title	Author(s)			
Aerodynamics	Parametric Sizing (PS)	Subsonic skin friction coefficient (analytical)	HYFAC			
Reference: HYFAC						
Brief Description: Calculation of skin friction coefficient for subsonic speeds using the Von-Schoenherr equation. First assuming a flat plate, then adding a correction for a wing and body.						
Assumptions			Applicability Subsonic regimes. WB configuration			
<ul style="list-style-type: none"> • Subsonic • Incompressible flow over a smooth flat plate • Adiabatic gas (air) for Mach numbers less than 5.0 						
Execution of Method						
Input Reynolds number R_e , wing thickness t , chord length c , fuselage diameter d , fuselage length l						



Analysis Description

$$1. \frac{C_{F_{Body}}}{C_{F_{Flat\ plate}}} = 1 + 1.5 \left(\frac{d}{l}\right)^{\frac{3}{2}} + 7 \left(\frac{d}{l}\right)^3$$

$$2. \frac{C_{F_{Wing}}}{C_{F_{flat\ plate}}} = 1 + 2 \left(\frac{t}{c}\right) + 60 \left(\frac{t}{c}\right)^4$$

3. Not sure how to use this yet:

$$\log 10 (R_N C_F) = \frac{0.242}{\sqrt{C_F}}$$

Output

C_F (subsonic)

Experience

Accuracy	Time to Calculate	General Comments
Not the most accurate.	Fast	Estimate for PS only.

Template adapted from Gary Coleman's thesis

Method Overview

Discipline	Design Phase	Method Title	Author(s)
Aerodynamics	Parametric Sizing (PS)	Transonic wave drag coefficient for WB, BB Supersonic wave drag coefficient for WB	Paul Czysz Gary Coleman

Reference:

1. Coleman, G. *Aircraft Conceptual Design – An Adaptable Parametric Sizing Methodology*.
2. Aprovitola, A., Dyblenko, O., Pezzella, G., and Viviani, A. “*Aerodynamic Analysis of a Supersonic Transport Aircraft at Low and High Speed Flow Conditions*.

Brief Description:

Calculation of skin friction coefficient for subsonic speeds using the Von-Schoenherr equation. First assuming a flat plate, then adding a correction for a wing and body.

Assumptions

- Transonic ($0.8 < M < 1.2$), supersonic
- Incompressible flow over a smooth flat plate
- Adiabatic gas (air) for Mach numbers less than 5.0

Applicability

Subsonic and supersonic regime. For supersonic, the equation comes method for Concorde analysis.

Execution of Method

Input

Transonic: Aircraft frontal area S_{front} , aircraft length L , planform area S_{pln} ,

Supersonic: Maximum body radius R_{max} , Maximum cross-sectional area S_{max} (S_{front}), Planform area S_{ref} , nose length l_N , tail length l_T , body length L

	SENIOR DESIGN: MAE 4351 Project	Ref.: MAE 4351-001-2021 Date: 11. Aug. 2023 Name: Gayathri Kola Status: Complete
---	---	---

Analysis Description

Transonic:

1. If $S_{front}/L^2 < 0.015$

$$(C_{Dwave})_{max} = \frac{S_{front}}{S_{pln}} \left[1.3862 \left(\frac{S_{front}}{L^2} \right) + 0.067 \right]$$

2. If $S_{front}/L^2 > 0.015$

$$(C_{Dwave})_{max} = \frac{S_{front}}{S_{pln}} \left[0.9536 \left(\frac{S_{front}}{L^2} \right)^3 - 1.916 \left(\frac{S_{front}}{L^2} \right)^2 + 1.3651 \left(\frac{S_{front}}{L^2} \right) + 0.1119 \right]$$

Supersonic:

$$1. C_{D_w} = \frac{24V}{L^3} \frac{S_{max}}{S_{ref}} = \frac{9\pi^2}{2} \left(\frac{R_{max}}{L} \right) \frac{S_{max}}{S_{ref}} = \frac{4.69}{4} \left[\left(\frac{R_{max}}{2l_N} \right)^2 + \left(\frac{R_{max}}{2l_T} \right)^2 \right] \frac{S_{max}}{S_{ref}}$$

Output

C_{D_w} (Transonic), C_{D_w} (Supersonic)

Experience

Accuracy	Time to Calculate	General Comments
	Fast	Estimate for PS only.

Template adapted from Gary Coleman's thesis

Raymer: CD supersonic – Pg. 432.

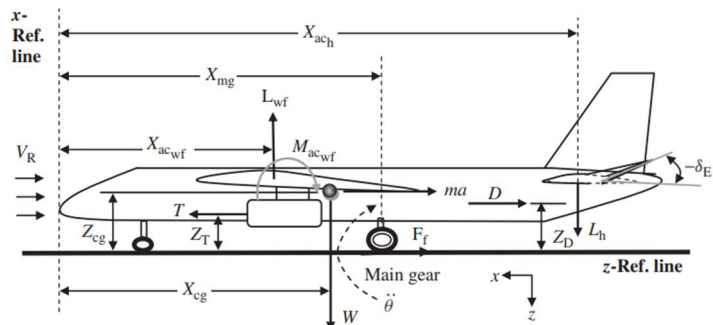
HYFAC: Induced drag factor, Vol 2 – Part 2.

STABILITY AND CONTROL

Method Overview					
Discipline	Design Phase	Method Title	Author(s)		
Stability and Control	Configuration Evaluation (CE)	Takeoff Rotation	M. Sadraey		
Reference:					
Sadraey, M. H. <i>Aircraft Design: A Systems Engineering Approach</i> . Wiley, Chichester, West Sussex, U.K, 2013.					
Brief Description:					
Provides a way to find the maximum elevator deflection angle to rotate about the main landing gear during takeoff. Has detailed methodology for estimating takeoff acceleration.					
Assumptions		Applicability			
<ul style="list-style-type: none"> • Large transport aircraft • $0.2V_{TO}$ (takeoff speed) 		Transport aircraft			
Execution of Method					
Input					
Lift-curve-slope $C_{L\alpha}$, lift coefficient C_L , control derivatives $C_{L\delta_e}$ and $C_{m\delta_e}$, Stability derivatives $C_{m\alpha}$ and C_{m_0}					
Analysis Description					

$$1. \delta_e = -\frac{C_{L\alpha}C_{m0} + C_{m\alpha}C_L}{C_{L\alpha}C_m\delta_e - C_L\delta_e C_{m\alpha}}$$

$$2. \sum M_{cg} = I_{yy_{mg}} \ddot{\theta} = -M_W + M_D - M_T + M_{Lwf} + M_{acwf} + M_{Lh} + M_a$$


Output
 $\ddot{\theta}$ for takeoff, δ_e for different trim conditions (same code)

Experience

Accuracy	Time to Calculate	General Comments
Unsure		Will go into the Control Surface Sizing code.

Template adapted from Gary Coleman's thesis

Method Overview

Discipline	Design Phase	Method Title	Author(s)
Stability and Control	Configuration Evaluation (CE)	Trim Drag	Nicolai & Carichner

Reference:

Fundamentals of Aircraft and Airship Design (Vol 1), Nicolai & Carichner 2012.

Brief Description:

Gives a way to calculate trim drag for TAC configuration that can be adapted to tailless aircraft with elevons. Will be using this method unless a better method is found.

Assumptions

- Load factor $n = 1$, most applicable for subsonic regimes.
- Extended to supersonic & hypersonic regimes.

Applicability

Mostly applicable to TAC aircraft.

Execution of Method
Input

Tail efficiency η_T , tail area S_T , tail lift coefficient C_{LT} , wing lift-curve-slope $C_{L\alpha}$, thrust T (all engines), z-location of thrust line z_T , wing area S_{ref} , stability derivatives $C_{m\delta}$ and $C_{L\delta}$ (from empirical relations).

Analysis Description

$$3. \delta_e = \frac{\left(\frac{x_w}{c}\right)\left(\frac{dC_L}{d\alpha}\right)_w \alpha - \left(\frac{Tz_T}{q_\infty S_{ref} c}\right)}{-\left(\frac{x_w}{c}\right)C_{L\delta} + C_{M\delta}}$$

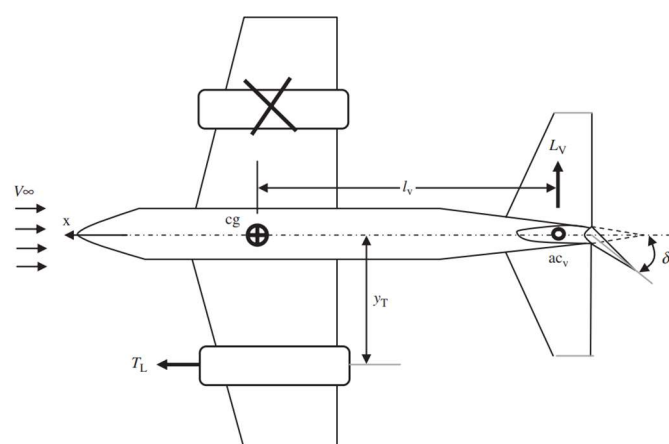
$$4. D_{trim} = \eta_T q_\infty S_T K_T C_{LT}^2$$

Output
 D_{trim} , δ_e for different trim conditions (same code)

Experience

Accuracy	Time to Calculate	General Comments
Unsure		Will go into the Control Surface Sizing code.

Template adapted from Gary Coleman's thesis

Method Overview					
Discipline	Design Phase	Method Title	Author(s)		
Stability and Control	Configuration Evaluation (CE)	One-Engine-Inoperative or Asymmetric thrust Crosswind Landing	M. Sadraey		
Reference:					
OEI: Sadraey, M. H. <i>Aircraft Design: A Systems Engineering Approach</i> . Wiley, Chichester, West Sussex, U.K, 2013. Crosswind Landing: Fundamentals of Aircraft and Airship Design (Vol 1), Nicolai & Carichner 2012.					
Brief Description: The two books above will be used to first find the maximum rudder deflection for OEI. If there is more than one engine on a single side of the plane, the book gives methods for multiple engines as well. For crosswind landing, simpler method is being used given in Nicolai compared to Sadraey, due to time constraints.					
Assumptions OEI: <ul style="list-style-type: none">• $C_{n_0} = 0$ (Symmetric aircraft)• Twin engines• No elevon deflection $\delta_e = 0$• sideslip angle $\beta = 0$ Crosswind landing: <ul style="list-style-type: none">• Sideslip angle $\beta = 11.5^\circ$• $0.2V_{TO}$ crosswinds		Applicability Transport aircraft			
Execution of Method					
Input OEI: Thrust from both engines T_L , y-location of engines from fuselage centerline y_T , wing area S_{ref} , wingspan b , control derivative $C_{n\delta_r}$, vertical tail area S_{VT} Crosswind landing: V_{TO} , $C_{n\beta}$, $C_{n\delta_r}$. Vary rudder deflection angle δ_r and fix sideslip angle β .					
Analysis Description					
1. OEI: $\delta_r = \frac{T_L y_T}{-\bar{q} S_{ref} b C_{n\delta_r}}$ 2. Crosswind Landing $C_n = 0 = C_{n\beta} \beta + C_{n\delta_r} \delta_r$ 					
Output					
Maximum rudder deflection angle δ_r					
Experience					
Accuracy Unsure	Time to Calculate	General Comments Will go into the Control Surface Sizing code.			
Template adapted from Gary Coleman's thesis					



Appendix C

This appendix serves to give codes written by the author.

AERODYNAMICS

Supersonic parasite drag estimation module given in Raymer. This has been included in Aeromodule.m of Synthesis code.

```
% Verifying Supersonic Parasite drag with XB-70 dimensions:  
% Reference: Base Pressure Measurements on the XB-70 Airplane at Mach 0.4 to 3.0, NASA-TM-X-1612.  
  
%[ft^2] Frontal area:  
Sfront = pi*((106/12)/2)^2;  
  
%[ft] Fuselage length:  
l = 189;  
  
%[-] Mach Number range  
M = 0:0.1:3;  
  
%[ft^2] Planform area  
Spln = 1184;  
  
%[deg] leading edge sweep angle:  
SweepLE = 65;  
  
%[-] Extracting supersonic drag coefficient from the function:  
for i = 1:length(M)  
    [CDo(i), CDw(i), Cdf(i)] = CDSupersonic(Sfront, l, M(i), SweepLE, Spln);  
end  
  
%% Initiates nicer colors for plots:  
% Plot settings code kindly provided by David Mexquitic  
Color = get(groot, 'DefaultAxesColorOrder');  
brown = Color(4,:); gold = Color(3,:);  
cielo = Color(6,:); red = Color(7,:);  
green = Color(5,:); blue = Color(1,:);  
orange = Color(2,:);  
  
Lw = 3; % Line width, used in plot command  
fSize = 15; % Text size, used in X & Y label  
  
% Plotting Commands  
legs = {'C_D_0', 'C_D_w', 'C_D_f'};  
figure('Name','FigureName','NumberTitle','off')  
plot(M, CDo(:), 'linewidth', Lw, 'Color', blue)  
% hold on  
% plot(M, CDw(:), 'linewidth', Lw, 'Color', green)  
% hold on  
% plot(M, Cdf(:), 'linewidth', Lw, 'Color', orange)  
% hold on  
box on; % adds a box i guess  
grid minor  
% legend(legs)  
set(gca, 'FontWeight', 'bold', 'FontSize', 14) % Sets the axis and fonts to bold  
set(gcf, 'Color','W') % Sets the figure background to white  
title('Supersonic Wave Drag Coefficient [XB-70]') % Title of the plot  
ylabel('Drag Coefficient {\it C_D_0}', 'FontSize', fSize) % Y axis label  
xlabel('Mach Number {\it M}', 'FontSize', fSize) % X axis label  
ylim([-inf inf])  
xlim([-inf inf])  
ax = gca; % axes handle  
ax.YAxis.Exponent = 0;  
  
% Sets nicer grid lines, i think AIAA does not use grids  
% set(gca, 'YMinorGrid', 'On','XMinorGrid', 'On')
```



```
function [CDo_ss, CDwave_ss, CSkinFriction_ss] = CDSupersonic(Amax, l, M, SweepLE, Splt)
% METHOD: RAYMER, Pg. 420, 432, 433
% ASSUMPTIONS: Supersonic regime

% INPUTS >>
% Amax [ft^2] - Maximum Cross-sectional area
% l [ft]       - body length: from nose to end.
% M [-]        - Mach number
% SweepLE [deg] - Leading Edge sweep angle
% Supersonic wave drag:

%[ft] Skin Roughness Value [Production sheet metal]
k = 1.33E-5;

%[-] Cut-off Reynolds Number of Supersonic: [flat plate + Mach correction factor]
R_ss = 44.62 * ((1/k)^1.053) * (M^1.16);

%[-] Supersonic skin friction drag:
CSkinFriction_ss = (0.455) / ((log10(R_ss)^2.58)*((1+0.144*(M^2))^0.65));

%[-] Sears Hack Wave Drag Coefficient:
CDWave_SHack = (9*pi/2) * (Amax/l)^2;

%[-] Wave drag efficiency factor: (Supersonic factor from 1.8 - 2.2)
EWD = 1.8;

%[-] Area ruled wave drag coefficient: !! Sweep in degrees
CDwave_ss = (EWD * (1 - (0.2*(M-1.2)^0.57)*(1 - (pi*(SweepLE^0.77)/100))) * CDWave_SHack) / Splt;

%[-] Estimated parasite drag coefficient
CDo_ss = CSkinFriction_ss + CDwave_ss;

end
```

Subsonic lift-curve-slope – Nicolai method test
% METHOD: NICOLAI, Pg. 46-49
% ASSUMPTIONS: Subsonic, delta wing, low-aspect ratio.

```
% INPUTS >>
% AR [-]      - Aspect ratio
% M [-]        - Mach number
% SweepLE [deg] - Leading Edge sweep angle

clc
clear
close

%[-] Mach Number
M = 0.5;

%[-] Aspect Ratio
AR1 = 1.5;
AR2 = 2.5;
AR3 = 3;

%[-] Constant for AR of delta wing
C1 = 5;
C2 = 3;
C3 = 2;

%[-] Some parameter
Beta = sqrt(1 - M^2);
```

	SENIOR DESIGN: MAE 4351 Project	Ref.: MAE 4351-001-2021 Date: 11. Aug. 2023 Name: Gayathri Kola Status: Complete
---	---	---

```
%[rad] Leading edge sweep
SweepLE = 75 * (pi/180);

%[-] lift-curve-slope for delta wing
CLAlpha1 = (2*pi*AR1) / (2 + sqrt(4 + ((AR1^2*Beta^2)*(1 + (tan(SweepLE)^2/Beta^2))))));
CLAlpha2 = (2*pi*AR2) / (2 + sqrt(4 + ((AR2^2*Beta^2)*(1 + (tan(SweepLE)^2/Beta^2))))));
CLAlpha3 = (2*pi*AR3) / (2 + sqrt(4 + ((AR3^2*Beta^2)*(1 + (tan(SweepLE)^2/Beta^2))))));

% %[rad] angle of attack
% alpha = 1 * (pi/180);

%[-] Lift coefficient
CL1 = @(alpha) (CLAlpha1 * alpha) + (C1 * alpha^2);
CL2 = @(alpha) (CLAlpha2 * alpha) + (C2 * alpha^2);
CL3 = @(alpha) (CLAlpha3 * alpha) + (C3 * alpha^2);

% Initiates nicer colors for plots:
% Plot settings code kindly given by David Mexquitic
Color = get(groot, 'DefaultAxesColorOrder');
brown = Color(4,:); gold = Color(3,:);
cielo = Color(6,:); red = Color(7,:);
green = Color(5,:); blue = Color(1,:);
orange = Color(2,:);

Lw = 3; % Line width, used in plot command
fSize = 15; % Text size, used in X & Y label

%% Plotting Commands
legs = {'AR = 1.5','AR = 2.5', 'AR = 3.0'};

figure('Name','FigureName','NumberTitle','off')
fplot(CL1, deg2rad([0 20]), 'linewidth', Lw, 'Color', blue)
hold on
fplot(CL2, deg2rad([0 20]), 'linewidth', Lw, 'Color', red)
hold on
fplot(CL3, deg2rad([0 20]), 'linewidth', Lw, 'Color', green)
box on; % adds a box i guess
legend(legs)
grid minor
set(gca, 'FontWeight', 'bold', 'FontSize', 14) % Sets the axis and fonts to bold
set(gcf, 'Color','W') % Sets the figure background to white
title('Non-Linear Subsonic Lift-curve-slope for Delta Wings') % Title of the plot
ylabel('Lift Coefficient {\it C_L}', 'FontSize', fSize) % Y axis label
xlabel('Angle of Attack {\it \alpha}', 'FontSize', fSize) % X axis label
ylim([-inf inf])
xlim([-inf inf])

% Sets nicer grid lines, i think AIAA does not use grids
% set(gca, 'YMinorGrid', 'On','XMinorGrid', 'On')
```

STABILITY AND CONTROL

Note, the code for Roskam (VI-VII) methods has been removed since it's more applicable for subsonic regime. A better generic way has been found for this analysis given in reference [62].

Longitudinal Verification Code (Week 6)

```
% Stability and Control: Longitudinal Verification
% Written by: Gayathri Kola
% Comment out other sections before running.
```



```
clc
clear
close

% SUBSONIC >>
%-----%
% METHOD >> Nicolai (tailless A/C)
% VARIABLE >> CMaoa, CmDeltaE
% VEHICLE DATA >> XB-70 | COMPARISON OF PREDICTIONS OF THE XB-70-1 LONGITUDINAL STABILITY AND CONTROL DERIVATIVES WITH FLIGHT RESULTS FOR SIX FLIGHT CONDITIONS
% ASSUMPTIONS >> No moment due to inlet, no canards, subsonic & supersonic regimes.

%[m] fuselage length:
lf = 57.61;
%[-] Mach number:
M = [0.76 0.75 1.22 1.22 1.61 2.39];
%[m] C.G. location:
Xcg = [0.221 0.234 0.228 0.209 0.220 0.212] * lf;
%[m] Mean aerodynamic chord:
CBar = 11.8;
%[m] x-dist from aircraft C.G. to aircraft A.C:
Xw = Xcg - CBar;
%[m^2] inlet capture area:
Si = 3.61;
%[rad] flow turning angle:
betaFlow = 0;
%[m^2] reference area:
Sref = 230.;
%[m] x-dist from inlet entrance to C.G:
li = 0;
%[-] Empirical Data: [subsonic]
dbeta_da0a = 0;
%[m] body diameter:
d = 2.54;
%[m] wingspan:
b = 32;

%[-] F parameter from Empirical data:
F = input('Input value of F for d/b:');
%[-] Aspect ratio:
AR = 1.751;
%[rad] Leading edge sweep angle:
SweepLE = 65.57 * (pi/180);

for i = 1:length(M)
    % Moment due to inlet is 0 since the inlets are located below wing.
    if M(i) > 1
        %[rad] some beta parameter:
        Beta(i) = sqrt(M(i)^2 - 1);
        %[-] Induced drag factor:
        K(i) = sqrt(M(i)^2 - 1)/4;
        %[-] wing lift curve slope based on linear theory & leading edge suction method:
        CLaoa_wb(i) = 1 / K(i);
    else
        %[rad] some beta parameter:
        Beta(i) = sqrt(1 - M(i)^2);
        %[-] wing lift curve slope:
        CLaoa_w(i) = (2*pi*AR) / (2 + sqrt(4 + ((AR^2*Beta(i)^2)*(1 + (tan(SweepLE)^2/Beta(i)^2)))));
        %[-] wing-body lift curve slope:
        CLaoa_wb(i) = F * CLaoa_w(i);
    end
    %[1/rad] Pitching moment as a function of AOA:
    CMaoa(1,i) = (-(Xw(i) / CBar)*CLaoa_wb(i));
end
```



```
%[-] XB-70's CMaoa Data for the given Mach numbers:  
CMaoaData = [-0.004 -0.00339 -0.00628 -0.00714 -0.00336 -0.00274];  
  
% Plot settings code kindly provided by David Mexquitic  
Color = get(groot, 'DefaultAxesColorOrder');  
brown = Color(4,:); gold = Color(3,:);  
cielo = Color(6,:); red = Color(7,:);  
green = Color(5,:); blue = Color(1,:);  
orange = Color(2,:);  
  
Lw = 3; % Line width, used in plot command  
fSize = 15; % Text size, used in X & Y label  
  
% Plotting Commands  
legs = {'Method: Nicolai', 'XB-70 Data'};  
% figure('Name','FigureName','NumberTitle','off')  
plot(M, CMaoaData/57.3, 'o', 'linewidth', Lw, 'Color', blue)  
hold on  
plot(M, CMaoaData, '--', 'linewidth', Lw, 'Color', green)  
hold on  
box on; % adds a box i guess  
grid minor  
legend(legs)  
set(gca, 'FontWeight', 'bold', 'FontSize', 14) % Sets the axis and fonts to bold  
set(gcf, 'Color', 'W') % Sets the figure background to white  
title('Subsonic, Supersonic C_m_alpha [XB-70 Verification]') % Title of the plot  
ylabel('{\it C_m_\alpha}', 'FontSize', fSize) % Y axis label  
xlabel('Mach Number {\it M}', 'FontSize', fSize) % X axis label  
ylim([-inf inf])  
xlim([-inf inf])  
ax = gca; % axes handle  
ax.YAxis.Exponent = 0;  
  
-----  
% Control Derivative: CmDeltaE (ROSKAM & SYSTEMS)  
  
%[-] HT efficiency: [assuming it is 1]  
nuh = 1;  
%[m^2] Elevon area: [two sides]  
Se = 3.623 * 2;  
%[m^2] Reference area:  
Sref = 166.761;  
%[-] Angle of attack effectiveness: [Ce/Cw = 0.1/0.9]  
tau_e = 0.25;  
%[m] fuselage length:  
lf = 32.614;  
%[m] mean aerodynamic chord:  
MAC = 11.369;  
%[-] Normalized elevon A.C: [same as the wing MAC, assuming]  
XBar_ace = 0.201;  
%[-] Normalized C.G. location: [baseline config]  
XBar_cg = linspace(0.173,0.258,31) * MAC;  
%[-] HT volume coefficeint: [baseline config]  
VBar_h = 0.043;  
%[-] Aspect ratio:  
AR = 1.939;  
%[rad] Leading edge sweep agnle:  
SweepLE = 52.629 * (pi/180);  
  
% Initialize a counter:  
i = 0;  
  
%[-] Mach number range:  
M = 0:0.1:3;
```



```
for i = 1:length(M)
    %[1/rad] pitching moment coefficeint due to elevon deflection:
    if M(i) < 1
        %[1/rad] Lift curve slope: (subsonic)
        Beta(i) = sqrt(1 - M(i)^2);
        Sub_CLaoa(i) = (2*pi*AR) / (2 + sqrt(4 + ((AR^2*Beta(i)^2)*(1 + (tan(SweepLE)^2/Beta(i)^2))))) ;
        CMDeltaE_Roskam(i) = -Sub_CLaoa(i) * nuh * (Se / Sref) * (XBar_cg(i) - XBar_ace) * tau_e;
        CMDeltaE_System(i) = -Sub_CLaoa(i) * nuh * VBar_h * tau_e;
    else
        %[1/rad] lift curve slope: (supersonic, hypersonic)
        Sup_CLaoa(i) = 1 / (sqrt(M(i)^2 - 1)/4);
        CMDeltaE_Roskam(i) = -Sup_CLaoa(i) * nuh * (Se / Sref) * (XBar_cg(i) - XBar_ace) * tau_e;
        CMDeltaE_System(i) = -Sup_CLaoa(i) * nuh * VBar_h * tau_e;
    end
end

% Selected key points from SR-71 data:
MData = [0.6 0.8 1.0 1.12 1.5 2.0 2.5];
CMDeltaE_Data = [-5 -4.8 -3.3 -2.0 -1.7 -1.5 -1.1] * 10^-3;

% Plot settings code kindly provided by David Mexquitic
Color = get(groot, 'DefaultAxesColorOrder');
brown = Color(4,:); gold = Color(3,:);
cielo = Color(6,:); red = Color(7,:);
green = Color(5,:); blue = Color(1,:);
orange = Color(2,:);

Lw = 2.5;      % Line width, used in plot command
fSize = 15; % Text size, used in X & Y label

% Plotting Commands
legs = {'Method: Roskam', 'Method: Sadraey', 'SR-71 Data'};
% figure('Name','FigureName','NumberTitle','off')
plot(M, CMDeltaE_Roskam/57.3, '--', 'linewidth', Lw, 'Color', blue)
hold on
plot(M, CMDeltaE_System/57.3, '--', 'linewidth', Lw, 'Color', green)
hold on
plot(MData, CMDeltaE_Data, '-o', 'linewidth', Lw, 'Color', gold)
box on; % adds a box i guess
grid minor
legend(legs)
set(gca, 'FontWeight', 'bold', 'FontSize', 14) % Sets the axis and fonts to bold
set(gcf, 'Color','W') % Sets the figure background to white
title('Control Derivative C_m_\delta_e Verification using SR-71 Data') % Title of the plot
ylabel('{\it C_m_\delta_e}', 'FontSize', fSize) % Y axis label
xlabel('Mach Number {\it M}', 'FontSize', fSize) % X axis label
ylim([-7 0]*10^-3)
xlim([-inf inf])
ax = gca; % axes handle
ax.YAxis.Exponent = 0;

% HYPERSONIC >
%-----
%-----%
% METHOD >> Systems Engineering (Generic)
% VARIABLE >> CMDeltaE
% VEHICLE DATA >> Space Shuttle Orbiter
% ASSUMPTIONS >>
% 1. Assume tail efficiency nuh =1;

% SPACE SHUTTLE DATA: Space Shuttle Orbiter and Subsystems by Whitman.

%[m^2] reference area or wing area:
```



```
Sref = 249.9;
%[m^2] elevon area: (total)
Se = 210 * 2;
%[m] wingspan:
b = 23.79;
%[m] reference body length:
lref = 32.77;
%[m] approximate length of moment arm: (from C.G. to elevon MAC) C.G envelope is from 65% to 67.5%
le = (0.95 - 0.675) * lref;
%[-] tail efficiency: (assume 1)
nuh = 1;
%[m] elevon chord:
Ce = 0.05 * lref;
%[m] wing root chord:
Cw = (3/4) * lref;
%[-] elevon chord to wing chord ratio:
Ce_Cw = Ce / Cw;
%[-] angle of attack effectiveness:
tau_e = input("Input Tau_e for Ce/Cw: ");
%[-] elevon volume coefficient:
VBar_h = (Se * le) / (Sref * b);
%[m^2] frontal area: [thermo report]
Sfront = 31.66;
%[m] altitude: [85,000 ft]
ALT = 25908;
%Hypersonic (L/D)max Kuchemann
[rho, SOS,~,~,~,~,~] = atmos(ALT);

%[rad] angle of attack range:
AOA = [45:-1:5] * (pi/180);

for j = 1:length(AOA)

    %Hypersonic CL Cruise
    cl_hs_cruise(j) = 2 * (sin(AOA(j))^2) * cos(AOA(j));

    %[1/rad] Lift-curve-slope:
    CLaoa_hyp(j) = cl_hs_cruise(j) / AOA(j);

    %[1/rad] pitching moment due elevon deflection:
    CMDeltaE_Hyp(j) = -CLaoa_hyp(j) * nuh * VBar_h * tau_e;
end

%[deg] change AOA to degrees:
AOA = AOA * (180/pi);

% Plot settings code kindly provided by David Mexquitic
Color = get(groot, 'DefaultAxesColorOrder');
brown = Color(4,:); gold = Color(3,:);
cielo = Color(6,:); red = Color(7,:);
green = Color(5,:); blue = Color(1,:);
orange = Color(2,:);

Lw = 3;      % Line width, used in plot command
fSize = 15; % Text size, used in X & Y label
% Plotting Commands
legs = {'Method: Sadraey'};
% figure('Name','FigureName','NumberTitle','off')
plot(AOA, CMDeltaE_Hyp(:)/57.3, '--', 'linewidth', Lw, 'Color', cielo)
box on; % adds a box i guess
grid minor
legend(legs)
set(gca, 'FontWeight', 'bold', 'FontSize', 14) % Sets the axis and fonts to bold
set(gcf, 'Color','W') % Sets the figure background to white
title('Hypersonic C_m\delta_e [Space Shuttle Verification]') % Title of the plot
ylabel('{\it C_m\delta_e}', 'FontSize', fSize) % Y axis label
```



```
xlabel('Angle of Attack {\it \alpha}', 'FontSize', fSize) % X axis label
ylim([-0.004 0])
xlim([-inf inf])
ax = gca; % axes handle
ax.YAxis.Exponent = 0;
```

Week 7: (Adding a lot of code because all I did was code this week, here's the summary)

1. Vertical Sizing code (for OEI & crosswind landings) [Completed]
2. Elevon Sizing code (for take-off rotation) [Needs refinement]
3. Control Surface geometry code based on preliminary AX-110 dimensions [Completed]
4. Neutral point verification (for Aerodynamics), [needs refinement, don't know why its giving high values]
5. Trim EOM code (for stability assessment) [Ongoing].

(1) Vertical tail sizing:

```
%> Stability and Control: Rudder Sizing for Asymmetric Thrust (or OEI)
%> Written by: Gayathri Kola, 7/13/2023
```

```
%> METHOD >>
%> Aircraft Design: A Systems Engineering Approach.
clc
clear
```

```
msg = 'User Question: Choose one of the following';
opts = ["Crosswind Landing @ landing" "OEI @ takeoff"];
choice = menu(msg,opts);
```

```
%> REQUIREMENTS >>
%-----
```

```
%> 1. Crosswind landing.
%> 2. OEI or Asymmetric thrust
```

```
%> MAIN IDENTIFICATION >>
%-----
```

```
%[-] Most unfavorable C.G. location:
BadCG = 1;
%[kg] Most unfavorable A/C weight:
Badm = 1;
%[m] Most unfavorable altitude:
BadALT = 1;
```

```
%> SPEEDS CONSIDERATIONS >>
%-----
```

```
%[m/s] Maximum crosswind speed: [SET]
Vw = 20.576;
%[m/s] Stall speed at approach ===== P&T:
Vs = 61.728;
%[m/s] Aircraft approach speed:
Va = 1.1*Vs;
%[m/s] total aircraft speed:
Vt = sqrt((Va^2) + (Vw^2)) ;
```

```
%> INPUTS >>
%-----
```



```
% %[m] Aircraft altitude:  
% ALT = 1;  
% %[kg/m^3, m/s] air density, speed of sound:  
% [rho,SOS,~,~,~,~,~] = atmos(ALT);  
rho = 1.225;  
%[-] vertical tail volume coefficient:  
Vv = 0.062;  
%[m] aircraft mass;  
m = 260000;  
  
%===== GEOM:  
  
%[m^2] wing area:  
Sref = 365;  
%[m^2] Projected side area:  
Ss = 404.4;  
%[m^2] Vertical tail area:  
Sv = 50;  
%[m] vertical tail span (height)  
bv = 8;  
%[m] x-dist from nose to C.G: (aft)  
Xcg = 31.313;  
%[m] x-dist from nose to center of A/C side area:  
Xca = 35.078;  
%[m] x-dist from C.G. to VT a.c:  
lvt = 27;  
%[m] wingspan:  
b = 60;  
%[m] aircraft length:  
lf = 63;  
%[m] y-dist between engines on either side:  
yT1 = 20;  
%[m] y-dist between engines on either side:  
yT2 = 40;  
  
%===== AERO:  
  
%[1/rad] vertical tail lift-curve-slope:  
CLaoaV = 4.5;  
  
%===== PROPULSION:  
  
%[-] Number of Engines on 1 side:  
NoOfEng = 2;  
%[N] single engine thrust:  
T = 140000;  
  
%===== ASSUME:  
  
%[-] side drag coefficient:  
CDy = 0.6;  
%[-] tail efficiency of VT:  
nuv = 0.96;  
%[-] sidewash due to sideslip:  
dsigma_dbeta = 0;  
%[1/rad] yawing moment bias:  
Cno = 0;  
%[1/rad] sideforce bias:  
Cyo = 0;  
%[-] parameter:  
Kf1 = 0.75;  
%[-] parameter:  
Kf2 = 1.35;  
  
% VERTICAL TAIL DESIGN >>
```



```
%-----  
%[-] rudder span-to-vertical tail span ratio: [Table 12.3]  
br_bv = input('Enter br/bv: ');\n%[-] rudder-to-vertical tail chord ratio: [Table 12.3]\ncr_cv = input('Enter cr/cv: ');\n%[-] angle of attack effectiveness: [Fig. 12.12]\ntau_r = input("Enter tau_r for chosen cr_cv: ");\n\n% QUICK MATHS >>\n%-----  
\n%[m] vertical tail mean chord:\nCBar_v = Sv/bv;\n%[m] x-dist from C.G (aft) to side area center:\ndc = Xca - Xcg;\n\n%[N] side-force due to crosswinds:\nFw = 0.5 * rho * (Vw^2) * Ss * CDy;\n\n%[rad] sideslip angle:\nbeta = atan(Vw/Va);\n\nif choice == 1\n    % STABILITY-CONTROL DERIVATIVES >>\n    %-----\n\n        %[1/rad] yawing moment due to sideslip:\n        CnBeta = Kf1 * CLaoaV * (1 - dsigma_dbeta) * nuv * (lvt*Sv/(b*Sref));\n        %[1/rad] sideforce moment due to sideslip:\n        CyBeta = -Kf2 * CLaoaV * (1 - dsigma_dbeta) * nuv * (Sv/Sref);\n        %[1/rad] Sideforce control derivative:\n        CyDeltaR = CLaoaV * nuv * tau_r * br_bv * (Sv/Sref);\n        %[1/rad] Yawing control derivative:\n        CnDeltaR = -CLaoaV * Vv * nuv * tau_r * br_bv;\n\n        % RUDDER DEFLECTION & SIDEWASH ANGLE >>\n        %-----\n\n        % Initial guess for deltaR and sigma\n        x0 = [0.0, 0.0];\n\n        % Call fsolve to solve the equations\n        options = optimoptions('fsolve', 'Display', 'iter', 'MaxIterations', 1000);\n        [result, ~] = fsolve(@(x) equations(x, rho, Vt, Vw, Sref, Ss, b, beta, CDy, Cno, CnBeta, CnDeltaR, Fw,\n        dc, Cyo, CyBeta, CyDeltaR), x0, options);\n\n        % Extract the results for deltaR and sigma\n        deltaR = result(1)*(180/pi);\n        sigma = result(2)*(180/pi);\n\n        disp('Solution:');\n        fprintf('deltaR: %.4f degrees\n', deltaR);\n        fprintf('sigma: %.4f degrees\n', sigma);\n\n        if deltaR > 30\n            disp('Too high rudder deflection angle, updating cr_cv = 1')\n            cr_cv = 1;\n        else\n            fprintf('Rudder deflection, deltaR = %.4f degrees for Crosswind Landing\n', deltaR)\n\n%-----
```



```
disp('Checking Asymmetric thrust (OEI) conditions: ...')
end

elseif choice == 2
% ASYMMETRIC THRUST >>
% -----
% [m/s] aircraft minimum controllable speed:
Vmc = 0.8 * Vs;

% [1/rad] Yawing control derivative:
CnDeltaR = -CLaoaV * Vv * nuv * tau_r * br_bv;

deltaR_OEI = ((T*(yT1/2))+(T*(yT2/2))) / (-0.5*rho*Sref*(Vmc^2)*b*CnDeltaR);
deltaR_OEI = deltaR_OEI * (180/pi);
fprintf('Rudder deflection, deltaR = %.4f degrees for Asymmetric thrust\n', deltaR_OEI)
if deltaR_OEI > 30
    disp('WARNING!! ----- High rudder deflection, change geometry')
    %[deg] rudder deflection max for minimum controllable speed:
    DeltaR_Vmc = 30;
    % [m/s] calculate minimum controllable speed in this case:
    Vmc_deltaR = sqrt( ((T*(yT1/2)) + (T*(yT2/2))) / (-0.5*rho*Sref*b*CnDeltaR*(DeltaR_Vmc/57.3)) );
    fprintf('The minimum controllable speed is Vmc = %.4f m/s for deltaR_Max = %.4f \n', Vmc_deltaR,
DeltaR_Vmc)
else
end

% VT GEOMETRY >>
% -----
% [m] rudder chord:
cr = cr_cv * CBar_v;
% [m] rudder span or height:
br = br_bv * bv;
% [m^2] rudder area:
Sr = br * cr;

fprintf('RUDDER GEOMETRY\n')
fprintf(' Rudder Chord = %.3f m \n Rudder Height = %.3f m \n Rudder Area = %.4f m^2 \n',cr,br,Sr)

end

% FUNCTION FILES >>
% -----
function F = equations(x, rho, Vt, Vw, Sref, Ss, b, beta, CDy, Cno, CnBeta, CnDeltaR, Fw, dc, Cyo, CyBeta, CyDeltaR)
% Extract variables from x vector
sigma = x(1);
deltaR = x(2);

% Equations
F(1) = 0.5 * rho * Vt^2 * Sref * b * (Cno + (CnBeta * (beta - sigma)) + (CnDeltaR * deltaR)) + (Fw *
dc * cos(sigma));
F(2) = 0.5 * rho * Vw^2 * Ss * CDy - 0.5 * rho * Vt^2 * Sref * (Cyo + (CyBeta * (beta - sigma)) +
(CyDeltaR * deltaR));
end

(2) Elevon Sizing code:
%% Stability and Control: Elevon design
% Written by: Gayathri Kola, 7/13/2023

% METHOD >>
```



```
% Aircraft Design: A Systems Engineering Approach
clc
clear
close

% 1. Takeoff rotation: Tricycle landing gear, 4-6 deg/s^2, 3-5s
% 2. Airport Altitude [m]:
% 3. Longitudinal trim.

% AIRPORT >>
%-----
%-----[m] Takeoff altitude:
ALT = 1;
%[kg/m^3] air density at altitude:
% [rho,SOS,~,~,~,~,~] = atmos(ALT);
rho = 1.225;
%[m] Cruise altitude:
ALT2 = 1;
%[kg/m^3] air density at cruise:
[rho2,SOS2,~,~,~,~,~] = atmos(ALT2);

% REQUIREMENTS >>
%-----
%[rad/^2] angular acceleration:
Adotdot = 12 * (pi/180);
%[-] Initial Ce_Ch [Elevon]
Ce_Ch = 1;
%[-] Initial be/bh = beng/b
be_bh = 1;
%[rad] Maximum up deflection:
DeltaE_UpMax = -25 * (pi/180);
%[rad] Maximum down deflection:
DeltaE_DownMax = 30 * (pi/180);

% INPUTS >>
%-----
%===== P&T =====
%[m/s] stall speed:
Vstall = 43.73;
%[m/s] minimum control speed:
Vc = 360 * 0.5144;

%===== GENERAL =====
%[kg] aircraft mass at takeoff:
m = 20000;
%[N] takeoff gross weight:
TOGW = m * 9.81;
%[m^2] Horizontal area:
Sh = 16;
%[-] aspect ratio:
AR = 8;
%[m^2] wing area:
Sref = 70;
%[-] rolling friction coefficient:
mu = 0.04;
%[rad] angle of attack:
aoa = 1 * (pi/180);
%[rad] fuselage angle of attack:
aoaf = 1 * (pi/180);
```



```
%[rad] takeoff stall angle of attack:  
aoasT0 = 12 * (pi/180);  
%[rad] takeoff angle of attack:  
aoaT0 = 1;  
%[m] wingspan:  
b = 23.66;  
  
%===== AERO  
%[m] mean aero chord:  
CBar = 2.96;  
%[-] lift coefficient @ takeoff:  
CLto = 0.797;  
%[-] drag coefficient @ takeoff:  
CDto = 0.067;  
%[N] drag @ takeoff:  
Dto = 0.5 * rho * (Vstall^2) * Sref * CDto;  
%[N] lift @ takeoff:  
Lto = 0.5 * rho * (Vstall^2) * Sref * CLto;  
%[N] wing-fuselage lift:  
Lwf = Lto;  
%[1/rad] lift-curve-slope wing:  
CLaoaw = 5.7;  
%[1/rad] lift-curve-slope horizontal tail:  
CLaoah = 4.3;  
%[1/rad] lift-curve-slope wing-fuselage:  
CLaoawf = 5.7;  
%[1/rad] pitching moment bias:  
Cmo = 0.05;  
%[1/rad] Lift coefficient bias:  
Clo = 0.24;  
%[1/rad] lift-curve-slope @ takeoff:  
CLaoa = 5.7;  
%[1/rad] pitching moment coefficient about a.c. of wing-fuselage:  
Cmacwf = 0.05;  
%[N-m] pitching moment about a.c. of wing-fuselage:  
Macwf = 0.5 * rho * (Vstall^2) * Cmacwf * Sref * CBar;  
  
%===== PROPULSION  
%[N] thrust of both engines:  
T = 28000 * 2;  
  
%===== GEOM  
%[m] main landing gear x-origin:  
Xmg = 0;  
%[m] x-dist from mg to most forward c.g. location:  
Xcg = 1.1;  
%[m] x-dist from mg to wing a.c. location:  
Xacwf = -0.8;  
%[m] x-dist from mg to elevon a.c. location:  
Xach = 11.3;  
%[m] z-dist from bottom of mg to drag line:  
Zd = 1.9;  
%[m] main landing gear z-origin:  
Zmg = 0;  
%[m] z-dist from bottom of mg to thrust line:  
Zt = -(1.7+0.3);  
%[m] z-dist from bottom of mg to most forward c.g.:  
Zcg = 1.7;  
%[rad] HT incidence angle:  
ih = -1 * (pi/180);  
%[rad] wing incidence angle:  
iw = 2 * (pi/180);  
%[m] x-dist from mg to HT a.c.:  
lh = 11.3;  
%[m]
```



```
h = Xcg/CBar;
%[m]
ho = Xacwf/CBar;
%[m] HT wingspan:
bh = 9;

%===== STRUCTURES =====
%[kg/m^2] moment of inertia of the main landing gear:
Iyymg = 150000;

%===== ASSUMPTION =====
nuh = 0.96;

% INPUTS >>
%-----

%[m/s^2] linear acceleration:
a = (T - Dto - (mu*(TOGW - Lto))) / m;

% CALCULATING MOMENTS >>
%-----
```

```
MW = TOGW*(Xmg-Xcg);
MD = Dto*(Zd-Zmg);
MT = T*(Zt-Zmg);
MLwf = Lwf*(Xmg-Xacwf);
Ma = m*a*(Zcg-Zmg);

% DESIRED HORIZONTAL TAIL LIFT @ TAKEOFF ROTATION >>
%-----
```

```
Lh = (MLwf + Macwf + Ma + MW + MD + MT - (Iyymg*Adotdot)) / (Xach - Xmg);
CLh = (2*Lh) / (rho*(Vstall^2)*Sh);

espo = (2*CLto) / (pi*AR);
desp_daoa = (2*CLaoaw) / (pi*AR);
eps = espo + (desp_daoa*iw);
aoah = iw + ih - eps;

ce_cw = [0 0.1 0.2 0.3 0.4 0.5 0.6 0.7];
taue_e = [0 0.28 0.4 0.53 0.6 0.67 0.74 0.8];

% Determine elevator chord:
tau_e = (aoah + (CLh/CLaoah)) / DeltaE_UpMax;
if tau_e > 1
    disp("Tau_e is greater than 1. \nElevon requirements cannot be met. \nMove landing gear location or
change elevon size.")
else
end
Ce_Ch2 = input("Enter CE/Ch for calculated Tau-e: ");

if Ce_Ch2 > 0.5
    Ce_Ch2 = 1;
else
end

% OTHER CODE INTEGRATION >>
%-----
```

```
%[deg] Twist angle:
```

	SENIOR DESIGN: MAE 4351 Project	Ref.: MAE 4351-001-2021 Date: 11. Aug. 2023 Name: Gayathri Kola Status: Complete
---	---	---

```

aoa_twist = 0.00001;
%[-] wing taper ratio:
lambda = 0;
%[1/rad] 2D lift-curve-slope:
aoa2d = 6.3;
%[deg] flap up zero-lift angle of attack
a_0 = -3;
%[deg] flap down zero-lift angle of attack
a_0_fd = -6;
%[-] %flap-to-wing span ratio
bf_b=0.6;

CL_TO_LL = Lifting_Line(Sref,AR,lambda,aoa_twist,iw,aoa2d,a_0,a_0_fd,b,bf_b);

% CONTROL DERIVATIVE CALCULATION >>
%-----

lh = lh+0.5;
VBar_h = (lh*Sh)/(Sref*CBar);
CMDeltaE = -CLaoah * nuh * VBar_h * be_bh * tau_e;
CLDeltaE = CLaoah * nuh * (Sh/Sref) * be_bh * tau_e;
CLhDeltaE = CLaoah * tau_e;

% ELEVON DEFLECTION FOR LONG TRIM, MOST AFT C.G >>
%-----

Qinf = 0.5*rho*(Vc^2);
CMaoa = (CLaoawf * ((h - ho)/CBar)) - (CLaoah*nuh*(Sh/Sref)*(1h/CBar)*(1-desp_daoa));
CL1 = (2*TOGW)/(rho*(Vc^2)*Sref);
Zt = -0.3;
DeltaE_Down = - (((T*Zt/(Qinf*Sref*CBar))+Cmo)*CLaoa) + ((CL1-CLo)*CMaoa) / ((CLaoa*CMDeltaE)-
(CMaoa*CLDeltaE));
DeltaE_Down_Deg = DeltaE_Down * (180/pi)

% ELEVON DEFLECTION FOR LONG TRIM, MOST FORWARD C.G >> INTEGRATE CODE
%-----



Vmax = 185; % m/s
Cmo = 0.05;
CLa = 5.2; %1/rad
CLa_wf = CLa;
lh2 = 11.3; % m from main landing gear
xcg1 = 0.5;
xcg2 = 1.1;

[De1,De2,VA] =
DeltaE(Vmax,Sref,Sh,CBar,Vstall,T,rho,Cmo,Zt,CLa,CLaoah,CLa_wf,m,CLo,lh2,desp_daoa,xcg1,xcg2);

plot(VA,De1, 'o',VA,De2, '*')
grid
xlabel ('Speed (knot)')
ylabel ('\delta_E (deg)')
legend('Most aft cg','Most forward cg')

% ELEVON STALL CHECK >>
%-----



%{
% fuselage lift angle:
aoast0 = 12;
aoaf = 2;
aoat0 = aoast0 - aoaf;

```



```
aoahT0 = (aoaT0*(1-desp_daoa)) + ih - espo;

aoah_stall = aoah_stall_DeltaE0 - Delta_aoahE;
%}

% ELEVON GEOMETRY >>
%-----

be = be_bh*b
CBar_h = Sh / b
Ce = Ce_Ch2 * CBar_h
Se = be*Ce

% OUTPUT INFO >>
%-----
(3) Control surface geometry:
clear all
close all
clc

% VOLUME COEFFICIENTS >>
%-----
% Written by: Carlos Carmona.
% METHOD: FLOPS for Weight Estimation.

% INPUTS & ASSUMPTIONS >>
SW= 215.43*3.281^2; %Wing Area in Ft^2
SPAN=20.92*3.281; %Span of the wing in ft
XL=32.50*3.281; %fuselage length in ft
WF= 4.5247*3.281; %max width of fuselage in ft
FLAPR=.33; %area ratio of horizontal control surface area to wing area. It is set to .33 by default as
that is typical of aircraft.
HHT=0; %this will range from 0 for elevons to a 1.0 for a direct T tail.
NEW=0; %number of wing mounted engines
VCMN=10; %Cruise Mach Number
SWEEP=68.74; %Sweep Angle of Wing
DF=1.75*3.281; %Maximum Fuselage Depth (height) in ft
NEF=9; %Number of Fuselage Mounted Engines. 8 turbine and 1 convertible Ramjet/Scramjet
NVERT=2; %number of Vertical Tails

HFAC=SW^2/(SPAN*XL); %Horizontal Tail Geometric Factor
VFAC=SPAN*SW/XL; %Vertical Tail Geometric Factor

HTVC=56.9*WF^.5*FLAPR^.82*(1-.46*HHT)*(1-.1*NEW)/(VCMN*SWEEP);
VTVC=.0035*SWEEP^.57*DF*(1+.2*HHT)*(1+.33*NEF)/VCMN*NVERT^.7;

SHT= HTVC*HFAC; %Horizontal Tail area ft^2
SVT=VTVC*VFAC; %Vertical Tail area ft^2

SHTm = SHT * 0.092903;
SVTm = SVT * 0.092903;

% HORIZONTAL TAIL (ELEVON) GEOMETRY >>
%-----
% Written by: Gayathri Kola.
% Shape: RIGHT TRAPEZOID
```



```
format long g
syms p1

% !! MORE INPUTS >>
%[m] Max fuselage width:
bf = 4.5247;
%[m] total wingspan:
bspan = 20.92;
%[deg] leading edge wing sweep:
SweepLE = SWEEP;

%[m^2] single elevon area:
Sht = SHTm / 2;
%[m] Available span on 1 side:
B = (bspan - bf) / 2;

% A bunch of trig:
z = tand(SweepLE);
Eqn1 = (2*Sht) == ((2*B) - p1)*(p1 * z);
roots1 = vpasolve(Eqn1,p1);
p11 = min(roots1);

%[m] elevon chord:
Ce = p11 * tand(SweepLE);
fprintf("=====1 ELEVON=====\\n")
fprintf('Elevon Shape: Right Trapezoid\\n')
fprintf('Elevon chord: Ce = %.4f [m]\\n', Ce)
fprintf('Elevon span (on 1 side): be = %.4f [m]\\n', B)
fprintf('Elevon area (single side): Sht = %.4f [m^2]\\n\\n', Sht)

% VERTICAL TAIL GEOMETRY >>
-----
% Written by: Gayathri Kola.
% Shape: RIGHT TRAPEZOID

% !! MORE INPUTS >>
%[m] Fuselage length:
lref = 32.5;
%[m] assume the vertical tail chord is 25% of fuselage length:
cv = lref * 0.25;
%[deg] VT sweep angle [based on SR-71]:
SweepVT = 33;
%[m^2] single elevon area:
Svt = SVTm / 2;

format long g
syms p2
% A bunch of trig:
y = tand(SweepVT);
Eqn2 = (2*Svt) == ((2*cv) - p2)*(p2 * y);
roots2 = vpasolve(Eqn2,p2);
p22 = min(roots2);
cvtip = cv - p22;

%[-] thickness ratio:
tc = 0.035;
roothick = tc * cv;
tipthick = tc * cvtip;

%[m] elevon chord:
bv = p22 * tand(SweepVT);
fprintf("=====1 VERTICAL TAIL=====\\n")
fprintf('Vertical Tail Shape: Right Trapezoid\\n')
fprintf('Vertical Tail Sweep: SweepVT = %.4f [deg] \\n', SweepVT)
fprintf('Vertical Tail Root chord (1 tail): Cvr = %.4f [m]\\n', cv)
```



```
fprintf('Vertical Tail tip chord (1 tail): Cvt = %.4f [m]\n', cvtip)
fprintf('Vertical Tail height (1 tail): bh = %.4f [m]\n', bv)
fprintf('Vertical Tail root thickness (bottom): tr = %.4f [m]\n', roothick)
fprintf('Vertical Tail tip thickness (top): tt = %.4f [m]\n', tiptthick)
fprintf('Vertical Tail area (single side): Svt = %.4f [m^2]\n', Svt)
```

(4) Neutral point code: (1)

```
%% Aerodynamics: Neutral Point
% Gayathri Kola: 7/18/2023
```

```
% METHOD >> RAYMER PAGE. 593
```

```
% REGIME >> SUBSONIC FIRST
clc
clear
close
```

```
% INPUTS >>
```

```
-----  
-----  
% AIRCRAFT: SR-71
```

```
%[-] tail efficiency [assume 1]
```

```
nuh = 0.97;
```

```
%[m^2] elevon area:
```

```
Se = 9.54;
```

```
%[m^2] wing area:
```

```
Sw = 166.76;
```

```
%[m^2] Inlet area (both):
```

```
Si = 1.858;
```

```
%[-] aspect ratio:
```

```
AR = 1.67;
```

```
%[rad] leading edge sweep angle:
```

```
SweepLE = 52 * (pi/180);
```

```
%[m] Root quarter-chord:
```

```
Cr_c4 = 18.29 * 18.29;
```

```
%[m] fuselage length:
```

```
lref = 32.61;
```

```
%[m] mean aerodynamic chord:
```

```
MAC = 12.19;
```

```
%[-] Normalized MAC of the WING by CBar:
```

```
XBar_acw = ((lref - MAC) + (0.25 * MAC)) / MAC;
```

```
%[-] Normalized MAC of ELEVON:
```

```
XBar_ace = (0.90 * lref) / MAC;
```

```
%[-] Normalized x-dist from nose to inlet entrance:
```

```
XBar_p = (0.20 * lref) / MAC;
```

```
%[-] C.G. location: 17% to 22% MAC -
```

```
XBar_cg = linspace(0.19,0.25,9);
```

```
%[-] Position of root quarter-chord as % fuselage length:
```

```
K_xaxis = Cr_c4 / lref;
```

```
%[-] Pitching moment factor:
```

```
Kfus = 0.04; % input("From Raymer, Fig. 16.14: ");
```

```
%[m] Maximum fuselage width:
```

```
Wf = 1.52;
```

```
%[1/deg] Fuselage pitching moment:
```

```
CMaoa_fus = (Kfus * Wf^2 * lref) / MAC * Sw;
```



```

%[m] altitude: [25,000 ft]
ALT = 7620;
%[kg/m^3, m/s] air density, speed of sound:
[rho, SOS,~,~,~,~,~] = atmos(ALT);

%[-] Mach number:
M = 0:0.1:0.8;
%[rad] angle of attack range:
AOA = linspace(0,14,9) * (pi/180);

for i = 1:length(M)

    %[m/s] aircraft velocity:
    VEL = M(i) * SOS;
    %[kg/m-s^2] Dynamic pressure:
    Qinif = 0.5 .* rho .* VEL^2;
    %[kg/s] engine mass flow rate:
    mdot = rho * Si * VEL;
    %[-] Vertical force (z-direction) produced by inlet front face due to turning of freestream flow, as a
    function of aoa:
    Fpaoa = mdot * VEL;

    %[-] beta factor:
    BF = sqrt(1 - M(i)^2);
    %[1/rad] subsonic lift-curve-slope:
    CLaoa = (2 * pi * AR) / (2 + sqrt( 4 + ( (AR^2)*(BF^2)) * (1 + ((tan(SweepLE)^2)/(BF^2))) ) );
    %[-] Constant C1:
    C1 = 4;
    %[-] lift coefficient for varying angle of attack:
    CL = (CLaoa * AOA(i)) + (C1 * AOA(i)^2);
    %[1/rad] lift-curve-slope:
    CLaoa1 = CL / AOA(i);
    %[1/rad] elevon lift-curve-slope:
    CLaoa_e = CLaoa1;

    %[-] downwash on tail:
    daoah_daoa = (1.62 * CLaoa1) / (pi * AR); %input('');
    %[-] rate of change in inlet angle of attack to A/C aoa:
    daoap_daoa = 0; % input('');

    % Splitting method into terms:
    term1 = (CLaoa1 * XBar_acw) - CMaoa_fus;
    term2 = (nuh * (Se / Sw) * CLaoa_e * daoah_daoa * XBar_ace);
    term3 = (Fpaoa / (Qinif * Sw)) * daoap_daoa * XBar_p;
    term4 = (nuh * (Se / Sw) * CLaoa_e * daoah_daoa);
    term5 = (Fpaoa / (Qinif * Sw)) * daoap_daoa;

    %[-] Normalized neutral point: by %MAC
    XBar_NP(i) = (term1 + term2 + term3) / (CLaoa1 + term4 + term5);

    %[1/rad] Pitching moment as a function of AOA:
    CMaoa(i) = -CLaoa1 * (XBar_NP(i) - XBar_cg(i));

    %[-] Static Margin:
    SM(i) = -CMaoa(i) / CLaoa1;

    %[-] -dist from nose to AC divided by MAC:
    Xc4 = XBar_acw;

end

```



```
Color = get(groot, 'DefaultAxesColorOrder');
brown = Color(4,:); gold = Color(3,:);
cielo = Color(6,:); red = Color(7,:);
green = Color(5,:); blue = Color(1,:);
orange = Color(2,:);

Lw = 3;      % Line width, used in plot command
fSize = 15; % Text size, used in X & Y label

figure(1)
plot(M,XBar_NP(:,1),'linewidth', Lw, 'Color', blue)
title("Neutral Point vs. Mach Number");
ylabel('Normalized Neutral Point, {\it NP}', 'FontSize', fSize) % Y axis label
xlabel('Mach Number {\it M}', 'FontSize', fSize) % X axis label
set(gca, 'FontWeight', 'bold', 'FontSize', 14) % Sets the axis and fonts to bold
set(gcf, 'Color','W') % Sets the figure background to white
ylim([-inf inf])
xlim([-inf inf])
box on; % adds a box i guess
grid minor
ax = gca; % axes handle
ax.YAxis.Exponent = 0;

figure(2)
plot(M,SM(:,1),'linewidth', Lw, 'Color', brown)
title("Static Margin vs. Mach Number");
ylabel('Static Margin, {\it SM}', 'FontSize', fSize) % Y axis label
xlabel('Mach Number {\it M}', 'FontSize', fSize) % X axis label
set(gca, 'FontWeight', 'bold', 'FontSize', 14) % Sets the axis and fonts to bold
set(gcf, 'Color','W') % Sets the figure background to white
ylim([-inf inf])
xlim([-inf inf])
box on; % adds a box i guess
grid minor
ax = gca; % axes handle
ax.YAxis.Exponent = 0;

figure(3)
plot(M,CMaoa(:,1),'linewidth', Lw, 'Color', green)
title("Pitching moment vs. Mach Number");
ylabel('{\it C_m\_alpha} [\circ]', 'FontSize', fSize) % Y axis label
xlabel('Mach Number {\it M}', 'FontSize', fSize) % X axis label
set(gca, 'FontWeight', 'bold', 'FontSize', 14) % Sets the axis and fonts to bold
set(gcf, 'Color','W') % Sets the figure background to white
ylim([-inf inf])
xlim([-inf inf])
box on; % adds a box i guess
grid minor
ax = gca; % axes handle
ax.YAxis.Exponent = 0;
% Plot settings code kindly provided by David Mexquitic
```

Neutral point – Normal force as a function of angle of attack function (Week 8)

```
function CNaoa = CN_aoa(M,SweepLE,AR)
%CNAOA Summary of this function goes here

%[-] beta factor for supersonic
beta = sqrt(M^2 - 1);

%[rad] converting to rad, input needs to be in degrees
SweepLE = SweepLE * (pi/180);

%[-] determining which line 0.25, 0.5, 1, 2, 3, 4, 5, 6.
Line = AR * tan(SweepLE);
Line = round(Line); % round to the nearest integer
```



```
%[-] finding the x-axis number:  
Linex = tan(SweepLE)/beta;  
  
if Linex > 1  
    Linex = 1;  
end  
  
% ALL TREND FITTED LINES >>  
%-----  
  
if Line >= 0 && Line <= 0.25  
    x = Linex;  
    y025 = @(x) (-265.68024648400000 * (x^6)) + (854.253665130585000 * (x^5)) - (1038.973525789330000 * (x^4)) + (579.634546890156000 * (x^3)) ...  
        - (132.664923269331000 * (x^2)) - (0.259241212956113 * x) + (4.076565220089410);  
    CNaoa_beta = y025(x);  
  
elseif Line >= 0.26 && Line <= 0.50  
    x = Linex;  
    y05 = @(x) (57.692307691104400 * (x^5)) - (166.229603726446000 * (x^4)) + (170.454545451619000 * (x^3)) - (69.369172493206900 * (x^2)) + ...  
        (4.266958042073380 * x) + (3.994405594310480);  
    CNaoa_beta = y05(x);  
  
elseif Line >= 0.51 && Line <= 1  
    x = Linex;  
    y1 = @(x) (119.281045551877000 * (x^6)) - (378.676469981670000 * (x^5)) + (452.491829395294000 * (x^4)) - (244.934783030301000 * (x^3)) ...  
        + (54.272902591153900 * (x^2)) - (4.690818230606960 * x) + (4.005008224842020);  
    CNaoa_beta = y1(x);  
  
elseif Line >= 1.01 && Line <= 2  
    x = Linex;  
    y2 = @(x) (0.033799533799595 * (x^2)) - (0.658344988345021 * x) + (4.022797202797220);  
    CNaoa_beta = y2(x);  
  
elseif Line >= 2.01 && Line <= 3  
    x = Linex;  
    y3 = @(x) (-0.123543123543072 * (x^2)) - (0.160093240093261 * x) + (3.993286713286740);  
    CNaoa_beta = y3(x);  
  
elseif Line >= 3 && Line <= 4  
    x = Linex;  
    y4 = @(x) (-0.189976689976675 * (x^2)) + (0.174522144522143 * x) + (3.999230769230790);  
    CNaoa_beta = y4(x);  
  
elseif Line >= 4.01 && Line <= 5  
    x = Linex;  
    y5 = @(x) (-1.719114219111360 * (x^4)) + (2.935120435111460 * (x^3)) - (1.178613053576560 * (x^2))  
+ (0.263655788629876 * x) + (4.000349650356470);  
    CNaoa_beta = y5(x);  
  
else  
    x = Linex;  
    y6 = @(x) (-0.145687645665021 * (x^4)) + (0.786713286681334 * (x^3)) - (0.756118881072325 * (x^2))  
+ (0.6098484816212 * x) + (3.999650349657570);  
    CNaoa_beta = y6(x);  
end  
  
%[1/rad] Normal force coefficient as a function of angle of attack:  
CNaoa = CNaoa_beta / beta;
```

End

Neutral point – Aerodynamic center per root chord function (Week 8)



```
function XacCr = Xac_CR(M, AR, SweepLE, Cr)
    %XAC_CR
    % METHOD >> DATCOM

    %[rad] converting to rad, input needs to be in degrees
    SweepLE = SweepLE * (pi/180);

    %[-] determining which line 1, 2, 3, 4, 5, 6.
    Line = AR * tan(SweepLE);
    Line = round(Line,2); % round to the nearest integer

    if M >= 0 && M <= 1
        % SUBSONIC:
        %[-] beta factor for supersonic
        beta = sqrt(1 - (M^2));
        %[-] finding the x-axis number:
        Linex = tan(SweepLE)/beta;

        if Linex > 1
            Linex = 1;
        end

        if Line >= 0 && Line <= 1
            x = Linex;
            yy1 = @(x) (0.01736111111143 * (x^3)) - (0.046130952380963 * (x^2)) - (0.011111111111084 * x)
+ 0.249761904761886;
            Xac_Cr = yy1(x);
        elseif Line >= 1.1 && Line <= 2
            x = Linex;
            yy2 = @(x) 0.34000;
            Xac_Cr = yy2(x);
        elseif Line >= 2.1 && Line <= 3
            x = Linex;
            yy3 = @(x) (0.390624999941792 * (x^5)) - (1.04166666453240 * (x^4)) + (0.963541666336823 *
(x^3)) - (0.33333332964685 * (x^2)) + (0.06083333396658 * x) ...
+ 0.41999999895126;
            Xac_Cr = yy3(x);
        elseif Line >= 3.1 && Line <= 4
            x = Linex;
            yy4 = @(x) (1.432291666627860 * (x^5)) - (3.255208333197520 * (x^4)) + (2.473958332906480 *
(x^3)) - (0.744791666205856 * (x^2)) + (0.173750000092696 * x) ...
+ 0.49999999867835;
            Xac_Cr = yy4(x);
        elseif Line >= 4.1 && Line <= 5
            x = Linex;
            yy5 = @(x) (0.19531250000000 * (x^4)) - (0.489004629627743 * (x^3)) + (0.358506944441615 *
(x^2)) + (0.036177248677632 * x) + 0.584503968254300;
            Xac_Cr = yy5(x);
        else
            x = Linex;
            yy6 = @(x) (0.195312499999091 * (x^4)) - (0.373263888890506 * (x^3)) + (0.184895833333940 *
(x^2)) + (0.11388888889051 * x) + 0.67458333333722;
            Xac_Cr = yy6(x);
        end
        XacCr = Xac_Cr;
    %     Xac = Xac_Cr * Cr;

    else
        % SUPERSONIC:
        %[-] beta factor for supersonic
        beta = sqrt(M^2 - 1);
        %[-] finding the x-axis number:
```



```
Linex = tan(SweepLE)/beta;

if Linex > 1
    Linex = 1;
end

if Line >= 0 && Line <= 1
    x = Linex;
    y1 = @(x) (-1.822916666773380 * (x^5)) + (4.68750000291040 * (x^4)) - (4.21875000436560 *
(x^3)) + (1.50000000349250 * (x^2)) - (0.21583333287264 * x) ...
+ 0.41999999916428;
    Xac_Cr = y1(x);
elseif Line >= 1.1 && Line <= 2
    x = Linex;
    y2 = @(x) (0.13020833331666 * (x^4)) - (0.22569444440705 * (x^3)) + (0.06770833331211 *
(x^2)) - (0.001984126983643 * x) + 0.499880952381169;
    Xac_Cr = y2(x);
elseif Line >= 2.1 && Line <= 3
    x = Linex;
    y3 = @(x) (-0.00000000000909 * (x^4)) + (0.011574074076634 * (x^3)) - (0.0486111111114951 *
(x^2)) + (0.006878306879230 * x) + 0.590079365079626;
    Xac_Cr = y3(x);
elseif Line >= 3.1 && Line <= 4
    x = Linex;
    y4 = @(x) (0.52083333333030 * (x^4)) - (1.041666666669700 * (x^3)) + (0.60416666664241 *
(x^2)) - (0.08333333332575 * x) + 0.67000000000311;
    Xac_Cr = y4(x);
elseif Line >= 4.1 && Line <= 5
    x = Linex;
    y5 = @(x) (0.39062500002728 * (x^4)) - (0.769675925928823 * (x^3)) + (0.529513888889596 *
(x^2)) - (0.119907407407254 * x) + 0.74972222222600;
    Xac_Cr = y5(x);
else
    x = Linex;
    y6 = @(x) (-0.52083333488553 * (x^5)) + (1.30208333604970 * (x^4)) - (1.041666667326350 *
(x^3)) + (0.322916667355457 * (x^2)) + (0.01750000125438 * x) ...
+ 0.81999999795762;
    Xac_Cr = y6(x);
end
XacCr = Xac_Cr;
%     Xac = Xac_Cr * Cr;

end
end
```

Neutral point verification using DATCOM and SR-71 data. (Week 8)

```
% Aerodynamics: Neutral Point
% Gayathri Kola: 7/18/2023
```

```
% METHOD >> DATCOM Section 4.1.4.2
% REGIME >> SUBSONIC & SUPERSONIC & HYPERSONIC
```

```
clc
clear all
close all
```

```
% METHOD VERIFICATION: SR-71 DATA.
```

```
% NOMENCLATURE >>
%-----
```

```
% INPUTS >>
%-----

AR = 1.939;
SweepC4 = 51 * (pi/180);
SweepLE = 52.629 * (pi/180);

CLaoao_p = 0;           % Only for double delta wings.
CNaooai = 1;
CNaooao_p = 1;

Si = 166.71;
So_p = 1;

Xac_cr_i = 1;
Xac_cri_o = 0;          % Only for double delta wings.

Cr = 18.45; %[m]

% BEIGN CODE >>
%-----

M = 0:0.05:3;

Xac_cr = zeros(size(M));

for i = 1:length(M)

    if M(i) >= 0 && M(i) <= 1
        beta = sqrt(1 - M(i)^2);
        % fprintf("Enter Matrix for Whichline for Mach numbers and re run");
        SweepLE1 = SweepLE * (180/pi);
        Xac_cr_i = Xac_CR(M(i), AR, SweepLE1, Cr);
        CLaoai = (2*pi*AR) / (2 + sqrt(((AR^2*beta^2) * (1 + ((tan(SweepC4)^2)/beta^2)) + 4));
        Xac_cr(i) = ((CLaoai * Si * Xac_cr_i) + (CLaoao_p * So_p * Xac_cri_o)) / ((CLaoai * Si) +
        (CLaoao_p * So_p));
        Xac = Xac_cr * Cr;

    elseif M(i) >= 1 && M(i) <= 5
        beta = sqrt(M(i)^2 - 1);
        WhichLine2 = AR * tan(SweepLE);
        F1(i) = tan(SweepLE) / beta; %[right side]
        F2(i) = beta / tan(SweepLE); %[left side]
        % fprintf("Enter Matrix for Whichline for Mach numbers and re run");
        SweepLE1 = SweepLE * (180/pi);
        CNaooai = CN_aoa(M(i), SweepLE1, AR);
        Xac_cr_i = Xac_CR(M(i), AR, SweepLE1, Cr);
        Xac_cr(i) = ((CNaooai * Si * Xac_cr_i) + (CNaooao_p * So_p * Xac_cri_o)) / ((CNaooai * Si) +
        (CNaooao_p * So_p));
        Xac = Xac_cr * Cr;

    else
        beta = sqrt(M(i)^2 - 1);
        WhichLine2 = AR * tan(SweepLE);
        F1(i) = tan(SweepLE) / beta; %[right side]
        F2(i) = beta / tan(SweepLE); %[left side]
        % fprintf("Enter Matrix for Whichline for Mach numbers and re run");
        SweepLE1 = SweepLE * (180/pi);
        CNaooai = CN_aoa(M(i), SweepLE1, AR);
        Xac_cr_i = Xac_CR(M(i), AR, SweepLE1, Cr);
    end
end
```



```
Xac_cr(i) = ((CNaoui * Si * Xac_cr_i) + (CNaao_p * So_p * Xac_cri_o)) / ((CNaoui * Si) +
(CNaao_p * So_p));
Xac = Xac_cr * Cr;
```

```
end
```

```
end
```

```
% PLOTTING >>
```

```
% Plot settings code kindly provided by David Mexquitic
Color = get(groot, 'DefaultAxesColorOrder');
brown = Color(4,:); gold = Color(3,:);
cielo = Color(6,:); red = Color(7,:);
green = Color(5,:); blue = Color(1,:);
orange = Color(2,:);

legs = {'Method: DATCOM with regression'};
plot(M, Xac_cr, ':', 'LineWidth', 4, 'Color', green)
title('Static Margin for SR-71');
grid on;
ax = gca; % axes handle
ax.YAxis.Exponent = 0;
ax.XAxis.LineWidth = 1.5;
ax.XAxis.Color = 'k';
ax.YAxis.LineWidth = 1.5;
ax.YAxis.Color = 'k';
set(gca, 'FontWeight', 'bold', 'FontSize', 10) % Sets the axis and fonts to bold
set(gcf, 'Color', 'W') % Sets the figure background to white
xlabel('Mach Number, {\it M}', 'FontSize', 12, 'fontWeight', 'bold');
ylabel('X_a_c/c_r', 'FontSize', 14, 'FontWeight', 'bold');
ylim([0 1])
xlim([-inf inf])
legend(legs);
```

Trim Equation of Motion (needs fixing), (week 8)

```
%> Stability and Control: Stability Assessment // TRIM EOMS (main script)
% Written by: Gayathri Kola, 7/15/2023.
```

```
% METHOD >> Trim EOM for Steady-State Straight Line Flight, B. Chudoba, M. Cook
% SPEED REGIME >> SUBSONIC
```

```
clc
clear all
close all
```

```
% GENERAL INPUTS >>
```

```
G = General_Inputs;
```

```
% ASSUMPTION >>
```

```
% Define the range of Mach numbers to iterate over
Mach_numbers = 0:0.1:0.8;
```

```
% Initialize arrays to store coefficients for each Mach number
CnBeta_array = zeros(size(Mach_numbers));
ClBeta_array = zeros(size(Mach_numbers));
CmAlpha_array = zeros(size(Mach_numbers));
```



```
Alpha_array = zeros(size(Mach_numbers));
Beta_array = zeros(size(Mach_numbers));
DeltaE_array = zeros(size(Mach_numbers));
DeltaA_array = zeros(size(Mach_numbers));
DeltaR_array = zeros(size(Mach_numbers));
CmDeltaE_array = zeros(size(Mach_numbers));
C1DeltaA_array = zeros(size(Mach_numbers));
CnDeltaR_array = zeros(size(Mach_numbers));
CLaoa_array = zeros(size(Mach_numbers));
CDaoa_array = zeros(size(Mach_numbers));

phi = 0;
psi = 0;

% BEIGN CODE >>
%-----

% Iterate over each Mach number
for i = 1:length(Mach_numbers)
    Mach = Mach_numbers(i);
    ALT = linspace(4,1000,Mach);
    [rho,a,~,~,~,~,~] = atmos(ALT);
    % Calculate airspeed (V) for the current Mach number
    V = Mach * a;

    % Iterate to find trim condition for the current Mach number
    alpha = 12 * (pi/180); % Assume zero angle of attack initially
    beta = 0 * (pi/180); % Assume zero sideslip angle initially
    delta_e = 5 * (pi/180); % Initial elevator deflection guess
    delta_a = 10 * (pi/180); % Initial aileron deflection guess
    delta_r = 10 * (pi/180); % Initial rudder deflection guess
    p = 0;
    r = 0;

    delta_e_prev = -1; % Previous elevator deflection guess
    delta_a_prev = -1; % Previous aileron deflection guess
    delta_r_prev = -1; % Previous rudder deflection guess

    % STRUCTURES >>
    %

Sub = Sub_Inputs(Mach,G,alpha);
Sup = Sup_Inputs(G, Mach);
Hyp = Hyp_Inputs(G,alpha);

% COEFFICIENTS >>
%-----

CLo = 0.3; % Lift coefficient at zero angle of attack
[CLaoa,~,~] = CL_aoa(Mach,G,alpha); % Lift coefficient slope

CDo = 0.03; % Drag coefficient at zero angle of attack
[CDaoa,~,~] = CD_aoa(Mach,G,alpha); % Drag coefficient slope

Cmo = 0; % Pitching moment coefficient at zero angle of attack
[Cmaoa,~,~] = Cm_aoa(rho,V,G,Sub,Sup,Hyp); % Pitching moment coefficient slope
[CmDeltaE,~,~] = Cm_DeltaE(G, Sub, Sup, Hyp); % Pitching moment coefficient due to elevator deflection

Clo = 0; % Rolling moment coefficient at zero angle of attack
[Clbeta,~,~] = Cl_beta(G,Sub,Sup,Hyp); % Rolling moment coefficient slope in the y-axis direction
[C1DeltaE,~,~] = C1_DeltaE(G,Sub,Sup,Hyp);
```



```
Clp = -0.05; % Rolling moment coefficient due to roll rate
Clr = 0.1; % Rolling moment coefficient due to yaw rate

Cno = 0; % Yawing moment coefficient at zero angle of attack
[Cnbeta,~,~] = Cn_Beta(G,Sub,Sup,Hyp); % Yawing moment coefficient slope in the y-axis direction
[CnDeltaR,~,~] = Cn_DeltaR(G,Sub,Sup,Hyp);
Cnp = 0; % Yawing moment coefficient due to roll rate
Cnr = 0; % Yawing moment coefficient due to yaw rate

T = 30000;
xt = 2;
yt = 0;
zt = 2;

while abs(delta_e - delta_e_prev) > 1e-6 || abs(delta_a - delta_a_prev) > 1e-6 || abs(delta_r - delta_r_prev) > 1e-6
    % Calculate aerodynamic forces and moments
    CL = CLo + (Claoa * alpha); % Lift coefficient
    CD = CDo + (Cdaoa * alpha); % Drag coefficient
    Cm = Cmo + (Cmaoa * alpha) + (CmDeltaE * delta_e); % Pitching moment coefficient
    Cl = Clo + (Clbeta * beta) + (ClDeltaE * delta_a) + (Clp * p) + (Clr * r); % Rolling moment coefficient
    Cn = Cno + (Cnbeta * beta) + (CnDeltaR * delta_r) + (Cnp * p) + (Cnr * r); % Yawing moment coefficient

    q = 0.5 * rho * V^2; % Dynamic pressure

    L = q * G.Sref * CL; % Lift force
    D = q * G.Sref * CD; % Drag force
    Y = q * G.Sref * (Cl + Clbeta * beta + Clp * p + Clr * r); % Side force

    % Calculate moments
    M = q * G.Sref * G.b * Cm; % Pitching moment
    L_roll = q * G.Sref * G.b * Cl; % Rolling moment
    N_yaw = q * G.Sref * G.b * Cn; % Yawing moment

    % Calculate trim equations
    eq1 = -L + (G.m * G.g * cos(G.gamma) * cos(phi)) + T*((-cos(phi)*cos(psi)*sin(alpha)) +
    (sin(phi)*cos(alpha))); % Vertical force balance equation
    eq2 = -D - (G.m * G.g * sin(G.gamma)) + T*((cos(phi)*cos(psi)*cos(alpha)) +
    (sin(phi)*sin(alpha))); % Horizontal force balance equation
    eq3 = Y + (G.m * G.g * sin(phi) * cos(G.gamma)) + T*(cos(phi)*sin(psi)); % Lateral force balance equation
    eq4 = M + T*((cos(phi)*cos(psi)*zt) - (sin(phi)*xt)); % Pitching moment balance equation
    eq5 = L_roll + T*cos(alpha)*((-cos(phi)*sin(psi)*zt) + (sin(phi)*yt)) +
    T*sin(alpha)*(cos(phi)*sin(psi)*xt - cos(phi)*cos(psi)*zt); % Rolling moment balance equation
    eq6 = N_yaw + T*sin(alpha)*(cos(phi)*sin(psi)*zt - sin(phi)*yt) +
    T*cos(alpha)*(cos(phi)*sin(psi)*xt - cos(phi)*cos(phi)*yt); % Yawing moment balance equation

    % Update control surface deflection guesses
    delta_e_prev = delta_e;
    delta_a_prev = delta_a;
    delta_r_prev = delta_r;

    % Solve for new control surface deflections
    delta_e = fsolve(@(de)eq1, delta_e_prev);
    delta_a = fsolve(@(da)eq2, delta_a_prev);
    delta_r = fsolve(@(dr)eq3, delta_r_prev);

    % Update angular rates (p and r)
    p = fsolve(@(p_var)eq5, p);
    r = fsolve(@(r_var)eq6, r);

    % Update angles of attack and sideslip
    alpha = (eq2 + G.m * G.g * sin(G.gamma)) / (0.5 * rho * V^2 * G.Sref);
```



```
beta = atan(eq3 / sqrt(eq1^2 + eq2^2));
end

% Store the coefficients for the current Mach number
CLaoa_array(i) = CL;
CDaoa_array(i) = CD;

CnBeta_array(i) = Cn;
ClBeta_array(i) = Cl;
CmAlpha_array(i) = Cm;
Alpha_array(i) = alpha;
Beta_array(i) = beta;
DeltaE_array(i) = delta_e;
DeltaA_array(i) = delta_a;
DeltaR_array(i) = delta_r;
CmDeltaE_array(i) = Cm * delta_e;
ClDeltaA_array(i) = Cl * delta_a;
CnDeltaR_array(i) = Cn * delta_r;
end

% PLOTTING >>
%-----
```

```
% Plot settings code kindly provided by David Mexquitic
Color = get(groot, 'DefaultAxesColorOrder');
brown = Color(4,:); gold = Color(3,:);
cielo = Color(6,:); red = Color(7,:);
green = Color(5,:); blue = Color(1,:);
orange = Color(2,:);

%-----
```

```
% AEROLOTS ----

% Plot ClBeta as a function of Mach number
figure;
plot(Mach_numbers, CLaoa_array/57.3, ':', 'linewidth', 4, 'Color', brown)
% title('ClBeta as a Function of Mach Number');
grid on;
ax = gca; % axes handle
ax.YAxis.Exponent = 0;
ax.XAxis.LineWidth = 1.5;
ax.XAxis.Color = 'k';
ax.YAxis.LineWidth = 1.5;
ax.YAxis.Color = 'k';
set(gca, 'FontWeight', 'bold', 'FontSize', 10) % Sets the axis and fonts to bold
set(gcf, 'Color', 'W') % Sets the figure background to white
xlabel('Mach Number, {\it M}', 'FontSize', 12, 'fontWeight', 'bold');
ylabel('C_L_\alpha', 'FontSize', 14, 'FontWeight', 'bold');

% Plot ClBeta as a function of Mach number
figure;
plot(Mach_numbers, CDaoa_array/57.3, ':', 'linewidth', 4, 'Color', brown)
% title('ClBeta as a Function of Mach Number');
grid on;
ax = gca; % axes handle
ax.YAxis.Exponent = 0;
ax.XAxis.LineWidth = 1.5;
ax.XAxis.Color = 'k';
ax.YAxis.LineWidth = 1.5;
ax.YAxis.Color = 'k';
set(gca, 'FontWeight', 'bold', 'FontSize', 10) % Sets the axis and fonts to bold
set(gcf, 'Color', 'W') % Sets the figure background to white
xlabel('Mach Number, {\it M}', 'FontSize', 12, 'fontWeight', 'bold');
ylabel('C_D_\alpha', 'FontSize', 14, 'FontWeight', 'bold');
```



```
%-----  
  
% Plot ClBeta as a function of Mach number  
figure;  
plot(Mach_numbers, CnBeta_array/57.3, ':', 'linewidth', 4, 'Color', cielo)  
% title('ClBeta as a Function of Mach Number');  
grid on;  
ax = gca; % axes handle  
ax.YAxis.Exponent = 0;  
ax.XAxis.LineWidth = 1.5;  
ax.XAxis.Color = 'k';  
ax.YAxis.LineWidth = 1.5;  
ax.YAxis.Color = 'k';  
set(gca, 'FontWeight', 'bold', 'FontSize', 10) % Sets the axis and fonts to bold  
set(gcf, 'Color', 'W') % Sets the figure background to white  
xlabel('Mach Number, {\it M}', 'FontSize', 12, 'fontWeight', 'bold');  
ylabel('C_n_\beta', 'FontSize', 14, 'FontWeight', 'bold');  
  
% Plot ClBeta as a function of Mach number  
figure;  
plot(Mach_numbers, ClBeta_array/57.3, ':', 'linewidth', 4, 'Color', brown)  
% title('ClBeta as a Function of Mach Number');  
grid on;  
ax = gca; % axes handle  
ax.YAxis.Exponent = 0;  
ax.XAxis.LineWidth = 1.5;  
ax.XAxis.Color = 'k';  
ax.YAxis.LineWidth = 1.5;  
ax.YAxis.Color = 'k';  
set(gca, 'FontWeight', 'bold', 'FontSize', 10) % Sets the axis and fonts to bold  
set(gcf, 'Color', 'W') % Sets the figure background to white  
xlabel('Mach Number, {\it M}', 'FontSize', 12, 'fontWeight', 'bold');  
ylabel('C_l_\beta', 'FontSize', 14, 'FontWeight', 'bold');  
  
% Plot CmAlpha as a function of Mach number  
figure;  
plot(Mach_numbers, CmAlpha_array/57.3, ':', 'linewidth', 4, 'Color', gold)  
% title('CmAlpha as a Function of Mach Number');  
grid on;  
ax = gca; % axes handle  
ax.YAxis.Exponent = 0;  
ax.XAxis.LineWidth = 1.5;  
ax.XAxis.Color = 'k';  
ax.YAxis.LineWidth = 1.5;  
ax.YAxis.Color = 'k';  
set(gca, 'FontWeight', 'bold', 'FontSize', 10) % Sets the axis and fonts to bold  
set(gcf, 'Color', 'W') % Sets the figure background to white  
xlabel('Mach Number, {\it M}', 'FontSize', 12, 'fontWeight', 'bold');  
ylabel('C_m_\alpha', 'FontSize', 14, 'FontWeight', 'bold');  
  
%-----  
% Plot CmAlpha as a function of Mach number  
figure;  
plot(Mach_numbers, DeltaR_array*(180/pi), ':', 'linewidth', 4, 'Color', red)  
% title('CmAlpha as a Function of Mach Number');  
grid on;  
ax = gca; % axes handle  
ax.YAxis.Exponent = 0;  
ax.XAxis.LineWidth = 1.5;  
ax.XAxis.Color = 'k';  
ax.YAxis.LineWidth = 1.5;  
ax.YAxis.Color = 'k';  
set(gca, 'FontWeight', 'bold', 'FontSize', 10) % Sets the axis and fonts to bold  
set(gcf, 'Color', 'W') % Sets the figure background to white  
xlabel('Mach Number, {\it M}', 'FontSize', 12, 'fontWeight', 'bold');
```



```
ylabel('\delta_r', 'FontSize', 14, 'FontWeight', 'bold');

% Plot CmAlpha as a function of Mach number
figure;
plot(Mach_numbers, Alpha_array*(180/pi),':', 'linewidth', 4, 'Color', green)
% title('CmAlpha as a Function of Mach Number');
grid on;
ax = gca; % axes handle
ax.YAxis.Exponent = 0;
ax.XAxis.LineWidth = 1.5;
ax.XAxis.Color = 'k';
ax.YAxis.LineWidth = 1.5;
ax.YAxis.Color = 'k';
set(gca, 'FontWeight', 'bold', 'FontSize', 10) % Sets the axis and fonts to bold
set(gcf, 'Color','W') % Sets the figure background to white
xlabel('Mach Number, {\it M}', 'FontSize', 12,'fontweight','bold');
ylabel('alpha', 'FontSize', 14, 'FontWeight', 'bold');

% Plot CmAlpha as a function of Mach number
figure;
plot(Mach_numbers, Beta_array*(180/pi),':', 'linewidth', 4, 'Color', blue)
% title('CmAlpha as a Function of Mach Number');
grid on;
ax = gca; % axes handle
ax.YAxis.Exponent = 0;
ax.XAxis.LineWidth = 1.5;
ax.XAxis.Color = 'k';
ax.YAxis.LineWidth = 1.5;
ax.YAxis.Color = 'k';
set(gca, 'FontWeight', 'bold', 'FontSize', 10) % Sets the axis and fonts to bold
set(gcf, 'Color','W') % Sets the figure background to white
xlabel('Mach Number, {\it M}', 'FontSize', 12,'fontweight','bold');
ylabel('beta', 'FontSize', 14, 'FontWeight', 'bold');

% Plot CmAlpha as a function of Mach number
figure;
plot(Mach_numbers, DeltaE_array*(180/pi),':', 'linewidth', 4, 'Color', orange)
% title('CmAlpha as a Function of Mach Number');
grid on;
ax = gca; % axes handle
ax.YAxis.Exponent = 0;
ax.XAxis.LineWidth = 1.5;
ax.XAxis.Color = 'k';
ax.YAxis.LineWidth = 1.5;
ax.YAxis.Color = 'k';
set(gca, 'FontWeight', 'bold', 'FontSize', 10) % Sets the axis and fonts to bold
set(gcf, 'Color','W') % Sets the figure background to white
xlabel('Mach Number, {\it M}', 'FontSize', 12,'fontweight','bold');
ylabel('delta_e', 'FontSize', 14, 'FontWeight', 'bold');

% Plot CmAlpha as a function of Mach number
figure;
plot(Mach_numbers, CmDeltaE_array/57.3,':', 'linewidth', 4, 'Color', cielo)
% title('CmAlpha as a Function of Mach Number');
grid on;
ax = gca; % axes handle
ax.YAxis.Exponent = 0;
ax.XAxis.LineWidth = 1.5;
ax.XAxis.Color = 'k';
ax.YAxis.LineWidth = 1.5;
ax.YAxis.Color = 'k';
set(gca, 'FontWeight', 'bold', 'FontSize', 10) % Sets the axis and fonts to bold
set(gcf, 'Color','W') % Sets the figure background to white
xlabel('Mach Number, {\it M}', 'FontSize', 12,'fontweight','bold');
ylabel('Cm_\delta_e', 'FontSize', 14, 'FontWeight', 'bold');
```

	SENIOR DESIGN: MAE 4351 Project	Ref.: MAE 4351-001-2021 Date: 11. Aug. 2023 Name: Gayathri Kola Status: Complete
---	---	---

```
% Plot CmAlpha as a function of Mach number
figure;
plot(Mach_numbers, ClDeltaA_array/57.3, ':', 'linewidth', 4, 'Color', brown)
% title('CmAlpha as a Function of Mach Number');
grid on;
ax = gca; % axes handle
ax.YAxis.Exponent = 0;
ax.XAxis.LineWidth = 1.5;
ax.XAxis.Color = 'k';
ax.YAxis.LineWidth = 1.5;
ax.YAxis.Color = 'k';
set(gca, 'FontWeight', 'bold', 'FontSize', 10) % Sets the axis and fonts to bold
set(gcf, 'Color','W') % Sets the figure background to white
xlabel('Mach Number, {\it M}', 'FontSize', 12, 'fontWeight', 'bold');
ylabel('Cl_\delta_a', 'FontSize', 14, 'FontWeight', 'bold');

% Plot CmAlpha as a function of Mach number
figure;
plot(Mach_numbers, CnDeltaR_array/57.3, ':', 'linewidth', 4, 'Color', gold)
% title('CmAlpha as a Function of Mach Number');
grid on;
ax = gca; % axes handle
ax.YAxis.Exponent = 0;
ax.XAxis.LineWidth = 1.5;
ax.XAxis.Color = 'k';
ax.YAxis.LineWidth = 1.5;
ax.YAxis.Color = 'k';
set(gca, 'FontWeight', 'bold', 'FontSize', 10) % Sets the axis and fonts to bold
set(gcf, 'Color','W') % Sets the figure background to white
xlabel('Mach Number, {\it M}', 'FontSize', 12, 'fontWeight', 'bold');
ylabel('Cn_\delta_r', 'FontSize', 14, 'FontWeight', 'bold');
```

Note: No more code was added for the final report because a lot were made. All files will be included in the data dump instead.

References

- [1] 1927 Spirit of St. Louis | Fantasy of Flight. *Fantasy of Flight*. <https://www.fantasyofflight.com/collection/aircraft/currently-not-showing-in-museum/golden-age/1927-spirit-of-st-louis/>. Accessed Jun. 11, 2023.
- [2] Hall, N. “The Spirit of St. Louis.” *Advanced Materials & Processes*, Vol. 161, No. 11, 2003, pp. 43–46.
- [3] New Aircraft: Gulfstream G700 | Private Jet Charter®. *Private Jet Charter*. <https://privatejetcharter.com/gulfstream-g700-private-jet-charter/>. Accessed Jun. 11, 2023.
- [4] Miller, L. S. SR-71 RSO Tells the Story of When His Blackbird Photographed All of the SA-2 SAM Sites in North Korea in One Mission before Doing an Emergency Landing in South Korea Because of an Engine Failure. *The Aviation Geek Club*. Accessed Jun. 11, 2023.
- [5] Hermeus. Quarterhorse. *Hermeus*. <https://www.hermeus.com/quarterhorse>.
- [6] Hermeus. Darkhorse. *Hermeus*. <https://www.hermeus.com/darkhorse>.
- [7] DARKHORSE. *Hermeus*. <https://www.hermeus.com/darkhorse>. Accessed Jun. 11, 2023.
- [8] Hermeus. Halcyon. *Hermeus*. <https://www.hermeus.com/halcyon>.
- [9] HALCYON. *Hermeus*. <https://www.hermeus.com/halcyon>. Accessed Jun. 11, 2023.
- [10] Chudoba, D. B. Design Project: Hypersonic Spirit of St. Louis. Jun 06, 2023.
- [11] Junell, W. *Designing a Wing Body Hypersonic Spirit of St. Louis: Detailed Analysis of Vehicle Synthesis and Geometry*. University of Texas at Arlington, Arlington, TX, 2023.
- [12] Blakely, N. *Trans-Atlantic Hypersonic Transport Aircraft: Reimagining the Spirit of St. Louis*. University of Texas at Arlington, Arlington, TX, 2023.
- [13] McDonnell Aircraft Company, and Czysz, P. *Hypersonic Research Facilities Study Volume 2*. Publication NASA CR 114326. McDonnell Douglas, California, 1970, p. 282.



- [14] North American X-15. Wikipedia, Aug 06, 2023.
- [15] North American X-15 HD Wallpapers and Backgrounds. *Wallpaper Abyss*. https://wall.alphacoders.com/by_sub_category.php?id=208905&name=North+American+X-15+Wallpapers. Accessed Aug. 11, 2023.
- [16] Aerospaceweb.Org | Ask Us - X-43 Accident Investigation. <https://aerospaceweb.org/question/investigations/q0116.shtml>. Accessed Aug. 11, 2023.
- [17] SPACE SHUTTLE ORBITER. <http://what-when-how.com/space-science-and-technology/space-shuttle-orbiter/>. Accessed Aug. 11, 2023.
- [18] Leone, D. Tu-144 Vs Concorde: The Concordski Was Bigger and Faster than Its Anglo-French Counterpart, but Its Glory Was Quite Short. Here's Why. *The Aviation Geek Club*. <https://theaviationgeekclub.com/tu-144-vs-concorde-the-concordski-was-bigger-and-faster-than-its-anglo-french-counterpart-but-its-glory-was-quite-short-heres-why/>. Accessed Jun. 23, 2023.
- [19] Chudoba, B. *Stability and Control of Conventional and Unconventional Aerospace Vehicle Configurations: A Generic Approach from Subsonic to Hypersonic Speeds*. Springer International Publishing, Cham, 2019.
- [20] Roskam, D. J. *Airplane Design Part VII: Determination of Stability, Control and Performance Characteristics*. Design, Analysis and Research Corporation, Lawrence, Kansas, 2017.
- [21] Moes, T. R. *Stability and Control Estimation Flight Test Results for the SR-71 Aircraft With Externally Mounted Experiments*. National Aeronautics and Space Administration, Dryden Flight Research Center, 2002.
- [22] Moes, T., Cobleigh, B., Cox, T., Conners, T., Iliff, K., and Powers, B. Flight Stability and Control and Performance Results from the Linear Aerospike SR-71 Experiment (LASRE). Presented at the 23rd Atmospheric Flight Mechanics Conference, Boston, MA, U.S.A., 1998.
- [23] Cox, T. H., and Marshall, A. "Longitudinal Handling Qualities of the Tu-144LL Airplane and Comparisons With Other Large, Supersonic Aircraft." *National Aeronautics and Space Administration, Dryden Flight Research Center*, 2000, p. 44.
- [24] Simon, S. *Development of the Vehicle Configuration Compendium: A Comprehensive Data-Information-Knowledge System to Aid in High-Speed Vehicle Design*. University of Texas at Arlington, 2022.
- [25] Nicolai, L. M., and Carichner, G. E. *Fundamentals of Aircraft and Airship Design*. American Institute of Aeronautics and Astronautics, Inc., Reston, Virginia, 2010.
- [26] Anderson, J. D. *Aircraft Performance & Design*. McGraw-Hill Education, 1999.
- [27] Yechout, T. R., Hallgren, W. F., Morris, S. L., and Bossert, D. E. *Introduction to Aircraft Flight Mechanics Performance, Static Stability, Dynamic Stability, and Classical Feedback Control*. American Institute of Aeronautics and Astronautics, Reston, UNITED STATES, 2003.
- [28] Sadraey, M. H. *Aircraft Design: A Systems Engineering Approach*. Wiley, Chichester, West Sussex, U.K, 2013.
- [29] USAF (United States Air Force) Stability and Control DATCOM (Data Compendium).
- [30] Raymer, D. P. *Aircraft Design: A Conceptual Approach*. American Institute of Aeronautics and Astronautics, Inc, Reston, VA, 2018.
- [31] Roskam, J. *Airplane Flight Dynamics and Automatic Flight Controls*. DARcorporation, 1998.
- [32] Warren Phillips. *Mechanics of Flight*. John Wiley & Sons, Inc., 2004.
- [33] Coleman, C. C., and Faruqi, F. A. "On Stability and Control of Hypersonic Vehicles."
- [34] Coleman, G., and Chudoba, B. A Generic Stability and Control Tool for Conceptual Design, Prototype Styem Overview. In *45th AIAA Aerospace Sciences Meeting and Exhibit*, American Institute of Aeronautics and Astronautics, 2007.
- [35] Coleman, G. J. "A Generic Stability And Control Tool For Flight Vehicle Conceptual Design: Aeromech Software Development." 2007.
- [36] Roskam, J. *Airplane Design II*. DARcorporation, Lawrence, Kan, 1986.
- [37] Anderson, Jr, J. D. *Fundamentals of Aerodynamics*. McGraw-Hill Education, 2017.
- [38] Roskam, J. *Airplane Design VI: Preliminary Calculation of Aerodynamic, Thrust and Power Characteristics*. DARcorporation, 1987.
- [39] Coleman, G. *AIRCRAFT CONCEPTUAL DESIGN – AN ADAPTABLE PARAMETRIC SIZING METHODOLOGY*. Dissertation. University of Texas at Arlington, Arlington, TX, 2010.
- [40] Czysz, P., and Vandekerckhove, J. Transatmospheric Launcher Sizing. In *Scramjet Propulsion*, American Institute of Aeronautics and Astronautics (AIAA), 2001.

- [41] Czysz, P., Bruno, C., and Chudoba, B. *Future Spacecraft Propulsion Systems and Integration: Enabling Technologies for Space Exploration*. Springer, Berlin, Heidelberg, 2018.
- [42] Ledford, T., and Harris, C. Hypersonic Convergence. Background and Methodology. Aerospace Vehicle Design (AVD) Laboratory, Feb 08, 2023.
- [43] Chudoba, B., Coleman, G., Oza, A., Gonzalez, L., and Czysz, P. *Solution-Space Screening of a Hypersonic Endurance Demonstrator*. Publication NF1676L-14425. 2012.
- [44] Murthy, T. K. S. *Computational Methods in Hypersonic Aerodynamics*. Springer Dordrecht, 1991.
- [45] Enkenhus, K., Wendt, J. F., and Pankhurst, R. C. *Aerodynamic Problems of Hypersonic Vehicles*. Advisory Group for Aerospace Research and Development (AGARD), 1972.
- [46] Rasmussen, M. *Hypersonic Flow*. Wiley, 1994.
- [47] Anderson Jr., J. D. *Hypersonic and High-Temperature Gas Dynamics, Second Edition*. American Institute of Aeronautics and Astronautics, Reston ,VA, 2006.
- [48] Mexquitic, D. *Designing a Wing-Body Hypersonic Spirit of St. Louis: Aerodynamics, Cost/Market*. University of Texas at Arlington, Arlington, TX, 2023.
- [49] Bartley, S., Urquidi, N., and Lurie, D. XB-70, SR-71, and TU-144: Large Supersonic Transports. Mar 22, 2006.
- [50] Whitman, D. G. "Space Shuttle Orbiter And Subsystems."
- [51] Gordon. Concorde SST. NASA, , 2017.
- [52] Lockheed Martin. *SR-71 Flight Manual*. 1989.
- [53] Eastwood, B. M. XB-70 Valkyrie: The Prototype Supersonic "Missile Truck" Disaster. 19FortyFive, Dec 28, 2022.
- [54] Eastwood, B. M. Tu-144: Russia's Dream of Building a Mach 2 Concorde Failed. 19FortyFive, Mar 21, 2022.
- [55] Zhang, B. The Concorde Flew across the Ocean for the First Time 42 Years Ago — Here's What It Was Like. *Business Insider*. <https://www.businessinsider.com/the-concorde-flew-across-the-ocean-for-the-first-42-years-ago-today-heres-what-it-was-like-2015-9>. Accessed Aug. 11, 2023.
- [56] 1:144 Lockheed SR-71 Blackbird Reconnaissance Aircraft Metal Plane Model, USAF. eBay. <https://www.ebay.com/itm/394731435686>. Accessed Aug. 11, 2023.
- [57] Supersonic, B. Boom - FlyBy - From Bomber to Supersonic Testbed: Explore the XB-70 Valkyrie with the National Museum of the U.S. Air Force. *Boom*. <https://boomsupersonic.com/flyby/xb70-from-bomber-to-supersonic-testbed>. Accessed Aug. 11, 2023.
- [58] Hutchison, H. C. North Korea Once Shot a Missile at an SR-71 Blackbird and Missed. *Business Insider*. <https://www.businessinsider.com/north-korea-shot-missile-sr-71-blackbird-2018-1>. Accessed Aug. 11, 2023.
- [59] Filseth, T. How Soviet Missiles Killed the XB-70 Without Firing a Shot. *The National Interest*. <https://nationalinterest.org/blog/buzz/how-soviet-missiles-killed-xb-70-without-firing-shot-197301>. Accessed Aug. 11, 2023.
- [60] Concorde Elevons and Rudder. *heritage-concorde*. <https://www.heritageconcorde.com/concorde-elevons-and-rudder>. Accessed Aug. 11, 2023.
- [61] Chudoba, B., and Cook, M. Trim Equations of Motion for Aircraft Design: Turning Flight, Pull-Up and Push-Over. Presented at the AIAA Atmospheric Flight Mechanics Conference and Exhibit, Austin, Texas, 2003.
- [62] Chudoba, B., and Cook, M. Trim Equations of Motion for Aircraft Design: Steady State Straight Line Flight. Presented at the AIAA Atmospheric Flight Mechanics Conference and Exhibit, Austin, Texas, 2003.
- [63] Roskam, J. *Airplane Design Part I-VII*. DARcorporation, 2002.
- [64] Hawthorne, P. J. *Results of Investigations on a 0.010-Scale 140A/B Configuration Space Shuttle Vehicle Orbiter Model 72-0 in the NASA/Langley Research Center Continuous Flow Hypersonic Tunnel (OA90)*. Publication NASA-CR-141805. 1975.
- [65] Wolowicz, C. H., and Yancey, R. B. *Summary of Stability and Control Characteristics of the XB-70 Airplane*. Publication NASA-TM-X-2933. 1973.
- [66] Wolowicz, C. H., and Yancey, R. B. *Comparisons of Predictions of the XB-70-1 Longitudinal Stability and Control Derivatives with Flight Results for Six Flight Conditions*. Publication NASA-TM-X-2881. 1973.
- [67] Carmona, C. *Conceptual Design of a Hypersonic Spirit of St. Louis*. University of Texas at Arlington, 2023.
- [68] Iliff, K., and Shafer, S. Extraction of Stability and Control Derivatives from Orbiter Flight Data. *NTRS*. https://www.nasa.gov/centers/dryden/pdf/88294main_H-1912.pdf. Accessed Jun. 25, 2023.
- [69] Prior, A. *Conceptual Hypersonic Transport Design*. University of Texas at Arlington, Aerospace Engineering Department, 2023.

	SENIOR DESIGN: MAE 4351 Project	Ref.: MAE 4351-001-2021 Date: 11. Aug. 2023 Name: Gayathri Kola Status: Complete
---	---	---

- [70] Coultron, J. *Conceptual Design of a Hypersonic Spirit of St. Louis: Propulsion, Structures and Landing Gear.* 2023.
- [71] Jo, S. *Designing a Wing-Body Hypersonic Spirit of St. Louis: Aerothermodynamics and Performance & Trajectory.* The University of Texas at Arlington, Arlington, TX, 2023.
- [72] Jones, B. *Hypersonic Spirit of St. Louis: Aerodynamic and Cost Analysis.* University of Texas at Arlington, Arlington, Texas.
- [73] Wells, D. The Flight Optimization System Weights Estimation Method. NASA, , 2017.
- [74] Dynamics of Flight: Stability and Control, 3rd Edition | Wiley. *Wiley.com.* <https://www.wiley.com/en-us/Dynamics+of+Flight%3A+Stability+and+Control%2C+3rd+Edition-p-9780471034186>. Accessed Jun. 18, 2023.
- [75] Leishman, J. G. “Flying Fast – Supersonic & Hypersonic Flight.” 2023. <https://doi.org/10.15394/eaglepub.2022.1066.n43>.
- [76] Roskam, J. *Airplane Design: Preliminary Sizing of Airplanes.* DARcorporation, 1985.
- [77] Mc Mahon, M. C., and Wentz, W. H. *An Experimental Investigation of the Flow Fields about Delta and Double-Delta Wings at Low Speeds.* Publication NASA-CR-521. 1966.
- [78] Goecke, S. A., Pembo, C., and Saltzman, E. J. *Base Pressure Measurements on the XB-70 Airplane at Mach Numbers from 0.4 to 3.0.* Publication NASA-TM-X-1612. 1968.
- [79] Aprovitola, A., Dyblenko, O., Pezzella, G., and Viviani, A. “Aerodynamic Analysis of a Supersonic Transport Aircraft at Low and High Speed Flow Conditions.” *Aerospace,* Vol. 9, No. 8, 2022, p. 411. <https://doi.org/10.3390/aerospace9080411>.
- [80] Samoylovitch, O., and Strelets, D. “Determination of the Oswald Efficiency Factor at the Aeroplane Design Preliminary Stage.” *Aircraft Design,* 2000.
- [81] Aerodynamic Study of the NASA’s X-43A Hypersonic Aircraft. <https://www.mdpi.com/2076-3417/10/22/8211>. Accessed Jun. 23, 2023.
- [82] OpenFOAM. <https://www.openfoam.com/>. Accessed Jun. 23, 2023.
- [83] OpenVSP. <https://openvsp.org/>. Accessed Jun. 23, 2023.
- [84] NASA. *Lockheed SR-71 Researcher’s Handbook.*